

# PULSED NUCLEAR QUADRUPOLE RESONANCE OF SPIN $3/2$ SOLIDS: DYNAMICS AND EQUILIBRIUM PROPERTIES

A Thesis Submitted  
in Partial Fulfilment of the Requirements  
for the Degree of

DOCTOR OF PHILOSOPHY

*by*  
ANIL KUMAR DUBEY

*to the*

DEPARTMENT OF CHEMISTRY  
INDIAN INSTITUTE OF TECHNOLOGY KANPUR

DECEMBER 1989

"...and miles to go before I sleep ."

- Robert Frost

CHM-1989-D-DUB-F

20 DEC 1991

CENTRAL LIBRARY  
U. T. KANPUR

Acc. No. A.112522

## STATEMENT

I hereby declare that the work embodied in this thesis entitled, PULSED NUCLEAR QUADRUPOLE RESONANCE OF SPIN  $3/2$  SOLIDS DYNAMICS AND EQUILIBRIUM PROPERTIES, is the result of investigations carried out by me in the Department of Chemistry Indian Institute of Technology Kanpur India.

This work, begun under the supervision of Professor P.T. Narasimhan, has been completed after his retirement under the guidance of Professor P. Raghunathan.

In keeping with the general practice of reporting scientific observations due acknowledgements have been made wherever the work described is based on the findings of other investigators.

KANPUR

December 1989

A. K. Dubey  
ANIL KUMAR DUBEY

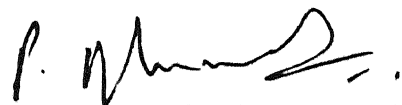


## CERTIFICATE I

*Certified that the work presented in this thesis entitled, 'PULSED NUCLEAR QUADRUPOLE RESONANCE SPECTROSCOPY OF SPIN 3/2 SOLIDS : DYNAMICS AND EQUILIBRIUM PROPERTIES by Mr. Anil Kumar Dubey has been completed under my guidance and has not been submitted elsewhere for a degree.*

Kanpur

December 1989



( Professor P. Raghunathan )

*Thesis Guide*

*Department of Chemistry*

*I.I.T. Kanpur*

DEPARTMENT OF CHEMISTRY  
INDIAN INSTITUTE OF TECHNOLOGY KANPUR, INDIA

CERTIFICATE II

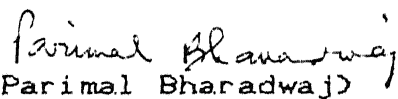
This is to certify that Mr. Anil Kumar Dubey has satisfactorily completed all the courses required for the Ph.D. Degree programme. The courses include :

Chm 505	Principles of Organic Chemistry
Chm 521	Chemical Binding
Chm 524	Modern Physical Methods in Chemistry
Chm 525	Principles of Physical Chemistry
Chm 534N	Electronics for Chemistry
Chm 545	Principles of Inorganic Chemistry
M 604N	Computer Programming
Chm 622N	Chemical Kinetics
Chm 634N	Symmetry and Molecular Structure
Chm 800	General Seminar
Chm 801	Special Seminar
Chm 900	Ph.D. Thesis

Mr. Anil Kumar Dubey was admitted to the candidacy for the Ph.D. degree in September 1984 after he successfully completed the written and oral qualifying examinations.

  
(S.S. Katiyar)

Head  
Department of Chemistry  
I.I.T. Kanpur

  
(Parimal Bharadwaj)

Convenor  
Departmental Post-Graduate  
Committee

I.I.T. Kanpur

## ACKNOWLEDGEMENTS

I thank Professor P.T. Narasimhan for introducing me to the subject of magnetic resonance and initiating me to the topic of research presented in this thesis. I am deeply indebted to Professor P. Raghunathan who guided me towards the completion of this work after Professor Narasimhan's retirement from this Institute. Without Professor Raghunathan's scientific discussions, constant support and encouragement, I would not have imagined the fruitful completion of this work.

I place on record the encouragement to pursue higher studies, provided by my guru Professor Sudhindra Nath Pal, a great teacher I have been taught by during my Bachelor's degree.

Dr. Narayanan Chandrakumar's support throughout the period of my thesis work was immense. The experiments in this thesis would not have come about without his help. Also, I am grateful to him for critically evaluating the theoretical part of this thesis.

I recall with pleasure my association with Dr. V. Ravishankar who has helped me shape my ideas about quadrupole precession a great deal.

My heartfelt thanks to Mr. S. Pandimani and Dr. S.C. Sivasubramanian for patiently assisting me in the computational part of this thesis.

I also thank Professor H.S. Mani for useful discussions and Dr. Parimal Bharadwaj for helping me read the crystal structure information of  $\text{HgCl}_2$ .

My association with the colleagues in the laboratory will remain unforgettable. This includes Drs (Mrs) Amrita Tripathi, Narsimha Reddy, S.C. Sivasubramanian and Ravinder Reddy ; and also A. Ramamoorthy, Sidharth Shankar Ray, V.G. Ju, Ilango and Kasi. The friends in IV Hall of Residence, namely, Drs Bhanu Pratap Singh, Manoj Kumar, G.P. Singh, Narayan Choudhuri, Srini, and also G. Ravindra Kumar, Ranjits, P.K. Choudhury, Sanjay Kumar, P. Tarakeshwar, Naveen Suyal and many others will always be remembered.

Lately my friendship with Arya Raychoudhuri, his wife Debasree and daughter Toku has been a great experience.

Last but not the least, many appreciation of the neat and patient typing done by Sri Bhagwat Prasad Pant and careful preparation of figures by Gauri Singh Thapa.

Anil Kumar Dubey

## SYNOPSIS

The subject matter of this dissertation is a study of the dynamics and equilibrium properties of a spin  $3/2$  pure nuclear quadrupole resonance (NQR) subjected to a scheme of radiofrequency (rf) radiation pulse perturbations. In magnetic resonance literature, the various schemes of rf radiation pulses are known collectively as multiple-pulse sequences.

A central theme that has guided our study is the behavior of the system's response right from zero-time to times of the order of  $\sim 8T_1$ , where  $T_1$  is the spin-(quadrupole)lattice relaxation time of the sample under study. The establishment of quasi-equilibrium state under varying conditions of the external parameters has been studied theoretically. Furthermore, wherever possible, appropriate experiments have been performed on model quadrupolar spin  $3/2$  solids to seek support for our theoretical findings. Very interestingly, it turns out that the mechanism of this quasi-equilibrium state leads to a characteristic prolongation of the quadrupolar relaxation time ( $T_1$ ), similar to previous findings on the prolongation of the spin-spin relaxation time ( $T_2$ ) in the case of pure dipolar solids. In addition to the abovementioned focal theme, our studies have enabled us to adapt several multiple-pulse cycles which have been in use for studies of dipolar solids; the effects

of these cycles on the various major interactions in quadrupolar solids, namely, electric field gradient (efg) inhomogeneity, torsional oscillations and dipole couplings, are studied theoretically.

The thesis consists of seven chapters. In Chapter I we have surveyed the essentials of the phenomenon of NQR. This has been presented vis-à-vis the phenomenon of nuclear magnetic resonance (NMR), and similarities and differences have been pointed out. This Chapter also discusses the importance and usefulness of multiple-pulse studies in NQR. A review of the work already done in multiple-pulse NQR is also presented in this Chapter, with a preview of the present work outlined towards the end of the Chapter.

In Chapter II we have presented the quantum mechanical background for the work presented in later chapters. After introducing all the Hamiltonians needed in the usual Cartesian basis of spin angular momentum operators, we present these Hamiltonians in terms of the single transition operators (STO) in a basis where the quadrupole Hamiltonian is diagonal. The choice of STO or fictitious spin  $1/2$  operators [A. Wokaun and R.R. Ernst, J. Chem. Phys. 67, 1752 (1977); S. Vega, J. Chem. Phys. 68, 5518 (1978)] turns out to be very suitable for describing the dynamics of the evolution of spin  $3/2$  nuclear assembly subjected to an rf field perturbation. We also introduce in this Chapter the quadrupole interaction frame (QIF); the high frequency

approximation for first order perturbation theory calculations; the observables of NQR experiments, namely, the magnetization operators for spin  $3/2$ ; the density operator; the high temperature approximation for the equilibrium density operator; the Liouville-von Neumann equation; and the pulse propagator. Also we describe in this Chapter the roles of the internal Hamiltonians in modifying NQR line shapes.

In Chapter III are presented the single pulse response and spin echo calculations for spin  $3/2$  NQR in a system of non-interacting nuclei. The purpose is to demonstrate, perhaps for the first time, the effectiveness of the STO formalism in typical spin  $3/2$  NQR calculations. We also demonstrate in this Chapter the applicability of STO formalism to analyse theoretically the zero-time resolution (ZTR) technique for the recovery of free induction decay (FID) completely in a spin  $3/2$  NQR system with non-axially symmetric efg. This is an extension of the recent work of Singh and Armstrong [M. Singh and R. L. Armstrong, J. Magn. Reson. 78, 538 (1988)] who have applied the same to study an axially symmetric spin  $3/2$  NQR.

In Chapter IV, we go to the next level of complexity in spin  $3/2$  NQR. Here we present a theoretical study of the multiple-pulse sequences, namely, Phase Alternated Pulse Sequence (PAPS) and WAUGH-HUBER-HAEBERLEN (WAHUHA) using Average Hamiltonian Theory (AHT) within the Magnus expansion framework. The cyclicity criterion, as it applies to a polycrystalline spin  $3/2$  NQR solid,

is explicitly stated; this enables us to formulate several multiple-pulse cycles which are adapted to the study of the major interactions in quadrupolar solids. The nuclear assembly is now considered as being no longer a non-interacting one and, therefore, heteronuclear dipolar interactions are taken into account. The homonuclear dipolar interactions are very weak in spin  $3/2$  NQR and are discarded. Also considered are the effects of impurity and torsional oscillations on the efg. A noteworthy result of this Chapter is the dependence of the effectiveness of the pulse sequences on crystal orientation and asymmetry parameter. Finally our experimental results on the effects of PAPS on spin  $3/2$  in powdered  $\text{KClO}_3$  ( $^{35}\text{Cl}$ ) are presented in this Chapter.

The generalized AHT within the framework of Floquet theorem has been found to be most appropriate to analyse theoretically the results of Ostroff-Waugh (OW) or Mansfield-Ware (MW) multiple-pulse sequence experiments in spin  $3/2$  NQR. Chapter V, therefore, starts with a detailed exposition of the Floquet theorem, the generalized AHT, and the derivation of equilibrium properties of spin  $3/2$  NQR therefrom, in the presence of periodic rf pulse perturbations. We also describe in this Chapter the advantages of the generalized AHT within the Floquet framework over AHT within the Magnus expansion framework and the conditions under which they yield similar results. The results of AHT in three formalisms, namely, Magnus expansion, Floquet theorem and



Krylov-Bogoliubov-Mitropolsky (KBMD) method, are compared in this Chapter.

Chapter VI gives the detailed results of our calculations performed for both single-crystal and powder samples of spin  $3/2$  NQR under the OW or MW pulse sequence. A Monte Carlo procedure based on 'systematic sampling' technique was used for powder averaging, and the Fortran program which performs the powder average is listed in Appendix A of the thesis.

Theoretical plots of the calculations are compared with the corresponding experimental results performed on powdered  $\text{HgCl}_2$  and  $\text{NaClO}_3$  ( $^{35}\text{Cl}$  resonance) samples. Attainment of a quasi-equilibrium state, viz., a spin-locked state, is demonstrated, both theoretically and experimentally. The dominant mechanism responsible for achieving this quasi-equilibrium state is the coupling of quadrupolar spins to the lattice via the oscillating efg due to the torsional oscillations. Unlike in NMR, the homonuclear dipolar interaction does not play any significant role in spin  $3/2$  NQR. The consequence of the above quasi-equilibrium is the persistence of the signal at times much longer than  $5T_1$ . This finding not only considerably generalizes and adapts the earlier work on spin 1 NQR by Maricq [M.M. Maricq, Phys. Rev. B33, 4501(1986)], but also enhances our understanding of NQR phenomena further.

In Chapter VII, we summarize the present work and the important conclusions drawn therefrom. We also point out the scope for future work in this Chapter.

The experiments carried out in this thesis have value from the standpoint of demonstration of theoretical predictions. In particular, the long-time behavior of the spin  $3/2$  quasi-equilibrium magnetization has been unequivocally demonstrated.

## TABLE OF CONTENTS

	<u>Page</u>
<u>Chapter I : Introduction</u>	1
I.A. A Survey of the Essentials of Pulsed NQR Experiments	1
I.B. Importance of Pulsed NQR of Spin $3/2$ Nuclei	19
I.C. The Usefulness of Multiple-Pulse Experiments	20
I.D. A Review of Multiple-pulse NQR	21
I.E. Motivation for the Present Work	24
I.F. A Preview of the Present Work	29
 <u>Chapter II : The Quantum Mechanical Background</u>	 34
II.A. The Hamiltonian of the System	34
II.B. The Description of the various Terms in Hamiltonian in Principle Axis System (QPAS)	43
II.C. The Cartesian Single Transition Operator (STO) Formalism	48
II.D. The Diagonalized $\mathcal{H}_Q$ Representation of the Hamiltonian Terms	54
II.E. The Quadrupole Interaction Frame (QIF) and Effective Hamiltonian Description the Spin System	61
II.F. The Observables in the NQR Experiment	77

II.G.	The Density Operator and the Observations in an NQR Experiment	81
II.H.	Pulse Sequence Propagators.	87
II.I.	The Equilibrium Density Operator	94
II.J.	The NQR Line Shape	95
II.K.	Summary	100
 <u>Chapter III: One- and Two-Pulse Responses and Application to Zero-Time Resolution (ZTR) Technique</u>		103
III.A.	A Special Property of the Quadrupole Hamiltonian for Spin $3/2$	103
III.B.	One-pulse Response	104
III.C.	Two-pulse Response	112
III.D.	The Zero-Time Resolution Technique Applied to NQR of Non-Axially Symmetric System containing Spin $3/2$ Nuclei	116
III.E.	Summary	129
 <u>Chapter IV: Spin <math>3/2</math> NQR in Powders : Multiple-Pulse Symmetry and Application of Average Hamiltonian Theory (AHT)</u>		130
IV.A.	Some Useful Properties of the Operators $\bar{L}$ , $\bar{M}$ , and $\bar{N}$	131
IV.B.	Cyclic, Periodic and Aperiodic Perturbations and Average Hamiltonian Theory (AHT)	133
IV.C.	Cyclic Multiple-Pulse Sequences for Spin $3/2$ NQR of Powders	145

		xvi
IV.D.	Response of Spin $3/2$ NQR Powders to Cyclic Multiple-Pulse Sequences	150
IV.E.	Experimental Details	157
IV.F.	Summary	161
Chapter V :	<u>NQR and Spin Thermodynamics in Spin <math>3/2</math> Systems Excited Periodically in Time : Use of the Floquet Theorem</u>	162
V.A.	Applications of Floquet Theorem to Periodic Quantum Mechanical Systems.	163
V.B.	Time-Periodic Quantum Mechanical System and the Floquet Theorem.	166
V.C.	Equilibrium Properties from Time Averages in Spin $3/2$ Solids	171
V.D.	The Krylov-Bogoliubov- Mitropolsky (KBMD) Method for Obtaining Average Hamiltonian Comparison with the Magnus Expansion and Floquet Theorem Methods	181
V.E.	Summary	188
Chapter VI :	<u>Pulsed Spin-Locking in the NQR of Spin <math>3/2</math> Solids : Theory and Experiments</u>	189
VI.A.	The Equilibrium Magnetization in the NQR of Spin $3/2$ Solids in the Pulsed Spin-Locking Experiment	189
VI.B.	Computation of Powder Average Response	196
VI.C.	Experimental Details and Results	209
VI.D.	Summary	235
Chapter VIII :	<u>Summary of Findings and Further Prospects</u>	236
REFERENCES		239
APPENDIX A		A1

## LIST OF FIGURES

<u>Figure</u>		<u>Page</u>
I.1:	Schematic experimental set up for pulsed NQR.	2
I.2:	An NQR experiment, viewed as a measurement of the response of a sample consisting of quadrupolar Nuclei ( $\text{Spins} \geq 1$ in units of $\hbar$ ) to a given excitation.	5
I.3:	Simple Energy level diagram for NMR of spin I in a static magnetic field ( $B_0$ ).	14
I.4	Spin 1 NQR ( $\eta = 0$ and $\neq 0$ ) and spin $3/2$ NQR ( $\eta = 0$ and $\neq 0$ ).	16
II.1	Relation between LABPAS y-axis and QPAS ( $x, y, z$ ) of one of the crystallites in the sample.	45
II.2	The matrix representation of the three single transition operators $I_x^{r-s}, I_y^{r-s}, I_z^{r-s}$ .	51
II.3	Schematic design of an NQR receiver that allows observations to be made of signal in QIF.	85
II.4	Schematic diagram showing (a) homogeneous broadening and (b) inhomogeneous broadening.	97
III.1	One-Pulse response.	105
III.2	Two-Pulse or spin echo sequence.	113
III.3	The first stage of the ZTR pulse technique.	118
IV.1	Natural and externally modified evolution of the state of a system.	134
IV.2	Evolution of a system under a cyclic perturbation.	137

IV.3	(a) A periodic perturbation.	
	(b) An aperiodic perturbation.	140
VI.1	Quasistationary magnetization vs various experimental parameters.	201
VI.2	Frequency domain signal of the $^{95}\text{Cl}$ resonance of (a) one pulse FID and (b) response to a spin-locking multiple-pulse sequence.	213
VI.3	The initial portion of the response to spin-locking multiple-pulse sequence of $^{95}\text{Cl}$ .	215
VI.4	Illustration of (a) the predicted evolution under effective Hamiltonian vs (b) the observed time-development of the magnetization for a time-periodic system.	217
VI.5	Time-domain response to OW or MW multiple-pulse sequence of the $^{95}\text{Cl}$ signal in $\text{NaClO}_3$ and $\text{HgCl}_2$	220

## LIST OF TABLES

Table

IV.1.	Transformations of $\bar{L}$ during PAPS	153
IV.2.	Transformations of $\bar{L}$ during WAHUA	155



## CHAPTER I

### INTRODUCTION

The subject matter of this dissertation is a study of the dynamics and equilibrium properties of a spin  $3/2$  pure nuclear quadrupole resonance (NQR) subjected to a scheme of radio-frequency (rf) radiation pulse perturbations. In magnetic resonance literature, the various schemes of rf radiation pulses are known collectively as multiple-pulse sequences.

#### I.A. A Survey of the Essentials of Pulsed NQR<sup>\*</sup> Experiments

In most pulsed NQR experiments, a multiple-pulse sequence is applied to a sample containing quadrupolar nuclei (spin  $\geq 1$  in units of  $\hbar$ ) initially at equilibrium in the inhomogeneous electric field created by the surrounding electronic charge cloud. The typical experimental arrangement is shown schematically in Figure I.1. The rf pulses excite the nuclear spins to a non-equilibrium state, from which much weaker rf signals are emitted and recorded. That state may be specified in detail by

---

<sup>\*</sup>From here onwards, NQR will mean pure NQR, i.e. NQR with no Zeeman field, unless specified otherwise.

Figure I.1: Schematic experimental set up for pulsed NQR. A sample is placed in the coil of a tuned rf circuit. The inhomogeneous electric field of the surrounding electronic charge cloud interacts with the quadrupolar nuclei to give rise to quantized energy levels. The nuclei in the sample distribute themselves among these energy levels according to the Maxwell-Boltzmann distribution law. rf pulses create an oscillating field  $B_1$  along the x-axis. Oscillating rf signals, emitted by the sample in the x-axis direction, are detected. The Cartesian coordinate system shown defines the laboratory frame.

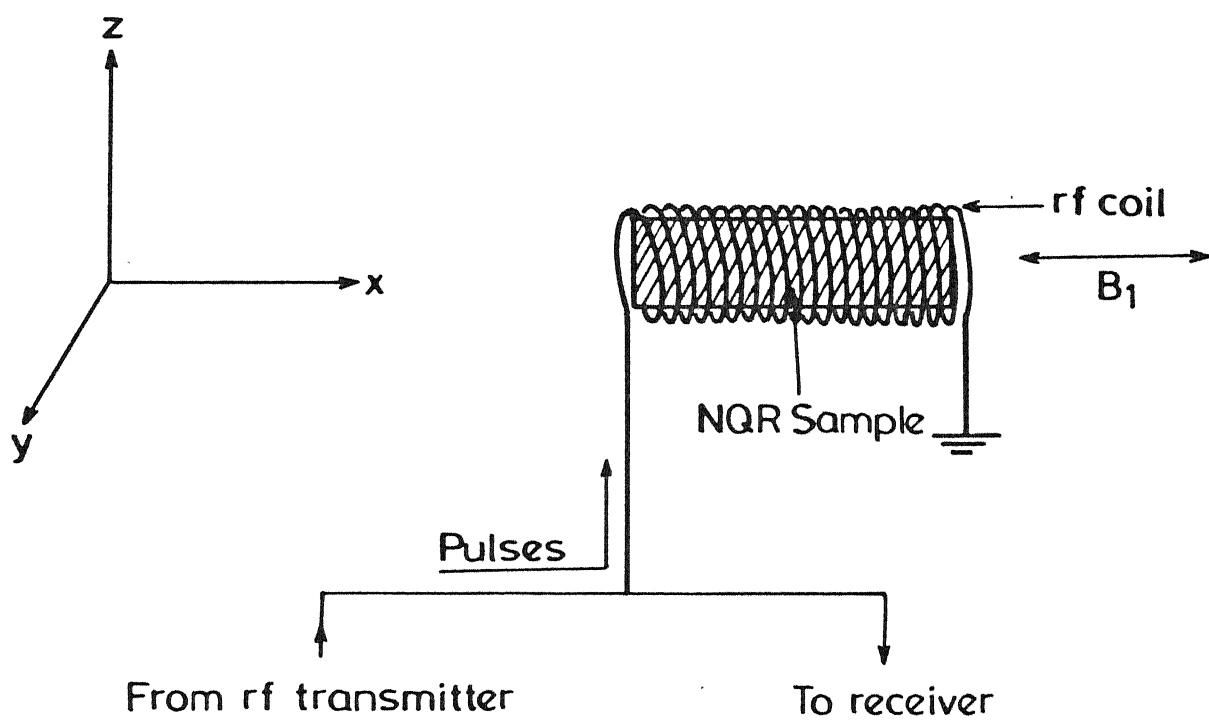


Figure I.1

a density operator. However, there is often one property of this perturbed spin state that is of particular interest. This property may then be considered to be the response of the spin system to the sequence of the applied rf pulses. Figure I.2 gives a schematic representation of the excitation process.

The rf pulses used to excite the sample are, most commonly, well approximated by rectangular shapes. The height of these rectangles represents the amplitude of the rf field. A multiple-pulse consisting of  $n$  pulses is schematically written as:

$$(\theta_1) \phi_1 - \tau_1 - (\theta_2) \phi_2 - \tau_2 - (\theta_3) \phi_3 - \tau_3 - \dots - (\theta_n) \phi_n - \tau_n$$

where  $\theta_i$  and  $\phi_i$  are the flip angle and phase of the  $i$ th pulse, respectively.  $\tau_i$  is the time that elapses between the  $i$ th and  $(i+1)$ th pulses. The flip angle is proportional to the duration of the rf pulse, and the name is reminiscent of the fact that, in the classical vector model of spin  $1/2$  nuclear magnetic resonance (NMR), it represents the angle by which the spin vector is rotated by application of the rf pulse for a certain duration [1-4]\*. Ideally, a certain pulse in the sequence is considered to be an impulse or Dirac's  $\delta$ -function.

---

\*All the references appear at the end of the last Chapter.

**Figure I.2:** An NQR experiment, viewed as a measurement of the response of a sample consisting of quadrupolar nuclei (spins  $\geq 1$  in units of  $\hbar$ ) to a given excitation. The excitation is typically a sequence of rf pulses with well-defined lengths and phases, possibly separated by delays.

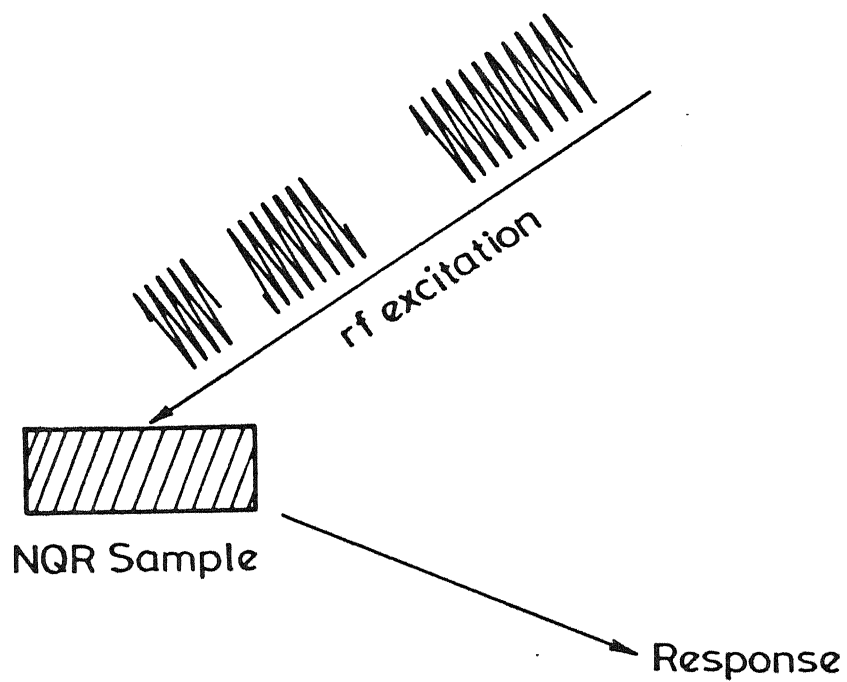


Figure I.2

The response is determined by the set of parameters involved in the experiment. Indeed, the response is modified not only by the parameters that can be manipulated externally, but also by the ones that are intrinsic to the system that is studied. When the rf amplitude is kept constant, the external parameters that are involved in a multiple-pulse experiment are the individual pulse lengths, rf-phases, interpulse time-durations and the resonance offset, a quantity defined as the difference between the radiofrequency and the resonance frequency of the spin. The parameters intrinsic to the NQR sample under study can all be put in two classes - (i) the strengths of spin-couplings and (ii) the distribution in the electric field gradient (efg) due to impurities, lattice defects and torsional motion of the units constituting the lattice. Some of the spin-coupling terms give rise to fine-structure in the response signal, thus making it rich in information content, while others make it structureless and hence less informative. This masking of information content of the response is known in magnetic resonance literature as line-broadening. Here it is worthwhile pointing out that, by manipulating the external parameters available to the experimenter, it is possible to enhance the information content of the response. These experiments in magnetic resonance are known collectively as selective-averaging or line-narrowing techniques. Later on, we shall deal with the mechanisms of line-broadening in NQR in general terms and also the techniques of

selective-averaging in detail. The distribution in efg invariably gives rise to broadening of NQR lines.

The focus of our attention in this thesis is the NQR of spin  $3/2$  systems. A central theme that has guided our study is the behavior of the response of the system right from zero-time to times of the order of  $\sim 8T_1$ , where  $T_1$  is the spin-(quadrupole) lattice relaxation time of the sample under study. The establishment of quasi-equilibrium state under varying conditions of the external parameters has been studied theoretically. Furthermore, wherever possible, appropriate experiments have been performed on model quadrupolar spin  $3/2$  solids to seek support for our theoretical findings. Very interestingly, it turns out that the mechanism of this quasi-equilibrium state leads to a characteristic prolongation of the quadrupolar relaxation time ( $T_1$ ), similar to previous findings on the prolongation of the spin-spin relaxation time ( $T_2$ ) in the case of pure dipolar solids. In addition to the above mentioned focal theme, our studies have enabled us to adapt several multiple-pulse cycles which have been in use for studies of dipolar solids; the effects of these cycles on the various major interactions in quadrupolar solids are studied theoretically.

Before we go into a discussion of the importance and usefulness of the present work, it may be worthwhile to point out the salient features of NQR vis-à-vis NMR in general, and how the spin  $1/2$  NMR, spin 1 NQR and spin  $3/2$  NQR compare with each other in particular. For the ensuing discussion, we have heavily drawn



upon the relevant material from standard monographs [1-4] and research papers [5-7].

The quantized energy levels in NMR have their origin in the magnetism which the nuclear spins possess inasmuch as they are created by the interaction of the nuclear magnetic moments with the applied static magnetic field. On the other hand, the NQR energy levels owe their origin to the electrostatic interaction of the electric quadrupole moment (which is due to the non-spherical charge distribution in the nucleus) with the efg due to the surrounding electronic charge cloud. This is a tensorial interaction [5-7].

The principal axis system of the efg tensor is chosen such that its diagonal components,  $V_{xx}$ ,  $V_{yy}$  and  $V_{zz}$  satisfy the condition [8],

$$|V_{zz}| \geq |V_{yy}| \geq |V_{xx}| \quad (I.1)$$

Here  $V$  is the electrostatic potential at the nucleus due to the surrounding electronic charges and  $V_{ij} = \frac{\partial^2 V}{\partial i \partial j}$ ;  $i, j = x, y, z$ .

It is assumed that the electric field at the site of the nucleus is produced entirely by charges external to it, in which case the Laplace equation,  $V_{xx} + V_{yy} + V_{zz} = 0$ , is satisfied. A measure of the deviation of the efg from cylindrical symmetry is given by a parameter  $\eta$ . In the NQR literature,  $\eta$  is known as the asymmetry parameter and is defined as

$$\eta = \left| \frac{V_{xx} - V_{yy}}{V_{zz}} \right| \quad (1.2)$$

The two constraints, Eqn I.1 and the Laplace equation, lead to the result that the value of  $\eta$  can vary between 0 and 1 only.  $\eta$  is zero for the axial symmetry of the efg tensor around z-axis of the principal axis system. In most chemical systems, the principal axis system is fixed in the molecule or crystal lattice which contains the quadrupolar nucleus or nuclei and is known in NQR literature as the quadrupole principal axis system (QPAS).

The non-spherical charge distribution is possible only in nuclei with spin  $\geq 1$ . We therefore have NQR of spin  $\geq 1$  only. This is unlike NMR where spin  $1/2$  is the most studied case.

In NMR the external static magnetic field defines the quantization axis for all the nuclei constituting the system. The situation is quite different in NQR. The quantization axis in this case is intrinsic to the system and an experimenter has no control over it. It is defined by the main component of the efg tensor, namely,  $V_{zz}$  in the QPAS. When we have a powder sample, which happens to be the case most commonly in NQR, each crystallite constituting the powder will have its own quantization axis and an external rf field perturbation will not have the same effect on nuclei in different crystallites. This one point makes the theoretical treatment of an NQR problem quite different from that of NMR.

Once the energy levels are created, the external rf field perturbation in a plane perpendicular to the quantization axis induces resonant transitions among them. In both NMR and NQR these transitions are magnetic dipole induced transitions, and hence the selection rule in both the cases is in general,  $\Delta m = \pm 1$ , where  $m$  is the magnetic quantum number for spin  $I$  and has values ranging from  $-I$  through  $+I$  in steps of unity. Seen from this point of view the term Nuclear Quadrupole Resonance is a misnomer [3]. It is interesting to mention here that, recently, using a dc superconducting quantum interference device (SQUID) detector Hahn et al [10-12] have been able to observe the effect of electric quadrupole induced transitions in spin  $3/2$  nuclear assembly - a phenomenon that is due to nuclear quadrupole resonance in the literal sense of the phrase.

The NMR energy levels for any spin  $I$  are determined by

$$E_m = m\gamma B_0, \quad (I.3)$$

where  $\gamma$  is the magnetogyric ratio and  $B_0$  the strength of the static magnetic field applied externally. The number of energy levels are, therefore,  $2I + 1$  and they are all non-degenerate. It is also clear from Eqn I.3 that the energy difference between any two adjacent levels is determined only by  $\gamma$  and  $B_0$ . Therefore, the levels are equidistant. In the particular case of spin  $1/2$  NMR, there are just two energy levels.

In the most simple case ( $\eta = 0$ ), the NQR energy levels for any spin  $I \geq 1$  are given by

$$E_m = A [3m^2 - I(I + 1)] \quad , \quad (I.4)$$

where,  $A = e^2 q Q / 4I(2I-1)$ ,  $Q$  is the quadrupole moment of the nucleus,  $eq$  is the magnitude of  $V_{zz}$  and  $e$  is the electronic charge.  $e^2 q Q$  is known as the quadrupole coupling constant (QCC). The above expression holds both for half-integral and integral spins. Here the energy levels are doubly degenerate in  $m$ , because the two states  $|+m\rangle$  and  $|-m\rangle$  have the same energy as is evident from Eqn I.4. Also, the energy difference between the adjacent pairs of levels will not be the same for various pairs of  $m$  values. Therefore, NQR energy levels are non-equidistant. For half-integral spins there are  $I+1/2$  non-equidistant energy levels all doubly degenerate, while for integral spins there are  $I+1$  non-equidistant energy levels where  $I$  of them are doubly degenerate and only one of them with  $m = 0$  is non-degenerate. It may be mentioned here that, for integral spins, when  $\eta \neq 0$ , the degeneracy is lifted completely, whereas for half-integral spins it is not. This follows from a special case of a general theorem due to Kramers [13]. Figures I.3 and I.4 illustrate the points we have discussed above.

In the general case, therefore, the spin 1 NQR system will have a non-degenerate three energy level pattern, labelled by the states  $|+1\rangle$ ,  $|0\rangle$  and  $|-1\rangle$ . Accordingly, a rf field applied in any arbitrary direction gives rise to three transitions, namely,  $|+1\rangle \leftrightarrow |0\rangle$ ,  $|0\rangle \leftrightarrow |-1\rangle$  and  $|+1\rangle \leftrightarrow |-1\rangle$ . The first two form a doublet with frequencies (in  $\text{rad sec}^{-1}$ )

$$\omega_{\pm} = \frac{3e^2 qQ}{4h} (1 \pm \eta/3) \quad (I.5)$$

The third transition ( $|+1\rangle \leftrightarrow |-1\rangle$ ) gives rise to a line at a very low frequency and is not of much interest. The intensities of the two members of the doublet are proportional to  $|\langle +1 | \mathcal{H}_{rf} | 0 \rangle|^2$  and  $|\langle -1 | \mathcal{H}_{rf} | 0 \rangle|^2$ , respectively. Here  $\mathcal{H}_{rf}$  is the Hamiltonian representing the radiofrequency field perturbation. The higher frequency line has a maximum intensity when the rf field lies in the x-direction of the QPAS, and the lower frequency line then has zero intensity. The opposite is true with the rf field in the y-direction of the QPAS. In other words, the spin 1 NQR resonant transitions are polarized (Figure I.4(a)).

The situation in spin 3/2 NQR is quite different. Although the presence of  $\eta$  leads to mixing of states  $|m\rangle$  differing by  $\Delta m = \pm 2$ , the energy eigenvalues are still doubly degenerate and are given as

$$E_{\pm 3/2} = 3A (1 + \eta^2/3)^{1/2} \quad ; \quad (I.6a)$$

$$E_{\pm 1/2} = -3A (1 + \eta^2/3)^{1/2} \quad . \quad (I.6b)$$

If an rf field is now applied, it is generally possible for four transitions to occur between eigenstates  $|m\rangle$  and  $|m'\rangle$  because of mixing of  $m$  states. The frequency for all the four transitions,

Figure I.3: (a) and (b): Simple energy level diagram for NMR of spin  $I$  in a static magnetic field ( $B_0$ ). (a) is for half-integral spin and (b) is for integral spin. All the adjacent levels are equidistant, as seen.

(c) and (d): Simple energy level diagram for NQR of spin  $I$  in a cylindrically symmetric electric field gradient (efg). (c) is for half-integral spin and (d) is for integral spin. The quantization axis in this case is defined by  $V_{zz}$  component of the efg in quadrupole principal axis system (QPAS). All the adjacent levels are not at equal difference in these cases as seen. Therefore, in these cases we have a degenerate (except  $m = 0$ ) and non-equidistant energy levels. Energy differences in all the diagrams are in arbitrary units.

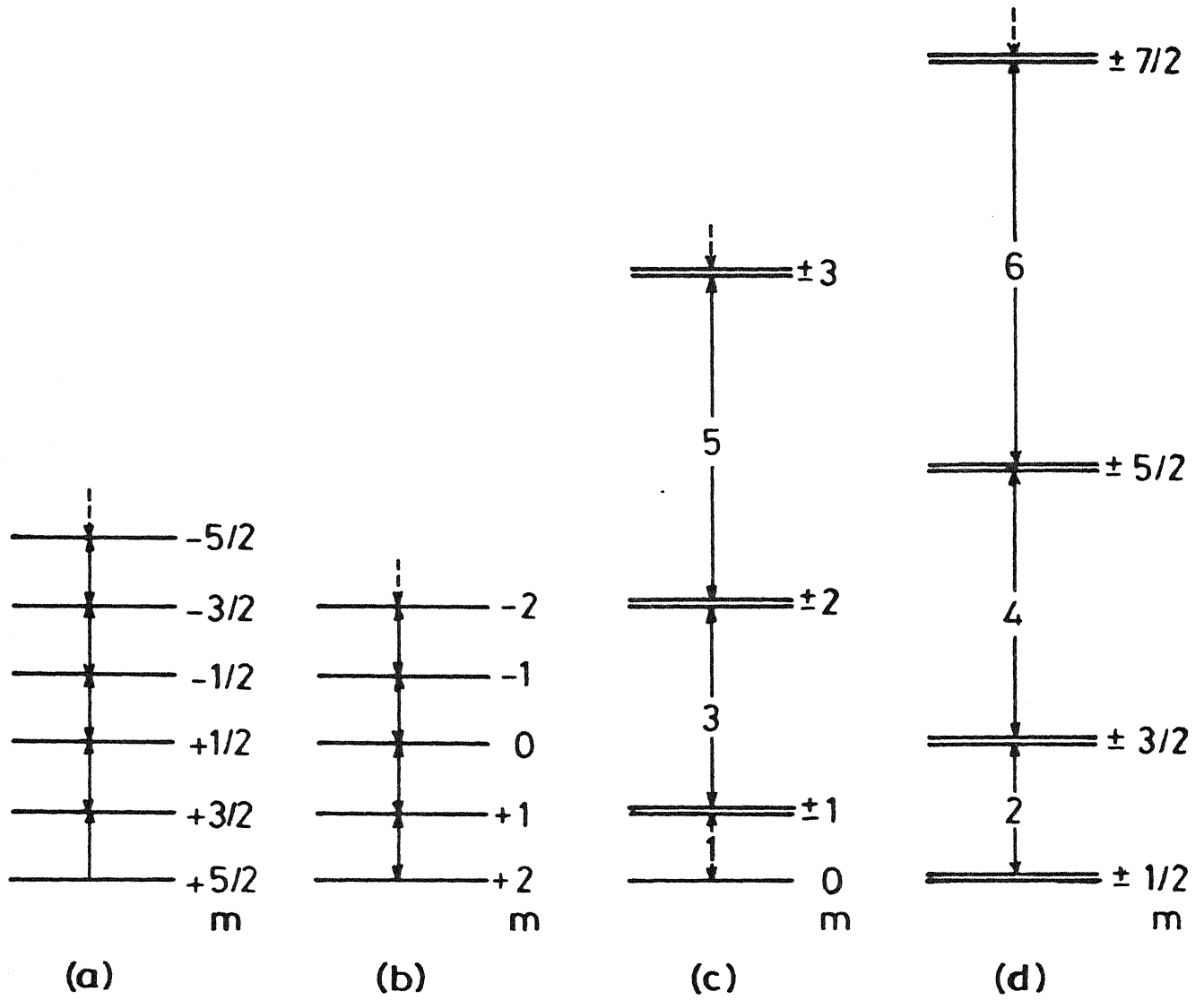


Figure I-3

**Figure I.4:** (a) Spin 1 NQR. For  $\eta = 0$ , we have a single resonant transition. For  $\eta \neq 0$ , there are three resonant transitions possible, as explained in the text. These transitions are linearly polarized.

(b) Spin  $3/2$  NQR. For both  $\eta = 0$  and  $\eta \neq 0$  only a single resonant transition is possible as shown. This transition involves all the energy levels and is not linearly polarized.



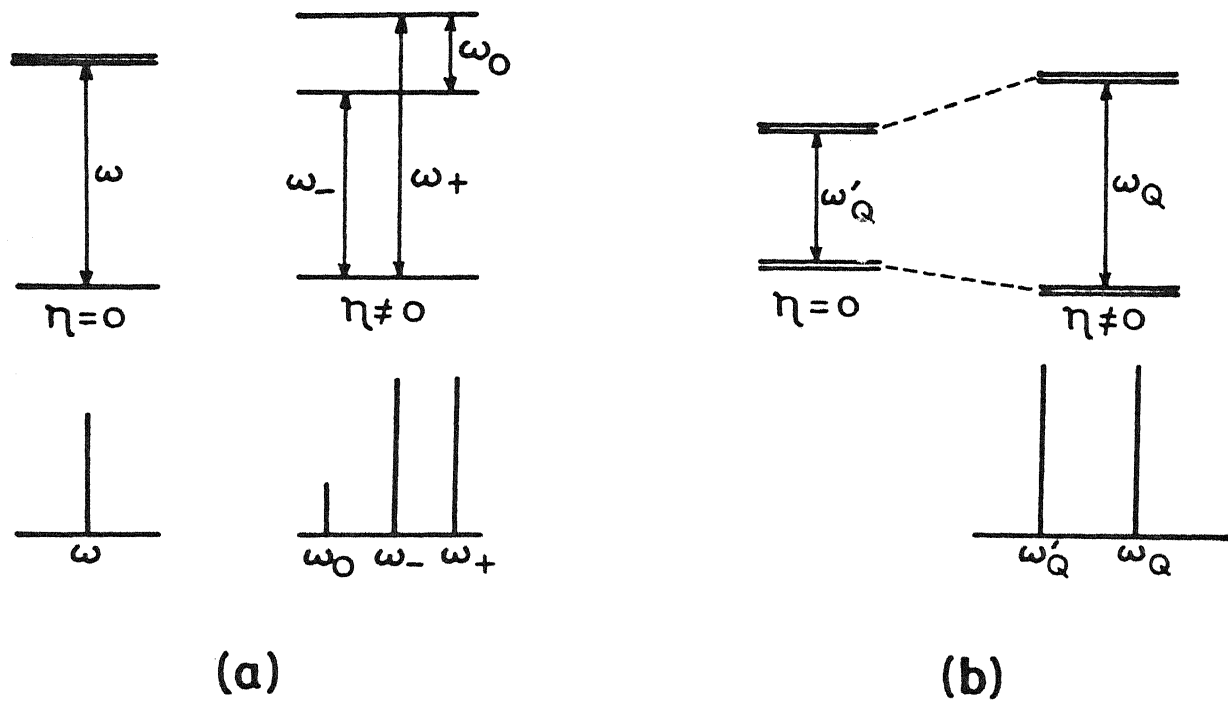


Figure I-4

namely,  $|+1/2\rangle \leftrightarrow |+3/2\rangle$ ,  $|+1/2\rangle \leftrightarrow |-3/2\rangle$ ,  $|-1/2\rangle \leftrightarrow |+3/2\rangle$  and  $|-1/2\rangle \leftrightarrow |-3/2\rangle$ , is given by (Figure I.4(b)).

$$\omega_a = \frac{6A}{h} (1 + \eta^2/3)^{1/2} \quad (I.7)$$

The transitions other than those corresponding to  $\Delta m = \pm 1$  are forbidden for axial symmetry and are expected to be weak except for large values of  $\eta$ . The transition frequencies in Eqn I.7 do not depend on the direction in the x-y plane in which the rf field is applied. Unlike spin 1 NQR, therefore, the transitions are unpolarized in this case.

We take the example of a sample of polycrystalline spin 1 NQR system. In a typical NQR experiment, it will be irradiated with an rf field of frequency that matches with one of the resonant frequencies of the spin. Let us also assume that the frequency of irradiation, in this example, corresponds to  $\omega_+$  as given in Eqn I.5 and Figure I.4(a). If the rf field is applied such that the oscillating magnetic field ( $B_1$ ) is in the direction of x-axis of laboratory frame, the system under consideration can closely, if not exactly, be made to resemble spin 1/2 NMR. This is because, of all the crystallites in the polycrystalline sample, only those that have their QPAS coinciding with the laboratory frame will favor their constituent nuclei to undergo resonant transitions. Only crystallites having this orientation in the powder are, therefore, excited. Also the rf field will connect only one pair

of energy levels out of three, namely, the one that has energy difference proportional to the angular frequency  $\omega_+$ . Under this circumstance, the spin 1 NQR system is well approximated by assuming it to be a two-level quantum system. The two energy levels of this system are the ones that are connected by resonant rf field irradiation. This also follows from the fictitious spin  $1/2$  formulation of the problem [14]. According to this formulation, in a multi-level quantum system, when we connect only two of the levels by an external resonant perturbation, we can model the system as a two-level system to an excellent approximation, disregarding non-resonant levels completely.

This however, cannot be the case in spin  $3/2$  NQR, where a single frequency radiation will connect all the four levels.

### I.B. Importance of Pulsed NQR of Spin $3/2$ Nuclei

Each of the quantum systems described above is representative of a class. An independent study of dynamics and equilibrium properties of each one of them, namely, spin  $1/2$  NMR, spin 1 NQR and spin  $3/2$  NQR under a scheme of rf perturbation pulses deserves merit in its own right. As pointed out earlier, spin  $1/2$  NMR is the most widely studied case [15-19]. While there also exist a few reports of the multiple-pulse studies in spin 1 NQR [20-33], there is a need to study multiple-pulse spin  $3/2$  NQR in more detail both theoretically and experimentally. The few studies that have been carried out in spin  $3/2$  systems will be described in section I.E.

From the point of view of applications of NQR, the spin  $3/2$  NQR has an additional importance. Only three nuclei out of eighty-seven naturally occurring NQR-active isotopes have spin 1. In contrast, spin  $3/2$  nuclei are thirty-two in number. A theoretical and experimental investigation of the kind presented here, therefore, may extend the benefits of a vital domain of techniques to a large variety of NQR systems.

### I.C. The Usefulness of Multiple-Pulse Experiments

The multiple-pulse experiments are very useful for measuring transient properties of spin systems both in NMR and NQR. In particular, they are extensively used for the measurement of relaxation times [34-38], for the study of diffusion processes [39] and for the investigation of chemical reactions [40-42]. Multiple-pulse experiments in solids, carried out on time scales of the order of  $T_2$ , show how the various factors contributing to the width of the resonance line respond to strong rf field perturbations. Also, these experiments reveal pulse sequence characteristics that lead to the narrowing of resonance line widths, thus yielding valuable information on the interactions leading to fine structure of the resonance lines [15-19]. Some of the multiple-pulse sequences, such as spin-locking sequences (SLS) of which the Ostroff-Waugh (OW) [43] or Mansfield-Ware (MW) [44] are examples, improve substantially the effective sensitivity of the NMR and the NQR signals if the individual echoes within each

spin-locked-spin-echo (SLSE) sequence [20,43-46] are coherently added. This sensitivity improvement accrues even without our taking recourse to the complicated double resonance schemes [47-50]. So versatile are the multiple-pulse experiments that they can be used nowadays for solid state NMR [15-19], high resolution NMR in liquids [51-54] and for NQR [55]. Indeed, such techniques, often called **spin-gymnastics**, have substantially extended the scope of magnetic resonance.

#### I.D. A Review of Multiple-Pulse NQR

The OW [43] or the MW [44] sequence, which we shall henceforth call as spin-locking sequence, is in general :

$$(\pi/2)_{\phi} - \tau - (\theta)_{\phi+\pi/2} - 2\tau - (\theta)_{\phi+\pi/2} - 2\tau - (\theta)_{\phi+\pi/2} \dots$$

It represents one of the first uses of pulsed rf fields for studying a powder system of spin 1 ( $^{14}\text{N}$  in polycrystalline  $\text{NaNO}_2$  at 77 K) NQR [20]. This sequence also represents one of the first uses of pulsed rf fields for selectively suppressing internal spin-interactions that cause homogeneous line-broadening of the resonance lines, thereby increasing the resolution of NMR lines in solids [43,44]. This particular sequence causes a refocusing of the transverse magnetization for periods much longer than  $T_2$ . In some respects, the effect is similar to the more familiar spin-locking by a constant amplitude continuous wave (CW) rf field

[56]. In the case of NQR also, the effects are very similar to those observed in the NMR experiment, namely, the persistence of the magnetization for long times compared with  $T_2$ . Initially, this was not conceptually reconcilable in light of differences between the origin of the interactions that give rise to the phenomena of NMR and of NQR in nuclear assemblies. The average Hamiltonian theory (AHT) within the framework of Magnus expansion [15-19,57,58] has been found to be a powerful theoretical tool to deal with analogous situations in spin  $1/2$  NMR. However, the AHT technique was thought to become intractable in spin 1 NQR case [21,22]. This is because the overall time-dependent Hamiltonian in the appropriate interaction representation in an NQR system is, in general, not cyclic in the sense of the system returning to its original state after the pulse sequence has been completed (see Chapter IV). This situation arises in a powder sample, as pointed out earlier, because the rf field has random orientations with respect to the individual QPAS of the crystallites constituting the powder. An explicit time evolution calculation [21,22] on a model system of dipolar coupled spin 1 nuclei, however, confirmed the refocusing of the spin magnetization in the multiple-pulse NQR experiment of  $^{14}\text{N}$  nuclei in  $\text{NaNO}_2$  powder sample, in the short-time regime ( $\sim T_2$ ). Later on, Maricq [33] gave a detailed theoretical analysis based on the generalized AHT within the framework of Floquet theorem [59-64]. Although the spin-locking sequence does not remain cyclic independent of the orientation of the rf field, Maricq has shown that the average

Hamiltonian approach can still be taken if one considers a single-crystal sample. In fact, this also has the advantage of revealing effects which are obscured in powdered samples. The result of single-crystal calculation can then be subjected to a powder-averaging procedure, taking into account the proper weightages for various orientations of the crystallites in the powder. Maricq also took into account the many-body nature of the interactions in the real system ( $\text{NaNO}_2$ ) in his theoretical analysis and successfully accounted for both the short ( $\sim T_2$ ) and long-time ( $\sim T_{1\rho}$ ) behavior of the overall magnetization. Incidentally, we mention here that earlier, generalized AHT was used by Maricq to settle the issue of the validity of the AHT for theoretical analysis of the multiple-pulse experiments in general [64]; furthermore, generalized AHT has also been used for the theoretical analysis of spin  $1/2$  NMR multiple-pulse experiments, namely, OW or MW and WAUGH-HUBER-HAEBERLEN (WAHUHA) [64-66].

In multiple-pulse experiments we confront not only a many-body system, but one which is driven by time-dependent external forces. Because the Hamiltonian corresponding to such a system is energy non-conservative, one cannot apply the normal methods of statistical thermodynamics to determine the equilibrium properties of the system. Maricq [65] showed how the Floquet solution for the time-dependent Schrödinger equation can be used to extend statistical thermodynamical ideas to systems evolving under a periodic time-dependent Hamiltonian. This was used by him to analyse theoretically the equilibrium properties of the overall

magnetization in spin  $1/2$  NMR [65] and spin 1 NQR [33] driven by a scheme of rf field perturbation sequences. Provotorov and co-workers [24,26,29] have also given a parallel theoretical analysis of the response of spin-locking sequence in a spin 1 NQR. Certain pulse sequences such as phase-alternated pulse sequence (PAPS) [67,68] and WAHUA remain cyclic irrespective of the orientation of the radiofrequency field in the QPAS of each crystallite in a powder. Osokin [23,25,27,30-32] has taken advantage of this special property of these multiple-pulse sequences, and has used the AHT within the framework of Magnus expansion to discuss the effects of these pulse sequences in spin 1 NQR experiments of  $^{14}\text{N}$  in  $\text{NaNO}_2$  polycrystalline sample.

### I.E. Motivation for the Present Work

All of the foregoing discussion has been about an NQR system of an assembly of spin 1 nuclei, where the multiple-pulse experiments have been carried out on one of the three possible resonances. Subsequent to the above work, there have been reports of experiments, from our laboratory [69-71] as well as elsewhere [72], on spins  $3/2$ ,  $5/2$  and  $7/2$ . The pulse sequences employed by these authors can be broadly classified into four categories:

(i)  $(\pi/2)_{\phi_1} - \{\tau - (\theta)_{\phi_1 + \pi/2} - \tau\}_n$  - the spin-locking sequence,

(ii)  $(\pi/2)_{\phi} - \{\tau - (\theta)_{-\phi} - 2\tau - (\theta)_{\phi} - \tau\}_n$  - the PAPS,



$$(iii) (\pi/2)_{\phi} \{-\tau-(\theta)_{\phi} -\tau-(\theta)_{\phi+\pi/2} -2\tau-(\theta)_{\phi+\pi/2} -(\phi+\pi/2)$$

$$-\tau-(\theta)_{\phi} -\tau\}_{\pi} - \text{the WAHUA ,}$$

$$\& (iv) (\pi/2)_{\phi} \{-\tau-(\theta)_{\phi} -\tau-(\theta)_{\phi+\pi/2} -2\tau-(\theta)_{\phi+\pi/2} -\tau-(\theta)_{\phi} -2\tau-(\theta)_{\phi}$$

$$-\tau-(\theta)_{\phi+\pi/2} -2\tau-(\theta)_{\phi+\pi/2} -\tau-(\theta)_{\phi} -\tau\}_{\pi} - \text{the Mansfield-Rhim-}$$

Elleman-Vaughan (MREV-8) [73-77],

where  $\phi = 0$  when rf pulses are applied in the x-direction of the laboratory frame. In the above, we have intentionally kept the phases  $\langle \phi \rangle$  of the pulses arbitrary. Unlike spin  $1/2$  NMR, as will be shown in Chapter II, in NQR  $\phi$  loses its usual meaning of representing directions in the rotating frame. Ainsbinder et al [72] have examined the spin-locking effect under the influence of Carr-Purcell-Meiboom-Gill (CPMG) sequence [78] both theoretically and experimentally in spin  $3/2$  NQR ( $^{85}\text{Cl}$  in polycrystalline samples of  $\text{SbCl}_3$ ,  $\text{C}_2\text{Cl}_6$  and  $\text{CCl}_3\text{COOH}$  at 77 K) and also in spin  $7/2$  NQR ( $^{123}\text{Sb}$  in polycrystalline  $\text{SbCl}_3$  sample at 77 K). Narsimha Reddy [69,70] has performed experiments using the pulse sequences of the categories (i) and (ii) listed above, with varying values of the pulse parameters  $\theta$ ,  $\phi$ ,  $\tau$  and offset from resonance conditions. His most important observation was that in the powdered sample of a spin  $3/2$  NQR system ( $^{85}\text{Cl}$  in  $\text{NaClO}_3$  and

KClO<sub>3</sub> polycrystalline sample at room temperature), spin-locking effect is observed for any value of  $\phi$ , the phase of the pulses in the sequence with respect to that of the preparatory first pulse. His experiments included well-known sequences such as OW or MW, PAPS, Carr-Purcell (CP) [35] and CPMG. Ravinder Reddy [71] reported experiments both on spin 3/2 and spin 5/2 NQR systems. His multiple-pulse sequences were from the first three categories listed above. His spin 3/2 experiments were on <sup>35</sup>Cl in the samples of NaClO<sub>3</sub>, KClO<sub>3</sub> and SbCl<sub>3</sub>. While experiments on NaClO<sub>3</sub> were done both on a single crystal and a powder, only powder samples were used in case of KClO<sub>3</sub> and SbCl<sub>3</sub>. For spin 5/2 experiments, a powder sample of KReO<sub>4</sub> was used and the nuclei studied were <sup>185</sup>Re and <sup>187</sup>Re. In all the spin-locking experiments, there is strong evidence for establishment of a quasi-equilibrium state for the overall magnetization under the spin-locked state. It means that the transverse magnetization, under multiple-pulse sequences of the type mentioned above, remains in the x-y plane of the laboratory frame for times much longer than the characteristic relaxation time of the system. The experiments in [71] using WAHUA also show lengthening of the characteristic relaxation rate constant. The theoretical analysis of these experiments as well as of MREV-8 [71] is a preliminary one and needs further investigation.

The other kind of multiple-pulse sequence that has been used to narrow the NQR lines is Lee-Goldburg (LG) [79] sequence. The possibility of application of this sequence has been discussed by

Pratt et al [80,81]. Mefed and Pavlov [82] used this sequence on  $^{127}\text{I}$  in a  $\text{CdI}_2$  single crystal ( $I = 5/2$ ). Their experiment was performed on the resonance line corresponding to the transition  $| \pm 1/2 \rangle \leftrightarrow | \pm 3/2 \rangle$  in  $^{127}\text{I}$  nuclei. They observed line-narrowing of the NQR line in a rotating reference frame that rotates with one of the components of the oscillating rf field. The free induction decay (FID) in this case was found to be  $\sim 25$  times slower than that in the laboratory frame. In his theoretical analysis, Pratt [81] considered dipolar couplings and distribution of electric field gradients due to static imperfections in the crystal lattice, to be the line-broadening interactions. His conclusion was that a multiple-pulse technique for partial suppression of the dipolar couplings followed by a spin-echo method for eliminating the inhomogeneous broadening would lead to enhanced sensitivity and resolution in NQR.

An alternative theoretical method of analysis of the response of LG sequence in spin  $3/2$  nuclear assembly has been used by Zueva [83]. In this procedure, the Hamiltonian is transformed to a generalized interaction frame, where a second moment calculation of the NQR line shape in the presence of the LG sequence is carried out. The second moment is shown to be smaller in magnitude when the LG sequence is used. The line-broadening interactions considered in this calculation are also the dipolar couplings and the distribution in efg.

Zueva and Kessel [84-86] have also reported a theoretical analysis of the response of a multiple-pulse sequence from an NQR

system of any half-integral nuclear spin assembly. In this analysis, the axially symmetric systems ( $\eta=0$ ) were considered. The theoretical analysis used was the same as has been described above for spin  $3/2$  systems, namely, the second moment calculations in generalized interaction representation for the line shape, in the presence of line-broadening interactions. These authors have also considered the following multiple-pulse sequences:

$$(i) \quad (\pi/2)_{\pi/2} - \{\tau - (\theta)_0 - 2\tau - (\theta)_0 - 2\tau - (\theta)_0 - 2\tau - (\theta)_0 - \tau\}_n,$$

$$\& (ii) \quad (\pi/2)_{\pi/2} - \{\tau - (\theta)_0 - 2\alpha\tau - (\theta)_0 - 2\tau - (\theta)_0 - 2\alpha\tau - (\theta)_0 - 2\tau - (\theta)_{\pi/2}$$

$$- 2\alpha\tau - (\theta)_{\pi/2} - 2\tau - (\theta)_{\pi/2} - 2\alpha\tau - (\theta)_{\pi/2} - \tau\}_n$$

( $\alpha =$  a positive integer).

They have been able to show that these pulse sequences are also very effective in line-narrowing of NQR lines in half-integral nuclear spin systems. We may also mention here that Ainsbinder and Furman [87] have given an independent theoretical framework based on Krylov-Bogoliubov-Mitropolsky (KBM) [18,88,89] averaging procedure and the canonical transformation technique to analyse multiple-pulse experiments for a general spin  $I$  with non-equidistant spectra. This theory offers an average Hamiltonian which is similar to the ones based on Magnus expansion [15-19,57,58] and on Floquet theory [64] in the lowest order

approximation. For higher order approximations, the differences start appearing. This theory, however, remains largely unexploited till date in magnetic resonance.

More recently, there have been reports on both experimental and theoretical studies of the kind where a modified Jeener-Broekaert (JB) sequence [90] has been used to transfer quadrupolar order into dipolar order in spin  $3/2$  pure NQR with line-broadening due to heteronuclear dipolar interaction [91] of  $^{35}\text{Cl}$ - $^{23}\text{Na}$  in  $\text{NaClO}_3$  and due to efg inhomogeneity [92] in  $\text{K}_2\text{OsCl}_6$ . In both the cases the nucleus studied was  $^{35}\text{Cl}$ . Theoretically, the introduction of the concept of spin temperature, corresponding to the Hamiltonians for internal interactions, has been very useful in predicting the correct experimental behavior of the overall magnetization. Also, the zero-time resolution (ZTR) [93] technique has been applied recently to recover the FID completely in an NQR experiment of spin  $3/2$  nuclei ( $^{35}\text{Cl}$  in  $\text{K}_2\text{OsCl}_6$ ) in axially symmetric case [94].

### I.F. A Preview of the Present Work

This study starts with the choice of a suitable operator formalism to describe the dynamics of the evolution of spin  $3/2$  nuclear assembly subjected to an rf field perturbation. The generators of the  $\text{SU}(4)$  Lie algebra [95,96], known in magnetic resonance as single transition operators [97] or fictitious spin  $1/2$  operators [98], provide a suitable choice. After introducing

all the Hamiltonians needed in the usual Cartesian basis of angular momentum operators, we present, in Chapter II, these Hamiltonians in terms of the single transition operators (STO) in a basis where the quadrupole Hamiltonian is diagonal. This is done for the mathematical convenience of the calculations in later Chapters. We also introduce in this Chapter the quadrupole interaction frame (QIF); the high-frequency approximation for first order perturbation theory calculations; the observables of NQR experiments, namely, the magnetization operators for spin  $3/2$ ; the density operator; the high temperature approximation for the equilibrium density operator; the Liouville-von Neumann equation; and the pulse propagator. In brief, this Chapter provides the quantum mechanical background for the work presented in later Chapters. Also we describe in this Chapter the roles of the internal Hamiltonians in modifying NQR line shapes.

In Chapter III are illustrated the single pulse response and spin echo calculations for spin  $3/2$  NQR in a system of non-interacting nuclei. The purpose is to demonstrate, perhaps for the first time, the effectiveness of the STO formalism in typical spin  $3/2$  NQR calculations. We also demonstrate in this Chapter the applicability of STO formalism to analyse theoretically the zero-time resolution technique for the recovery of FID completely in a spin  $3/2$  NQR system with non-axially symmetric efg. This is an extension of the recent work of Singh and Armstrong [94] who have applied the same to study an axially symmetric spin  $3/2$  NQR.

In Chapter IV, we go to the next level of complexity in spin  $3/2$  NQR. Here we present a theoretical study of the multiple-pulse sequences, namely, PAPS and WAHUA using AHT within the Magnus expansion framework. The cyclicity criterion, as it applies to a polycrystalline spin  $3/2$  NQR solid, is explicitly stated; this enables us to formulate several multiple-pulse cycles which are adapted for studying the major interactions in quadrupolar solids. The nuclear assembly is now considered as being no longer a non-interacting one and, therefore, heteronuclear dipolar interactions are taken into account. The homonuclear dipolar interactions are very weak in spin  $3/2$  NQR and are discarded. Also considered are the effects of impurity and torsional oscillations on the efg. A noteworthy result of this Chapter is the dependence of the effectiveness of the pulse sequences on crystal orientation and asymmetry parameter. Finally, our experimental results on the effects of PAPS on spin  $3/2$  in  $\text{KClO}_3$  ( $^{35}\text{Cl}$ ) are presented.

The generalized AHT in the framework of Floquet theorem has been found to be most appropriate to analyse theoretically the results of OW or MW pulse sequence experiments in spin  $3/2$  also, as in spin  $1/2$  NMR and spin 1 NQR. Chapter V therefore starts with a detailed exposition of the Floquet theorem, the generalized AHT, and the derivation of equilibrium properties of spin  $3/2$  NQR therefrom, in the presence of periodic rf pulse perturbations. The theory presented in this Chapter is in the same spirit as that of Maricq [33,64-66] but for the spin  $3/2$  NQR

experiment itself. We also describe in this Chapter the advantages of the generalized AHT within the Floquet framework over AHT within the Magnus expansion framework and the conditions in which they yield similar results. The results of AHT in three formalisms, namely, Magnus expansion, Floquet theorem and Krylov-Bogoliubov-Mitropolsky (KBMD) method, are compared in this Chapter.

Chapter VI gives the detailed results of our calculations performed for both single-crystal and powder samples of spin  $3/2$  NQR under the OW or MW pulse sequence. A Monte Carlo procedure based on the 'systematic sampling' technique was used for powder averaging, and the Fortran program which performs the powder average is listed in Appendix A.

The theoretical plots are compared with the experimental results performed on powdered  $\text{HgCl}_2$  and  $\text{NaClO}_3$  ( $^{35}\text{Cl}$  resonance) samples. Attainment of a quasi-equilibrium state, viz., a spin-locked state, is demonstrated, both theoretically and experimentally. The dominant mechanism responsible for achieving this quasi-equilibrium state is the coupling of quadrupolar spins to the lattice via the oscillating efg due to the torsional oscillations. Unlike in NMR, the homonuclear dipolar interaction does not play any significant role in spin  $3/2$  NQR [99,100]. The consequence of the above quasi-equilibrium is persistence of the signal even at times much longer than  $5T_1$ . This finding not only considerably generalizes and adapts the earlier work on spin 1 NQR by Maricq [33], but also enhances our understanding of NQR phenomena further.



In Chapter VII, we summarize the present work and the important conclusions drawn therefrom. We also point out the scope for future work in this Chapter.

Overall, the thesis has been written up in a style that blends the quantum mechanical and magnetic resonance languages, with the jargon of the latter predominating somewhat. This is meant to be in keeping with our belief that current problems of NQR dynamics and equilibrium properties are topics of research with an intrinsic interest. On the other hand, certain details which may seem somewhat elementary have been treated at length in this thesis, and this has been done intentionally to make up for the absence of such treatment in currently available monographs, textbooks and other dissertations.

The experiments carried out in this thesis have value from the standpoint of demonstration of theoretical predictions. In particular, the long-time behavior of the spin  $3/2$  quasi-equilibrium magnetization has been unequivocally demonstrated.

## CHAPTER II

### THE QUANTUM MECHANICAL BACKGROUND

#### II.A. The Hamiltonian of the System

The interactions of nuclear spins that occur in a quadrupole nuclear assembly can be described by a Hamiltonian of the following general form [1-4]:

$$\mathcal{H} = \mathcal{H}_Q + \mathcal{H}_{rf} + \mathcal{H}_{int} \quad , \quad (\text{II.1})$$

where we have also included the interaction of the quadrupolar system with the external radiofrequency field perturbation.  $\mathcal{H}$  has units of radians per second or energy divided by  $\hbar$ .  $\mathcal{H}_Q$ , the quadrupole Hamiltonian, corresponds to the interaction of the electric quadrupole moment of the nucleus with the surrounding electric field gradient (efg) due to electronic charge cloud.  $\mathcal{H}_{rf}$ , known as the radiofrequency (rf) Hamiltonian, describes the interaction of the quadrupolar nuclei with a linearly oscillating rf field.  $\mathcal{H}_{int}$  stands for internal Hamiltonians, and it represents all other internal interactions of the nuclei that constitute the NQR system. The internal interactions include coupling between pairs of spins and between spins and internal oscillating fields and field gradients.

The Hamiltonians take the most simple form in their own principal axis system (PAS). To begin with therefore, it is convenient to define each of the three terms on the right hand side of Eqn II.1 in a different coordinate system. We adopt the following notation for this purpose:

<u>Coordinate system</u>	<u>Notation</u>
Quadrupole PAS (QPAS)	x, y, z
Laboratory PAS (LABPAS)	x, y, z
Internal interaction PAS (IPAS)	x', y', z'

The Quadrupole Hamiltonian:  $\mathcal{H}_Q$

The QPAS is defined by the principal components of the efg tensor as described in Chapter I (p.9). The single-particle quadrupole Hamiltonian in this coordinate system is given by [1-4]:

$$\mathcal{H}_Q = \frac{\omega_Q}{6} [3I_z^2 - I^2 + \frac{\eta}{2} (I_+^2 + I_-^2)] ; \quad (\text{II.2})$$

$$= \frac{\omega_Q}{\sqrt{6}} [T_{20}^Q + \frac{\eta}{\sqrt{3}} T_{22}^Q(S)] \quad (\text{II.2a})$$

$\omega_Q$  is in frequency units and is given by:

$$\omega_Q = 6A = \frac{3e^2 qQ}{2I(2I-1)\hbar}$$

A is the same as defined in Eqn I.4.  $T_{20}^Q$  and  $T_{22}^Q(S)$  in Eqn II.2a are the rank two irreducible spherical tensors:

$$T_{22}^Q(S) = (1/\sqrt{2}) [T_{22}^Q + T_{2-2}^Q]$$

For spin 3/2 NQR,  $\omega_Q$  is the one and only resonance frequency.  $\eta$  is the asymmetry parameter defined in Chapter I (p.9,10).  $I$ 's are the components, or linear combinations thereof, of the total angular momentum operator of the nuclear spin.

#### The Radiofrequency (rf) Hamiltonian: $\mathcal{H}_{rf}$

Here we assume the classical field form of radiofrequency radiation. This form is quite appropriate for describing most of the magnetic resonance phenomena. The interaction of the radiofrequency radiation field with a nuclear spin is described by  $\mathcal{H}_{rf}$ . We place the axis of the rf coil along the y-axis of LABPAS defined earlier. The explicit form of the single particle  $\mathcal{H}_{rf}$  in LABPAS is then :

$$\mathcal{H}_{rf} = -\omega_1(t) \cos(\omega t + \phi) I_y \quad ; \quad \text{(II.3)}$$

$$= -i\omega_1(t) \cos(\omega t + \phi) T_{11}^{rf}(S) \quad . \quad \text{(II.3a)}$$

$\omega_1(t)$  equals  $\gamma B_1(t)$ , where  $\gamma$  is the magnetogyric ratio of the nucleus that is being irradiated.  $B_1(t)$  is the rf magnetic field amplitude.  $\omega$  and  $\phi$  are the frequency and phase of the rf,

respectively. In multiple-pulse experiments, typically the rf field is applied in pulses that are ideally rectangles, so that  $\omega_1(t)$  is piecewise constant, taking on the values 0 and  $\omega_1^0$  only.  $\omega_1^0$  will be referred to as the nominal rf amplitude. Also, typically  $\omega$  is constant and  $\phi$  is piecewise constant. The first pulse in these experiments, known as the preparatory pulse, has  $\phi = 0$ . Other pulses in the sequence will have different values for  $\phi$  depending on the kind of experiment being performed. Some of the examples of the form of multiple-pulse sequences have already been given in Chapter I (p. 21, 24 and 28).  $T_{11}^{rf}(S) = (1/\sqrt{2}) [T_{11}^{rf} + T_{1-1}^{rf}]$  in Eqn II.3a is a first rank tensor.

### The Internal Hamiltonians: $\mathcal{H}_{int}$

The internal interactions that play a role in the dynamics of the NQR are of different physical origins. We describe below the Hamiltonians corresponding to each one of them.

#### 1. The efg inhomogeneity Hamiltonian: $D_\omega \mathcal{H}_Q$

The single particle efg inhomogeneity Hamiltonian in the QPAS is:

$$D_\omega \mathcal{H}_Q = D_\omega \frac{\omega_Q}{6} [3I_z^2 - I^2 + \frac{\eta}{2} (I_+^2 + I_-^2)] \quad ; \quad (II.4)$$

$$= D_\omega \frac{\omega_Q}{\sqrt{6}} [T_{20}^Q + \frac{\eta}{\sqrt{3}} T_{22}^Q(S)] \quad . \quad (II.4a)$$

It causes inhomogeneous broadening of NQR lines.  $D_\omega$  is a function that is introduced phenomenologically to take into account the distribution of resonance frequencies around the centre frequency  $\omega_Q$ . This distribution of frequencies is the result of the efg inhomogeneity [102-105]. Dislocations and strains in the crystal or powder grain cause random distortions in the intermolecular interactions and a corresponding random distribution of electric field gradients at nuclear sites. Strains may result from the crystal growth process, cold work or from cooling the sample under study. Disorder in the crystal also causes a similar distribution. The most appropriate distribution function in this case is the Gaussian distribution function:

$$g(\omega - \omega_Q) = [\exp - (\omega - \omega_Q)^2 / (2\delta^2)] / (2\pi\delta^2)^{1/2}, \quad (\text{II.5})$$

where

$$\int_{-\infty}^{\infty} g(\omega - \omega_Q) d\omega = 1 \quad (\text{II.6})$$

and

$$\delta = \frac{1}{T_2^*} = \frac{(\Delta\omega)_{1/2}}{(2\ln 2)^{1/2}}; \Delta\omega = \omega - \omega_Q \quad (\text{II.7})$$

is the root-mean-square deviation in  $\Delta\omega$  and  $(\Delta\omega)_{1/2}$  is the half width of the NQR line at half intensity.  $T_2^*$  is the effective spin-spin (transverse) relaxation time.  $\omega$  is a frequency away from the centre frequency  $\omega_Q$ .

## 2. The Torsional Oscillation Hamiltonian: $\mathcal{H}_T$

In the NQR sample, molecules containing the quadrupolar nucleus undergo torsional motions about the three principal axes of the field gradient. Let us denote the axes fixed in space (fixed QPAS) by  $(x, y, z)$ , and the axes fixed in the molecule (oscillating QPAS) by  $(x', y', z')$ . For small rotations  $\theta_x, \theta_y, \theta_z$ , about the three axes  $x', y'$  and  $z'$ , respectively, it may then be shown that the components of the field gradient tensor in the two coordinate systems are related by the following equations [8,103,106] :

$$V_{xx} = (1 - \theta_y^2, -\theta_z^2) V_{x',x'} + \theta_z^2 V_{y',y'} + \theta_y^2 V_{z',z'},$$

$$V_{yy} = \theta_z^2 V_{x',x'} + (1 - \theta_x^2, -\theta_z^2) V_{y',y'} + \theta_x^2 V_{z',z'},$$

$$V_{zz} = \theta_y^2 V_{x',x'} + \theta_x^2 V_{y',y'} + (1 - \theta_x^2, -\theta_y^2) V_{z',z'},$$

$$V_{xy} = V_{yx} = -\theta_z V_{x',x'} + (\theta_x \theta_y + \theta_z) V_{y',y'} - \theta_z \theta_y \theta_{z',z'},$$

$$V_{yz} = V_{zy} = \theta_y \theta_z V_{x',x'} - \theta_x V_{y',y'} - (\theta_y \theta_z - \theta_x) V_{z',z'},$$

$$V_{zx} = V_{xz} = -\theta_y V_{x',x'} - \theta_x \theta_z V_{y',y'} + (\theta_x \theta_z + \theta_y) V_{z',z'},$$

(II.8)

Substituting  $V_{x',x'} = \frac{eq}{2} (\eta-1)$ ,  $V_{y',y'} = -\frac{eq}{2} (\eta+1)$  and  $V_{z',z'} = eq$ , the relations in (II.8) can be rewritten as:

$$V_{xx} = \frac{eq}{2} [-\eta(\theta_y^2 + 2\theta_z^2, -1) - (1 - 3\theta_y^2, )]$$

$$V_{yy} = \frac{eq}{2} [\eta(\theta_x^2 + 2\theta_z^2, -1) - (1 - 3\theta_x^2, )]$$

$$V_{zz} = \frac{eq}{2} [-\eta(\theta_x^2, -\theta_y^2, ) - (3\theta_x^2 + 3\theta_y^2, -2)]$$

$$V_{xy} = V_{yx} = \frac{eq}{2} [-\eta(2\theta_z + \theta_x \theta_y, ) - 3\theta_x \theta_y, ]$$

$$V_{yz} = V_{zy} = \frac{eq}{2} [\eta(\theta_y \theta_z + \theta_x, ) + 3(\theta_x, -\theta_y \theta_z, )]$$

$$V_{zx} = V_{xz} = \frac{eq}{2} [-\eta(\theta_y, -\theta_x \theta_z, ) + 3(\theta_y, +\theta_x \theta_z, )]$$

(II.9)

Eqs II.9 lead to the following form for the single-particle torsional oscillation Hamiltonian in the fixed OPAS:

$$\begin{aligned} \mathcal{H}_T = & A_T(I_X^2 - I_Y^2) + B_T(I_Y^2 - I_Z^2) + C_T(I_Z^2 - I_X^2) \\ & + D_T(I_X I_Y + I_Y I_X) + E_T(I_Y I_Z + I_Z I_Y) + F_T(I_Z I_X + I_X I_Z), \end{aligned}$$

(II.10)



where

$$A_T = \frac{\omega_Q}{8} [\eta(1-2\bar{\theta}_x^2)]$$

$$B_T = -\frac{\omega_Q}{8} [1-(\eta+3)\bar{\theta}_x^2]$$

$$C_T = \frac{\omega_Q}{8} [1+(\eta-3)\bar{\theta}_y^2]$$

$$D_T = -\frac{\omega_Q}{8} [3\bar{\theta}_x, \bar{\theta}_y, +\eta(\bar{\theta}_x, \bar{\theta}_y, +2\bar{\theta}_z)]$$

$$E_T = \frac{\omega_Q}{8} [3(\bar{\theta}_x, -\bar{\theta}_y, \bar{\theta}_z) + \eta(\bar{\theta}_x, +\bar{\theta}_y, \bar{\theta}_z)]$$

$$F_T = \frac{\omega_Q}{8} [3(\bar{\theta}_y, +\bar{\theta}_x, \bar{\theta}_z) - \eta(\bar{\theta}_y, -\bar{\theta}_x, \bar{\theta}_z)]$$

$\bar{\theta}_i = \theta_i^2 - \langle \theta_i^2 \rangle$ ;  $i = x', y', z'$ .  $\langle \theta_i^2 \rangle$  is the thermal average of  $\theta_i^2$ .

For our later discussions, the torsional Hamiltonian also needs to be expressed in terms of irreducible spherical tensors. The fixed QPAS  $(x,y,z)$  and the oscillating QPAS  $(x,y',z')$  can be related by the Euler angle rotations  $\Omega \equiv (\alpha\beta\gamma)$ . The torsional oscillation Hamiltonian in fixed QPAS can then also be written as:

$$\mathcal{H}_T = \frac{\omega_Q}{9} [ \{ \sqrt{6} D_{02}^2(\Omega) + \eta(D_{22}^2(\Omega) + D_{-22}^2(\Omega)) \} T_{2-2}^Q$$

$$- \{ \sqrt{6} D_{01}^2(\Omega) + \eta(D_{21}^2(\Omega) + D_{-21}^2(\Omega)) \} T_{2-1}^Q$$

$$\begin{aligned}
& + \{ \sqrt{6} D_{00}^2(\Omega) + \eta (D_{20}^2(\Omega) + D_{-20}^2(\Omega)) \} T_{20}^{\alpha} \\
& - \{ \sqrt{6} D_{0-1}^2(\Omega) + \eta (D_{2-1}^2(\Omega) + D_{-2-1}^2(\Omega)) \} T_{2-1}^{\alpha} \\
& + \{ \sqrt{6} D_{0-2}^2(\Omega) + \eta (D_{2-2}^2(\Omega) + D_{-2-2}^2(\Omega)) \} T_{2-2}^{\alpha} \} \quad , \quad (\text{II.10a})
\end{aligned}$$

where  $D_{mm}^l$ 's are the Wigner rotation matrices for Euler angle rotation  $\Omega \equiv (\alpha\beta\gamma)$ . They are related to the rotation angles described above as  $\theta_x$ ,  $\theta_y$ , and  $\theta_z$ . The assumption that rotations are infinitesimal, has also been used in Eqn II.10a.

### 3. The Dipole Hamiltonian: $\mathcal{H}_D$

Another contribution to  $\mathcal{H}_{\text{int}}$  is the dipole coupling. This coupling can be of two kinds. When both the nuclei being coupled by the interaction are of the same species, we have a homonuclear dipole coupling. The coupling of the resonant nucleus with other non-resonant nuclei in the sample is considered as heteronuclear dipole coupling. This Hamiltonian is a two-particle Hamiltonian. We describe here the explicit form for both the abovementioned cases :

Expressed in its own principal axis system (DPAS), the dipole coupling between  $i$  and  $j$  nuclei is given by [16] :

$$\mathcal{H}_D = \omega_{ij} (1/\sqrt{6}) (2I_{z'i} I_{z'j} - I_{y'i} I_{y'j} - I_{x'i} I_{x'j}) ; \quad (\text{II.11})$$

$$= \omega_{ij} T_{20}^D \quad . \quad (\text{II.11a})$$

Here  $\omega_{ij} = -2\gamma_i\gamma_j\hbar\gamma(3/2)r_{ij}^{-3}$ .  $r_{ij}$  is the distance between nuclei  $i$  and  $j$ .  $\gamma_i$  and  $\gamma_j$  are the magnetogyric ratios of the  $i$  and  $j$  nuclei, respectively. The principal axis system is defined such that the  $z$ -axis is along  $r_{ij}$ , the internuclear vector.  $T_{20}^D$  in Eqn II.11a is the rank two irreducible spherical tensor operator.

A point to be noted at this stage is that when homonuclear dipole coupling is significant in the sample under study, we have to take into account the two-particle nature of the full Hamiltonian. The total Hamiltonian is now a sum of single-particle Hamiltonians pertaining to each nucleus; while for the dipole term, the sum will be over each distinct pair of nuclei. In all our calculations, where homonuclear dipolar interaction is considered to be present, this summation will be implied, even when not mentioned explicitly. In the particular case of the quadrupole Hamiltonian we will assume that the QPAS's of the two nuclear spins coincide. Also  $\omega_{ai} = \omega_{aj} = \omega_a$ ;  $\eta_i = \eta_j = \eta$ .

## II.B. The Description of the Various Terms in the Hamiltonian in the same Principal Axis System (QPAS)

In the present study, the magnitude of the quadrupole Hamiltonian will be the largest. It is, therefore, convenient to describe the system when all the terms in the total Hamiltonian are written in QPAS. The efg inhomogeneity (Eqn II.4) and the torsional oscillation (Eqn II.10) Hamiltonians are already in QPAS. In this section we transform  $\mathcal{H}_{rf}$  and  $\mathcal{H}_D$  also to the QPAS.

### The rf Hamiltonian $\mathcal{H}_{rf}$ , in QPAS

The  $\mathcal{H}_{rf}$  has been defined in Eqn II.3 along the y-axis of LABPAS. The relative orientation of this y-axis and the QPAS depends on the crystal orientation. In a powder sample, crystallites will be randomly oriented in all possible directions. In general, we can represent the relation between y-axis of LABPAS and the axes of the QPAS by two angles  $(\theta_L, \phi_L)$  as shown in Figure II.1. Clearly,

$$y = x \sin \phi_L \sin \theta_L + y \cos \theta_L + z \cos \phi_L \sin \theta_L, \quad (\text{II.12})$$

and also

$$I_y = \sin \phi_L \sin \theta_L I_{Lx} + \cos \theta_L I_{Ly} + \cos \phi_L \sin \theta_L I_{Lz}. \quad (\text{II.13})$$

Thus, in QPAS we get from Eqn II.3:

$$\mathcal{H}_{rf} = -\omega_1(t) \cos(\omega t + \phi) (\sin \phi_L \sin \theta_L I_{Lx} + \cos \theta_L I_{Ly} + \cos \phi_L \sin \theta_L I_{Lz}). \quad (\text{II.14})$$

### The Dipole Hamiltonian $\mathcal{H}_D$ , in QPAS

In this case also, we shall assume for generality that the DPAS and QPAS are randomly oriented with respect to each other. We can then express  $\mathcal{H}_D$  in the QPAS by using (in II.11a) the appropriate Wigner matrix for that transformation [16,21,22]

Figure II.1: Relation between LABPAS y-axis and QPAS (x,y,z) of one of the crystallites in the sample.  $n$  is the projection of  $y$  on the x-z plane.  $\theta_L$  is the angle between  $y$  and  $n$ .  $\phi_L$  is the angle between  $n$  and  $z$ . Projection of  $y$  on  $y$  is therefore  $y \cos \theta_L$ . Projection of  $z$  on  $n$  is  $z \cos \phi_L$ . Projection of  $z \cos \phi_L$  on  $y$  is  $z \cos \phi_L \cos(\pi/2 - \theta_L) = z \cos \phi_L \sin \theta_L$ . Similarly, projection of  $x$  on  $y$  is  $x \sin \phi_L \cos(\pi/2 - \theta_L) = x \sin \phi_L \sin \theta_L$ . Therefore,  $y = x \sin \phi_L \sin \theta_L + y \cos \theta_L + z \cos \phi_L \sin \theta_L$ .

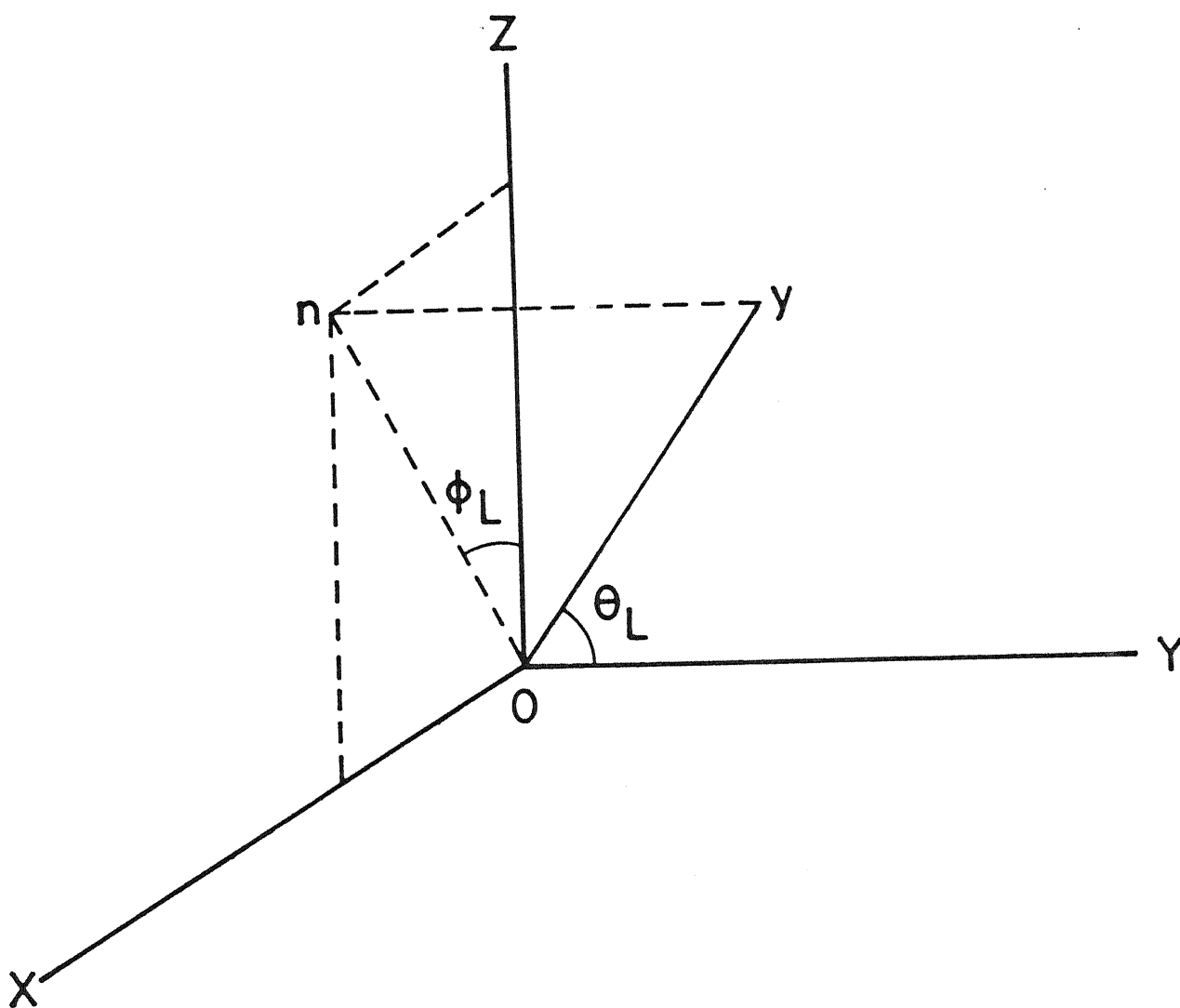


Figure II.1

$$\frac{1}{\omega_{ij}} \mathcal{E}_D = \sum_{m=-2}^2 D_{0-m}^2 T_{2m}^D (-1)^m ; \quad (\text{II.15})$$

$$\begin{aligned} &= \sqrt{(3/8)} \sin^2 \theta_D \{ T_{22}^D \exp(-2i\phi_D) + T_{2-2}^D \exp(+2i\phi_D) \\ &\quad - \sqrt{(3/8)} \sin 2\theta_D \{ T_{21}^D \exp(-i\phi_D) - T_{2-1}^D \exp(i\phi_D) \} \\ &\quad + (1/2)(3\cos^2 \theta_D - 1) T_{20}^D \} ; \end{aligned} \quad (\text{II.16})$$

$$\begin{aligned} &= \sqrt{(3/8)} \sin^2 \theta_D \cos 2\phi_D (I_{xi} I_{xj} - I_{yi} I_{yj}) \\ &\quad + \left[ \frac{3\cos^2 \theta_D - 1}{2\sqrt{6}} \right] (2I_{zi} I_{zj} - I_{xi} I_{xj} - I_{yi} I_{yj}) \\ &\quad + \sqrt{(3/8)} \{ \sin^2 \theta_D \sin 2\phi_D (I_{xi} I_{yj} + I_{yi} I_{xj}) \\ &\quad + \sin 2\theta_D \sin \phi_D (I_{yi} I_{zj} + I_{zi} I_{yj}) \\ &\quad + \sin 2\theta_D \cos \phi_D (I_{zi} I_{xj} + I_{xi} I_{zj}) \} . \end{aligned} \quad (\text{II.17})$$

From Eqn II.17, after rearrangement, we obtain

$$\begin{aligned} \mathcal{E}_D &= \omega_{ij} \{ a I_{xi} I_{xj} + a I_{yi} I_{yj} + a I_{zi} I_{zj} \\ &\quad + b(I_{xi} I_{yj} + I_{yi} I_{zj}) + c(I_{xi} I_{zj} + I_{zi} I_{xj}) + d(I_{yi} I_{zj} + I_{zi} I_{yj}) \} , \end{aligned} \quad (\text{II.18})$$

where

$$a_x = \sqrt{(3/2)} \sin^2 \theta_D \cos 2\phi_D - \sqrt{(1/6)} (3 \cos^2 \theta_D - 1) ,$$

$$a_y = -\sqrt{(3/2)} \sin^2 \theta_D \sin 2\phi_D - \sqrt{(1/6)} (3 \cos^2 \theta_D - 1) ,$$

$$a_z = \sqrt{(2/3)} (3 \cos^2 \theta_D - 1) ,$$

$$b = \sqrt{(3/2)} \sin^2 \theta_D \sin 2\phi_D ,$$

$$c = \sqrt{(3/2)} \sin 2\theta_D \cos \phi_D ,$$

$$d = \sqrt{(3/2)} \sin 2\theta_D \sin \phi_D .$$

Eqn II.18 is the dipole Hamiltonian in QPAS.

### II.C. The Cartesian Single Transition Operator (STO) Formalism

Wokaun and Ernst [97,54] and Vega [98] have developed an operator formalism which has been found to be very useful in describing spin 3/2 NQR. We shall presently express the Hamiltonian terms described in Sections II.A and II.B in terms of STO's. In this section we describe their definitions, commutation and other properties. We mention in passing that STO's are generators of SU(4) Lie Algebra [95,96]. Its use in NQR is not new. A very similar operator formalism constructed out of



Pauli matrices was used by Leppelmeier and Hahn [107] to study spin-lattice relaxation phenomenon in spin 3/2 NQR. Also, the operators used by Singh and Armstrong [94] and Ramachandran and Murthy [108] are very closely related to STO's.

The single transition operators  $I_x^{r-s}$ ,  $I_y^{r-s}$ ,  $I_z^{r-s}$ ,  $I_+^{r-s}$  and  $I_-^{r-s}$  refer to the transition between two energy levels  $|r\rangle$  and  $|s\rangle$ . All other energy levels are disregarded, and the subsystem is treated as a fictitious two-level system. The single transition operators associated with the transition between  $|r\rangle$  and  $|s\rangle$ , which may represent a zero-, single-, or multiple-quantum transition are defined in the following way:

$$\langle i | I_x^{r-s} | j \rangle = 1/2(\delta_{ir} \delta_{js} + \delta_{is} \delta_{jr}),$$

$$\langle i | I_y^{r-s} | j \rangle = 1/2(-\delta_{ir} \delta_{js} + \delta_{is} \delta_{jr}),$$

$$\langle i | I_z^{r-s} | j \rangle = 1/2(\delta_{ir} \delta_{jr} - \delta_{is} \delta_{js}). \quad (\text{II.19})$$

The matrix representations of these three operators (Figure II.2), lead us after elimination of rows and columns containing only zeroes, to the Pauli matrices.

It is easily seen that reversing the order of indices leads to the relations

$$I_x^{s-r} = I_x^{r-s},$$

$$I_Y^{s-r} = -I_Y^{r-s} ,$$

$$I_Z^{s-r} = -I_Z^{r-s} . \quad (II.20)$$

These sign changes have to be taken into account when constructing single transition operators for arbitrary eigenstates  $|r\rangle$  and  $|s\rangle$ .

The three operators belonging to a particular transition between  $|r\rangle$  and  $|s\rangle$  obey the standard commutation relations for Pauli spin matrices:

$$[I_\alpha^{r-s}, I_\beta^{r-s}] = iI_\gamma^{r-s} , \quad (II.21)$$

where  $\alpha, \beta, \gamma = x, y, z$  and their cyclic permutations.

For operators describing two connected transitions that involve three distinct states  $|r\rangle$ ,  $|s\rangle$  and  $|t\rangle$ , the following commutation rules hold :

$$[I_X^{r-t}, I_X^{s-t}] = [I_Y^{r-t}, I_Y^{s-t}] = (1/2)I_Y^{r-s} ,$$

$$[I_Z^{r-t}, I_Z^{s-t}] = 0 ,$$

$$[I_X^{r-t}, I_Y^{s-t}] = (1/2)I_X^{r-s} ,$$

$$[I_X^{r-t}, I_Z^{s-t}] = -(1/2)I_Y^{r-t} ,$$

$$[I_Y^{r-t}, I_Z^{s-t}] = (1/2)I_X^{r-t} . \quad (II.22)$$

Figure II.2: Matrix representation of the three single transition operators  $I_x^{r-s}$ ,  $I_y^{r-s}$  and  $I_z^{r-s}$ . They are represented in the eigenbasis of the corresponding Hamiltonian [54].

CENTRAL LIBRARY  
 Acc. No. A112522

$$I_X^{r-s} = \begin{array}{c} \begin{array}{cc} & |r\rangle \\ \begin{array}{c} 0 \\ \langle r| \end{array} & \begin{array}{c} 0 \\ \langle r| \end{array} \end{array} & \begin{array}{cc} & |s\rangle \\ \begin{array}{c} 1/2 \\ \langle r| \end{array} & \begin{array}{c} 0 \\ \langle r| \end{array} \end{array} \\ \hline \begin{array}{cc} & |r\rangle \\ \begin{array}{c} 1/2 \\ \langle s| \end{array} & \begin{array}{c} 0 \\ \langle s| \end{array} \end{array} & \begin{array}{cc} & |s\rangle \\ \begin{array}{c} 0 \\ \langle s| \end{array} & \begin{array}{c} 0 \\ \langle s| \end{array} \end{array} \end{array}$$

$$I_Z^{r-s} = \begin{array}{c} \begin{array}{cc} & |r\rangle \\ \begin{array}{c} 0 \\ \langle r| \end{array} & \begin{array}{c} 1/2 \\ \langle r| \end{array} \end{array} & \begin{array}{cc} & |s\rangle \\ \begin{array}{c} 0 \\ \langle r| \end{array} & \begin{array}{c} -1/2 \\ \langle r| \end{array} \end{array} \\ \hline \begin{array}{cc} & |r\rangle \\ \begin{array}{c} 0 \\ \langle s| \end{array} & \begin{array}{c} 0 \\ \langle s| \end{array} \end{array} & \begin{array}{cc} & |s\rangle \\ \begin{array}{c} -1/2 \\ \langle s| \end{array} & \begin{array}{c} 0 \\ \langle s| \end{array} \end{array} \end{array}$$

$$I_+^{r-s} = I_x^{r-s} + iI_y^{r-s} = |r\rangle\langle s| ,$$

$$I_-^{r-s} = I_x^{r-s} - iI_y^{r-s} = |s\rangle\langle r| = (I_+^{r-s})^\dagger . \quad (\text{II.27})$$

Because the  $y$  component is reversed in sign if we permute the indices, we have formally :

$$I_-^{r-s} = I_+^{s-r} . \quad (\text{II.28})$$

However it is desirable to use ordered indices such that  $m_r > m_s$ , to ensure that the raising and lowering operators increase and decrease the magnetic quantum numbers respectively :

$$I_+^{r-s} |s\rangle = |r\rangle ,$$

$$I_-^{r-s} |r\rangle = |s\rangle . \quad (\text{II.29})$$

#### II.D. The Diagonalized $\mathcal{H}_Q$ Representation of the Hamiltonian Terms

In order to follow conveniently the evolution of the assembly of quadrupolar nuclei in the single transition operator formalism, we diagonalize  $\mathcal{H}_Q$ , the main term in the overall Hamiltonian. Also, all other Hamiltonian terms are expressed in this representation. This representation is denoted throughout by a

superscript prime ('). In general, this diagonalization does not represent a pure rotation. However, since the quadrupole Hamiltonian is Hermitian, it can be diagonalized by a unitary transformation and such a transformation need not always represent a rotation. In such a case we can no longer assign probability weights  $P_m$  to states  $|m\rangle$  with respect to any choice of the z-axis in space, but only to a different set of orthonormal states which would, in general, be linear superpositions of states characterized by magnetic quantum number [109].

The unitary transformation that diagonalizes the quadrupole Hamiltonian is

$$R = \begin{bmatrix} \cos\xi/2 & 0 & \sin\xi/2 & 0 \\ 0 & \cos\xi/2 & 0 & -\sin\xi/2 \\ -\sin\xi/2 & 0 & \cos\xi/2 & 0 \\ 0 & \sin\xi/2 & 0 & \cos\xi/2 \end{bmatrix},$$

(II.30)

where  $\tan\xi = \eta/\sqrt{3}$ . Also  $R^{-1}$  is the transpose of Eqn II.30.

The exponential operator form of this unitary transformation is

$$R = \exp [ +i(I_Y^{1-3} - I_Y^{2-4})\xi ] \quad , \quad (\text{II.30a})$$

where  $\tan\xi = \eta/\sqrt{3}$ . It is interesting to point out here that since  $\mathcal{H}_Q$  (for spin 3/2) has degenerate eigenvalues, the unitary matrix  $R$  that diagonalizes it is not unique [110]. For instance, in place of Eqn II.29a we can construct another unitary transformation that achieves the aforesaid diagonalization:

$$R_1 = R_1^{-1} = \begin{bmatrix} \cos\xi/2 & 0 & \sin\xi/2 & 0 \\ 0 & -\cos\xi/2 & 0 & \sin\xi/2 \\ \sin\xi/2 & 0 & -\cos\xi/2 & 0 \\ 0 & \sin\xi/2 & 0 & \cos\xi/2 \end{bmatrix} \quad ,$$

(II.30b)

where  $\tan\xi = \eta/\sqrt{3}$ .

When we apply a Zeeman field, the degeneracy of the energy levels is lifted. The unitary transformation that will now diagonalize the Hamiltonian will be unique.

Using Eqn II.30 in Eqn II.1 we obtain

$$\mathcal{H}' = \mathcal{H}'_Q + \mathcal{H}'_{rf} + \mathcal{H}'_{int}, \quad (\text{II.31})$$

where, for example,  $\mathcal{H}'_{rf}$  represents  $R\mathcal{H}_{rf}R^{-1}$ . We give here the form of various terms in the right hand side of Eqn II.31 in terms of the single transition operators:

$$\mathcal{H}'_Q = K(I_Z^{1-2} - I_Z^{3-4}) = K\bar{L} \quad ; \quad (\text{II.32})$$

$$\bar{L} = (I_Z^{1-2} - I_Z^{3-4}) \quad , \quad (\text{II.32a})$$

$$\text{where } K = \frac{\omega}{2} (1 + \eta^2/3)^{1/2} .$$

Also from Eqn II.4, the efg inhomogeneity Hamiltonian is

$$D_\omega \mathcal{H}'_Q = D_\omega K(I_Z^{1-2} - I_Z^{3-4}) = D_\omega K\bar{L} . \quad (\text{II.33})$$

From Eqn II.14 we obtain

$$\begin{aligned} \mathcal{H}'_{rf} = & -\omega_1(t) \cos(\omega t + \phi) [ \sin\theta_L \sin\phi_L \{ -(\sqrt{3}\cos\xi + \sin\xi)(I_X^{1-2} + I_X^{3-4}) \\ & + (I_X^{1-4} + I_X^{2-3}) + (\sqrt{3}\sin\xi - \cos\xi)(I_X^{1-4} - I_X^{2-3}) \} \\ & + \cos\theta_L \{ (\sin\xi - \sqrt{3}\cos\xi)(I_Y^{1-2} + I_Y^{3-4}) - (I_Y^{1-4} - I_Y^{2-3}) \} \end{aligned}$$



$$\begin{aligned}
& +(\sqrt{3}\sin\xi+\cos\xi)(I_Y^{1-4}+I_Y^{2-3})\} \\
& +\sin\theta_L\cos\phi_L\{(I_Z^{1-4}-I_Z^{2-3})+2\cos\xi(I_Z^{1-4}+I_Z^{2-3})+2\sin\xi(I_X^{1-3}-I_X^{2-4})\}; \\
& \quad \quad \quad (II.34)
\end{aligned}$$

From Eqn II.10 we obtain

$$\begin{aligned}
\mathcal{E}'_T &= A'_T(I_Z^{1-2}-I_Z^{3-4})+B'_T(I_X^{1-3}+I_X^{2-4})-C'_T(I_Y^{1-3}+I_Y^{2-4})-D'_T(I_Y^{1-2}-I_Y^{3-4}) \\
& \quad -E'_T(I_X^{1-2}-I_X^{3-4}), \quad \quad \quad (II.35)
\end{aligned}$$

where

$$\begin{aligned}
A'_T &= \{2\sqrt{3}A_T\sin\xi-\sqrt{3}B_T(\sqrt{3}\cos\xi+\sin\xi)+\sqrt{3}C_T(\sqrt{3}\cos\xi-\sin\xi)\}, \\
B'_T &= \{-2\sqrt{3}A_T\cos\xi-\sqrt{3}B_T(\sqrt{3}\sin\xi-\cos\xi)+\sqrt{3}C_T(\sqrt{3}\sin\xi+\cos\xi)\}, \\
C'_T &= 2\sqrt{3}D_T, \\
D'_T &= 2\sqrt{3}E_T, \\
E'_T &= 2\sqrt{3}F_T;
\end{aligned}$$

and from Eqn II.18 we obtain

$$\mathcal{E}'_D = \omega_{ij}[a_X\{-(\sqrt{3}\cos\xi+\sin\xi)(I_{Xi}^{1-2}+I_{Xi}^{3-4})+(I_{Xi}^{1-4}+I_{Xi}^{2-3})\}$$

$$+(\sqrt{3}\sin\xi-\cos\xi)(I_{xi}^{1-4}-I_{xi}^{2-3})$$

$$x(-(\sqrt{3}\cos\xi+\sin\xi)(I_{xj}^{1-2}+I_{xj}^{3-4})+(I_{xj}^{1-4}+I_{xj}^{2-3}))$$

$$+(\sqrt{3}\sin\xi-\cos\xi)(I_{xj}^{1-4}+I_{xj}^{2-3})$$

$$+a_y\{(-\sqrt{3}\cos\xi+\sin\xi)(I_{yi}^{1-2}+I_{yi}^{3-4})-(I_{yi}^{1-4}-I_{yi}^{2-3})$$

$$+(\sqrt{3}\sin\xi+\cos\xi)(I_{yi}^{1-4}-I_{yi}^{2-3})\}$$

$$x(-(\sqrt{3}\cos\xi+\sin\xi)(I_{yj}^{1-2}+I_{yj}^{3-4})-(I_{yj}^{1-4}-I_{yj}^{2-3}))$$

$$+(\sqrt{3}\sin\xi+\cos\xi)(I_{yj}^{1-4}+I_{yj}^{2-3})$$

$$+a_z\{(I_{zi}^{1-4}-I_{zi}^{2-3})+2\cos\xi(I_{zi}^{1-4}+I_{zi}^{2-3})+2\sin\xi(I_{xi}^{1-3}-I_{xi}^{2-4})\}$$

$$x\{(I_{zj}^{1-4}-I_{zj}^{2-3})+2\cos\xi(I_{zj}^{1-4}+I_{zj}^{2-3})+2\sin\xi(I_{xj}^{1-3}-I_{xj}^{2-4})\}$$

$$+b\{(-(\sqrt{3}\cos\xi+\sin\xi)(I_{xi}^{1-2}+I_{xi}^{3-4})+(I_{xi}^{1-4}+I_{xi}^{2-3}))$$

$$+(\sqrt{3}\sin\xi-\cos\xi)(I_{xi}^{1-4}-I_{xi}^{2-3})\}$$

$$x(-(\sqrt{3}\cos\xi+\sin\xi)(I_{yj}^{1-2}+I_{yj}^{3-4})-(I_{yj}^{1-4}-I_{yj}^{2-3}))$$

$$+(\sqrt{3}\sin\xi+\cos\xi)(I_{yj}^{1-4}+I_{yj}^{2-3})$$

$$+((-\sqrt{3}\cos\xi+\sin\xi)(I_{Yi}^{1-2}+I_{Yi}^{3-4})-(I_{Yi}^{1-4}-I_{Yi}^{2-3}))$$

$$+(\sqrt{3}\sin\xi+\cos\xi)(I_{Yi}^{1-4}-I_{Yi}^{2-3}))$$

$$\times(-( \sqrt{3}\cos\xi+\sin\xi)(I_{Xj}^{1-2}+I_{Xj}^{3-4})+(I_{Xj}^{1-4}+I_{Xj}^{2-3}))$$

$$+(\sqrt{3}\sin\xi-\cos\xi)(I_{Xj}^{1-4}+I_{Xj}^{2-3}))$$

$$+c((-\sqrt{3}\cos\xi+\sin\xi)(I_{Xi}^{1-2}+I_{Xi}^{3-4})+(I_{Xi}^{1-4}+I_{Xi}^{2-3}))$$

$$+(\sqrt{3}\sin\xi-\cos\xi)(I_{Xi}^{1-4}-I_{Xi}^{2-3}))$$

$$\times((I_{Zj}^{1-4}-I_{Zj}^{2-3})+2\cos\xi(I_{Zj}^{1-4}+I_{Zj}^{2-3})+2\sin\xi(I_{Xj}^{1-3}-I_{Xj}^{2-4}))$$

$$+((I_{Zi}^{1-4}-I_{Zi}^{2-3})+2\cos\xi(I_{Zi}^{1-4}+I_{Zi}^{2-3})+2\sin\xi(I_{Xi}^{1-3}-I_{Xi}^{2-4}))$$

$$\times(-( \sqrt{3}\cos\xi+\sin\xi)(I_{Xj}^{1-2}+I_{Xj}^{3-4})+(I_{Xj}^{1-4}+I_{Xj}^{2-3}))$$

$$+(\sqrt{3}\sin\xi-\cos\xi)(I_{Xj}^{1-4}-I_{Xj}^{2-3}))$$

$$+d((-\sqrt{3}\cos\xi+\sin\xi)(I_{Yi}^{1-2}+I_{Yi}^{3-4})-(I_{Yi}^{1-4}-I_{Yi}^{2-3}))$$

$$+(\sqrt{3}\sin\xi+\cos\xi)(I_{Yi}^{1-4}+I_{Yi}^{2-3}))$$

$$x \langle (I_{zj}^{1-4} - I_{zj}^{2-3}) + 2\cos\xi(I_{zj}^{1-4} + I_{zj}^{2-3}) + 2\sin\xi(I_{xj}^{1-3} - I_{xj}^{2-4}) \rangle$$

$$+ \langle (I_{zi}^{1-4} - I_{zi}^{2-3}) + 2\cos\xi(I_{zi}^{1-4} + I_{zi}^{2-3}) + 2\sin\xi(I_{xi}^{1-3} - I_{xi}^{2-4}) \rangle$$

$$x \langle (-\sqrt{3}\cos\xi + \sin\xi)(I_{yj}^{1-2} + I_{yj}^{3-4}) - (I_{yj}^{1-4} - I_{yj}^{2-3})$$

$$+ (\sqrt{3}\sin\xi + \cos\xi)(I_{yj}^{1-4} + I_{yj}^{2-3}) \rangle]$$

(II.36)

## II.E. The Quadrupole Interaction Frame (QIF) and Effective Hamiltonian Description of the Spin System

The interaction representation provides a relatively simple and convenient means for calculating the pulse response of an ensemble of nuclear spins experiencing electric quadrupole coupling [21,22,107,111]. The procedure which we adopt here is completely analogous to the rotating frame concept in NMR, where the laboratory frame Hamiltonian consisting of a main time-independent part and a much smaller but time-dependent perturbation (the coupling of the magnetic moments of the spins to the rf magnetic field), is transformed in the interaction picture into a new Hamiltonian consisting of a low-field time-independent part  $\tilde{\mathcal{H}}$  and time-dependent parts oscillating at frequencies  $\omega$  and  $2\omega$ . Since these oscillating terms are far from

resonance in the interaction picture, they exert a negligible torque on the spin system, the evolution of which may then, to an excellent approximation, be described by  $\tilde{\mathcal{H}}$  alone. This procedure of dropping the oscillating terms in the interaction representation is completely equivalent to the standard first-order perturbation theory used to tackle time-dependent quantum mechanical problems [112].

In the quadrupolar case, the transformation involved in the interaction representation does not correspond to a rotation and has no simple geometrical interpretation. Nevertheless, in what follows, we will see how the interaction representation can be used in our case in a way completely analogous to its better known use in NMR [3,4,113]. Rather than dealing with the quadrupole interaction frame transformation specifically, it is useful to describe the general quantum mechanical procedure for a change of reference frames [114].\*

A change of reference frames is defined by a unitary transformation  $U_{IF}(t)$ , which may be time-dependent. If  $|\psi(t)\rangle$  is the state of a system at time  $t$  in the original frame, the state at time  $t$  in the new frame is  $|\tilde{\psi}(t)\rangle$ :

$$|\tilde{\psi}(t)\rangle = U_{IF}(t) |\psi(t)\rangle \quad (II.37)$$

Given that  $\mathcal{H}$  is the Hamiltonian in the original frame, the

---

\* We are not considering boosts here.

Hamiltonian  $\tilde{\mathcal{H}}$  in the new frame may be found by the following argument. In their respective frames,  $|\psi(t)\rangle$  and  $|\tilde{\psi}(t)\rangle$  evolve according to the Schrödinger equation :

$$i \frac{d}{dt} |\psi(t)\rangle = \mathcal{H} |\psi(t)\rangle \quad , \quad (\text{II.38})$$

$$i \frac{d}{dt} |\tilde{\psi}(t)\rangle = \tilde{\mathcal{H}} |\tilde{\psi}(t)\rangle \quad . \quad (\text{II.39})$$

Substituting Eqn II.37 into Eqn II.39:

$$i \frac{dU}{dt} {}_{\text{IF}} |\psi(t)\rangle + i U {}_{\text{IF}} \frac{d}{dt} |\psi(t)\rangle = \tilde{\mathcal{H}} |\tilde{\psi}(t)\rangle \quad . \quad (\text{II.40})$$

Using Eqn II.38 :

$$[i (\frac{dU}{dt} {}_{\text{IF}}) + U {}_{\text{IF}} \mathcal{H}] |\psi(t)\rangle = \tilde{\mathcal{H}} |\tilde{\psi}(t)\rangle \quad . \quad (\text{II.41})$$

Eqn II.41 implies that :

$$\tilde{\mathcal{H}} = i (\frac{dU}{dt} {}_{\text{IF}}) U {}_{\text{IF}}^{-1} + U {}_{\text{IF}} \mathcal{H} U {}_{\text{IF}}^{-1} \quad . \quad (\text{II.42})$$

This expression for  $\tilde{\mathcal{H}}$  holds even if  $\mathcal{H}$  is time dependent.

The specific example of the quadrupole interaction frame (QIF) transformation employs a unitary transformation given by

$$U_0(t) = \exp(i\mathcal{H}_0 t) \quad , \quad (\text{II.43})$$

where

$$\begin{aligned}
 \mathcal{H}'_0 &= \mathcal{H}'_Q + \Delta \mathcal{H}'_Q = (1+\Delta) \mathcal{H}'_Q \\
 &= (1+\Delta) K (I_z^{1-2} - I_z^{3-4}) \\
 &= K' (I_z^{1-2} - I_z^{3-4}) \\
 &= K' \bar{L} \quad ; (K' = (1+\Delta)K) , \quad (\text{II.44})
 \end{aligned}$$

is the quadrupole Hamiltonian plus the resonance offset. To distinguish the special on-resonance case  $\Delta = 0$ , we will denote the coefficient by  $K^0$ .

Applying Eqn II.42 to Eqn II.31 :

$$\begin{aligned}
 \tilde{\mathcal{H}} &= i \left\{ \frac{d \exp(i\mathcal{H}'_0 t)}{dt} \exp(-i\mathcal{H}'_0 t) \right. \\
 &\quad \left. + \exp(i\mathcal{H}'_0 t) (\mathcal{H}'_Q + \mathcal{H}'_{rf} + \mathcal{H}'_{int}) \exp(-i\mathcal{H}'_0 t) \right\} \\
 &= -\mathcal{H}'_0 + U_0 \mathcal{H}'_Q U_0^{-1} + U_0 \mathcal{H}'_{rf} U_0^{-1} + U_0 \mathcal{H}'_{int} U_0^{-1} \\
 &= -\Delta \mathcal{H}'_Q + \tilde{\mathcal{H}}'_{rf} + \tilde{\mathcal{H}}'_{int} , \quad (\text{II.45})
 \end{aligned}$$

where

$$\tilde{\mathcal{H}}'_Q = \exp(i\mathcal{H}'_0 t) \mathcal{H}'_Q \exp(-i\mathcal{H}'_0 t) = \mathcal{H}'_Q , \quad (\text{II.46})$$

because

$$[\mathcal{H}'_0, \mathcal{H}'_Q] = 0 \quad . \quad (II.47)$$

To evaluate the expressions of the kind in Eqn II.46, we note that the operators involved satisfy the cyclic commutation relations in the sense that, if

$$[P, Q] = i\pi R \quad ,$$

$$[Q, R] = i\pi P \quad ,$$

$$\text{and } [R, P] = i\pi Q \quad ,$$

with  $\pi = 1, 1/2$  or  $-1/2$  and with P, Q, R representing the single transition operators or their linear combinations, we get the following transformation relations :

$$\exp(-i\theta P) Q \exp(i\theta P) = Q \cos \pi \theta + R \sin \pi \theta$$

$$\exp(-i\theta P) R \exp(i\theta P) = R \cos \pi \theta - Q \sin \pi \theta \quad . \quad (II.48)$$

Also, of course, if

$$[P, Q] = 0, \text{ then}$$

$$\exp(-i\theta P) Q \exp(i\theta P) = Q \quad . \quad (II.50)$$

Using Eqns II.48 and II.50 to evaluate  $\tilde{\mathcal{H}}'_{rf}$  and  $\tilde{\mathcal{H}}'_{int}$ , we arrive at the following expressions for the terms in the Hamiltonian in QIF:

$$\tilde{\mathcal{H}}'_{rf} = -\omega_1(t) \cos(\omega t + \phi) [\sin \theta_L \sin \phi_L \{-(\sqrt{3} \cos \xi + \sin \xi)\}]$$



$$\begin{aligned}
& x \{ (I_X^{1-2} + I_X^{3-4}) \cos K' t - (I_Y^{1-2} - I_Y^{3-4}) \sin K' t \} \\
& + (I_X^{1-4} + I_X^{2-3}) + (\sqrt{3} \sin \xi - \cos \xi) (I_X^{1-4} - I_X^{2-3}) \} \\
& + \cos \theta_L \{ (\sin \xi - \sqrt{3} \cos \xi) (I_Y^{1-2} + I_Y^{3-4}) \cos K' t + (I_X^{1-2} - I_X^{3-4}) \sin K' t \} \\
& - (I_Y^{1-4} - I_Y^{2-3}) + (\sqrt{3} \sin \xi + \cos \xi) (I_Y^{1-4} + I_Y^{2-3}) \} \\
& + \sin \theta_L \cos \phi_L \{ (I_Z^{1-4} - I_Z^{2-3}) + 2 \cos \xi (I_Z^{1-4} + I_Z^{2-3}) \\
& + 2 \sin \xi \{ (I_X^{1-3} - I_X^{2-4}) \cos K' t - (I_Y^{2-4} + I_Y^{1-3}) \sin K' t \} \} ] ,
\end{aligned}
\tag{II.51}$$

$$\tilde{\mathcal{H}}'_{int} = D_{\omega} \tilde{\mathcal{H}}'_Q + \tilde{\mathcal{H}}'_T + \tilde{\mathcal{H}}'_D .
\tag{II.52}$$

The expression for each of the Hamiltonian terms in Eqn II.52 is as follows :

$$D_{\omega} \tilde{\mathcal{H}}'_Q = D_{\omega} \mathcal{H}'_Q = D_{\omega} K (I_Z^{1-2} - I_Z^{3-4}) ,
\tag{II.53}$$

$$\begin{aligned}
\mathcal{H}'_T &= A'_T (I_Z^{1-2} - I_Z^{3-4}) \\
&+ B'_T \{ (I_X^{1-3} + I_X^{2-4}) \cos K' t - (I_Y^{1-3} - I_Y^{2-4}) \sin K' t \} \\
&- C'_T \{ (I_Y^{1-3} + I_Y^{2-4}) \cos K' t + (I_X^{1-3} - I_X^{2-4}) \sin K' t \}
\end{aligned}$$

$$\begin{aligned}
& -D_T' \langle (I_Y^{1-2} - I_Y^{3-4}) \cos K' t + (I_X^{1-2} + I_X^{3-4}) \sin K' t \rangle \\
& -E_T' \langle (I_X^{1-2} - I_X^{3-4}) \cos K' t - (I_Y^{1-2} + I_Y^{3-4}) \sin K' t \rangle \quad (II.54)
\end{aligned}$$

The dipole Hamiltonian will take different forms in QIF depending upon the kind of the nuclei that are dipole-coupled to each other. We have two distinct cases, namely, the heteronuclear dipole and the homonuclear dipole. We give below the expressions for both of them in QIF.

Let us denote the dipole-coupled nuclei as  $i$  and  $j$ . Also, let  $i$  be the non-resonant nucleus and  $j$  the resonant one. The transformation to QIF therefore, is carried out with respect to  $\mathcal{H}_0'$  of  $j$ th nucleus, i.e.,

$$\tilde{\mathcal{H}}_{D(\text{hetero})}' = \exp(i\mathcal{H}_{0j}' t) \mathcal{H}_D' \exp(-i\mathcal{H}_{0j}' t) \quad (II.55)$$

Using Eqn II.36 for the expression of  $\mathcal{H}_D'$  and Eqns II.49 and II.50, we write the following expression for  $\tilde{\mathcal{H}}_{D(\text{hetero})}'$ :

$$\begin{aligned}
\tilde{\mathcal{H}}_{D(\text{hetero})}' &= \omega_{ij} [a_{Xj} I_{Xi} \{-(\sqrt{3} \cos \xi + \sin \xi) \\
& \quad \times \langle (I_{Xj}^{1-2} + I_{Xj}^{3-4}) \cos K' t - (I_{Yj}^{1-2} - I_{Yj}^{3-4}) \sin K' t \rangle \\
& \quad + (I_{Xj}^{1-4} + I_{Xj}^{2-3}) + (\sqrt{3} \sin \xi - \cos \xi) \langle (I_{Xj}^{1-4} - I_{Xj}^{2-3}) \rangle \}
\end{aligned}$$

$$\begin{aligned}
& +a_y I_{yi} \{(\sin\xi - \sqrt{3}\cos\xi)(I_{yj}^{1-2} + I_{yj}^{3-4})\cos K't + (I_{xj}^{1-2} - I_{xj}^{3-4})\sin K't) \\
& \quad - (I_{yj}^{1-4} - I_{yj}^{2-3}) + (\sqrt{3}\sin\xi + \cos\xi)(I_{yj}^{1-4} + I_{yj}^{2-3})\} \\
& +a_z I_{zi} \{(I_{zj}^{1-4} - I_{zj}^{2-3}) + 2\cos\xi(I_{zj}^{1-4} + I_{zj}^{2-3}) \\
& \quad + 2\sin\xi((I_{xj}^{1-3} - I_{xj}^{2-4})\cos K't - (I_{yj}^{2-4} + I_{yj}^{1-3})\sin K't)\} \\
& +b[I_{xi} \{(\sin\xi - \sqrt{3}\cos\xi)(I_{yj}^{1-2} + I_{yj}^{3-4})\cos K't + (I_{xj}^{1-2} - I_{xj}^{3-4})\sin K't) \\
& \quad - (I_{yj}^{1-4} - I_{yj}^{2-3}) + (\sqrt{3}\sin\xi + \cos\xi)(I_{yj}^{1-4} + I_{yj}^{2-3})\} \\
& + I_{yi} \{-(\sqrt{3}\cos\xi + \sin\xi)(I_{xj}^{1-2} + I_{xj}^{3-4})\cos K't - (I_{yj}^{1-2} - I_{yj}^{3-4})\sin K't) \\
& \quad + (I_{xj}^{1-4} + I_{xj}^{2-3}) + (\sqrt{3}\sin\xi - \cos\xi)(I_{xj}^{1-4} - I_{xj}^{2-3})\} \\
& +c[I_{xi} \{(I_{zj}^{1-4} - I_{zj}^{2-3}) + 2\cos\xi(I_{zj}^{1-4} + I_{zj}^{2-3}) \\
& \quad + 2\sin\xi((I_{xj}^{1-3} - I_{xj}^{2-4})\cos K't - (I_{yj}^{2-4} + I_{yj}^{1-3})\sin K't)\} \\
& + I_{zi} \{-(\sqrt{3}\cos\xi + \sin\xi)(I_{xj}^{1-2} + I_{xj}^{3-4})\cos K't - (I_{yj}^{1-2} - I_{yj}^{3-4})\sin K't) \\
& \quad + (I_{xj}^{1-4} + I_{xj}^{2-3}) + (\sqrt{3}\sin\xi - \cos\xi)(I_{xj}^{1-4} - I_{xj}^{2-3})\} \\
& +d[I_{yi} \{(I_{zj}^{1-4} - I_{zj}^{2-3}) + 2\cos\xi(I_{zj}^{1-4} + I_{zj}^{2-3})
\end{aligned}$$



$$+a_y \{ (\sin \xi - \sqrt{3} \cos \xi) (I_{y_i}^{1-2} + I_{y_i}^{3-4}) \cos K' t + (I_{x_i}^{1-2} - I_{x_i}^{3-4}) \sin K' t \}$$

$$- (I_{y_i}^{1-4} - I_{y_i}^{2-3}) + (\sqrt{3} \sin \xi + \cos \xi) (I_{y_i}^{1-4} + I_{y_i}^{2-3}) \}$$

$$\times \{ (\sin \xi - \sqrt{3} \cos \xi) (I_{y_j}^{1-2} + I_{y_j}^{3-4}) \cos K' t + (I_{x_j}^{1-2} - I_{x_j}^{3-4}) \sin K' t \}$$

$$- (I_{y_j}^{1-4} - I_{y_j}^{2-3}) + (\sqrt{3} \sin \xi + \cos \xi) (I_{y_j}^{1-4} + I_{y_j}^{2-3}) \}$$

$$+a_z \{ (I_{z_i}^{1-4} - I_{z_i}^{2-3}) + 2 \cos \xi (I_{z_i}^{1-4} + I_{z_i}^{2-3})$$

$$+ 2 \sin \xi (I_{x_i}^{1-3} - I_{x_i}^{2-4}) \cos K' t - (I_{y_i}^{2-4} + I_{y_i}^{1-3}) \sin K' t \}$$

$$\times \{ (I_{z_j}^{1-4} - I_{z_j}^{2-3}) + 2 \cos \xi (I_{z_j}^{1-4} + I_{z_j}^{2-3})$$

$$+ 2 \sin \xi (I_{x_j}^{1-3} - I_{x_j}^{2-4}) \cos K' t - (I_{y_j}^{2-4} + I_{y_j}^{1-3}) \sin K' t \}$$

$$+b \{ -(\sqrt{3} \cos \xi + \sin \xi) (I_{x_i}^{1-2} + I_{x_i}^{3-4}) \cos K' t - (I_{y_i}^{1-2} - I_{y_i}^{3-4}) \sin K' t \}$$

$$+ (I_{x_i}^{1-4} + I_{x_i}^{2-3}) + (\sqrt{3} \sin \xi - \cos \xi) (I_{x_i}^{1-4} - I_{x_i}^{2-3}) \}$$

$$\times \{ (\sin \xi - \sqrt{3} \cos \xi) (I_{y_j}^{1-2} + I_{y_j}^{3-4}) \cos K' t + (I_{x_j}^{1-2} - I_{x_j}^{3-4}) \sin K' t \}$$

$$- (I_{y_j}^{1-4} - I_{y_j}^{2-3}) + (\sqrt{3} \sin \xi + \cos \xi) (I_{y_j}^{1-4} + I_{y_j}^{2-3}) \}$$

$$+ \{ (\sin \xi - \sqrt{3} \cos \xi) (I_{y_i}^{1-2} + I_{y_i}^{3-4}) \cos K' t + (I_{x_i}^{1-2} - I_{x_i}^{3-4}) \sin K' t \}$$

$$\begin{aligned}
& -(I_{Yi}^{1-4} - I_{Yi}^{2-3}) + (\sqrt{3}\sin\xi + \cos\xi)(I_{Yi}^{1-4} + I_{Yi}^{2-3})\} \\
& \times \{-(\sqrt{3}\cos\xi + \sin\xi)(I_{Xj}^{1-2} + I_{Xj}^{3-4})\cos K't - (I_{Yj}^{1-2} - I_{Yj}^{3-4})\sin K't) \\
& \quad + (I_{Xj}^{1-4} + I_{Xj}^{2-3}) + (\sqrt{3}\sin\xi - \cos\xi)(I_{Xj}^{1-4} - I_{Xj}^{2-3})\} \\
& + c\{-(\sqrt{3}\cos\xi + \sin\xi)(I_{Xi}^{1-2} + I_{Xi}^{3-4})\cos K't - (I_{Yi}^{1-2} - I_{Yi}^{3-4})\sin K't) \\
& \quad + (I_{Xi}^{1-4} + I_{Xi}^{2-3}) + (\sqrt{3}\sin\xi - \cos\xi)(I_{Xi}^{1-4} - I_{Xi}^{2-3})\} \\
& \times \{(I_{Zj}^{1-4} - I_{Zj}^{2-3}) + 2\cos\xi(I_{Zj}^{1-4} + I_{Zj}^{2-3}) \\
& \quad + 2\sin\xi((I_{Xj}^{1-3} - I_{Xj}^{2-4})\cos K't - (I_{Yj}^{2-4} + I_{Yj}^{1-3})\sin K't)\} \\
& + \{(I_{Zi}^{1-4} - I_{Zi}^{2-3}) + 2\cos\xi(I_{Zi}^{1-4} + I_{Zi}^{2-3}) \\
& \quad + 2\sin\xi((I_{Xi}^{1-3} - I_{Xi}^{2-4})\cos K't - (I_{Yi}^{2-4} + I_{Yi}^{1-3})\sin K't)\} \\
& \times \{-(\sqrt{3}\cos\xi + \sin\xi)(I_{Xj}^{1-2} + I_{Xj}^{3-4})\cos K't - (I_{Yj}^{1-2} - I_{Yj}^{3-4})\sin K't) \\
& \quad + (I_{Xj}^{1-4} + I_{Xj}^{2-3}) + (\sqrt{3}\sin\xi - \cos\xi)(I_{Xj}^{1-4} - I_{Xj}^{2-3})\} \\
& + d\{(\sin\xi - \sqrt{3}\cos\xi)(I_{Yi}^{1-2} + I_{Yi}^{3-4})\cos K't + (I_{Xi}^{1-2} - I_{Xi}^{3-4})\sin K't) \\
& \quad - (I_{Yi}^{1-4} - I_{Yi}^{2-3}) + (\sqrt{3}\sin\xi + \cos\xi)(I_{Yi}^{1-4} + I_{Yi}^{2-3})\}
\end{aligned}$$

$$\begin{aligned}
& \times \{ (I_{zj}^{1-4} - I_{zj}^{2-3}) + 2\cos\xi (I_{zj}^{1-4} + I_{zj}^{2-3}) \\
& \quad + 2\sin\xi (I_{xj}^{1-3} - I_{xj}^{2-4}) \cos K't - (I_{yj}^{2-4} + I_{yj}^{1-3}) \sin K't \} \\
& + \{ (I_{zi}^{1-4} - I_{zi}^{2-3}) + 2\cos\xi (I_{zi}^{1-4} + I_{zi}^{2-3}) \\
& \quad + 2\sin\xi (I_{xi}^{1-3} - I_{xi}^{2-4}) \cos K't - (I_{yi}^{2-4} + I_{yi}^{1-3}) \sin K't \} \\
& \times \{ (\sin\xi - \sqrt{3}\cos\xi) (I_{yj}^{1-2} + I_{yj}^{3-4}) \cos K't + (I_{xj}^{1-2} - I_{xj}^{3-4}) \sin K't \\
& \quad - (I_{yj}^{1-4} - I_{yj}^{2-3}) + (\sqrt{3}\sin\xi + \cos\xi) (I_{yj}^{1-4} + I_{yj}^{2-3}) \} ] .
\end{aligned}$$

(II.58)

As pointed out earlier, in the QIF we can drop the terms from  $\tilde{\mathcal{H}}_{rf}'$  and  $\tilde{\mathcal{H}}_{int}'$ , that oscillate at  $\omega$  or  $2\omega$ . This leads to the following expressions for the terms in the Hamiltonian:

$$\begin{aligned}
\tilde{\mathcal{H}}_{rf}' &= -\omega_1(t) [ k(I_x^{1-2} + I_x^{3-4}) + l(I_y^{1-2} - I_y^{3-4}) + m(I_y^{1-2} + I_y^{3-4}) \\
& \quad + n(I_x^{1-2} - I_x^{3-4}) + p(I_x^{1-3} - I_x^{2-4}) + q(I_y^{1-3} + I_y^{2-4}) ] \\
&= -\omega_1(t) \bar{N} ,
\end{aligned}$$

(II.59)

where

$$k = -(1/2)\sin\theta_L \sin\phi_L (\sqrt{3}\cos\xi + \sin\xi)\cos\phi ,$$

$$l = -(1/2)\sin\theta_L \sin\phi_L (\sqrt{3}\cos\xi + \sin\xi)\sin\phi ,$$

$$m = -(1/2)\cos\theta_L (\sqrt{3}\cos\xi - \sin\xi)\cos\phi ,$$

$$n = (1/2)\cos\theta_L (\sqrt{3}\cos\xi - \sin\xi)\sin\phi ,$$

$$p = \sin\theta_L \cos\phi_L \sin\xi \cos\phi ,$$

$$q = \sin\theta_L \cos\phi_L \sin\xi \sin\phi ,$$

(II.60)

and

$$\bar{N} = k(I_X^{1-2} + I_X^{3-4}) + l(I_Y^{1-2} - I_Y^{3-4}) + m(I_Y^{1-2} + I_Y^{3-4}) ;$$

$$+ n(I_X^{1-2} - I_X^{3-4}) + p(I_X^{1-3} - I_X^{2-4}) + q(I_Y^{1-3} + I_Y^{2-4})$$

(II.60a)

$$\tilde{\mathcal{H}}_T' = A_T' (I_Z^{1-2} - I_Z^{3-4}) = A_T' \bar{L} ;$$

(II.61)

$$\tilde{\mathcal{H}}_{D(\text{hetero})}' = F_X \{ (I_{Xj}^{1-4} + I_{Xj}^{2-3}) + (\sqrt{3}\sin\xi - \cos\xi) (I_{Xj}^{1-4} - I_{Xj}^{2-3}) \}$$

$$+ F_Y \{ -(I_{Yj}^{1-4} - I_{Yj}^{2-3}) + (\sqrt{3}\sin\xi + \cos\xi) (I_{Yj}^{1-4} + I_{Yj}^{2-3}) \}$$

$$+ F_Z \{ (I_{Zj}^{1-4} - I_{Zj}^{2-3}) + 2\cos\xi (I_{Zj}^{1-4} + I_{Zj}^{2-3}) \} ,$$

(II.62)

$$\text{where } F_X = \omega_{ij} (a_X I_{Xi} + b I_{Yi} + c I_{Zi}) ,$$

$$F_Y = \omega_{ij} (a_Y I_{Yi} + b I_{Xi} + d I_{Zi}) ,$$

$$F_Z = \omega_{ij} (a_Z I_{Zi} + c I_{Xi} + d I_{Yi}) .$$

(II.63)



$$\tilde{\chi}_{D(\text{homo})}' = \omega_{ij} [a_x \{ (1/2) (\sqrt{3} \cos \xi + \sin \xi)^2$$

$$x \langle (I_{xi}^{1-2} + I_{xi}^{3-4}) (I_{xj}^{1-2} + I_{xj}^{3-4}) + (I_{yi}^{1-2} - I_{yi}^{3-4}) (I_{yj}^{1-2} - I_{yj}^{3-4}) \rangle +$$

$$(I_{xi}^{1-4} + I_{xi}^{2-3}) (I_{xj}^{1-4} + I_{xj}^{2-3})$$

$$+ (\sqrt{3} \sin \xi - \cos \xi) \langle (I_{xi}^{1-4} + I_{xi}^{2-3}) (I_{xj}^{1-4} - I_{xj}^{2-3}) + (I_{xi}^{1-4} - I_{xi}^{2-3}) (I_{xj}^{1-4} + I_{xj}^{2-3}) \rangle$$

$$+ (\sqrt{3} \sin \xi - \cos \xi)^2 (I_{xi}^{1-4} - I_{xi}^{2-3}) (I_{xj}^{1-4} - I_{xj}^{2-3}) \rangle$$

$$+ a_y \{ (1/2) (\sqrt{3} \cos \xi - \sin \xi)^2$$

$$x \langle (I_{yi}^{1-2} + I_{yi}^{3-4}) (I_{yj}^{1-2} + I_{yj}^{3-4}) + (I_{xi}^{1-2} - I_{xi}^{3-4}) (I_{xj}^{1-2} - I_{xj}^{3-4}) \rangle +$$

$$(I_{yi}^{1-4} - I_{yi}^{2-3}) (I_{yj}^{1-4} - I_{yj}^{2-3})$$

$$- (\sqrt{3} \sin \xi + \cos \xi) \langle (I_{yi}^{1-4} + I_{yi}^{2-3}) (I_{yj}^{1-4} - I_{yj}^{2-3}) + (I_{yi}^{1-4} - I_{yi}^{2-3}) (I_{yj}^{1-4} + I_{yj}^{2-3}) \rangle$$

$$+ (\sqrt{3} \sin \xi + \cos \xi)^2 (I_{yi}^{1-4} + I_{yi}^{2-3}) (I_{yj}^{1-4} + I_{yj}^{2-3}) \rangle$$

$$+ a_z \{ (I_{zi}^{1-4} - I_{zi}^{2-3}) (I_{zj}^{1-4} - I_{zj}^{2-3})$$

$$+ 2 \cos \xi \langle (I_{zi}^{1-4} - I_{zi}^{2-3}) (I_{zj}^{1-4} + I_{zj}^{2-3}) + (I_{zi}^{1-4} + I_{zi}^{2-3}) (I_{zj}^{1-4} - I_{zj}^{2-3}) \rangle$$

$$+ 4 \cos^2 \xi (I_{zi}^{1-4} + I_{zi}^{2-3}) (I_{zj}^{1-4} + I_{zj}^{2-3}) \rangle$$

$$+2\sin^2\xi\{(I_{xi}^{1-3}-I_{xi}^{2-4})(I_{xj}^{1-3}-I_{xj}^{2-4})+(I_{yi}^{1-3}+I_{yi}^{2-4})(I_{yj}^{1-3}+I_{yj}^{2-4})\}$$

$$+b((1/2)(3\cos^2\xi-\sin^2\xi)$$

$$x\{(I_{xi}^{1-2}+I_{xi}^{3-4})(I_{yj}^{1-2}+I_{yj}^{3-4})-(I_{yi}^{1-2}-I_{yi}^{3-4})(I_{xj}^{1-2}-I_{xj}^{3-4})+$$

$$(I_{yi}^{1-2}+I_{yi}^{3-4})(I_{xj}^{1-2}+I_{xj}^{3-4})-(I_{xi}^{1-2}-I_{xi}^{3-4})(I_{yj}^{1-2}-I_{yj}^{3-4})\}$$

$$-(I_{xi}^{1-4}+I_{xi}^{2-3})(I_{yj}^{1-4}-I_{yj}^{2-3})+(I_{yi}^{1-4}-I_{yi}^{2-3})(I_{xj}^{1-4}+I_{xj}^{2-3})\}$$

$$-(\sqrt{3}\sin\xi-\cos\xi)\{(I_{xi}^{1-4}-I_{xi}^{2-3})(I_{yj}^{1-4}-I_{yj}^{2-3})+(I_{yi}^{1-4}-I_{yi}^{2-3})(I_{xj}^{1-4}-I_{xj}^{2-3})\}$$

$$+(\sqrt{3}\sin\xi+\cos\xi)\{(I_{xi}^{1-4}+I_{xi}^{2-3})(I_{yj}^{1-4}+I_{yj}^{2-3})+(I_{yi}^{1-4}+I_{yi}^{2-3})(I_{xj}^{1-4}+I_{xj}^{2-3})\}$$

$$+(3\sin^2\xi-\cos^2\xi)\{(I_{xi}^{1-4}-I_{xi}^{2-3})(I_{yj}^{1-4}+I_{yj}^{2-3})+(I_{yi}^{1-4}+I_{yi}^{2-3})(I_{xj}^{1-4}-I_{xj}^{2-3})\}$$

$$+c(-(\sqrt{3}\cos\xi+\sin\xi)\sin\xi\{(I_{xi}^{1-2}+I_{xi}^{3-4})(I_{xj}^{1-3}-I_{xj}^{2-4})+(I_{yi}^{1-2}-I_{yi}^{3-4})(I_{yj}^{1-3}+I_{yj}^{2-4})$$

$$+(I_{xi}^{1-3}-I_{xi}^{2-4})(I_{xj}^{1-2}+I_{xj}^{3-4})+(I_{yi}^{1-3}+I_{yi}^{2-4})(I_{yj}^{1-2}-I_{yj}^{3-4})\}$$

$$+(I_{xi}^{1-4}+I_{xi}^{2-3})(I_{zj}^{1-4}-I_{zj}^{2-3})+(I_{zi}^{1-4}-I_{zi}^{2-3})(I_{xj}^{1-4}+I_{xj}^{2-3})\}$$

$$+2\cos\xi\{(I_{xi}^{1-4}+I_{xi}^{2-3})(I_{zj}^{1-4}+I_{zj}^{2-3})+(I_{zi}^{1-4}+I_{zi}^{2-3})(I_{xj}^{1-4}+I_{xj}^{2-3})\}$$

$$+(\sqrt{3}\sin\xi-\cos\xi)\{(I_{xi}^{1-4}-I_{xi}^{2-3})(I_{zj}^{1-4}-I_{zj}^{2-3})+(I_{zi}^{1-4}-I_{zi}^{2-3})(I_{xj}^{1-4}-I_{xj}^{2-3})\}$$

$$+2\cos\xi(\sqrt{3}\sin\xi-\cos\xi)\{(I_{xi}^{1-4}-I_{xi}^{2-3})(I_{zj}^{1-4}+I_{zj}^{2-3})+(I_{zi}^{1-4}+I_{zi}^{2-3})(I_{xj}^{1-4}-I_{xj}^{2-3})\}$$

$$\begin{aligned}
& +d(-(\sqrt{3}\cos\xi - \sin\xi)\sin\xi\langle(I_{Yi}^{1-2} + I_{Yi}^{3-4})(I_{Xj}^{1-3} - I_{Xj}^{2-4}) - (I_{Xi}^{1-2} - I_{Xi}^{3-4})(I_{Yj}^{1-3} + I_{Yj}^{2-4}) \\
& + (I_{Xi}^{1-3} - I_{Xi}^{2-4})(I_{Yj}^{1-2} + I_{Yj}^{3-4}) - (I_{Yi}^{1-3} + I_{Yi}^{2-4})(I_{Xj}^{1-2} - I_{Xj}^{3-4})\rangle \\
& - \langle(I_{Yi}^{1-4} - I_{Yi}^{2-3})(I_{Zj}^{1-4} - I_{Zj}^{2-3}) + (I_{Zi}^{1-4} - I_{Zi}^{2-3})(I_{Yj}^{1-4} - I_{Yj}^{2-3})\rangle \\
& - 2\cos\xi\langle(I_{Yi}^{1-4} - I_{Yi}^{2-3})(I_{Zj}^{1-4} + I_{Zj}^{2-3}) + (I_{Zi}^{1-4} + I_{Zi}^{2-3})(I_{Yj}^{1-4} - I_{Yj}^{2-3})\rangle \\
& + (\sqrt{3}\sin\xi + \cos\xi)\langle(I_{Yi}^{1-4} + I_{Yi}^{2-3})(I_{Zj}^{1-4} - I_{Zj}^{2-3}) + (I_{Zi}^{1-4} - I_{Zi}^{2-3})(I_{Yj}^{1-4} + I_{Yj}^{2-3})\rangle \\
& + 2\cos\xi(\sqrt{3}\sin\xi + \cos\xi)\langle(I_{Yi}^{1-4} + I_{Yi}^{2-3})(I_{Zj}^{1-4} + I_{Zj}^{2-3}) + (I_{Zi}^{1-4} + I_{Zi}^{2-3})(I_{Yj}^{1-4} + I_{Yj}^{2-3})\rangle\}.
\end{aligned}$$

(II.64)

A few comments about the truncated Hamiltonians in QIF are in order. The process of truncation has projected out the time-independent parts from the various Hamiltonians that commute with the main term in the total Hamiltonian namely, the quadrupole Hamiltonian  $\mathcal{H}_Q$ . These truncated Hamiltonians are also known as the secular part of the respective Hamiltonians. From Eqns II.33 and II.61 it is clear that- save for the coefficients ( $D_\omega K$  in II.33 and  $A'_T$  in II.61) - the secular part of the torsional Hamiltonian has the same form as the efg inhomogeneity Hamiltonian. It is obvious also from the physics of the situation. Torsional oscillations of the units in the sample of which the quadrupolar nucleus is a part, modulate the efg at the site of the nucleus. This results in a time-averaged shift in the NQR frequency of the

system.  $D_{\omega} K$  in Eqn II.33 also is a description of distribution of NQR frequencies (with proper weightages) around the centre frequency. Both can be taken into account by assigning appropriate values to the parameter  $\Delta$  in our calculations. The secular part of the torsional oscillation Hamiltonian is also responsible for quadrupolar relaxation of the system [2,100,101]

## II.F. The Observables in the NQR Experiment

The signal that is observed in any NQR experiment is due to the voltage that is induced in the detector by the magnetization of the system under study. In other words, the signal is proportional to the bulk magnetization of the NQR sample along the axis of the detector coil. We define therefore, the laboratory frame observable at the radiation frequency  $\omega$  in the NQR experiment to be the magnetization operator given by :

$$B_1 = \cos(\omega t + \phi_1) I_y \quad , \quad (\text{II.65})$$

where  $\phi_1$  tells us about the phase of the detected NQR signal.  $\phi_1$  is an experimentally adjustable parameter and is related to the phase of the detector. A point to be noted here is that the phase  $\phi$  of the pulses and also of the magnetization operator correspond, in NMR, to the directions in the x-y plane of the rotating frame, i.e. Zeeman Interaction Frame. As pointed out earlier, QIF has no simple geometrical interpretation. An analogous assignment of directions corresponding to phases in NQR is therefore meaningless.

For an arbitrary orientation of the axis of the detector coil with respect to QPAS, Eqn II.65 will take the form :

$$B_1 = \cos(\omega t + \phi_s) (\sin\phi_L \sin\theta_L I_{LX} + \cos\theta_L I_{LY} + \cos\phi_L \sin\theta_L I_{LZ}) \quad (II.66)$$

Using the transformation Eqn II.30 to transform II.66 to the frame where  $\mathcal{H}_Q$  is diagonal, we obtain :

$$\begin{aligned} B_1' = \cos(\omega t + \phi_s) [ & \{ -( \sqrt{3} \cos\xi + \sin\xi ) ( I_X^{1-2} + I_X^{3-4} ) + ( I_X^{1-4} + I_X^{2-3} ) \\ & + ( \sqrt{3} \sin\xi - \cos\xi ) ( I_X^{1-4} - I_X^{2-3} ) \} \sin\theta_L \sin\phi_L \\ & + \{ -( \sqrt{3} \cos\xi - \sin\xi ) ( I_Y^{1-2} + I_Y^{3-4} ) - ( I_Y^{1-4} - I_Y^{2-3} ) \\ & + ( \sqrt{3} \sin\xi + \cos\xi ) ( I_Y^{1-4} + I_Y^{2-3} ) \} \cos\theta_L \\ & \{ ( I_Z^{1-4} - I_Z^{2-3} ) + 2 \cos\xi ( I_Z^{1-4} + I_Z^{2-3} ) \\ & + 2 \sin\xi ( I_X^{1-3} - I_X^{2-4} ) \} \sin\theta_L \cos\phi_L ] \quad (II.67) \end{aligned}$$

In QIF Eqn II.67 will take the form :

$$\begin{aligned} \tilde{B}_1' = \cos(\omega t + \phi_s) [ & \{ -( \sqrt{3} \cos\xi + \sin\xi ) \{ ( I_X^{1-2} + I_X^{3-4} ) \cos K' t - \\ & ( I_Y^{1-2} - I_Y^{3-4} ) \sin K' t \} + ( I_X^{1-4} + I_X^{2-3} ) \end{aligned}$$

$$\begin{aligned}
& +(\sqrt{3}\sin\xi - \cos\xi)(I_X^{1-4} - I_X^{2-3})\sin\theta_L \sin\phi_L \\
& +\{-(\sqrt{3}\cos\xi - \sin\xi)(I_Y^{1-2} + I_Y^{3-4})\cos K't + (I_X^{1-2} - I_X^{3-4})\sin K't\} \\
& -(I_Y^{1-4} - I_Y^{2-3}) + (\sqrt{3}\sin\xi + \cos\xi)(I_Y^{1-4} + I_Y^{2-3})\cos\theta_L \\
& +\{(I_Z^{1-4} - I_Z^{2-3}) + 2\cos\xi(I_Z^{1-4} + I_Z^{2-3}) \\
& + 2\sin\xi[(I_X^{1-3} - I_X^{2-4})\cos K't - (I_Y^{2-4} + I_Y^{1-3})\sin K't]\sin\theta_L \cos\phi_L\} .
\end{aligned}$$

(II.68)

The part that is time dependent in Eqn II.68 does not contribute to the signal we observe. Therefore, we truncate in the usual way, i.e. ignoring terms which oscillate rapidly (or of order  $\omega_Q$  and higher) we obtain :

$$\begin{aligned}
\tilde{B}_1 &= k_g(I_X^{1-2} + I_X^{3-4}) + l_g(I_Y^{1-2} - I_Y^{3-4}) + m_g(I_Y^{1-2} + I_Y^{3-4}) \\
&+ n_g(I_X^{1-2} - I_X^{3-4}) + p_g(I_X^{1-3} - I_X^{2-4}) + q_g(I_Y^{1-3} + I_Y^{2-4}) \\
&= \bar{N}_g
\end{aligned}$$

(II.69)

where

$$\begin{aligned}
 k_s &= -(1/2) \sin \theta_L \sin \phi_L (\sqrt{3} \cos \xi + \sin \xi) \cos \phi_s , \\
 l_s &= -(1/2) \sin \theta_L \sin \phi_L (\sqrt{3} \cos \xi + \sin \xi) \sin \phi_s , \\
 m_s &= -(1/2) \cos \theta_L (\sqrt{3} \cos \xi - \sin \xi) \cos \phi_s , \\
 n_s &= (1/2) \cos \theta_L (\sqrt{3} \cos \xi - \sin \xi) \sin \phi_s , \\
 p_s &= \sin \theta_L \cos \phi_L \sin \xi \cos \phi_s , \\
 q_s &= \sin \theta_L \cos \phi_L \sin \xi \sin \phi_s ,
 \end{aligned}
 \tag{II.70}$$

and

$$\begin{aligned}
 \bar{N}_s &= k_s (I_X^{1-2} + I_X^{3-4}) + l_s (I_Y^{1-2} - I_Y^{3-4}) + m_s (I_Y^{1-2} + I_Y^{3-4}) \\
 &\quad + n_s (I_X^{1-2} - I_X^{3-4}) + p_s (I_X^{1-3} - I_X^{2-4}) + q_s (I_Y^{1-3} + I_Y^{2-4}) .
 \end{aligned}
 \tag{II.70a}$$

Eqn II.69 is the expression used for the calculation of the laboratory frame signal under various experimental situations as will be seen in the following. The in-phase signal ( $B_{in}$ ) will be obtained when  $\phi_s = 0$ . Similarly when  $\phi_s = \pi/2$ , the signal ( $B_{out}$ ) is out of phase.

## II.G. The Density Operator and the Observations in an NQR experiment

The interaction frame is more than a mathematical trick. Due to the usual design of a typical pulsed NQR spectrometer, experimental observations have a lot to do with the interaction frame. To show this, it is first necessary to present the quantum mechanical description of a statistical assembly of spin systems and observables [115-118]

### The Density Operator

A spin system is described by a density operator  $\rho(t)$ . If the system is in a pure state  $|\psi(t)\rangle$ , the corresponding density operator is :

$$\rho(t) = |\psi(t)\rangle\langle\psi(t)| \quad . \quad (II.71)$$

The system may also be and generally is, in a mixed state or an incoherent superposition of states. In that case it cannot be described by a single ket, but can be described by the density operator :

$$\rho(t) = \sum_{nm} C_{nm}(t) |n\rangle\langle m| \quad , \quad (II.72)$$

Where  $\{|n\rangle\}$  is a complete basis of orthonormal states and is chosen according to the convenience that can result in tackling the problem at hand.  $\rho(t)$  is Hermitian, so that  $C_{nm} = C_{mn}^*$ .



The evolution of  $\rho(t)$  is governed by the Liouville-von Neumann equation [119,115,116] :

$$\frac{d\rho(t)}{dt} = i[\rho(t), \mathcal{H}] \quad . \quad (II.73)$$

The formal solution to Eqn II.73 is :

$$\rho(t) = U(t)\rho(0)U(t)^{-1} \quad , \quad (II.74)$$

where the time - evolution operator  $U(t)$  may generally be written :

$$U(t) = T \exp(-i \int_0^t \mathcal{H}(t') dt') \quad . \quad (II.75)$$

Using the Dyson time-ordering operator  $T$  [120];  $U(t)$  is commonly called the propagator in magnetic resonance literature. The same propagator governs the evolution of pure states :

$$|\psi(t)\rangle = U(t)|\psi(0)\rangle \quad (II.76)$$

Given the density operator the expectation value  $b$  of an observable represented by Hermitian operator  $B$ , can be expressed as a trace :

$$b = \text{Tr}(B\rho) \quad . \quad (II.77)$$

The laboratory frame observable in an NQR experiment is typically the  $y$ -component of the bulk nuclear magnetization in the

x-y plane of the laboratory. The corresponding observable operator is  $B_{out}$  in Eqn II.65 with  $\phi_s = \pi/2$ . Thus the observed signal  $S(t)$ , is :

$$S(t) = \text{Tr} [B_{out} U_L(t) \rho(0) U_L(t)^{-1}] \quad (II.78)$$

Here  $U_L(t)$  is the propagator in the laboratory frame.

Eqns II.37 and II.43 imply that the propagator  $U(t)$  in the interaction frame is related to that in the laboratory frame by :

$$U_L(t) = \exp(-i\omega_0 t) U(t) \quad (II.79)$$

Substituting Eqn II.79 into II.78, it can be shown that :

$$S(t) = \text{Tr} [B_{out} U(t) \rho(0) U(t)^{-1}] \cos \omega t - \text{Tr} [B_{in} U(t) \rho(0) U(t)^{-1}] \sin \omega t \quad (II.80)$$

where  $B_{in}$  is obtained by putting  $\phi_s = 0$  in Eqn II.69.

In NQR experiments the detected signal corresponds to the coefficients of  $\cos \omega t$  and  $\sin \omega t$  in Eqn II.80 and they are known as in- and out-of-phase components of the signal respectively. The signal components in an NQR experiment can either be in - or out-of-phase or both.

Experimentally, the signal  $S(t)$  is divided into two, which are mixed separately with two rf reference signals, one

proportional to  $\cos\omega t$  and the other to  $\sin\omega t$ . The two results after mixing are then passed through separate low-pass audio filters. Sending the signal through low-pass filter is mathematically equivalent to the throwing away of high-frequency terms, i.e., going from Eqn II.68 to Eqn II.69. This process of mixing and filtering has the effect of extracting signals that are proportional to the coefficients of  $\cos\omega t$  and  $\sin\omega t$ . The two extracted signals are stored as the real and imaginary parts of a complex signal  $S_+(t)$  :

$$S_+(t) = -\text{Tr}[B_+ U(t) \rho(0) U(t)^{-1}] \quad , \quad (\text{II.81})$$

with  $B_+ = B_{in} + iB_{out}$ . The experimental arrangement is illustrated in Figure II.3.

The above discussion illustrates the point that in NQR, just as in NMR, the experiments are performed in an interaction frame. However, there are important differences between an NMR and an NQR experiment. In NQR this interaction frame does not rotate with the magnetic field component of the external rf field perturbation, while in NMR the Zeeman interaction frame coincides with a frame rotating in the same sense as one of the two circularly polarized components of the rf magnetic field. In NQR there is no simple geometrical relationship between the quadrupole interaction frame and any frame associated with the rf.

It is pertinent to mention here that, unlike in NMR of spin  $1/2$ , the classical notion of precession of angular momentum

Figure II.3: Schematic design of an NQR receiver that allows observations to be made of the signal in QIF. Signals ( $\text{dB}_{\text{in(out)}}$ / $\text{dt}$ ) near the rf receiver frequency are mixed independently with rf references with a  $\pi/2$  phase difference. This mixing with  $\pi/2$  and 0 rf reference is equivalent to multiplying the  $B_{\text{out}}$  and  $B_{\text{in}}$  components of the signal by  $\cos\omega t$  and  $\sin\omega t$ , respectively. The complex audio signal after filtering corresponds to the in- and out-of-phase components of the signal that we observe. Passing through low-pass filters is mathematically equivalent to throwing away of the high-frequency terms in QIF in lowest order perturbation theory.

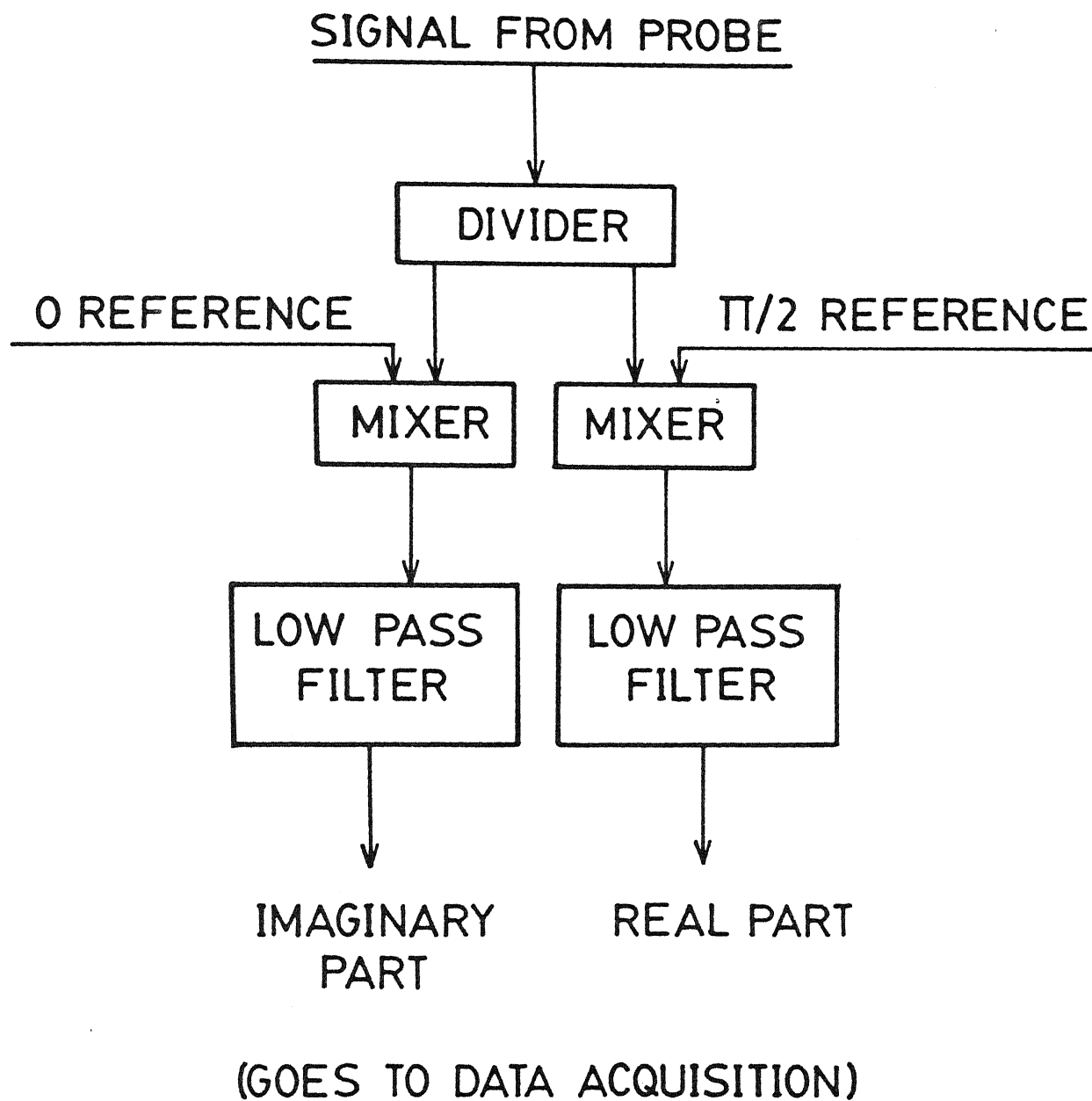


Figure II-3

completely breaks down in the case of NQR [121]. The full quantum mechanical solution of the problem [121] in case of spin 1 and  $3/2$  in quadrupole field does not give anything analogous to the classical Larmor precession. In NQR, therefore, it is useful to talk only about resonant absorption of the nuclei from the applied external field that causes the transitions. In NMR of spin  $1/2$ , the dropping out of oscillating terms, when viewed classically, corresponds to the neglect of the effect of the counter-rotating component of the oscillating rf magnetic field. When not neglected, this component of the oscillating rf magnetic field gives rise to the Bloch-Siegert shift [122]. This, however, is not the case in NQR. We can not associate the oscillating terms in QIF to the dropping of one of the components of linearly oscillating rf magnetic field. As stated earlier, we can only say that this process corresponds to a first order perturbation treatment of the time-dependent quantum mechanical system. The selective excitation ( $+3/2 \leftrightarrow +1/2$  or  $-3/2 \leftrightarrow -1/2$ ) experiment [123-125] using circularly polarized rf field can be understood with the help of Wigner-Eckart theorem [126-129] without invoking the misleading concept of precession of angular momentum in quadrupolar nuclei and its coupling with the circularly polarized rf of the correct sense.

## II.H. Pulse Sequence Propagators

### 1. General Remarks

The effect of an rf pulse sequence on a spin system is given

by the propagator, defined most generally in Eqn II.75. Eqn II.75 can be viewed in several ways. The exponential operator can be expanded in a series :

$$U(t) = T \left[ 1 - i \int_c^t \mathcal{H}(t') dt' - \frac{1}{2} \left( \int_0^t \mathcal{H}(t') dt' \right)^2 + \dots \right] . \quad (\text{II.82})$$

The time-ordering operator  $T$ , performs the following function:

$$T \mathcal{H}(t_1) \mathcal{H}(t_2) = \begin{cases} \mathcal{H}(t_1) \mathcal{H}(t_2) , & t_1 \geq t_2 \\ \mathcal{H}(t_2) \mathcal{H}(t_1) , & t_1 < t_2 \end{cases} . \quad (\text{II.83})$$

Use of Eqn II.83 enables us to write Eqn II.82 as

$$U(t) = 1 - i \int_0^t dt_1 \mathcal{H}(t_1) - \frac{1}{2} \int_0^t dt_1 \int_0^{t_1} dt_2 \mathcal{H}(t_1) \mathcal{H}(t_2) + \dots . \quad (\text{II.84})$$

Eqn II.84 is the Dyson series expression for a propagator [120]. If the Hamiltonian is piecewise constant, equal to  $\mathcal{H}_1, \mathcal{H}_2, \mathcal{H}_3, \dots$ , during successive intervals of length  $t_1, t_2, t_3, \dots$ , the propagator can be written as

$$U(t) = \exp(-i\mathcal{H}_n t_n) \dots \exp(-i\mathcal{H}_2 t_2) \exp(-i\mathcal{H}_1 t_1) . \quad (\text{II.85})$$

$$t = \sum_i t_i \quad . \quad (II.86)$$

If the Hamiltonian varies continuously in time, one may imagine the total time interval  $t$  to be divided into many small subintervals during which the Hamiltonian is essentially constant. Then an expression like Eqn II.85 holds to an increasingly good approximation as the number of subintervals increases. Thus, for a general time-dependent Hamiltonian :

$$U(t) = \lim_{N \rightarrow \infty} \exp(-i\mathcal{H}(t) t/N) \dots \exp(-i\mathcal{H}(2t/N) t/N) \exp(-i\mathcal{H}(t/N) t/N). \quad (II.87)$$

The expression in Eqn II.75 can be thought of as a shorthand for Eqn II.87

The interaction frame Hamiltonian during an ideal pulse sequence is piecewise constant. Propagators for Hamiltonians that are not piecewise constant are considered in detail in Chapter IV and also in Chapter V.

## 2. The propagator and the geometrical view of evolution of the density operator in a multiple-pulse NQR experiment

In NQR experiments, it is generally a good approximation to consider the individual quadrupolar nuclei to be isolated spins during a pulse, since the scalar couplings are very small compared to typical values of  $\omega_1^0$ . The Hamiltonian during a pulse is therefore :



$$\tilde{\mathcal{H}}' \cong \tilde{\mathcal{H}}'_{rf} \quad . \quad (II.88)$$

Mention may be made here of the fact that when the duration for which the pulse is on is very long, as for example in zero-time resolution pulse as explained in Chapter III, the internal Hamiltonians can no longer be neglected even during the pulse. This will be elaborated in detail in Chapter III.

If the pulse is of duration  $\tau$ , the propagator for this duration is :

$$U(\tau) = \exp [-i\tilde{\mathcal{H}}'_{rf}\tau] \quad . \quad (II.89)$$

From Eqn II.59 it is clear that in QIF the Hamiltonian of the system during the pulse is time-independent. When the pulse is off, i.e., during the time interval between two pulses, the time-development of the system is governed by

$$\tilde{\mathcal{H}}' \cong \tilde{\mathcal{H}}'_{int} \quad . \quad (II.90)$$

With the corresponding propagator given by :

$$U(t) = \exp [-i\tilde{\mathcal{H}}'_{int}t] \quad . \quad (II.91)$$

The density operator at any time  $t$ , is (Eqn II.72)

other by an orthogonal transformation. This orthogonal transformation is a rotation in a  $(2I+1)^2-1$  dimensional vector space of column vectors whose components are the independent parameters defined above. In the particular case of spin  $3/2$  the vector space is 15-dimensional.

The most general state of a quantum mechanical spin system is best described by the well-known irreducible spherical tensor operators [128-129]. They provide physical insight into the process of creation and destruction of various order polarizations during the evolution of the system under various perturbations, both external and internal. The density operator for spin  $I$ , resolved into the components of irreducible spherical tensors, has the form [117,130,131]

$$\rho_I(t) = (1/2I+1) \left[ 1 + \sum_{k=1}^{2I} \sum_{q=-k}^k T_{kq}(I) P_{kq}(t) \right] \quad , \quad (\text{II.96})$$

where  $T_{kq}(I)$  is  $k$ th rank irreducible spherical tensor for spin  $I$ , and the polarizations  $P_{kq}(t)$  are in general time-dependent. Both

$T_{kq}$  and  $P_{kq}$  satisfy the Hermiticity constraint :

$$\begin{aligned} (T_{kq})^\dagger &= (-1)^q T_{k,-q} \quad , \\ P_{kq}^* &= (-1)^q P_{k,-q} \quad . \end{aligned} \quad \left| \quad (\text{II.97}) \right.$$

Clearly, the evolution of the system of nuclear spins  $I$  is a rotation of column vectors whose components are the polarizations

$P_{kq}(t)$ ;  $k=1, \dots, 2I$ ;  $q=-k, \dots, +k$ . Evolution under rf pulses (rank 1 tensor, Eqn II.3a) conserves the rank  $k$  of  $P_{kq}$ , but changes  $q$ ; evolution under internal Hamiltonians (rank 2 tensors, Eqns II.4a, II.10a and II.11a) does not conserve the  $k$ th rank polarization.

For spin  $1/2$ ,  $k=1$ ;  $q=-1, 0, +1$ . The rotations referred to above are in 3-dimensions and the polarizations are all rank 1, i.e. the vector polarizations. The rotations of these vector polarizations can be visualized by using Bloch vector model [132] and they represent the rotations we are familiar with in 3-dimensions. In usual magnetic resonance experiments only vector polarizations (rank 1 polarization) are detectable.

For spins  $I \geq 1$ , higher rank polarizations i.e. tensor polarizations, also contribute to the evolution of the system and a simple Bloch vector kind of geometrical picture is then not possible. For example in spin 1, rank 2 polarizations come into play and the evolution of the system is on a surface of 8-dimensional sphere.

For spin  $3/2$  nuclear ensemble, the tensor polarizations of rank 1, 2 and 3 contribute to the evolution of the system. Mention may be made here that in usual NMR experiments also for nuclei with spin  $I \geq 1$ , it is only the vector polarization (i.e. rank 1 polarization), that is detected.

In spite of the physical insight the irreducible spherical tensors provide, we have not used this basis for our calculations

here. Instead, we have resolved the density operator for the mathematical convenience in single transition operator basis :

$$\rho(t) = a_0 \mathbf{1} + \sum_{i,j} \sum_{p=X,Y,Z} a_p^{i-j}(t) I_p^{i-j} . \quad (\text{II.98})$$

For spin  $3/2$ ;  $i, j = 1, 2, \dots, 4$ . The single transition operators are an over-representation of the space spanned by spin  $I$ . Nevertheless, as will be seen in the following, it is quite useful for NQR spin-dynamics problems.

### II.1. The equilibrium density operator

The pulse sequence propagator acts on the initial density operator, transforming it to a final density operator according to the Liouville-von Neumann equation II.73. If the initial density operator describes a spin system at equilibrium, it is given by :

$$\rho_{eq} = \exp(-\mathcal{H} / kT) / \text{Tr}[\exp(-\mathcal{H}/kT)] , \quad (\text{II.99})$$

where  $\mathcal{H}$  is the Hamiltonian of the system with no rf fields present. Since the dominant term in  $\mathcal{H}$  is the quadrupole term and since  $\omega_Q \ll kT$  at temperatures above a few degrees K, it is a good approximation to write :

$$\rho_{eq} = [1 + \mathcal{H}_Q / kT] / N . \quad (\text{II.100})$$

Here  $N$  is the total number of spin states, or the dimension of the system. This is the high temperature approximation [3,4,17,133]. The unit operator part of  $\rho_{eq}$ , commutes with all propagators and does not contribute to the observed signals. Therefore, it is usually dropped along with the constant of proportionality multiplying  $\mathcal{H}_0$ , which only determines the absolute signal amplitude, leaving an initial reduced equilibrium density operator of  $\mathcal{H}_0$ .

The equilibrium density operator being proportional to  $\mathcal{H}_0$ , is a second rank tensor (Eqn II.a). The first or the preparatory pulse prepares the system for observation in the x-y plane of the laboratory. The density operator during this time evolves in a 5-dimensional subspace of the full space. It is only after this pulse, when internal Hamiltonians come into play, that various order polarizations start getting mixed and for all subsequent times the evolution is in the full space of spin I.

## II.J. The NQR Line Shapes

### 1. General Remarks

The various external rf field perturbation schemes affect the different internal static and dynamic interactions in a bulk sample differently. The overall magnetic resonance signal, i.e. the resonance line shape, depends markedly on these interactions and any modification of them results in a suitably modulated line

shape. It is therefore essential to evaluate very closely the relation between the internal interactions and the line shape.

All contributions to a magnetic resonance line can be broadly classified as homogeneous or inhomogeneous. The purest form of a homogeneous line is the one without separate contributions to different parts of the line, i.e. all the nuclei in that line make identical contributions with their intrinsic linewidths the same as the composite. There are then no spectral shifts with respect to each other due to individual contributions. An inhomogeneously broadened line, on the other hand is a sum of non-overlapping individual lines. The line shape in this case is determined by a distribution of shifts. Although there may be some life-time broadening connected with individual spectral packets, no coupling between them exists\*. Figure II.4 illustrates pictorially the ideas so far discussed [134-136].

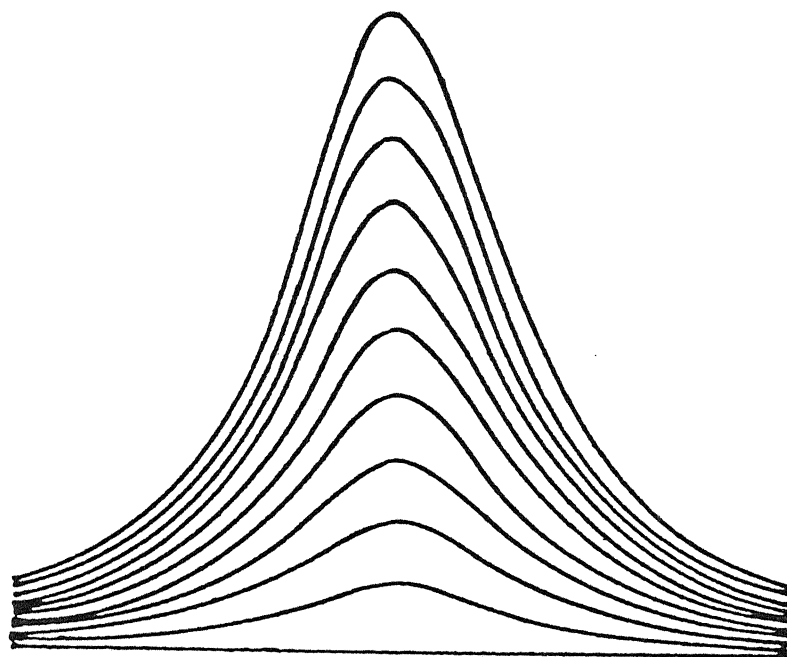
The following are some of the interactions in solids that will give rise to a homogeneous broadening of the magnetic resonance line shape :

- (a) Dipolar interaction between like spins
  - (b) Spin-lattice relaxation
  - (c) Interaction with the radiation field
  - (d) Motionally narrowed fluctuations in the local field,
- etc.

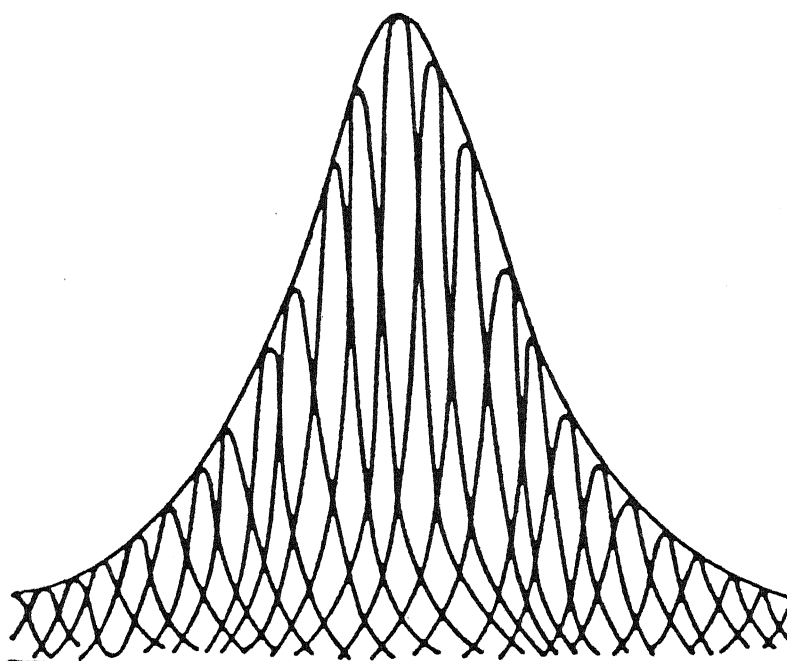
---

\*In case there is a coupling between the spectral packets, the line is known as a heterogeneous line.

Figure II.4 : Schematic diagram showing (a) homogeneous broadening and (b) inhomogeneous broadening [135,136].



(a)



(b)

Figure II.4



Some typical sources of inhomogeneous broadening include :

- (a) Hyperfine interactions
- (b) Anisotropy broadening
- (c) Dipolar broadening between spins with different Larmor frequencies (heteronuclear dipolar interaction)
- (d) Inhomogeneities in the electric field gradient (efg) in pure quadrupole resonance and
- (e) The applied magnetic field in the case of NMR.

The broadening due to dipolar interaction deserves a special note. Both homo- and heteronuclear dipole couplings give rise to a variation in the local fields at the site of the resonant nucleus. Thus, in principle, we should have an inhomogeneously broadened line in both the cases. However, in the case of homonuclear dipole interaction, the energy absorbed at one frequency of the dipolar broadened resonance line is quickly transferred to all the spins, whether or not they are in a local field exactly corresponding to the applied rf frequency [134,137,138]. This assumption is justified because of the possibility of mutual spin-flips between neighboring nuclei brought about by the dipolar interactions. Thus in this case the line becomes homogeneous. In the heteronuclear dipole case, the mutual spin flip between neighboring nuclei becomes difficult as their Larmor frequencies are 'too far apart. Therefore, the line remains inhomogeneous.

In case of spin-lattice relaxation the spin-flip, and hence

the transfer of energy to the lattice, comes about because of the coupling of the spins with the appropriate lattice modes. The broadening is again homogeneous. Since the other interactions do not interest us in the present work, we shall not discuss them here.

## 2. The spin 3/2 NQR Line Shape

The static inhomogeneous contributions to the NQR line shape comes mainly from efg inhomogeneity and also to a lesser extent from heteronuclear dipole interactions.

The homogeneous line-width in an NQR system has its major contribution from coupling of the quadrupolar nuclei to the oscillating efg due to various modes of lattice vibrations. In our calculations this line-width will be described by the secular part of the torsional oscillation Hamiltonian, Eqn.II.61. Unlike in solid state NMR of protons, the homonuclear dipole Hamiltonian contributes to the homogeneous line-width of the line in a very insignificant manner. Generally, this is because of the large size of the quadrupolar nuclei and their low magnetogyric ratios as compared to that of a proton. The calculations of Gutowsky and Woessner [101] show that the torsional oscillation is  $10^8$  to  $10^{10}$  times more powerful in relaxing the quadrupolar nuclei than the dipole coupling.

## II.K. Summary

This Chapter serves as the foundation for the ones that follow. After introducing all the Hamiltonians that are at work

in spin  $3/2$  NQR in the usual Cartesian basis of angular momentum operators, we have presented these Hamiltonians in a representation where it is most convenient to follow mathematically the time-development of the system. To begin with, the Hamiltonians are defined in their respective principal axis systems(PAS). The quadrupole Hamiltonian is the main term in the overall Hamiltonian and, therefore, all the other Hamiltonians are then expressed in the Quadrupole Principal Axis System(QPAS). To simplify later mathematical developments, all the Hamiltonians are now converted to a representation where the quadrupole Hamiltonian  $\mathcal{H}_Q$  is diagonal. The concept of quadrupole interaction frame (QIF) is then introduced, and all the Hamiltonians are transformed to QIF. In complete agreement with the lowest order perturbation theory, the oscillating terms are dropped here from all the Hamiltonian operator terms. The choice of the operator formalism for simpler description of the system is the generators of the  $SU(4)$  Lie algebra, known in magnetic resonance as single transition operators or fictitious spin  $1/2$  operators. This completes our task of defining the Hamiltonian of the system for applications to different problems in later Chapters.

We also have described in this Chapter the observables in the NQR experiment. The concept of the density operator and how it helps to follow the time-development of the NQR system using Liouville-von Neumann equation has also been introduced. The

experimental procedure of detecting an NQR signal has been correlated with the calculation of the expectation value of the observable in NQR using the density operator.

A detailed description of the propagators in multiple - pulse experiments has also been included in this Chapter along with a geometrical picture of the evolution of density operator in the space spanned by the basis operators of the spin system.

This Chapter concludes with a discussion of the nature of the internal Hamiltonians and how they modify the NQR line shapes.

In Chapter III, we shall apply the formalism developed here to some simple problems, namely the single pulse response and the two pulse response. Also, the formalism will be applied to the zero-time resolution technique in non-axially symmetric NQR of spin  $3/2$  nuclei.

## CHAPTER III

### ONE- AND TWO- PULSE RESPONSES AND APPLICATION TO ZERO-TIME RESOLUTION (ZTR) TECHNIQUE

In this Chapter the formalism developed in Chapter II is employed for some very well-known phenomena in NQR, namely, the one-puls. response known also as the free induction decay (FID) and the two-pulse response, otherwise known as the spin echo phenomenon. The explicit solutions presented here have been obtained in the past using the standard time-dependent perturbation theory to solve the Schrödinger equation [6] and also the density operator technique [1,139,140] where the solution is obtained by manipulating explicit matrices. Our purpose is to demonstrate the fact that the diagonalized  $\mathcal{H}_Q$  representation and the single transition operator formalism lead to a relative simplification of the typical NQR dynamics calculations. Also, we shall demonstrate theoretically, perhaps for the first time, the validity of zero-time resolution technique to non-axially symmetric NQR of spin 3/2 solids.

#### III.A. A Special Property of the Quadrupole Hamiltonian for Spin 3/2

The quadrupole Hamiltonian in 3/2 space satisfies

$$\mathcal{H}_Q^2 = K^2 \mathbf{1} \quad , \quad \text{(III.1)}$$

where  $K = \frac{\omega}{2} (1 + \eta^2/3)^{1/2}$ .

This was first observed by Pratt [111] in a special basis. Later it was noted by Ravishankar [121] that this property is basis independent. Hence

$$\exp(-i\mathcal{H}_a t) = \cos Kt - \frac{i\mathcal{H}_a}{K} \sin Kt, \quad (\text{III.2})$$

so that the corresponding density operator at any time  $t$ , can also be written in a basis-independent manner as

$$\rho(t) = \rho(0) + \left( \frac{1}{2K} \sin 2Kt + \frac{\sin^2 Kt}{K^2} \mathcal{H}_a \right) [\rho(0), \mathcal{H}_a],$$

(III.3)

where  $\rho(0)$  is the density operator at time 0. We shall be using this property in the following wherever required (see the two pulse response, Section III.C).

### III.B. One-Pulse Response

Let us consider the effect of a single rf pulse (as shown in Figure III.1) on the equilibrium reduced density operator. We have made the simplifying assumption that our assembly is a system of non-interacting nuclei. This problem may now be solved for a very general case of arbitrary flip angle and phase for the pulse. The solution in this form shall be used in forthcoming Sections and later Chapters.

Figure III.1: One-pulse response.

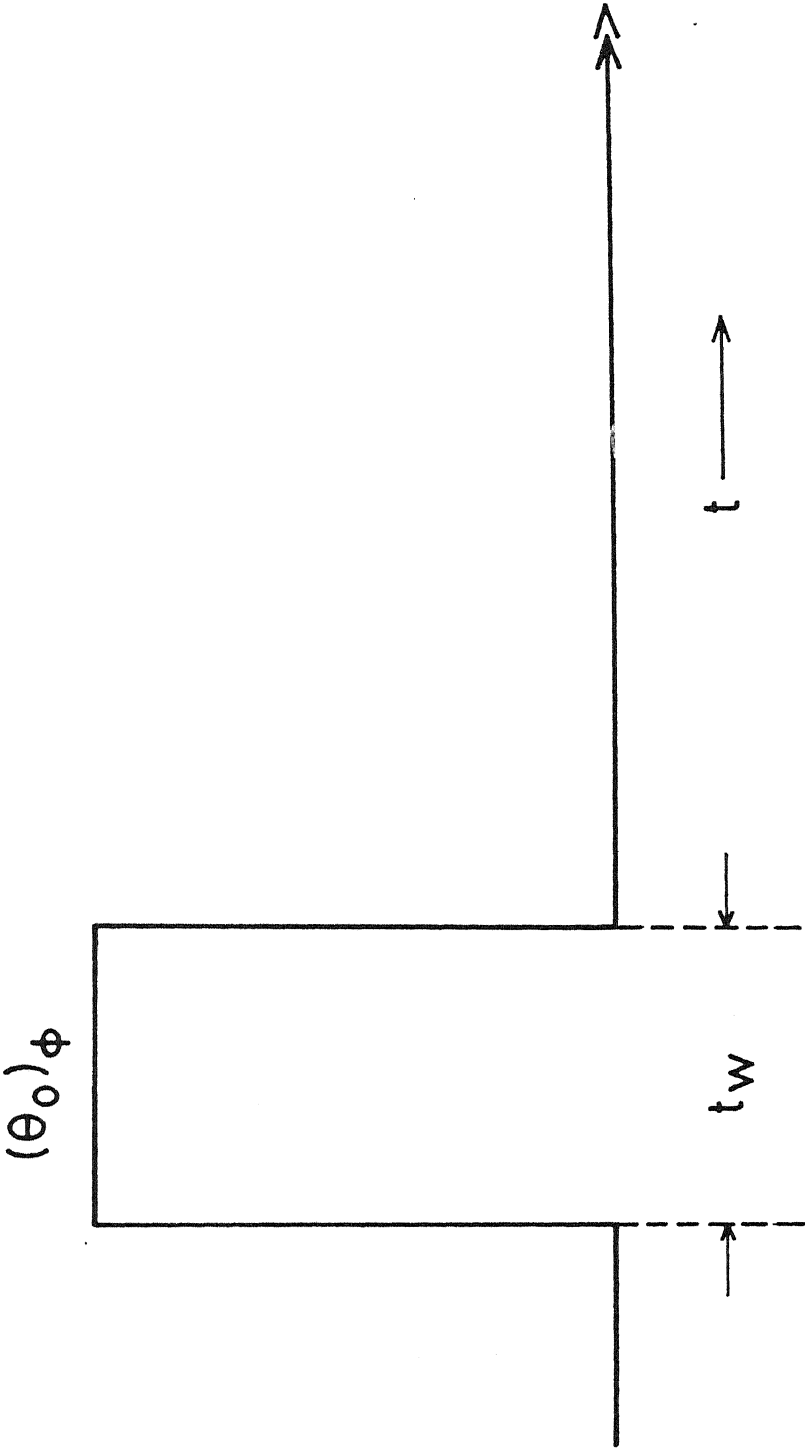


Figure III.1



From Eqn II.100, the reduced equilibrium density operator is

$$\rho_{eq} = \mathcal{H}_Q = K \bar{L} \quad (III.4)$$

The one pulse propagator, from Eqn II.89, is

$$U(t_w) = \exp [-i \tilde{\mathcal{H}}_{rf}' t_w] \quad (III.5)$$

where  $\tilde{\mathcal{H}}_{rf}'$  is defined in Eqn II.59. Using Eqn II.74 :

$$\begin{aligned} \rho(t_w) &= U(t_w) \mathcal{H}_Q U(t_w)^{-1} \\ &= \exp [-i \tilde{\mathcal{H}}_{rf}' t_w] K \bar{L} \exp [i \tilde{\mathcal{H}}_{rf}' t_w] \quad (III.6) \end{aligned}$$

From Eqn II.89, we have

$$\mathcal{H}_{rf}' t_w = -\omega_1^0 \bar{N} t_w = \bar{N} \theta_0 \quad (III.7)$$

where  $-\omega_1^0 t_w = \theta_0$ . Therefore Eqn III.6 gives

$$\rho(t_w) = K \exp(-i \bar{N} \theta_0) \bar{L} \exp(i \bar{N} \theta_0) \quad (III.8)$$

To evaluate Eqn III.8, we use the Baker-Campbell-Hausdorff (BCH) formula [141-151]. It states that for two non-commutative operators A and B, i.e. if  $[A, B] \neq 0$ , then

$$\exp(-iAt) B \exp(iAt)$$

$$= B - (it)[A, B] + \frac{(it)^2}{2!} [A, [A, B]] - \frac{(it)^3}{3!} [A, [A, [A, B]]] + \dots$$

(III.9)

Using Eqn III.9 in Eqn III.8, we obtain :

$$\rho(t_w) = K' \langle \bar{L} \cos(\theta_0 r) - \frac{i\bar{M}}{r} \sin(\theta_0 r) \rangle, \quad \text{(III.10)}$$

where

$$\begin{aligned} \bar{M} = & -ik(I_Y^{1-2} - I_Y^{3-4}) + il(I_X^{1-2} + I_X^{3-4}) + im(I_X^{1-2} - I_X^{3-4}) \\ & -in(I_Y^{1-2} + I_Y^{3-4}) - ip(I_Y^{1-3} + I_Y^{2-4}) + iq(I_X^{1-3} - I_X^{2-4}), \end{aligned}$$

(III.11)

and  $k, l, m, n, p$  and  $q$  were defined already in Eqn II.60. Also, it can be shown that

$$[\bar{N}, \bar{L}] = \bar{M} \quad , \quad \text{(III.12a)}$$

$$[\bar{N}, \bar{M}] = r^2 \bar{L} \quad , \quad \text{(III.12b)}$$

$$[\bar{M}, \bar{L}] = \bar{N} \quad , \quad \text{(III.12c)}$$

where

$$r^2 = k^2 + l^2 + m^2 + n^2 + p^2 + q^2 \quad . \quad (\text{III.12d})$$

Eqn III.10 is the density operator in QIF after a pulse. In principle we can go ahead and calculate the expectation value of the signal using Eqns III.10 and II.69 in Eqn II.77. In order to compare the result with that in the literature, we shall further simplify the situation. We shall assume the case of a single crystal where the rf is applied at resonance ( $\Delta=0$ ) along the y-axis ( $\phi=0$ ;  $\theta_L = \phi_L=0$ ) or along the x-axis ( $\phi=0$ ;  $\theta_L = \phi_L=\pi/2$ ) of the QPAS. Therefore  $K' = K$ , and

(a) detector along y-axis

$$\bar{L} = I_z^{1-2} - I_z^{3-4} \quad , \quad (\text{III.13})$$

$$\bar{N} = \frac{1}{2}(\sin \xi - \sqrt{3}\cos \xi)(I_y^{1-2} + I_y^{3-4}) \quad , \quad (\text{III.14})$$

$$\bar{M} = \frac{1}{2}i(\sin \xi - \sqrt{3}\cos \xi)(I_x^{1-2} - I_x^{3-4}) \quad . \quad (\text{III.15})$$

Also  $r$  reduces to  $r_y$  given by :

$$r_y = \frac{1}{2}(\sin \xi - \sqrt{3}\cos \xi) \quad . \quad (\text{III.16})$$

Therefore Eqn III.10 in this special case reduces to :

$$\rho_y(t_w) = K[(I_z^{1-2} - I_z^{3-4})\cos(\theta_y) + (I_x^{1-2} - I_x^{3-4})\sin(\theta_y)] \quad , \quad (\text{III.17})$$

$$\text{where } \theta_y = \theta_o r_y \quad . \quad (\text{III.17a})$$

(b) Detector along the x-axis :

$$\bar{L} = (I_z^{1-2} - I_z^{3-4}) \quad , \quad (\text{III.18})$$

$$\bar{M} = \frac{1}{2} (I_y^{1-2} - I_y^{3-4}) (\sqrt{3} \cos \xi + \sin \xi) \quad , \quad (\text{III.19})$$

$$\bar{N} = -\frac{1}{2} (I_x^{1-2} + I_x^{3-4}) (\sqrt{3} \cos \xi + \sin \xi) \quad , \quad (\text{III.20})$$

and  $r$  will reduce to  $r_x$  given by :

$$r_x = \frac{1}{2} (\sqrt{3} \cos \xi + \sin \xi) \quad . \quad (\text{III.21})$$

Therefore

$$\tilde{\rho}_x(t_w) = K \{ (I_z^{1-2} - I_z^{3-4}) \cos(\theta_x) + (I_y^{1-2} - I_y^{3-4}) \sin(\theta_x) \} \quad , \quad (\text{III.22})$$

$$\text{where } \theta_x = \theta_o r_x \quad . \quad (\text{III.22a})$$

The corresponding magnetization operator required to calculate the signal from Eqn III.22 is (from Eqn II.69):

$$\tilde{B}_x = -\left(\frac{1}{2}\right)(\sqrt{3}\cos\xi + \sin\xi)(I_Y^{1-2} - I_Y^{3-4}), \quad (\text{III.23})$$

where the phase of the detector  $\phi_s = \pi/2$ . Therefore,

$$\langle \tilde{B}_x \rangle = -\left(\frac{K}{2}\right)(\sqrt{3}\cos\xi + \sin\xi)\sin(\theta_x) \quad (\text{III.24})$$

In the laboratory frame, from Eqn II.80:

$$\langle B_x \rangle = +\left(\frac{K}{2}\right)(\sqrt{3}\cos\xi + \sin\xi)\sin(\theta_x)\sin Kt. \quad (\text{III.25})$$

Substituting for various parameters gives the value of the signal to be :

$$\langle B_x \rangle = \frac{\omega_a}{12}(3+\eta^2)^{1/2}(3+\eta)\sin\left(\frac{\theta}{2} \cdot \frac{(3+\eta)}{(3+\eta^2)^{1/2}}\right)\sin\left(\frac{\omega_a}{6} \cdot (3+\eta^2)t\right). \quad (\text{III.26})$$

From Eqn III.26, the laboratory frame signal for the axially symmetric case ( $\eta=0$ ) is :

$$\langle B_x \rangle_{\eta=0} = \frac{\omega_a}{4}\sqrt{3}\sin((\sqrt{3}/2)\theta_0)\sin((\omega_a/2)t). \quad (\text{III.27})$$

The results III.25 and III.26 compare with the reported expressions for the same [1,2]. It can also easily be shown that there will not be any signal along y and z-axis of QPAS. Also, even along x-axis a signal is possible only when the phase of the

detector  $\phi_s = \pi/2$ . The point to be noted is that phases of the applied rf and detector respectively differ by  $\pi/2$ .

### III.C. Two-Pulse Response :

In this section we consider the effect of the following (Figure III.2) two pulse scheme on the density operator at equilibrium. If the density operator at time  $t > \tau + t_w$  is given by  $\rho(t)$ , then

$$\rho(t) = Q(t-\tau)^{-1} P(t_w)^{-1} Q(\tau)^{-1} \rho(t_w)^{-1} \rho_{eq} P(t_w) Q(\tau) P(t_w) Q(t-\tau), \quad (\text{III.28})$$

where

$$P(t_w) = \exp(i\tilde{\mathcal{H}}_{rf} t_w) = \exp(i\bar{N} \theta_o) = \exp(i(I_x^{1-2} + I_x^{3-4}) \theta_x), \quad (\text{III.29})$$

$$Q(\tau) = \exp(i\mathcal{H}_Q \tau) = \exp(i\Delta_l K (I_z^{1-2} - I_z^{3-4}) \tau), \quad (\text{III.30})$$

$$Q(t-\tau) = \exp(i\Delta_l K (I_z^{1-2} - I_z^{3-4}) (t-\tau)) \quad (\text{III.31})$$

In writing Eqn III.28, we assumed that both the rf pulses are applied along the x-axis of QPAS of a single crystal sample, so that  $\theta_L = \phi_L = \pi/2$ , the phases of both the pulses being  $\phi=0$ . The evolution in QIF in between the two pulses and also after the second pulse is under the quadrupolar Hamiltonian. This is

Figure III.2: Two-pulse or Spin Echo sequence.

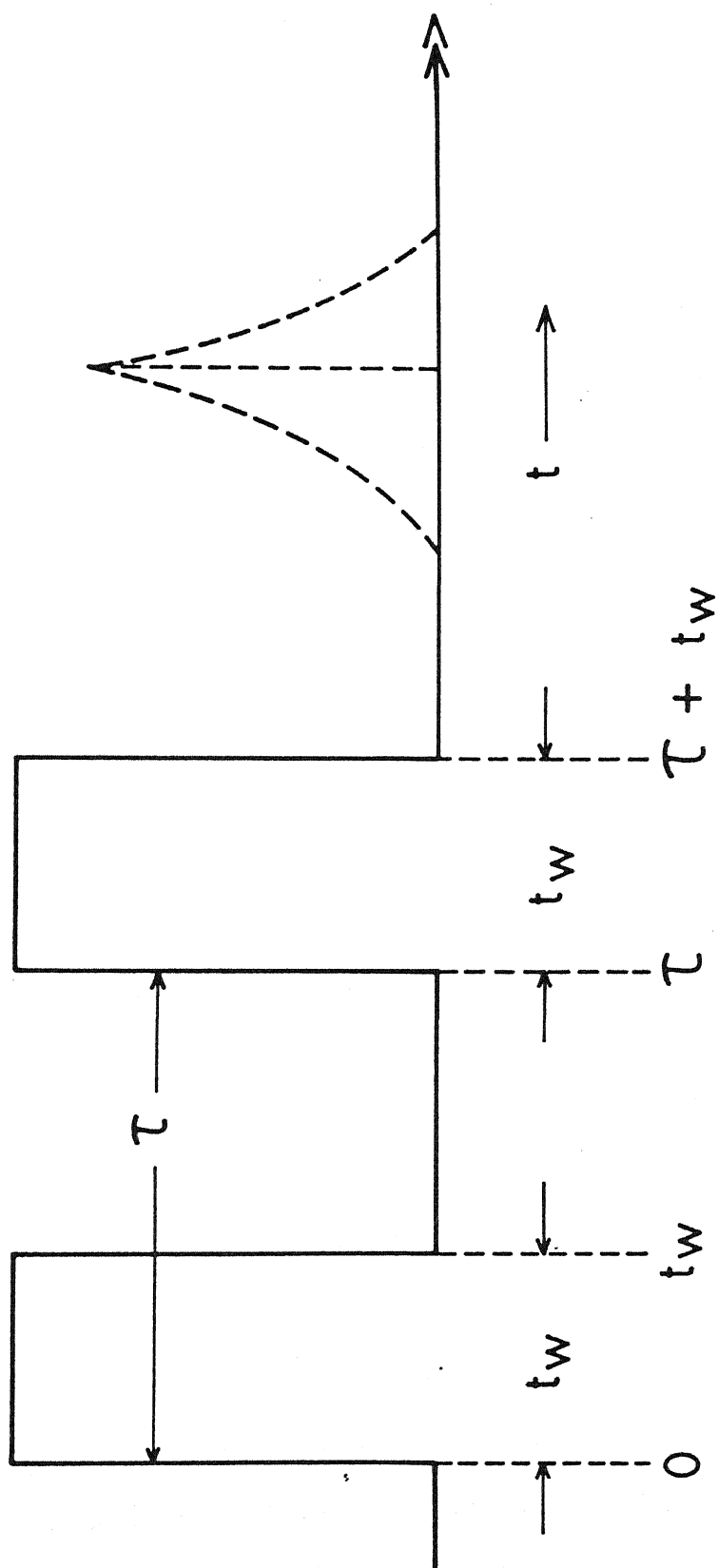


Figure III.2



because we have assumed electric field gradient inhomogeneity in the crystal to see the spin echo effect.  $\Delta_l$  is a factor that incorporates the effect of efg inhomogeneity in Eqns III.30 and III.31.

Using the commutation relations of the single transition operators and Eqn. III.3, we get from Eqn III.26 the expression for density operator at time  $t = \tau + t_w$  as follows:

$$\rho(t) = \alpha_1(I_z^{1-2} - I_z^{3-4}) + \beta_1(I_y^{1-2} - I_y^{3-4}) + \gamma_1(I_x^{1-2} + I_x^{3-4}), \quad (\text{III.32})$$

where

$$\alpha_1 = K (\cos^2 \theta_x - \sin^2 \theta_x \cos(\Delta_l K \tau)) \quad , \quad (\text{III.33a})$$

$$\begin{aligned} \beta_1 = K [\sin(\Delta_l K \tau) \sin \theta_x (\Delta_l K(t-\tau)) - \sin \theta_x - \cos \theta_x (1 + \cos(\Delta_l K \tau)) \\ \times \cos(\Delta_l K(t-\tau))] \quad , \quad (\text{III.33b}) \end{aligned}$$

$$\begin{aligned} \gamma_1 = K [\sin \theta_x \cos \theta_x (1 + \cos(\Delta_l K \tau)) \sin(\Delta_l K(t-\tau)) - \\ \sin(\Delta_l K \tau) \sin \theta_x \cos(\Delta_l K(t-\tau))] \quad . \quad (\text{III.33c}) \end{aligned}$$

The signal  $B_x$  will appear along the x-axis of QPAS. The expression also clearly shows that there can be two signals corresponding to two detector phases  $\phi_s = 0$  and  $\pi/2$ .

When  $\phi_s = 0$ ,

$$\langle B_x \rangle_{\phi_s=0} = -\frac{1}{2} (\sqrt{3}\cos\xi + \sin\xi) \beta_1. \quad (\text{III.34})$$

Also, when  $\phi_s = \pi/2$ ,

$$\langle B_x \rangle_{\phi_s=\pi/2} = -\frac{1}{2} (\sqrt{3}\cos\xi + \sin\xi) \gamma_1. \quad (\text{III.35})$$

Egns III.34 and II.33 can be easily translated into the expression reported [1,2] by substituting for parameters. In this case also there will not be any signal along y and z axis of QPAS.

### III.D. The Zero-Time Resolution Technique applied to NQR of non-axially symmetric systems containing spin 3/2 Nuclei

#### 1. General Remarks

In solids the initial portion of a free induction decay (FID) signal, that has important information, often becomes unobtainable, especially when strong spin-spin coupling among the resonant nuclei is present. This is due to the following:

- (i) The FID function  $F(t)$ , has its temporal origin at approximately the centre of the rf pulse; the NQR signal is not normally observable while the rf excitation pulse is on, so that the effective measurement time of the  $F(t)$  is typically only one-half of the rf pulse length;
- (ii) more seriously, electronic causes also contribute, that is, the initial portion of the FID is masked due to rf transients arising from

- (a) finite  $Q$  (quality-factor) of the various resonant circuits excited by the rf pulse, and
- (b) saturation of the high - gain signal amplifier circuits (on the rf receiver side) due to the feed through of rf power from the excitation pulse [93,152].

In solid state NMR spectroscopy, several techniques have been developed to overcome this problem [90,93,153-156]. Zero-time resolution (ZTR) technique [93,156], so called because it permits one to resolve the signal near time  $t = 0$ , has been found to be simpler and much superior to other methods available in the literature.

In NQR of spin  $3/2$  with a non-zero dipole-dipole coupling among resonant nuclei also, finite recovery time potentially can distort the FID. The possibility of overcoming this finite recovery time was discussed for the first time by Pratt [111]. He used the solid echo sequence of Powles and Strange [153]. More recently Singh and Armstrong [94] have applied the ZTR technique to a spin  $3/2$  system in an axially symmetric electric field gradient ( $\eta=0$ ). But the scope of their work is limited because most of the compounds studied in NQR spectroscopy possess non-axially symmetric electric field gradient ( $\eta \neq 0$ ) [2,157,158]. The purpose of this section is to analyse theoretically the general validity of ZTR method for non-axially symmetric spin  $3/2$  systems also.

## 2. ZTR technique applied to NQR of non-axially symmetric spin $3/2$ systems

ZTR pulse is shown in the following figure :

Figure III.3: The first stage of the ZTR pulse technique. The short initial  $\pi/2$  pulse is followed by a long spin-locking pulse that is phase shifted by  $\pi/2$  with respect to it.

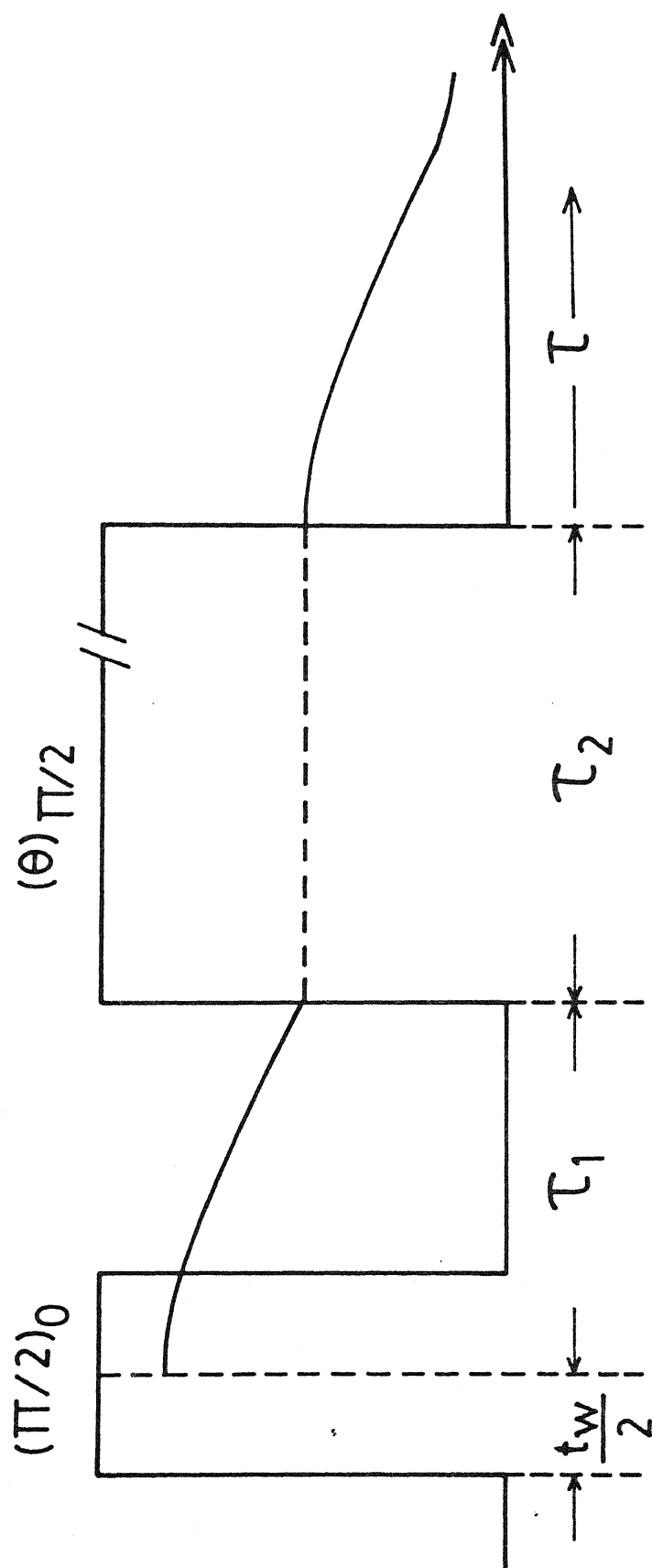


Figure III.3

As is apparent from the above figure, it is essentially a combination of the basic one-pulse experiment followed by one or more spin-locking pulses. The success of this method in recovering the shape of the free induction decay of the equilibrium magnetization following a single rf pulse has been predicted [93] to be dependent on the ability of the long rf pulse to prepare the spin system in the spin-locked state [159,160], that is, on the existence of a spin temperature in the QIF. The effect of the ZTR pulse sequence on a spin 3/2 quadrupolar system can now be evaluated.

The reduced equilibrium density operator of the system under study is (Eqn II.100):

$$\rho_{eq} \simeq \mathcal{H}_Q = K\bar{L} \quad (III.4)$$

Also, we assume a homonuclear dipole coupled nuclear assembly. Therefore, apart from the driving rf Hamiltonian the system will evolve under secular part of the dipole Hamiltonian during ZTR sequence. Let us assume that the pulses are applied at resonance along the y-axis of the laboratory frame. The rf Hamiltonian for the first pulse ( $\phi=0$ ) is, from Eqn II.59,

$$\tilde{\mathcal{H}}_{rf(\alpha)}' = -\omega_{1(\alpha)}(t) \bar{N}_1, \quad (III.36)$$

where

$$\bar{N}_1 = k_1 (I_X^{1-2} + I_X^{3-4}) + m_1 (I_Y^{1-2} + I_Y^{3-4}) + p_1 (I_X^{1-3} - I_X^{2-4}) ,$$

(III.37)

with

$$k_1 = -\left(\frac{1}{2}\right) \sin \theta_L \sin \phi_L (\sqrt{3} \cos \xi + \sin \xi) ,$$

$$m_1 = \left(\frac{1}{2}\right) \cos \theta_L (\sin \xi - \sqrt{3} \cos \xi) ,$$

$$p_1 = \sin \theta_L \cos \phi_L \sin \xi .$$

(III.38)

Eqn III.37 has been derived from Eqns II.80 by putting  $\phi = 0$ .

Similarly, the rf Hamiltonian for the second pulse ( $\phi = \pi/2$ ) is given again, from Eqn II.59, to be :

$$\tilde{\mathcal{H}}'_{rf(z)} = -\omega_{1(2)}(t) \bar{N}_2 ,$$

(III.39)

where

$$\bar{N}_2 = k_1 (I_Y^{1-2} - I_Y^{3-4}) - m_1 (I_X^{1-2} - I_X^{3-4}) + p_1 (I_Y^{2-4} + I_Y^{1-3}) .$$

(III.40)

Also,

$$[\bar{N}_1, \bar{L}] = -i\bar{N}_2 ,$$

(III.41)

$$[\bar{N}_2, \bar{L}] = i\bar{N}_1 \quad , \quad (\text{III.42})$$

$$[\bar{N}_1, \bar{N}_2] = ir_1^2 \bar{L} \quad , \quad (\text{III.43})$$

where

$$r_1^2 = k_1^2 + m_1^2 + p_1^2 \quad . \quad (\text{III.44})$$

The effect of the first pulse of duration  $t_w$ , on the initial density operator is :

$$\tilde{\rho}(t_w) = \exp(+i\omega_{1(\alpha)} t_w \bar{N}_1) K \bar{L} \exp(-i\omega_{1(\alpha)} t_w \bar{N}_1) \quad (\text{III.45})$$

$$= K \{ \bar{L} \cos(\omega_{1(\alpha)}(t) t_w r_1) - \frac{N_2}{r_1} \sin(\omega_{1(\alpha)} t_w r_1) \} \quad . \quad (\text{III.46})$$

For a  $\pi/2$  pulse\*,  $\omega_{1(\alpha)} t_w = \pi/2$ , therefore,

$$\tilde{\rho}(t_w) = -\frac{K}{r_1} \bar{N}_2 \quad . \quad (\text{III.47})$$

---

\*When we are using a powder sample, ' $\pi/2$ ' pulse means a pulse that gives the maximum signal intensity and it corresponds to  $0.86 \pi$ , rather than the single crystal value of  $0.5 \pi$ . A good discussion and derivation of this is given in Petersen's Ph.D. thesis [161].



If we assume the initial applied  $\pi/2$  pulse to be a  $\delta$ -function, then  $t_w \cong 0$ .

After the excitation pulse, and in the absence of any further rf fields, the evolution of the density operator for the spin system is described by

$$\tilde{\rho}(\tau_1 + t_w) = - \frac{K}{r_1} U(\tau_1) \tilde{N}_2 U(\tau_1)^{-1}, \quad (\text{III.48})$$

where

$$U(\tau_1) = \exp(-i \tilde{\mathcal{H}}'_{D(\text{homo})} \tau_1) \quad (\text{III.49})$$

In Eqn III.49,  $\tilde{\mathcal{H}}'_{D(\text{homo})}$  is the time-independent secular part of the homonuclear dipole Hamiltonian given in Eqn II.58.

Now when the second long spin-locking rf pulse is applied, the operator governing the evolution of the system is :

$$U(\tau_2) = \exp(i(\tilde{\mathcal{H}}'_{rf(z)} + \tilde{\mathcal{H}}'_{D(\text{homo})}) \tau_2) \quad (\text{III.50})$$

The second pulse is a soft pulse and its duration is long. Therefore, the effect of  $\tilde{\mathcal{H}}'_{D(\text{homo})}$  can no longer be neglected even during the pulse being on, and hence its inclusion in Eqn III.50. Also  $\tilde{\mathcal{H}}'_{rf(z)} \gg \tilde{\mathcal{H}}'_{D(\text{homo})}$ ; therefore, it is useful to go to a second interaction representation [153] defined by :

$$U_{IF(rf(z))} = \exp(i \tilde{\mathcal{H}}'_{rf(z)} t) \quad (\text{III.51})$$

Labeling  $\tilde{\mathcal{H}}_{D(homo)}''$  as that part of  $\tilde{\mathcal{H}}_{D(homo)}'$  which commutes

with  $\bar{N}_z$ , only  $\tilde{\mathcal{H}}_{D(homo)}''$  is effective in driving the spin system evolution in this interaction representation during the time  $\tau_2$ . Denoting the density operator in the interaction representation of the rf as  $\tilde{\rho}$ , one has :

$$\tilde{\rho}(\tau_2) = \exp(-i\tilde{\mathcal{H}}_{D(homo)}''\tau_2)\tilde{\rho}(0)\exp(i\tilde{\mathcal{H}}_{D(homo)}''\tau_2), \quad (III.52)$$

$$\text{where } \tilde{\rho}(0) = \tilde{\rho}(\tau_1 + t_w) \quad (III.53)$$

At a time  $\tau$  after the spin-locking second pulse has been switched off ,

$$\begin{aligned} & \tilde{\rho}(t_w + \tau_1 + \tau_2 + \tau) \\ &= -\frac{K}{r_1} \exp(-i\tilde{\mathcal{H}}_{D(homo)}'\tau) \{ \exp(-i\tilde{\mathcal{H}}_{D(homo)}''\tau_2) \exp(-i\tilde{\mathcal{H}}_{D(homo)}'\tau_1) \bar{N}_z \\ & \times \exp(i\tilde{\mathcal{H}}_{D(homo)}'\tau_1) \exp(i\tilde{\mathcal{H}}_{D(homo)}''\tau_2) \} \exp(i\tilde{\mathcal{H}}_{D(homo)}'\tau) \quad (III.54) \end{aligned}$$

For the first pulse along the y-axis of the laboratory frame, the magnetization operator is given by putting  $\phi = \pi/2$  in Eqns II.69

and II.70. This can easily be seen to be nothing but  $\bar{N}_2$  given in Eqn III.40. Therefore,

$$\langle \bar{N}_2(t) \rangle = \text{Tr} \{ \tilde{\rho}(t) \bar{N}_2 \} , \quad (\text{III.55})$$

where  $t$  in this case is given by

$$t = t_w + \tau_1 + \tau_2 + \tau \quad (\text{III.56})$$

If Eqn III.55 is to be identical with the FID then  $\rho(t_w + \tau_1 + \tau_2)$  must be diagonal, or else the off-diagonal elements must have no effects on the further evolution of  $\langle \bar{N}_2 \rangle$  after the spin-locking pulse, so that  $\langle \bar{N}_2(t) \rangle$  evolves as though the matrix were diagonal at  $\tau = 0$ . It appears that for  $\tau_2 \gg T_2$ , the latter seems to be the case, although this cannot be shown rigorously. We, therefore, present a semi-rigorous argument that the off-diagonal matrix elements will make a negligible contribution to the evolution of  $\langle \bar{N}_2(t) \rangle$  provided that  $\tau_2 \gg T_2$ . For further justification we have to rely on experimental results.

The useful analogy given by Vollmers et al [93] in case of NMR can also be invoked here. If there exists a component of magnetization along the  $y$ -axis of laboratory frame that is out of phase by  $\pi/2$ , it disappears in a time equal to several  $T_2$ 's due to the effect of the Hamiltonian  $\tilde{\mathcal{H}}'_{D(\text{homo})}$ . The Hamiltonian  $\tilde{\mathcal{H}}''_{D(\text{homo})}$  has the same form with respect to  $\tilde{\mathcal{H}}'_{rf(2)}$  in the second interaction frame as  $\tilde{\mathcal{H}}'_{D(\text{homo})}$  has with respect to  $\mathcal{H}_0$  in QIF,

except for a constant factor. Therefore, its effect in the second interaction frame should be to cause the decay of any component of magnetization in a direction transverse to the direction of  $\tilde{\mathcal{H}}'_{rf(2)}$  at a rate that is inverse to the constant factor. Since  $\tilde{\mathcal{H}}'_{D(homo)}$  and  $\tilde{\mathcal{H}}''_{D(homo)}$  commute with  $\bar{L}$  and  $\bar{N}_2$ , respectively, the magnetization components\*  $\langle \bar{L} \rangle$  and  $\langle \bar{N}_2 \rangle$  would be unaffected. After the magnetization transverse to the direction of  $\tilde{\mathcal{H}}'_{rf(2)}$  has decayed, we may expect that when the spin-locking pulse is removed, the out-of-phase magnetization along the y-axis will be the only net magnetization, and will commence decaying again with the same time dependence as originally, but with the time origin at the end of the spin-locking pulse.

To return to our derivation, the exponential operator in Eqn III.48 can be expanded in a power series so that the density operator at time  $\tau_1$ , can be written as (putting  $t_w = 0$  in the  $\delta$ -pulse limit):

$$\begin{aligned}
 - \frac{\tau_1}{K} \rho(\tau_1) = \bar{N}_2 - \frac{i\tau_1}{1!} [\tilde{\mathcal{H}}'_{D(homo)}, \bar{N}_2] \\
 + \frac{i^2 \tau_1^2}{2!} [\tilde{\mathcal{H}}'_{D(homo)}, [\tilde{\mathcal{H}}'_{D(homo)}, \bar{N}_2]] + \dots \quad (III.57)
 \end{aligned}$$

$$\rho(\tau_1) = \sum_{j=1}^N \chi_{j2}(\tau_1) \bar{N}_{j2} + \sum_{j,k} \chi_{jk1}(\tau_1) \bar{N}_{j1} \bar{L}_k + \dots \quad (III.58)$$

---

\* The magnetization component corresponding to  $\bar{L}$  is not directly detectable in NQR experiments.

Eqn III.58 follows from Eqn III.57 when the commutators are evaluated and various terms collected. The first term in Eqn III.58 is diagonal while all the rest of the terms are nondiagonal, becoming more complex as the order of the terms increases. If we have physically equivalent nuclei in the system,  $\chi_{j2}$  is independent of  $j$  and the first term in Eqn III.58 reduces to  $\chi_2(\tau_1)\bar{N}_2$ . For the case where all the nuclei are not equivalent, it is advantageous to rewrite the first term as

$$\sum_{j=1}^N \chi_{j2}(\tau_1)\bar{N}_{j2} = \chi_2(\tau_1)\bar{N}_2 + \sum_{j=1}^N \chi_{j2}(\tau_1) - \chi_2(\tau_1)\bar{N}_{j2} ; \quad (\text{III.59})$$

$$\chi_2(\tau_1) = \frac{1}{N} \sum_{j=1}^N \chi_{j2}(\tau_1) . \quad (\text{III.60})$$

It is rigorously shown in Eqn III.61 below that  $\tilde{\mathcal{H}}_{D(\text{homo})}''$ , the dominant term in  $\tilde{\mathcal{H}}_{D(\text{homo})}'$ , does not affect  $\langle \bar{N}_2 \rangle$  during the spin-locking pulse.

$$\begin{aligned} \langle \bar{N}_2(t_w + \tau_1 + \tau_2) \rangle &= \text{Tr} \{ \rho(t_w + \tau_1 + \tau_2) \bar{N}_2 \} \\ &= -\frac{K}{r_1} \text{Tr} \{ \exp(-i \tilde{\mathcal{H}}_{D(\text{homo})}'' \tau_2) \exp(-i \tilde{\mathcal{H}}_{D(\text{homo})}' \tau_1) \bar{N}_2 \\ &\quad \times \exp(i \tilde{\mathcal{H}}_{D(\text{homo})}' \tau_1) \exp(i \tilde{\mathcal{H}}_{D(\text{homo})}'' \tau_2) \bar{N}_2 \} \end{aligned}$$

$$\begin{aligned}
&= -\frac{K}{r_1} \text{Tr}(\exp(-i \tilde{\mathcal{H}}_{D(\text{homo})}^{\prime} \tau_1) \bar{N}_2 \exp(+i \tilde{\mathcal{H}}_{D(\text{homo})}^{\prime} \tau_1) \bar{N}_2) \\
&= \langle \bar{N}_2(t_w + \tau_1) \rangle \\
&= \chi_2(\tau_1) \text{Tr}(\bar{N}_2^2) \quad ; \quad (\text{III.61})
\end{aligned}$$

in the above the first exponential has been cycled to the end of the product, where it commutes with  $\bar{N}_2$  and cancels with its complex conjugate. Thus, regardless of  $\tau_2$ , the magnitude of  $\langle \bar{N}_2 \rangle$  is the same at the end of the spin-locking pulse as at the beginning (those terms in  $\tilde{\mathcal{H}}_{D(\text{homo})}^{\prime}$  which produce spin-lattice relaxation in the second interaction frame, and thus somewhat attenuate  $\langle \bar{N}_2 \rangle$ , have been truncated).

In view of the semi-rigorous nature of the arguments developed above the ultimate test is the experimental results. The successful use of the ZTR method in NQR applications is limited only by the ability of the spin-spin interactions to achieve a state of quasi-equilibrium during the time  $\tau_2$  of the spin-locking pulse. For a strongly inhomogeneous system, where neighboring spins are isolated from one another, the dipolar coupling cannot bring about this situation in the second interaction frame. The response of the spin system following the long pulse can then not be expected to reproduce faithfully the true FID. If there is inhomogeneous broadening but still effective spin-spin interaction either throughout the entire

## CHAPTER IV

### SPIN $3/2$ NQR IN POWDERS : MULTIPLE-PULSE SYMMETRY AND APPLICATION OF AVERAGE HAMILTONIAN THEORY (AHT)

In this Chapter we present a theoretical study of the response of a spin  $3/2$  NQR powder sample to several multiple-pulse sequences which are frequently exploited in solid-state NMR. Also proposed are some suitably adapted multiple-pulse sequences with their possible influence on internal interactions of a powder sample. The guideline for designing our multiple-pulse sequences has been their symmetry property with respect to the spin  $3/2$  NQR powder sample. A critical analysis of the cyclicity criterion of these sequences in the present context has been made. It is interesting to point out that the symmetry of some of the multiple-pulse sequences proposed by us is independent of the crystal orientation parameters. Also some of them preserve their cyclicity irrespective of the flip angle chosen for the pulses in the sequence. The Average Hamiltonian Theory (AHT) within the framework of Magnus expansion has been used to study the effect of some typical (e.g. PAPS and WAHUHA) cyclic multiple-pulse sequences on the system's response. Our theoretical findings for PAPS have been demonstrated by a  $^{35}\text{Cl}$  NQR experiment on  $\text{KClO}_3$  powder.

#### IV. A. Some useful Properties of the Operators $\bar{L}$ , $\bar{M}$ and $\bar{N}$

Before we enter the main theme of this Chapter, it is pertinent here to point out the mathematical properties which characterize the operators  $\bar{L}$ ,  $\bar{M}$  and  $\bar{N}$  defined in Eqns II.32a, II.60a and III.11, respectively. The subscripts 1,2 and 3 on  $\bar{M}$  and  $\bar{N}$  distinguish the different phases ( $\phi$ ) involved in k,l,m,n,p and q in Eqn II.60. The properties defined here, therefore, are true for these subscripted operators also.

It has been observed by us earlier (Chapter III) that the operators  $\bar{L}$ ,  $\bar{M}$  and  $\bar{N}$  in spin 3/2 NQR are analogues of the corresponding angular momentum operators  $I_z$ ,  $I_y$  and  $I_x$ , respectively, in spin 1/2 NMR.  $\bar{L}$ ,  $\bar{M}$  and  $\bar{N}$  have the additional properties of carrying information about the crystal orientation parameters, the asymmetry parameter and the phase of the externally applied rf field. We list here their most important properties :

(a) The commutation relations (reproduced from Eqns III.12a-d) are :

$$[\bar{N}, \bar{L}] = \bar{M} \quad , \quad \text{(IV.1a)}$$

$$[\bar{N}, \bar{M}] = r^2 \bar{L} \quad , \quad \text{(IV.1b)}$$

$$[\bar{M}, \bar{L}] = \bar{N} \quad , \quad \text{(IV.1c)}$$



where

$$r^2 = k^2 + l^2 + m^2 + n^2 + p^2 + q^2 \quad (\text{IV.1d})$$

Also

$$\bar{L}^2 = \frac{1}{4} 1 \quad (\text{IV.2a})$$

$$\bar{M}^2 = -\frac{1}{4} r^2 1 \quad (\text{IV.2b})$$

$$\bar{N}^2 = \frac{1}{4} r^2 1 \quad (\text{IV.2c})$$

Egns IV.2a-c lead to the following properties of their respective exponential operators :

$$\exp(i\bar{L}t) = 1\cos(t/2) + 2i\bar{L}\sin(t/2) \quad (\text{IV.3a})$$

$$\exp(i\bar{M}t) = 1\cosh(tr/2) + \frac{2i\bar{M}}{r}\sinh(tr/2) \quad (\text{IV.3b})$$

$$\exp(i\bar{N}t) = 1\cos(tr/2) + \frac{2i\bar{N}}{r}\sin(tr/2) \quad (\text{IV.3c})$$

Egns IV.3a-c lead to the following form of the evolution of the density operator :

$$\begin{aligned} \rho(t) &= \exp(-i\bar{L}t) \rho(0) \exp(i\bar{L}t) \\ &= \rho(0) + \left\{ i\sin t + 4\sin^2(tr/2)\bar{L} \right\} [\rho(0), \bar{L}] \quad (\text{IV.4a}) \end{aligned}$$

$$\rho(t) = \exp(-i\bar{M}t)\rho(0)\exp(i\bar{M}t)$$

$$= \rho(0) + \left\{ (1/r)\sinh(tr) + \frac{\sinh(tr/2)}{(r/2)^2} \bar{M} \right\} [\rho(0), \bar{M}] ,$$

(IV.4b)

$$\rho(t) = \exp(-i\bar{N}t)\rho(0)\exp(i\bar{N}t)$$

$$= \rho(0) + \left\{ (1/r)\sin(tr) + \frac{\sin(tr/2)}{(r/2)^2} \bar{N} \right\} [\rho(0), \bar{N}] .$$

(IV.4c)

We will use all the abovementioned properties of  $\bar{L}$ ,  $\bar{M}$  and  $\bar{N}$  in the Sections that follow and also in later Chapters.

#### IV.B. Cyclic, Periodic and Aperiodic Perturbations and Average Hamiltonian Theory (AHT)

The general trend in much of the recent magnetic resonance research is to prepare a system, or to let it evolve, under an externally controlled Hamiltonian or under a Hamiltonian with certain symmetry or transformation properties (see Figure IV.1). It is necessary on many occasions to implement a specific desired Hamiltonian, perhaps different from the natural unperturbed Hamiltonian, of the system. In other words, whereas the system might naturally evolve under its propagator  $U(t)$ , we apply a

Figure IV.1 : Natural and externally modified evolution of the state of a system [162]

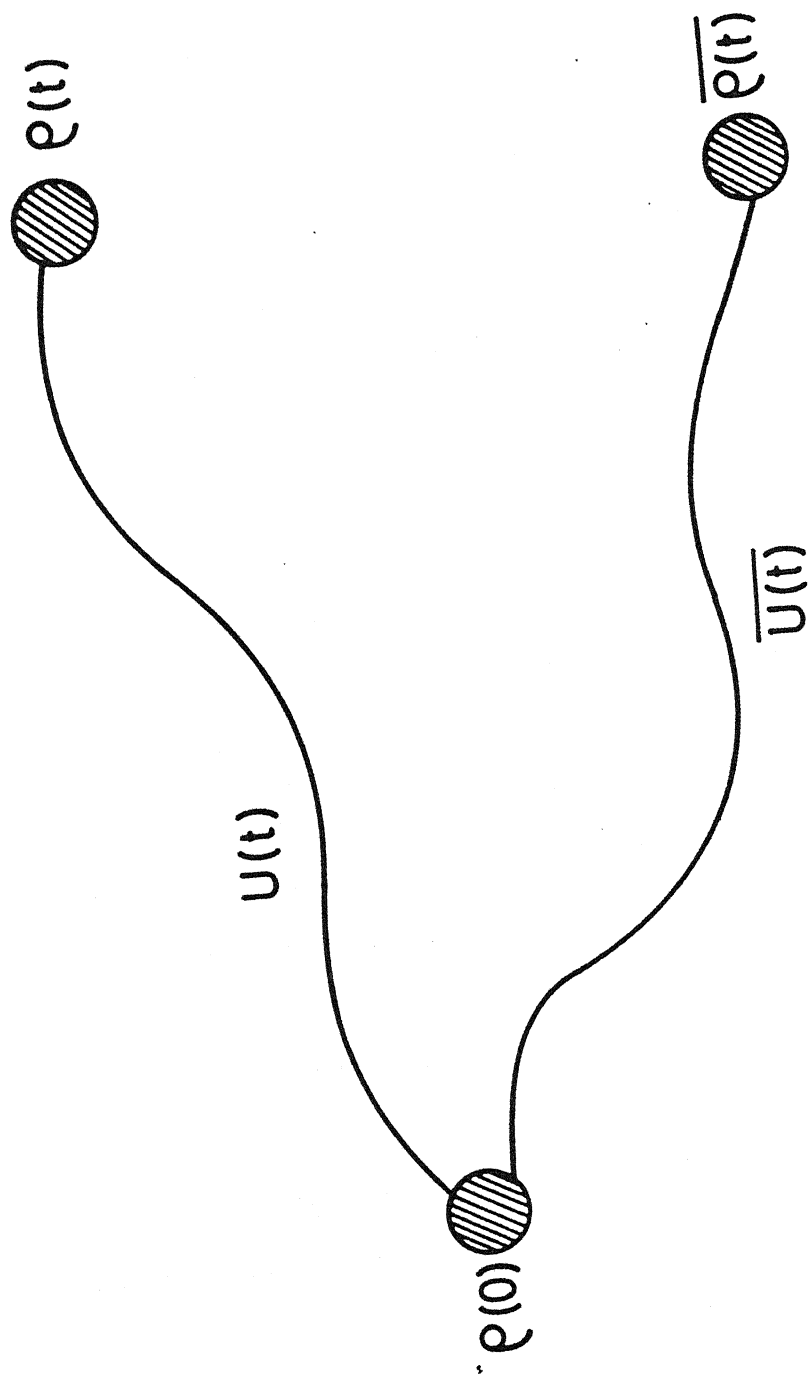


Figure IV.1

perturbation so that the system evolves under a different propagator  $\bar{U}(t)$ , due to a Hamiltonian  $\bar{\mathcal{H}}$ , arriving perhaps at a different state at time  $t$ . The perturbation needed may be a coherent one, such as a sequence of rf pulses, a mechanical rotation, or perhaps an incoherent one such as heating the sample or applying pressure to the system. In order to exploit the symmetry or transformation properties to its maximum, we shall be concerned here about the design of cyclic and periodic sequences of coherent pulse perturbation schemes. We, therefore, define below the terms cyclic, periodic and aperiodic perturbations.

#### 1. Cyclic Perturbations

A cyclic perturbation has the property of returning the system to its original state after the cycle is complete. In other words, if the state of the system at the initial time  $t$  is specified by  $\rho(t)$ , and  $t_c$  is the cycle-time of the cyclic perturbation scheme, then

$$\rho(t + t_c) = \rho(t) \quad . \quad (IV.5)$$

A cyclic perturbation can be depicted as shown in Figure IV.2. Eqn IV.5 implies that, when  $U$  is cyclic,

$$\rho(t+t_c) = U(t_c, t) \rho(t) U(t_c, t)^{-1} = \rho(t) \quad . \quad (IV.6)$$

Eqn IV.6 makes it evident that, for a cyclic sequence of rf field perturbations,

Figure IV.2 : Evolution of a system under a cyclic  
Perturbation

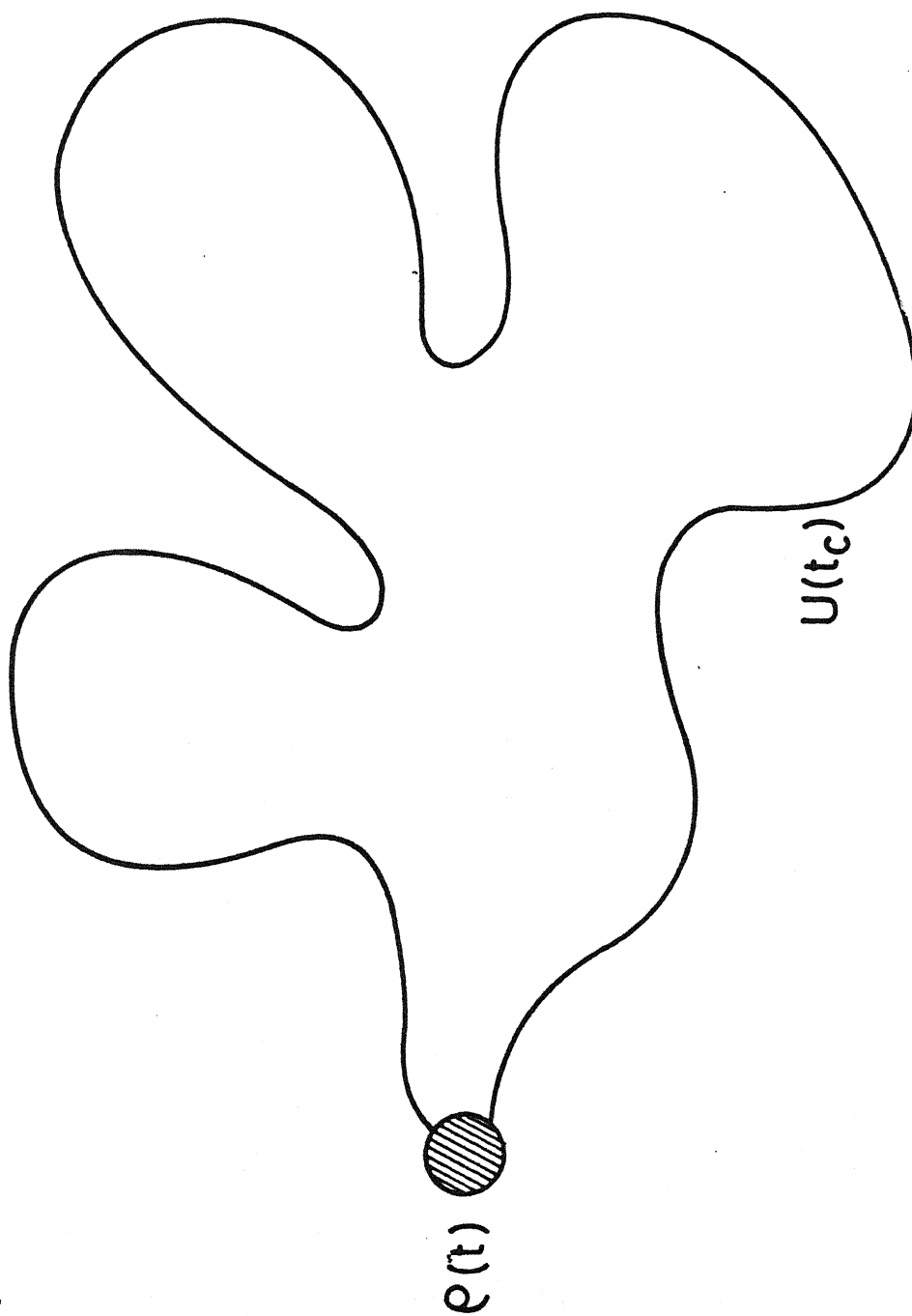


Figure IV.2

$$U(t_c, t) = T \exp \left[ -i \int_t^{t_c} \tilde{\mathcal{H}}'_{rf}(t') dt' \right] = 1 \quad (\text{IV.7})$$

## 2. Periodic Perturbations

The requirement that a sequence be periodic is :

$$\mathcal{H}_{rf}(t) = \mathcal{H}_{rf}(t + t_p) \quad , \quad (\text{IV.8})$$

where  $t_p$  is the periodicity of the Hamiltonian. In other words, if a perturbation keeps recurring at fixed time intervals of  $t_p$ , it is periodic. Pictorially it can be depicted as in Figure IV.3(a).

## 3. Aperiodic Perturbations

The perturbations that do not have the abovementioned property of recurring at fixed time intervals (the characteristic time  $t_p$  is absent) are aperiodic. This is shown pictorially in Figure IV.3(b).

If a cyclic perturbation sequence is repeated more than once, each cycle constitutes a period and the perturbation scheme also becomes periodic, with  $t_c = t_p$ . It is to be noted that there may be sub-time-intervals  $t_h$ , with  $nt_h = t_p = t_c$ , where  $n$  is a non-zero positive integer, when the perturbation is periodic (but need not be cyclic). Also, it is very clear from the above discussions that periodicity does not imply cyclicity and vice



Figure IV.3 : (a) A periodic perturbation. (b) An aperiodic perturbation [162]

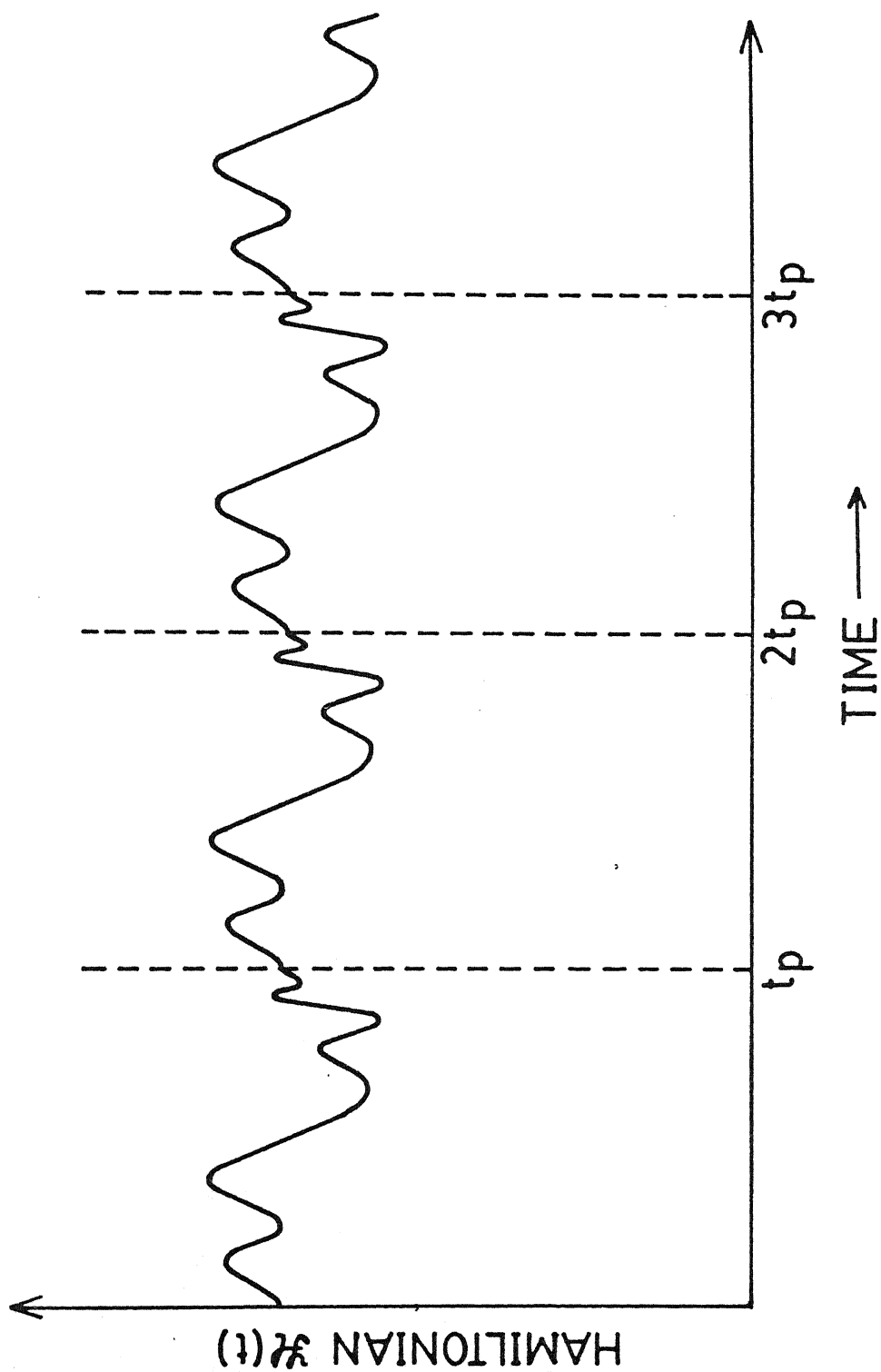


Figure IV.3(a)

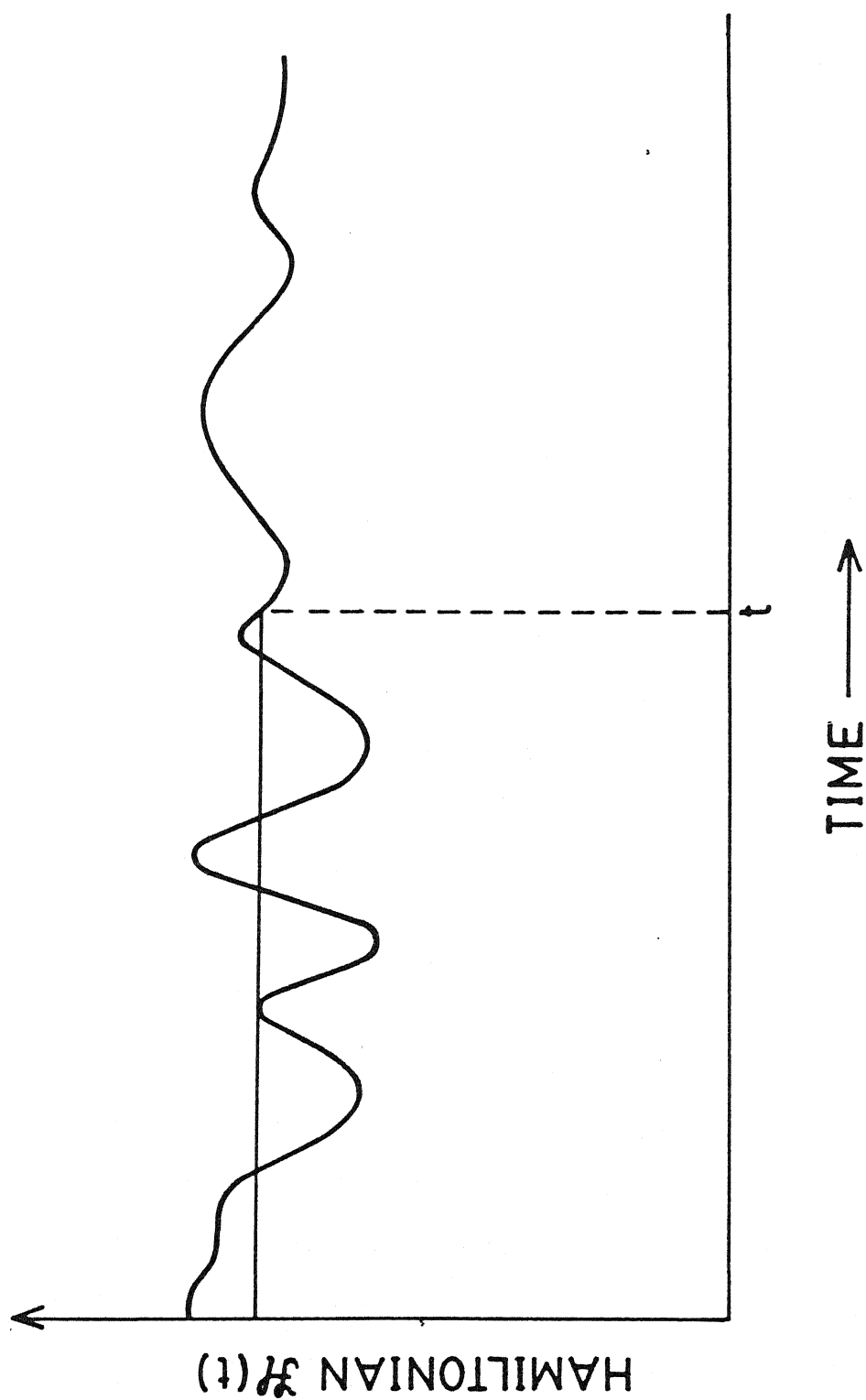


Figure IV.3(b)

versa. When an rf pulse perturbation scheme is both periodic and cyclic, then

$$\mathcal{H}_{rf}(t) = \mathcal{H}_{rf}(t + Nt_c) \quad , \quad (\text{IV.9a})$$

$$U_{rf}(Nt_c, t) = 1 \quad , \quad (\text{IV.9b})$$

where  $N$  is a non-zero positive integer. It is to be noted that Eqns IV.9a and IV.9b do not impose any constraint on subperiods and (or) subcycles.

When the perturbation on a system is cyclic it is enough to know the behavior of the system over one cycle. For subsequent cycles the same behavior is repeated so that [16,83]

$$\rho(Nt_c) = [\rho(t_c)]^N \quad . \quad (\text{IV.10})$$

#### 4. Average Hamiltonian Theory

The theory that best accounts for the design of specific Hamiltonians (and therefore propagators) under coherent perturbation is Average Hamiltonian Theory (AHT). Suppose the Hamiltonian is time-dependent (owing to, for example, an applied perturbation), as depicted in Figures IV.3 and IV.4. A question that arises is : can we find a time-dependent Hamiltonian  $\bar{\mathcal{H}}$ , which can induce evolution of the system through  $\bar{U}(t)$  to the same state as  $\mathcal{H}(t)$  would induce at time  $t$  ? The answer is yes ,and

that  $\bar{\mathcal{H}}$  is the Magnus Hamiltonian given by [18-19, 57, 58, 163, 164] :

$$\bar{\mathcal{H}} = \bar{\mathcal{H}}^{(0)} + \bar{\mathcal{H}}^{(1)} + \bar{\mathcal{H}}^{(2)} + \dots, \quad (\text{IV.11})$$

where

$$\bar{\mathcal{H}}^{(0)} = \frac{1}{t} \int_0^t \mathcal{H}(t') dt', \quad (\text{IV.12})$$

is the average Hamiltonian. The next two terms in this series are :

$$\bar{\mathcal{H}}^{(1)} = -\frac{1}{2t} \int_0^t \int_0^{t'} [\mathcal{H}(t'), \mathcal{H}(t'')] dt'' dt', \quad (\text{IV.13})$$

and

$$\begin{aligned} \bar{\mathcal{H}}^{(2)} = & -\frac{1}{6t} \int_0^t \int_0^{t'} \int_0^{t''} \{ [\mathcal{H}(t'), [\mathcal{H}(t''), \mathcal{H}(t''')]] \\ & + \mathcal{H}(t'''), [\mathcal{H}(t''), \mathcal{H}(t')] ] \} dt''' dt'' dt'. \quad (\text{IV.14}) \end{aligned}$$

If Eqn IV.11 converges rapidly, so that  $\bar{\mathcal{H}}^{(k)}$  are small for  $k \neq 0$ , then the average Hamiltonian  $\bar{\mathcal{H}}^{(0)}$  provides a good description of the system and other  $\bar{\mathcal{H}}^{(k)}$ 's are correction terms. The problem of

convergence of Magnus expansion has been discussed in the literature [21,64,165,166]. By applying a perturbation we have, therefore, taken a system which would have evolved under some Hamiltonian  $\mathcal{H}$  and caused it to evolve effectively under  $\bar{\mathcal{H}}^{(0)}$  as in Figure IV.1. The trick is to realize the desired  $\bar{\mathcal{H}}^{(0)}$  by appropriate perturbations that can be implemented experimentally, such as employing PAPS and WAHUA sequences to be discussed in the next Section. Note that, in general,  $\bar{\mathcal{H}}$  and  $\bar{\mathcal{H}}^{(0)}$  depend on  $t$ , but if  $\mathcal{H}(t)$  is periodic and the evolution is cyclic, then the same  $\bar{\mathcal{H}}$  and  $\bar{\mathcal{H}}^{(0)}$  hold at all integral multiples of  $t_c$ . If  $\mathcal{H}(t)$  is not periodic the approach is still useful, since one can effectively impose an  $\bar{\mathcal{H}}$  which produces a particular desired final state  $\bar{\rho}(t)$  at time  $t$  (Figure IV.1). It is interesting to point out here that the average Hamiltonian theory for cyclic perturbation schemes is related to Berry's geometrical phase [167-169]. In the Section that follows, we shall adapt the ideas discussed here for the particular case of spin 3/2 NQR to design cyclic rf pulse perturbation schemes.

#### IV.C. Cyclic Multiple-Pulse Sequences for Spin 3/2 NQR of Powders

##### 1. The Phase Alternated Pulse Sequence (PAPS)

It is a two-pulse cycle in which the phases of the pulses differ by  $\pi$ . It may be represented as

$$(\pi/2)_{\phi}, -\left\{ \tau - (\theta)_{\phi+\pi} - 2\tau - (\theta)_{\phi} - \tau \right\}_n \quad . \quad (\text{IV.15})$$

It is seen from above that the cycle time  $t_c = 4\tau$ . We shall examine below its cyclicity. In the  $\delta$ -pulse limit we obtain, for the cycle pulse propagator,

$$U = \exp(-i\theta\bar{N}_2) \exp(-i\theta\bar{N}_1), \quad (\text{IV.16})$$

where  $\bar{N}$  is given by Eqn II.80. The subscripts 1 and 2 on  $\bar{N}$  represent the phases  $\phi+\pi$  and  $\phi$ , respectively, of the pulses in the cycle. Since  $\cos(\phi+\pi) = -\cos\phi$  and  $\sin(\phi+\pi) = -\sin\phi$ , Eqn IV.16 reduces to :

$$U = \exp(-i\theta\bar{N}) \exp(+i\theta\bar{N}) = 1. \quad (\text{IV.17})$$

Therefore PAPS is cyclic for any value of  $\phi$  in IV.15. From the above discussion it is clear that all the following cycles represent experimentally feasible PAPS sequences for spin 3/2 NQR:

$$(1) \quad (\pi/2)_{\phi}, -\left\{ \tau-(\theta)_{\pi} - 2\tau-(\theta)_{\phi} - \tau \right\}_n, \quad (\text{IV.18a})$$

$$(11) \quad (\pi/2)_{\phi}, -\left\{ \tau-(\theta)_{\phi} - 2\tau-(\theta)_{\pi} - \tau \right\}_n, \quad (\text{IV.18b})$$

$$(111) \quad (\pi/2)_{\phi}, -\left\{ \tau-(\theta)_{3\pi/2} - 2\tau-(\theta)_{\pi/2} - \tau \right\}_n, \quad (\text{IV.18c})$$

$$\& (1v) \quad (\pi/2)_{\phi}, -\left\{ \tau-(\theta)_{\pi/2} - 2\tau-(\theta)_{3\pi/2} - \tau \right\}_n. \quad (\text{IV.18d})$$

It is also clear from the above discussion that the multiple-pulse sequences in Eqns IV.18 remain cyclic irrespective of the orientation of the individual crystallites in a powder sample. This conclusion for spin  $3/2$  NQR is similar to that of Osokin [23,25,31] in the context of spin 1 NQR. It, therefore, seems to be true for any spin  $I$ . Also  $\theta$  and  $\phi'$ , the flip angle of the cycle pulses and phase of the preparatory pulse, respectively, can have any value. Usually one takes  $\theta = \pi/2$  and  $\phi' = 0$ .

## 2. The Waugh-Huber-Haeberlen (WAHHA) pulse Sequence

It is a four-pulse cycle with cycle time  $t_c = 6\tau$  and is represented as :

$$(\pi/2)_{\phi'} - \left\{ \tau - (\theta)_{\phi_1 + \pi} - \tau - (\theta)_{\phi_2} - 2\tau - (\theta)_{\phi_2 + \pi} - \tau - (\theta)_{\phi_2} - \tau \right\}_n$$

(IV.19)

In the  $\delta$ -pulse limit, the pulse propagator for this sequence is :

$$U = \exp(-i\theta\bar{N}_4) \exp(-i\theta\bar{N}_3) \exp(-i\theta\bar{N}_2) \exp(-i\theta\bar{N}_1),$$

(IV.20)

where, as before,  $\bar{N}$  is given by Eqn II.60. The subscripts 1,2,3 and 4 on  $\bar{N}$  represent the phases  $\phi_1 + \pi$ ,  $\phi_2$ ,  $\phi_2 + \pi$  and  $\phi_1$  of the pulses, respectively, in the pulse sequence. Again, since  $\cos(\phi + \pi) = -\cos \phi$  and  $\sin(\phi + \pi) = -\sin \phi$ , we have



$$U = \exp(-i\theta\bar{N}_1)\exp(i\theta\bar{N}_2)\exp(-i\theta\bar{N}_2)\exp(i\theta\bar{N}_1) = 1 .$$

(IV.21)

Therefore WAHUA is cyclic for any value of  $\phi$  in IV.19. One of the examples of WAHUA for spin 3/2 NQR is

$$(\pi/2)_{\phi} \left\{ \tau-(\theta)_{\pi} \tau-(\theta)_{\pi/2} -2\tau-(\theta)_{3\pi/2} \tau-(\theta)_0 \tau \right\}_n ;$$

(IV.22)

Another example is :

$$(\pi/2)_{\phi} \left\{ \tau-(\theta)_{5\pi/4} \tau-(\theta)_{\pi/4} -2\tau-(\theta)_{5\pi/4} \tau-(\theta)_{\pi/4} \tau \right\}_n .$$

(IV.23)

### 3. The Carr-Purcell (CP) Pulse Sequence

This pulse sequence consists of two pulses in the cycle, both with a flip angle of  $\pi$  and having the same phase. It may be represented as :

$$(\pi/2)_{\phi} \left\{ \tau-(\pi)_{\phi} -2\tau-(\pi)_{\phi} \tau \right\}_n .$$

The cycle time  $t_c$  is  $4\tau$ . The cycle propagator is

$$U = \exp(-i\pi\bar{N}) \exp(-i\pi\bar{N}) \quad (\text{IV.25})$$

$$= \exp(-2i\pi\bar{N})$$

$$= i \cos(\pi r) + \frac{2i\bar{N}}{r} \sin(\pi r) \quad (\text{IV.26})$$

Eqn IV.26 is obtained using IV.3c. It is clear from Eqn IV.26 that Carr-Purcell sequence is, in general, not cyclic for a spin 3/2 powder sample. However, it will be cyclic for all those crystallites for which  $r = 1$ . In the Carr-Purcell-Meiboom-Gill (CPMG) modification of the CP sequence, the phase difference between the preparatory pulse and the cycle pulses is  $\pi/2$ . As Eqn IV.26 is independent of  $\phi$ , CPMG pulse sequence is also not cyclic, in general, for spin 3/2 NQR.

#### 4. The Ostroff-Waugh (OW) Pulse Sequence

This multiple pulse sequence consists of a train of  $\pi/2$  pulses. The first pulse and the rest of the pulses in the train have a phase difference of  $\pi/2$ . This sequence may be represented as

$$(\pi/2)_0 - \tau - \left\{ \tau - (\pi/2)_{\pi/2} - \tau \right\}_n \quad (\text{IV.27})$$

In NMR, four of the pulses in the sequence constitute a cycle, with cycle time  $t_c = 8\tau$ . We shall examine here the case of spin 3/2 NQR. The cycle pulse propagator for IV.27 is

$$U = \exp\left(-\frac{i\pi}{2} \bar{N}\right) \exp\left(-\frac{i\pi}{2} \bar{N}\right) \exp\left(-\frac{i\pi}{2} \bar{N}\right) \exp\left(-\frac{i\pi}{2} \bar{N}\right),$$

(IV.28)

where  $\bar{N}$  is given by substituting  $\phi = \pi/2$  in Eqn II.60. Therefore,

$$U = \exp(-2\pi i \bar{N})$$

$$= 1 \cos(\pi r) + \frac{i\pi \bar{N}}{r} \sin(\pi r), \quad \text{(IV.29)}$$

where the last step has been obtained using Eqn IV.3c. Therefore, from Eqn IV.28 it is clear that OW is cyclic (with cycle time  $t_c = 8\tau$ ) only for those crystallites in a powder spin  $3/2$  sample that have their crystal orientation and asymmetry parameter such as to make  $r = 1$ . However, as will be seen in Chapter VI, a different approach based only on the periodicity criterion for the pulse perturbation can still be made for handling the problem using AHT.

In the following Section, we examine the effect of some of the cyclic multiple-pulse sequences on the internal Hamiltonians of spin  $3/2$  powder sample. Our approach is based on AHT for cyclic multiple-pulse sequences within Magnus expansion framework.

#### IV.D. Response of Spin $3/2$ NQR Powders to Cyclic Multiple-Pulse Sequences

##### 1. General Remarks

When a spin  $3/2$  NQR powder sample is irradiated by a cyclic

multiple-pulse sequence, the behavior of the system is described by AHT, provided we observe the system only at specified observation windows, i.e., only after a cycle is complete. By making a judicious choice of cyclic multiple-pulse sequences we can introduce time dependence in the line-broadening internal interactions in such a way that their average Hamiltonian commutes with the initial density operator  $\rho(0)$  prepared from the equilibrium density operator  $\rho_{eq}$  by a preparatory pulse [170], i.e.,

$$[\rho(0), \bar{H}] = 0 \quad . \quad (IV.30)$$

$\rho(0)$  thus becomes a constant of the motion during the cyclic interaction with the rf, and the line-broadening internal interactions under consideration do not contribute to the evolution of the system. In effect, we achieve line-narrowing. In this Section we calculate the average Hamiltonian using Magnus expansion for the line-broadening internal interactions, namely, efg inhomogeneity and heteronuclear dipole coupling. The commutators of these average Hamiltonians with  $\rho(0)$  are then evaluated. Homonuclear dipole coupling is very weak and is discarded for this study. Also, conclusions regarding torsional oscillations will be the same as that for efg inhomogeneity.

## 2. The Effect of Cyclic Multiple-Pulse Sequences on the efg Inhomogeneity and Torsional Oscillation Hamiltonian

The major line-broadening interactions in quadrupolar solids

are efg inhomogeneity and the effect of torsional oscillations. The Hamiltonians corresponding to both these interactions have a common structure and may be represented as (Eqns II.33 and II.61):

$$\Delta_i \mathcal{H}_Q = \Delta_i K \bar{L} \quad , \quad (\text{IV.31})$$

where  $\Delta_i$  is a parameter that takes into account the shift of resonance frequency from the centre frequency due to efg inhomogeneity or due to the secular part of the torsional oscillation Hamiltonian.

(a) The Phase Alternated Pulse Sequence (PAPS)

We shall now consider the pulse given in IV.18a and its effect on the Hamiltonian given in Eqn IV.31. The pulse cycle in IV.18a is :

$$\left\{ \tau - (\theta)_{\pi} - 2\tau - (\theta)_0 - \tau \right\}_n \quad . \quad (\text{IV.32})$$

For the average Hamiltonian, therefore, we look at the transformations of  $\bar{L}$  during PAPS. We present the result in Table IV.1.

Therefore, using Eqn IV.12, we obtain the average Hamiltonian for efg inhomogeneity and torsional Hamiltonian during the cycle IV.32 as,

$$\Delta_i \bar{\mathcal{H}}_Q^{(0)} = \Delta_i K \left\{ \bar{L} \cos\left(\frac{\theta r}{2}\right) + \frac{i\bar{M}}{r} \sin\left(\frac{\theta r}{2}\right) \right\} \cos\left(\frac{\theta r}{2}\right) \quad . \quad (\text{IV.33})$$

Table IV.1 : Transformations of  $\bar{L}$  during PAPS\*

Interval	Time	$\mathcal{H}_{rf}$	$U_{rf}^{-1}$	$\tilde{L}$
$\delta_1$	$0 \leq t < \tau$	0	1	$\bar{L}$
Pulse 1	$\tau$	$-\bar{N}$	$\exp(i\theta\bar{N})$	Undefined
$\delta_2$	$\tau < t \leq 3\tau$	0	1	$\bar{L}\cos(\theta r) + \frac{i\bar{M}}{r}\sin(\theta r)$
Pulse 2	$3\tau$	$+\bar{N}$	$\exp(-i\theta\bar{N})$	Undefined
$\delta_3$	$3\tau < t \leq 4\tau$	0	1	$\bar{L}$

If the preparatory pulse has flip-angle  $\theta_0$ , from Eqn III.10 we can write the initial density operator as :

$$\rho(0) = K \left\{ \bar{L} \cos(\theta_0 r) - \frac{i\bar{M}}{r} \sin(\theta_0 r) \right\} \quad \text{(III.10)}$$

The commutator is easily evaluated. After some algebra, the result is

$$[\rho(0), \Delta_i \bar{\mathcal{H}}_Q^{(0)}] = \Delta_i K^2 [\bar{L}, \bar{M}] \left( \frac{1}{r} \right) \left\{ \sin(\theta_0 r) + \sin((\theta + \theta_0)r) \right\}.$$

(IV.34)

Eqn IV.34 will go to zero only when  $\theta r = \theta_0 r = \pi$ . Therefore, those crystallites in a powder that have  $r = 1$  will not see the

---

\* $\bar{N}$  is obtained from Eqn II.60a by putting  $\phi=0$ .

effect of efg inhomogeneity and torsional oscillations, when  $\theta_o = \theta = \pi$ . For all other orientations of the crystallites efg and torsional oscillations will contribute to the line-broadening. For a single crystal with  $r = 1$ , PAPS with  $\theta_o = \theta = \pi$  will show a line-narrowing.

(b) The WAUGH-HUBER-HAEBERLEN (WAHUHA) Pulse Sequence

We will consider the following cycle (Eqn IV.22) :

$$\left\{ \tau - (\theta)_{\pi} - \tau - (\theta)_{\pi/2} - 2\tau - (\theta)_{3\pi/2} - \tau - (\theta)_o - \tau \right\}_n \quad (\text{IV.35})$$

We look at the transformations of  $\bar{L}$  during WAHUHA. In Table IV.2 below we present the results.

From Table IV.2, the average Hamiltonian for the efg inhomogeneity and torsional oscillation Hamiltonian can be calculated. We present the final results below :

$$\Delta_1 K \bar{\mathcal{H}}_a^{(o)} = \frac{1}{3} \left\{ \left\{ 1 + \cos(\theta r) + \cosh(\theta r) \cos(\theta r) \right\} \bar{L} + \frac{2i\bar{M}}{r} \sin(\theta r) + \frac{i\bar{N}}{r} \sinh(\theta r) \cos(\theta r) \right\} \quad (\text{IV.36})$$

When  $\theta r = \pi/2$ , Eqn IV.36 reduces to

$$\Delta_1 K \bar{\mathcal{H}}_a^{(o)} = \frac{1}{3} \left\{ \bar{L} + \frac{2i\bar{M}}{r} \right\} \quad (\text{IV.37})$$

Table IV.2 : Transformations of  $\bar{L}$  during WAHUHA\*

Interval	Time	$\mathcal{H}_{rf}$	$U_{rf}^{-1}$	$\tilde{L}$
$\delta_1$	$0 \leq t < \tau$	0	1	$\bar{L}$
Pulse 1	$\tau$	$-\bar{N}$	$\exp(i\theta\bar{N})$	Undefined
$\delta_2$	$\tau < t \leq 2\tau$	0	1	$\bar{L}\cos(\theta\tau) + \frac{i\bar{M}}{\tau}\sin(\theta\tau)$
Pulse 2	$2\tau$	$+\bar{M}$	$\exp(-i\theta\bar{M})$	Undefined
$\delta_3$	$2\tau < t \leq 4\tau$	0	1	$\{\bar{L}\cosh(\theta\tau) - \frac{i\bar{N}}{\tau}\sinh(\theta\tau)\}$ $x\cos(\theta\tau) + \frac{i\bar{M}}{\tau}\sin(\theta\tau)$
Pulse 3	$4\tau$	$-\bar{M}$	$\exp(i\theta\bar{N})$	Undefined
$\delta_4$	$4\tau < t \leq 5\tau$	0	1	$\bar{L}\cos(\theta\tau) + \frac{i\bar{M}}{\tau}\sin(\theta\tau)$
Pulse 4	$5\tau$	$\bar{N}$	$\exp(-i\theta\bar{M})$	Undefined
$\delta_5$	$5\tau < t \leq 6\tau$	0	1	$\bar{L}$

It can be shown that Eqn IV.36 does not commute with the initial density operator (Eqn III.10) for  $\theta \neq 0$ . Therefore, the interesting conclusion may be made that WAHUHA will not be effective in removing broadening due to efg inhomogeneity and torsional oscillations from the NQR line shape of a spin 3/2 powder sample.

\* $\bar{N}$  and  $\bar{M}$  are obtained from Eqs II.60a and III.11, respectively, by putting  $\phi = 0$ .



### 3. The Effect of PAPS on Heteronuclear Dipole Interaction in a Spin 3/2 Single Crystal Sample

The calculation of the average Hamiltonian corresponding to heteronuclear dipole coupling in a powder sample becomes very complicated. We, therefore, present here the result of our calculations for a single crystal sample [171]. We consider the rf field as being applied along the x-axis of the OPAS and we assume the single-crystal to consist of physically equivalent quadrupolar nuclei. We give here only the final result :

The average Hamiltonian is

$$\begin{aligned}
 \bar{\mathcal{H}}_{D(\text{hetero})}^{(0)} = & C_1(I_X^{1-4} + I_X^{2-3}) + C_2 \left\{ (I_X^{1-4} - I_X^{2-3}) \cos\left(\frac{\theta_r}{2}\right) \right. \\
 & \left. - (I_Y^{2-4} + I_Y^{3-1}) \sin\left(\frac{\theta_r}{2}\right) \right\} \cos\left(\frac{\theta_r}{2}\right) \\
 & + C_3 \left\{ (I_Y^{1-4} - I_Y^{2-3}) \cos\left(\frac{\theta_r}{2}\right) - (I_X^{1-3} - I_X^{2-4}) \sin\left(\frac{\theta_r}{2}\right) \right\} \cos\left(\frac{\theta_r}{2}\right) \\
 & + C_4(I_Y^{1-4} + I_Y^{2-3}) + C_5 \left\{ (I_Z^{1-4} - I_Z^{2-3}) \cos\left(\frac{\theta_r}{2}\right) \right. \\
 & \left. + (I_Y^{1-2} + I_Y^{3-4}) \sin\left(\frac{\theta_r}{2}\right) \right\} \cos\left(\frac{\theta_r}{2}\right) \\
 & + C_6(I_Z^{1-4} + I_Z^{2-3})
 \end{aligned}
 \tag{IV.38}$$

where

$$C_1 = F_x ; C_2 = F_x (\sqrt{3} \sin \xi - \cos \xi) ; C_3 = -F_y ;$$

$$C_4 = F_y (\sqrt{3} \sin \xi + \cos \xi) ; C_5 = F_z ; \text{ and } C_6 = 2F_z \cos \xi .$$

(IV.39)

(For the definition of F's, see Eqn II.63)

Also,

$$[\rho(o), \bar{\rho}_{D(\text{hetero})}(o)] = 0 , \quad (IV.40)$$

$$\text{when } \theta_r = \theta_o = \pi \quad (IV.41)$$

Therefore, we can conclude that, when condition IV.41 is satisfied, heteronuclear dipole interaction does not contribute to the NQR line shape in a single crystal containing spin 3/2 nuclei. We infer that, for particular orientations of crystallites in a powder sample, the heteronuclear dipole coupling is removed even in powder samples. In the next Section we present our experimental result of the response of spin 3/2 powder sample during PAPS, which essentially demonstrates the theory developed above.

#### IV.E. Experimental Details

In this Section, we present our experimental result on

application of PAPS to the  $^{35}\text{Cl}$  NQR of a powder sample of  $\text{KClO}_3$ . The experiment was performed using a Bruker CXP-90 NMR Spectrometer at the Central Leather Research Institute Madras, India. Of course, the dc magnetic field had been switched off during the experiment. A two-pulse program, in which the second pulse with alternating phases would occur between 1 and 4095 counts during a loop, was written, and data were acquired at the end of each cycle. The first pulse was set to be a ' $\pi$ ' pulse. The peak transmitter power employed was  $\approx 400$ -500 Watts corresponding to a ' $\pi$ ' flip angle of 26  $\mu\text{secs}$ . A standard wide-line NMR probe (10 mm diameter) tuned to oscillate at a frequency of 20-32 MHz was employed. The phase of the pulses in the cycle could be controlled in ' $\pi/2$ ' steps by using the pulse-list feature of the system's Z-17c pulser. The spectral width chosen was  $1/4\tau$ , where  $2\tau$  is the separation between the  $\theta$  pulses in the PAPS cycle. The ambient temperature was maintained to be  $21 \pm 1^\circ\text{C}$ .

$\text{KClO}_3$  is an ionic crystal and has a monoclinic structure with 2 molecules per unit cell at room temperature [2,172]. There is unit positive charge on the positive ion ( $\text{K}^+$ ) and unit negative charge on the  $\text{ClO}_3^-$  ions, and the direct influence of neighboring ions on the field gradient can be appreciable [173]. We present the experimental parameters and the spectrum obtained on the next page. The prolongation of the signal for a time as long as  $\sim 400$  msec is an indication of the removal of efg inhomogeneity effect, torsional oscillations and heteronuclear dipole coupling.

Figure IV.4: Time domain response of  $^{35}\text{Cl}$  signal in  $\text{KClO}_3$  powder ( $\omega_a = 28.100$  MHz) to PAPS ; experimental parameters  $\tau = 95$   $\mu\text{secs}$ .  $\theta = \pi$ ,  $\Delta = 0.021$ .

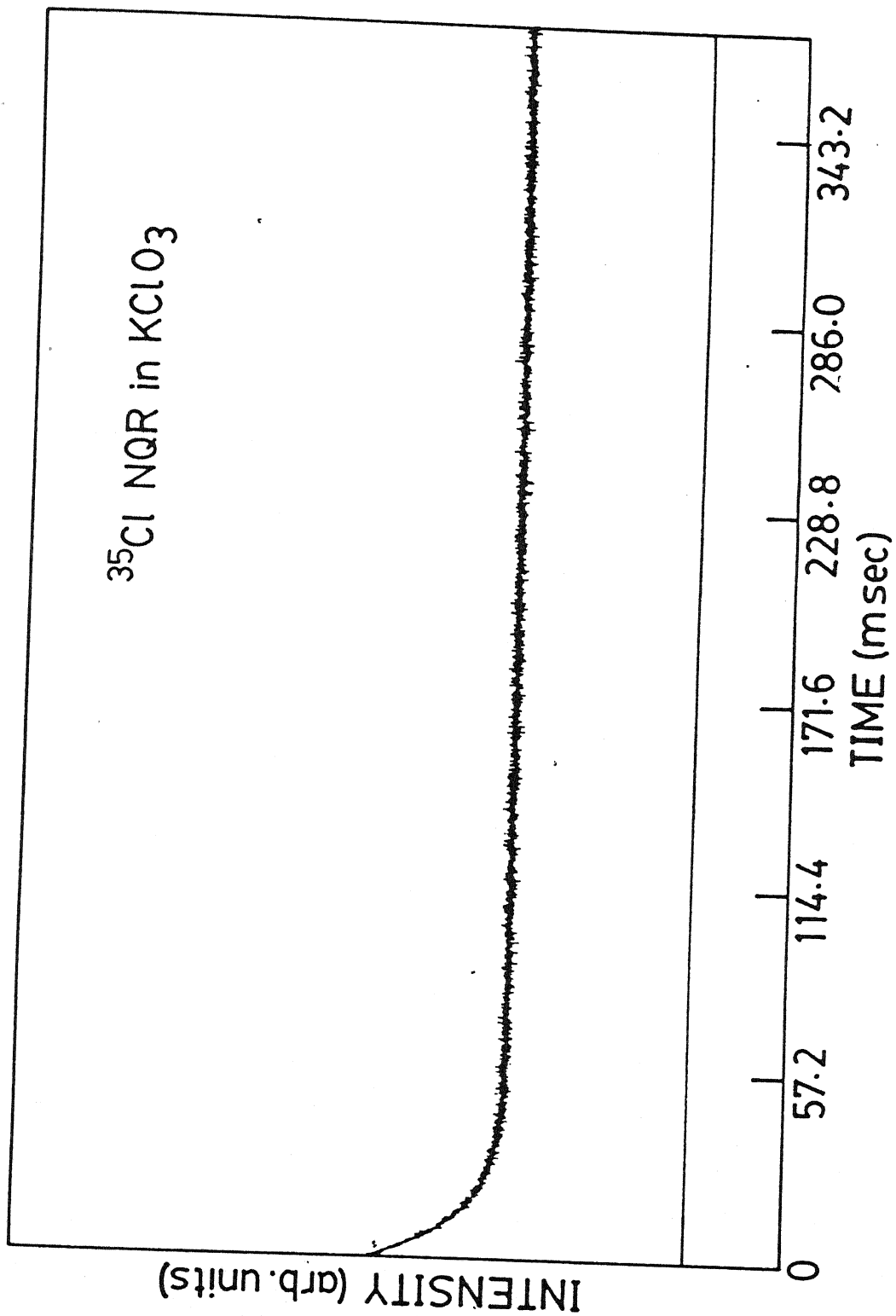


Figure IV.4

#### IV.F. Summary

In this Chapter, we have set forth our results regarding useful mathematical properties of the operators  $\bar{L}$ ,  $\bar{M}$  and  $\bar{N}$ . It turns out that these three operators describe completely the dynamics of an assembly of non-interacting spin  $3/2$  nuclei. We have critically examined the cyclicity of the well-known multiple-pulse sequences and how they can be adapted for spin  $3/2$  NQR spectroscopy of powder samples. The Average Hamiltonian Theory has been used to calculate the effect of PAPS and WAHUA on the major internal Hamiltonians of spin  $3/2$  NQR system. Also, explicitly brought out in this Chapter is the manner in which the pulse sequences influencing the internal Hamiltonians depend on crystal orientation and asymmetry parameter. Finally, we have presented our experimental results on the use of PAPS in  $^{35}\text{Cl}$  resonance of  $\text{KClO}_3$  powder sample. Both theory and experiment enable us to conclude that the efg inhomogeneity and torsional oscillation Hamiltonian can effectively be removed from the system for those crystallites having  $\theta_0 = \theta = \pi$ , during a PAPS experiment. Furthermore, our PAPS calculations for a single crystal show that heteronuclear dipole coupling is also removed completely for flip angles  $\theta_0 = \theta = \pi$ ; the same should hold true in a powder at least for some orientations of individual crystallites with respect to the rf coil axis. In case of WAHUA, line-broadening features due to quadrupole coupling and torsional effects, are not suppressed. However, a WAHUA experiment was not performed by us.

## CHAPTER V

### NQR AND SPIN THERMODYNAMICS IN SPIN $3/2$ SYSEMS EXCITED PERIODICALLY IN TIME : USE OF THE FLOQUET THEOREM

In the rest of the thesis we present our studies of the behavior of spin  $3/2$  quadrupolar nuclear ensemble when subjected to the multiple-pulse scheme referred to earlier as spin-locking pulse. This combined system of spin  $3/2$  nuclear spins and the spin-locking multiple-pulse sequence constitutes a quantum mechanical system characterized by a Hamiltonian with temporal periodicity. This is an example of a class of quantum mechanical systems the analysis of which is best done using Floquet Theorem.

The use of Floquet theorem enables us to model the natural periodic-time-dependent Hamiltonian by a time-independent Floquet Hamiltonian.

To understand the equilibrium properties of a many-body system with an energy-conserving Hamiltonian, one often takes recourse to the powerful tools provided by statistical mechanics. However, a quantum mechanical system of which the Hamiltonian is time-periodic is energy non-conservative and is, as such, intractable by the methods of statistical mechanics. It is here that the model Floquet Hamiltonian (which is time-independent and hence energy-conserving) comes into its own in rendering the methods of statistical mechanics more amenable. We shall

elaborate upon the abovementioned ideas in this Chapter, keeping in mind the spin  $3/2$  quadrupolar system with time-periodic Hamiltonian. To start with, however, we present a brief review of the applications of Floquet theorem to quantum mechanical systems in general. The earlier applications of Floquet theorem in magnetic resonance are also pointed out in this review section.

## V.A. Applications of Floquet Theorem to Periodic Quantum Mechanical Systems

### 1. General Remarks

Mathematically, Floquet theorem helps us to write down the solutions of a system of linear differential equations with periodic coefficients [60,174]. The solutions of the differential equations of a quantized system interacting with a sinusoidal monochromatic field can be written as a Fourier series. As far back as the years 1883-1900, Floquet [59] studied the solutions of such linear differential equations with periodic coefficients, and Poincaré [175] considered the construction of the solutions. It was next used by Bloch to analyse the Schrödinger equation for a periodic potential. The statement of the Bloch theorem [176] is in fact the Floquet theorem as applied to the spatial periodicity of a crystal lattice. The Floquet theorem was later used by Autler and Townes [177] to obtain the wave function for the two-level system in terms of infinite continued fractions. However, the application of Floquet theorem to quantum systems began to grow only after the mid-1960s [61,178-180].



In a well-known paper Shirley [61] reformulated the problem of the interaction of a quantum system with a strong oscillating field by relating the solution of the Schrödinger equation to a time-independent infinite Floquet matrix. While this is literally a semiclassical theory which nowhere involves explicit field quantization, Shirley has shown that his Floquet states can be interpreted physically as quantum field states. Indeed, his Floquet quasienergy diagram is identical to the dressed atom picture derived by Cohen-Tannoudji and Haroche [181]. Shirley's work and its subsequent application to various problems by Young et al [182] was all for finite-basis-set systems. A noteworthy development after this was its generalization to a system characterized by infinite Hilbert space [63]. Barone et al [62] have applied the Floquet theory within the framework of Shirley's method to the interaction of stationary and moving, neutral two-level atomic or molecular systems with monochromatic linearly and circularly polarized electromagnetic radiation. Recently, Ho et al [183-186] have extended the single-mode Floquet formalism of Shirley to a generalized many-mode Floquet theory yielding a practical non-perturbative technique for the semiclassical treatment of the interaction of a quantum system with several monochromatic oscillating fields. Ho et al have illustrated the theory by a detailed study of the population dynamics of a three-level system driven by two monochromatic radiation fields. Also, Maricq [194] has applied it to solve the problem of the

low-energy scattering by a vibrating molecule.

In fact the list of applications of Floquet theorem is quite extensive. A comprehensive survey of different Floquet approaches for two-level systems published before 1976 is given by Dion and Hirschfelder [187] which also includes a description of the nine Floquet theorems. Some of the earlier applications of Floquet theory to excited atomic and molecular states in strong fields can be found in the review by Bayfield [188]. Recent developments in semiclassical Floquet theories for intense-field multiphoton processes have been reviewed by Chu [186].

## 2. Applications to Magnetic Resonance

The earliest known application of Floquet theorem in magnetic resonance is by Bucci et al [189-191]. A strong, continuous rf field can cause a multiple-quantum resonance, in continuous wave (cw) experiments, to shift in frequency [192-193] in analogy to Bloch-Siegert effects [122]. Bucci et al [189] using Floquet theorem confirmed these effects quantitatively and formulated a new theoretical approach which circumvents the rotating frame (in spin  $1/2$  NMR) by using the second quantization formalism [190]. This work led to multiple-quantum experiments with two different rf fields which involve the absorption of  $p$  photons from one wave and the simultaneous emission of  $p \pm 1$  photons to the other wave [191]. Maricq has used the Floquet solution for the evolution operator of a spin  $1/2$  NMR [64-66] and also the single resonant

frequency irradiation of a spin 1 NQR system in a multiple-pulse experiment [33]. The periodicity referred to in these experiments is of the multiple-pulse sequences in the interaction frame. The effective Hamiltonian thus obtained has been used to examine the equilibrium properties of the system [33,64-66,195]. Recently [196] Maricq has also used the method of second quantization [197] to study the relaxation and equilibrium of a spin system coupled to a radiation field. The idea of Shirley's Floquet states have been successfully used in the study of multi-photon NMR [198,199]. A semiclassical approach involving the development of the method of transformations to rotating coordinate frames, particularly suitable for magnetic resonance problems, has been recently reviewed by Series [200].

We now present in the following the Floquet Theorem and its application to study the dynamics and equilibrium properties of a spin  $3/2$  solid when irradiated with a periodic multiple-pulse sequence. We have adapted the method of Maricq [64-66] for this purpose. In the following Section we present Floquet theorem and a derivation of Floquet Hamiltonian to study the experiments of the kind mentioned above..

#### V.B. Time-Periodic Quantum Mechanical Systems and the Floquet Theorem

The time-dependent Schrödinger equation is

$$\frac{d U(t)}{dt} = -iH(t)U(t) , \quad (V.1)$$

assumption,  $\mathcal{H}(t+t_p) = \mathcal{H}(t)$ , it follows that  $V(t)$  must be a solution to Schrödinger equation with the initial condition  $V(t=0) = U(t_p)$ . Next we set  $W(t) = U(t)U(t_p)$ . By operating with  $U(t_p)$  from the left on both sides of Schrödinger equation for  $U(t)$  (Eqn. V.1) it follows that  $W(t)$  is also a solution with the initial condition  $W(t=0) = U(t_p)$ . From the uniqueness of the solution we must then have  $W(t) = V(t)$  or  $U(t+t_p) = U(t)U(t_p)$ . From the definition of the operator  $P(t)$  we have

$$P(t+t_p) = U(t+t_p) \exp [i(t+t_p)\bar{\mathcal{H}}] \quad (V.4)$$

Using the previous result we obtain

$$P(t+t_p) = U(t)U(t_p) \exp [i(t+t_p)\bar{\mathcal{H}}] \quad (V.5)$$

Because  $U(t_p) = \exp(-i\bar{\mathcal{H}}t_p)$ , the above two time-independent factors cancel, leaving  $U(t)\exp(i\bar{\mathcal{H}}t)$  which is just  $P(t)$ . Thus  $P(t+t_p) = P(t)$  completing the proof.

It is to be noted that the order of the factors on the right hand side of Eqn. V.3 is important. If these factors are reversed, the resulting  $P(t)$  will not be periodic unless  $U(t_p)$  commutes with  $U(t)$  for all  $t$ , which need not be true.

It may be pointed out here that in a sense  $\bar{\mathcal{H}}$  is an effective time-independent Hamiltonian for the system. More precisely, if the time-scale for secular changes is large

compared to the period  $t_p$ , the time-averaged state vector, averaged over a period  $t_p$  evolves as if  $\bar{\mathcal{H}}$  were the Hamiltonian. Essentially we have modelled the natural Hamiltonian of the system which is time-dependent by an effective time-independent Hamiltonian, namely, the Floquet Hamiltonian.

We now substitute Eqn V.3 into the Schrödinger equation (Eqn V.1). This gives

$$\frac{dP(t)}{dt} = -i\mathcal{H}(t)P(t) + iP(t)\bar{\mathcal{H}}, \quad (V.6)$$

with  $P(0) = 1$ . Eqn V.6 is a system of linear differential equations. A perturbation scheme is obtained by invoking the following power series expansions.

$$P(t) = \sum_{n=1}^{\infty} \lambda^n P_n(t), \quad (V.7)$$

$$\bar{\mathcal{H}} = \sum_{n=1}^{\infty} \lambda^n \bar{\mathcal{H}}_n, \quad (V.8)$$

and with the substitution  $\mathcal{H} \longrightarrow \lambda\mathcal{H}$ . It is to be noted that Eqn V.7 is a time-dependent power series in  $\lambda$ , whereas Eqn V.8 is a time-independent power series in  $\lambda$ . The factor  $\lambda$  has been introduced to keep track of the various orders and is set to 1 in the end. Next we substitute Eqns V.7 and V.8 into Eqn V.6. After some algebra we obtain the main result :

$$P_n(t) = -i \int_0^t P \left( \mathcal{H}(t') P_{n-1}(t') - \sum_{k=1}^{n-1} P_k(t') \bar{\mathcal{H}}_{n-k} \right) dt',$$

(V.9)

$$\text{and } \bar{\mathcal{H}}_n = \frac{1}{t_p} \int_0^{t_p} P \left( \mathcal{H}(t') P_{n-1}(t') - \sum_{k=1}^{n-1} P_k(t') \bar{\mathcal{H}}_{n-k} \right) dt'.$$

(V.10)

The  $\bar{\mathcal{H}}_n$  are obtained with the additional requirement that each  $P_n(t)$  be periodic with period  $t_p$ . It is to be noted that the two zeroth-order terms are  $P_0 = 1$  and  $\bar{\mathcal{H}}_0 = 0$ .

In magnetic resonance applications, all the above calculations are assumed to have been done in the interaction frame of the main term in the total Hamiltonian of the system.

Maricq [64] has shown the equivalence of Magnus expansion terms (Eqn IV.11) and Floquet Hamiltonian terms given by Eqn V.10, provided the latter is evaluated at times  $t = t_p$ . The correspondence between the two series is

$$\bar{\mathcal{H}}_{n(F)} = \bar{\mathcal{H}}_M^{(n-1)}, \quad (V.11)$$

where  $\bar{\mathcal{H}}_{n(F)}$  is  $n$ th order Floquet Hamiltonian and  $\bar{\mathcal{H}}_M^{(n-1)}$ , the  $(n-1)$ th order Magnus Hamiltonian.

The  $n$ th-order term in Eqn V.10 is easily obtained and the expansion of  $P(t)$  is evaluated concurrently with  $\bar{\mathcal{H}}$ . This can

potentially be used to follow the evolution of the system within each cycle. This, in essence, removes the restriction of observation of the system only at stroboscopic points in the observation windows. Maricq [64] has given a proof of the fact that the series for  $\exp(-i\bar{\mathcal{H}}_p t)$  converges in mathematical sense. Thus, the power series  $\bar{\mathcal{H}} = \sum_{n=1}^{\infty} \lambda^n \bar{\mathcal{H}}_n$  must also converge. Often in many experimental situations the energy level is not sharp but spread around a central value because of the various broadening mechanisms which we have earlier discussed. Under such conditions, Maricq has concluded that in order that the Floquet Hamiltonian series converges rapidly one must irradiate the system always above resonance. In fact, it has been shown by Maricq that the decay of the quasi-stationary magnetization at long times is the consequence of the failure of series Floquet Hamiltonians (or Magnus Hamiltonians) to converge. We shall adapt Maricq's arguments for our particular system under study.

In the next Section we will show how the model Floquet Hamiltonian can be used to study the equilibrium properties of a periodically perturbed quadrupolar spin 3/2 system.

## V.C. Equilibrium Properties from Time Averages in Spin 3/2 Solids

The purpose of this Section is to derive the expression for the equilibrium magnetization of a system of spin 3/2 nuclear ensemble which is subjected to a time-periodic external

perturbation. The corresponding Hamiltonian will be explicitly time-dependent. This precludes the direct application of ensemble averaging procedure to arrive at the equilibrium properties of the system. One approach to surmount this problem is to approximate the time-periodic system by another that evolves under a time-independent effective Hamiltonian, namely, the Floquet Hamiltonian described in the last Section. The disadvantage of this procedure is that one is then confronted by the question of the uniqueness of  $\bar{\mathcal{H}}$  (Floquet Hamiltonian is not unique; in fact each of its eigenvalues is only defined within an additive constant of  $n\pi/t_p$ , for a non-zero positive integer  $n$ ). In order to arrive at an equilibrium value that is independent of the choice of  $\bar{\mathcal{H}}$ , an alternative route is taken to calculate the equilibrium magnetization from the time average of  $M(t)$ . This procedure is based on the following argument.

A macroscopic collection of quadrupolar spin  $3/2$  nuclei in a solid sample will obey the mixing property [202-204]. The mixing property guarantees that if a nonequilibrium population of spin states is introduced locally, so that only a small portion of the sample is affected, then after a time the nonequilibrium state will spread uniformly throughout the sample via spin diffusion. A dynamical system that obeys this mixing property is ergodic [203,204]. In the case of a conservative Hamiltonian governing the spin system, this guarantees the equality between



the time average of the magnetization (expectation value taken along the rf detector coil axis)

$$M_{eq} = \lim_{T \rightarrow \infty} \left( \frac{1}{T} \right) \int_0^T \text{Tr} B \rho(t) dt, \quad (V.12)$$

and the ensemble average :

$$\frac{M_{eq}}{M_i} = \frac{\text{Tr}(Q \mathcal{K} \text{Tr}(\mathcal{K}B))}{\text{Tr} \mathcal{K}^2 \text{Tr}(QB)}, \quad (V.13)$$

where  $Q$  is a traceless Hermitian operator and is defined to be the initial reduced density operator (immediately after the preparatory pulse) and is the same as  $\rho(0)$  defined in Eqn. III.10 ( $t_v \approx 0$ ). Also,  $B$  is the magnetization operator already defined in Eqn II.69. We explore in the following the extension of the time-average approach for calculating equilibrium properties in spin 3/2 NQR experiment, to a periodic time-dependent Hamiltonian.

Calculations of the magnetization using the Floquet form for the evolution operator leads to an equilibrium value of :

$$M_{eq} = \lim_{T \rightarrow \infty} \left( \frac{1}{T} \right) \int_0^T \text{Tr} \left\{ B P(t) \exp(-i\bar{H}t) \rho(0) \exp(i\bar{H}t) P^\dagger(t) \right\} dt.$$

(V.14)

Here  $U(t) = P(t) \exp(-i\bar{H}t)$  is the propagator for the time-periodic

Schrödinger equation (Eqn V.1). By interchanging the order of  $P^\dagger(t)$  and the remainder of the expression in the trace, we can consider the magnetization to arise from the product of two terms : the quantity  $\mathcal{R}(t) = \exp(-i\bar{\mathcal{H}}t)\rho(0)\exp(i\bar{\mathcal{H}}t)$ , in which the spin system appears to evolve under an energy-conservative Hamiltonian  $\bar{\mathcal{H}}$  and the time-periodic observable

$$P^\dagger(t)BP(t) . \quad (V.15)$$

The limit, as  $T \rightarrow \infty$ , of the integral in Eqn V.14 is non-zero only if the integrand has a component that is constant. This is because, as the time variation is periodic, the integral will be sweeping two equal and opposite areas such as those of a sinusoidal function. This results in the value of the integral becoming zero.

Whether the integral in Eqn V.14 will have a constant component, depends on the Fourier spectra of the operators  $P^\dagger(t)BP(t)$  and  $\mathcal{R}(t)$ . Because  $P(t)$  has a periodicity of  $t_p$ , we can expand  $P^\dagger(t)BP(t)$  in a Fourier series, obtaining :

$$P^\dagger(t)BP(t) = \sum_k B_k \exp(ik2\pi t/t_p) , \quad (V.16)$$

whereby the spectrum is discrete. In order that a particular frequency component  $B_k$ , contributes to the time average, the operator  $\mathcal{R}(t)$  must include a component that oscillates with

frequency  $-k2\pi/t_p$ . Application of the spectral theorem to  $\tilde{\mathcal{K}}$  provides the following expansion for  $\mathcal{R}(t)$  :

$$\mathcal{R}(t) = \exp\left\{-it \int \lambda d\lambda |\lambda\rangle\langle\lambda|\right\} \rho(0) \exp\left\{it \int \lambda d\lambda |\lambda\rangle\langle\lambda|\right\}, \quad (\text{V.17})$$

where  $\tilde{\mathcal{K}}$  is assumed to have a continuous spectrum of eigenvalues  $\lambda$ . Now, since

$$\{|\lambda\rangle\langle\lambda|\}^n = |\lambda\rangle\langle\lambda|, \quad (\text{V.18})$$

therefore,

$$\exp\left\{-it \int \lambda d\lambda |\lambda\rangle\langle\lambda|\right\} = \exp(-it\lambda) \left\{\int d\lambda |\lambda\rangle\langle\lambda|\right\}. \quad (\text{V.19})$$

And Eqn V.17 reduces to

$$\begin{aligned} \mathcal{R}(t) &= \exp(-it\lambda) \left\{\int d\lambda |\lambda\rangle\langle\lambda|\right\} \rho(0) \left\{\int d\lambda |\lambda\rangle\langle\lambda|\right\} \exp(it\lambda) \\ &= \iint d\lambda d\lambda' \exp\left\{-i(\lambda - \lambda')t\right\} |\lambda\rangle\langle\lambda| \rho(0) |\lambda'\rangle\langle\lambda'|. \end{aligned} \quad (\text{V.20})$$

From Eqn V.20 it is apparent that the range of frequencies is dictated by the differences between the eigenvalues of  $\bar{\mathcal{H}}$  and the line shape is determined by the matrix elements of  $\rho(0)$  or equivalently of  $Q$  in the basis of the eigenstates of  $\bar{\mathcal{H}}$  (the line shape is the Fourier transform of the autocorrelation function of  $M(t)$  [205]). Now the counter-rotating component from Eqn V.20 is given by

$$\exp \left\{ -i(\lambda - \lambda') t \right\} = \exp \left\{ -ik2\pi t / t_p \right\} \quad , \quad (V.21)$$

$$\text{i.e. } \lambda - \lambda' = k2\pi / t_p$$

$$\text{or } \lambda - k2\pi / t_p = \lambda' \quad . \quad (V.22)$$

Combining the term in Eqn V.18 that is proportional to  $\exp(ik2\pi t / t_p)$  with the counter-rotating component given by Eqn V.22, we get from Eqn V.20 the equilibrium magnetization as

$$M_{eq} = \sum_k' \int d\lambda \langle \lambda - k2\pi / t_p | B_k | \lambda \rangle \langle \lambda | \rho(0) | \lambda - k2\pi / t_p \rangle .$$

(V.23)

The prime over summation indicates that the sum over  $k$  includes only those terms for which  $\lambda - k2\pi / t_p$  is an eigenvalue of  $\bar{\mathcal{H}}$ . This is an alternative way of saying that we are taking only the

diagonal elements to find out the trace which gives us the magnetization vector. The terms with  $k \neq 0$  represent the contribution from transitions between states with different energies. The trace in Eqn V.23 will be non-zero only when  $\lambda = \lambda - k2\pi/t_p$ .

The use of Eqn V.20 requires knowledge of the eigenstates of  $\bar{\mathcal{H}}$ . This is readily obtained for systems in which a small groups of spins interact strongly among themselves but weakly with the rest of the sample. In that case the matrix operators that describe the interactions within the group are of a manageable size and can be diagonalized. However, in more general circumstances, where strong interactions between many spins are involved the above expression is not very convenient.

Eqn V.20 for the equilibrium magnetization can be transformed into a more appealing form under the assumption that only the  $k=0$  term in the Fourier series contributes significantly to the sum, i.e., only the constant components of  $P^\dagger(t)BP(t)$  and  $\mathcal{H}(t)$  are significant. This assumption is valid under the following circumstance:  $|\lambda_i - \lambda_j| < 2\pi/t_p$  for all eigenvalue pairs of  $\bar{\mathcal{H}}$ . If this is the case, then the spectrum of  $\mathcal{H}(t)$  lies entirely within the frequencies  $-\pi/t_p$  and  $\pi/t_p$ , whereby  $\lambda - k2\pi/t_p$  is an eigenvalue of  $\bar{\mathcal{H}}$  only for  $k=0$ . Eqn V.20 reduces, under these circumstances, to

$$M_{eq} = \int d\lambda \langle \lambda | \left\{ P^\dagger(t) B P(t) \right\}_{av} | \lambda \rangle \langle \lambda | \rho(0) | \lambda \rangle, \quad (V.24)$$

where  $B_0$  is the zero Fourier coefficient of the Fourier expansion of  $P^\dagger(t)BP(t)$ , i.e.

$$B_0 = \frac{1}{T} \int_0^T P^\dagger(t)BP(t)dt \quad (V.25)$$

Each of the operators  $\{P^\dagger(t)BP(t)\}_{av}$  and  $\rho(0)$  can be written as the sum of two terms : one operator that commutes with  $\bar{\mathcal{H}}$  and is diagonal in the  $|\lambda\rangle$  basis, and a second that is completely off diagonal. Clearly, the diagonal part of  $\rho(0)$  is the equilibrium density operator. We consider for a moment a conservative system, i.e., one with  $P(t) = 1$ . If the energy is the only constant of motion, two important properties hold true : First, any operator that commutes with the Hamiltonian must be expressible as a function of it, and second, the system is ergodic [203,204]. In the case of a time-periodic Hamiltonian,  $\bar{\mathcal{H}}$  plays the role of the constant of motion, although it does so only at intervals of  $t_p$ . Nevertheless, we use the first property to write the diagonal portion of the initial density operator as

$$\text{diag}\{\rho(0)\} = \rho_{eq} = f(\bar{\mathcal{H}}) = \sum_{\lambda} f(\lambda) |\lambda\rangle\langle\lambda| \quad (V.26)$$

If there were a second constant of motion,  $\rho_{eq}$  should be expanded in a basis of simultaneous eigenfunctions of the two constants of motion, and therefore would be a function of both the operators. The second property enables us to use the laws of

statistical mechanics to determine the function  $f(\lambda)$ . This is achieved by maximizing the entropy  $S$ , of the system

$$S = -k_B \text{Tr} \left\{ \rho_{eq} \ln(\rho_{eq}) \right\} , \quad (V.27)$$

subject to the constraints that the density operator is normalized, i.e.,  $\int d\lambda f(\lambda) = 1$ , and subject to the energy constraint  $\langle E_i \rangle = \text{Tr}(\bar{\mathcal{H}} \rho_{eq})$ . Using the methods of undetermined multipliers [206] we obtain the result as

$$f(\lambda) = \frac{1}{Z} \exp(-\beta_{eq} \lambda) \cong 1 - \beta_i \frac{\text{Tr}(\bar{\mathcal{H}} Q)}{\text{Tr} \mathcal{H}^2} \lambda , \quad (V.28)$$

where  $Z$  is the partition function. The high-temperature approximation is invoked to expand the exponential, and the equilibrium inverse temperature  $\beta_{eq}$ , is written in terms of the initial inverse temperature ( $\beta_i$ ) from energy conservation [133] Eqn V.28 is substituted into Eqn V.26 to find  $\rho_{eq}$ , which in turn, is used to replace the diagonal part of  $\rho(0)$  in Eqn V.25 to give

$$M_{eq} = \int d\lambda \langle \lambda | \left\{ P^\dagger(t) B P(t) \right\}_{av} | \lambda \rangle \left[ 1 - \beta_i \frac{\text{Tr} \bar{\mathcal{H}} Q}{\text{Tr} \mathcal{H}^2} \lambda \right] . \quad (V.29)$$

This is easily rearranged into the desired form

$$M_{eq} = -\beta_i \frac{\langle \text{Tr} \bar{Q} \rangle \langle \text{Tr} \langle P^\dagger(t) B P(t) \rangle_{av} \bar{Q} \rangle}{\text{Tr} \bar{Q}^2} \quad (V.30)$$

and in the application of this equation in the next Chapter to spin-locking experiment in NQR of spin 3/2 it is normalized by dividing by the initial magnetization  $M_i$  given by

$$M_i = -\beta_i \text{Tr} \{ Q \} \quad (V.31)$$

Therefore,

$$\frac{M_{eq}}{M_i} = \frac{\langle \text{Tr} \bar{Q} \rangle \langle \text{Tr} \langle P^\dagger(t) B P(t) \rangle_{av} \bar{Q} \rangle}{\langle \text{Tr} \bar{Q}^2 \rangle \langle \text{Tr} Q B \rangle} \quad (V.32)$$

It is useful at this point, to indicate some relevant features concerning the above derivation. Eqn V.32 is quite similar to the ensemble average given in Eqn. V.13; simply the magnetization operator  $B$  is replaced by  $\langle P^\dagger(t) B P(t) \rangle_{av}$ , the average taken over one period in the numerator. This similarity underlies the relevance of the effective Hamiltonian, which is responsible for the evolution of the system over one period, in determining the equilibrium properties of the spin system. On the other hand, the appearance of the periodic operator  $P(t)$ , signifies that the behavior of the spins during the entire period must be accounted for, in order to predict the true behavior of  $M_{eq}$ .



The solution for  $M_{eq}$  given by Eqn V.32 is valid only under the condition that the spectrum of  $\bar{\mathcal{H}}$  lies completely within the frequency interval  $(-\pi/t_p, \pi/t_p)$ . This is the same condition that applies to the truncation of the series expansion for  $\bar{\mathcal{H}}$  in Eqn V.10. Therefore, in the case in which we wish to use the perturbation solutions for the Floquet form of the propagator, the condition that allows the series to be truncated also allows us to use the result of Eqn V.32 to calculate the equilibrium magnetization. Of course, if an internal interaction of the system causes the line to spread beyond  $\pm \pi/t_p$ , then Eqn V.32 applies only approximately.

#### V.D. The Krylov-Bogoliubov-Mitropolsky (KBMD) Method for Obtaining Average Hamiltonian: Comparison with the Magnus Expansion and Floquet Theorem Methods

The substitution of a time-dependent Hamiltonian by a corresponding time-independent effective or average Hamiltonian in solving different physical problems is of much current interest not only in magnetic resonance studies [29,33,65,66,208-210], but also in coherent optics [186] and solid state physics [211]. A careful evaluation of the various techniques employed for obtaining average Hamiltonian, therefore becomes pertinent. Choice of a particular technique closely depends on many factors. The average Hamiltonians obtained are in general approximations

to the corresponding natural time-dependent Hamiltonian and are usually represented as series expansion. The convergence of this series solution, both in the mathematical and practical sense (from the viewpoint of experiments), needs to be studied thoroughly. Also the mathematical conditions imposed on the existence of average Hamiltonians in various techniques need to be kept in mind so that, in a given experimental situation, the appropriate technique of choice describes the true experimental behavior.

We confine ourselves here to three averaging procedures employed so far in explaining and designing magnetic resonance experiments. Two of these techniques, namely, Magnus expansion (see Chapter IV) and Floquet theorem (see Section B of this Chapter) based average Hamiltonians have already been described. We now give a brief account of the KBM method and then examine the relative merits of the three techniques in the context of pulsed magnetic resonance experiments. Our description of this technique is based on the account given by Mehring [18] which is a simpler version of the original derivation given by Buishvili and Manabde [89].

The KBM averaging method is connected with the existence of a certain change of variables, whereby it becomes possible to eliminate the explicit time-dependence with any desired degree of accuracy relative to a small parameter, i.e., it permits the exact solution of the problem to be approximated by the solution

of a corresponding conservative problem much simpler than the original one. It is to be noted here that the KBM method is the most general way of setting up an average Hamiltonian because it does not depend upon the nature of the time-dependence of the system's true Hamiltonian. It is therefore useful for problems where stochastic averaging or aperiodic perturbations are involved. Its use for the particular case of time-periodic systems may now be illustrated.

Since the excitation of the system is periodic both the Hamiltonian and density operator can be conveniently expressed by the Fourier series

$$\mathcal{H}(t) = \sum_{n=-\infty}^{n=\infty} \hat{H}_n \exp(i\omega_n t), \quad (\text{V. 33})$$

and

$$\rho(t) = \sum_{m=-\infty}^{m=\infty} P_m(t) \exp(i\omega_m t); \quad (\text{V. 34})$$

where

$$\hat{H}_n = \frac{1}{t_p} \int_0^{t_p} dt \mathcal{H}(t) \exp(-i\omega_n t); \quad \omega_n = \frac{2\pi}{t_p} n. \quad (\text{V. 35})$$

Also  $\rho_m(t)$  corresponds to the slow motion evolution. Inserting Eqns. V.33 and V.34 into Liouville-von Neumann equation (Eqn II.73) leads to

$$\left\{ \frac{d}{dt} \rho_m(t) + i\omega_m \rho_m(t) + i \sum_k \hat{H}_{m-k} \rho_k(t) \right\} \exp(i\omega_m t) = 0.$$

(V.36)

The zeroth component  $\rho_0(t)$ , known as the slowly moving part of  $\rho(t)$ , can be easily derived from (V.36) and is given by

$$\frac{d}{dt} \rho_0(t) + i \hat{H}_0 \rho_0(t) + i \sum_{k \neq 0} \hat{H}_{-k} \rho_k(t) = 0.$$

(V.37)

In a zeroth order approximation the sum over  $k \neq 0$  can be neglected and we obtain

$$\rho_0(t) = \exp(-it\hat{H}_0) \rho_0(t=0), \quad (V.38)$$

where

$$\hat{H}_0 = \frac{1}{t} \int_0^t P dt \mathcal{H}(t), \quad (V.39)$$

according to Eqn V.38. Eqn V.39 is the same result as was obtained earlier for the zeroth order term using Magnus expansion (Eqn IV.12) and also using Floquet theorem (Eqns V.9 and V.10). The deviation, however, occurs in the higher order corrections. To obtain the higher-order terms it is convenient to Laplace transform Eqns V.36 and V.37, whereby we obtain

$$(S+i\omega_m)\rho_m(S)+i\hat{H}_m\rho_0(S)+i\sum_{k\neq 0}\hat{H}_{m-k}\rho_k(S)=0, \quad (V.40)$$

for  $m \neq 0$ , and

$$S\rho_0(S)+i\hat{H}_0\rho_0(S)+i\sum_{k\neq 0}\hat{H}_{-k}\rho_k(S)=\rho(0), \quad (V.41)$$

where

$$\rho_m(S) = \int_0^{\infty} dt \rho_m(t) \exp(-st), \quad (V.42)$$

and where the initial condition  $\rho_{m\neq 0}(t=0)=0$ ;  $\rho_0(t=0)=\rho(0)$ . We are essentially looking for an expression of the form

$$(S+i\hat{H})\rho_0(S)=\rho(0) \quad (V.43)$$

where

$$\hat{H} = \hat{H}^{(0)} + \hat{H}^{(1)} + \hat{H}^{(2)} + \dots, \quad (V.44)$$

which has the solution

$$\rho_0(t) = \exp(-it\hat{H})\rho(0), \quad (V.45)$$

for the time evolution of the 'secular' part of the density operator. The higher order terms are obtained by solving Eqn V.40 for  $\rho_m(S)$  and inserting it, after redefinition as  $\rho_k(S)$ , into Eqn V.41. For the secular motion part ( $|S| \ll \omega_m$ ),  $S+i\omega_m$  is

replaced by  $i\omega_m$  and we get the first two terms of the series in Eqn V.44 as

$$\hat{H}^{(0)} = \hat{H}_0, \quad (V.46)$$

$$\hat{H}^{(1)} = - \sum_{k>0} \frac{1}{\omega_k} \left[ \hat{H}_{-k}, \hat{H}_k \right]. \quad (V.47)$$

Expressing  $\hat{H}^{(1)}$  in the notation of Eqn IV.13, we get  $\hat{H}^{(1)}$  as

$$\hat{H}^{(1)} = -\frac{1}{2t} \int_0^t dt \int_0^t dt' \left[ \mathcal{H}(t) - \bar{\mathcal{H}}^{(0)}, \mathcal{H}(t') - \bar{\mathcal{H}}^{(0)} \right] \quad (V.47a)$$

Comparing Eqns IV.13 and V.47a, it is evident that both the average Hamiltonians are equal if  $\bar{\mathcal{H}}^{(0)} = \hat{H}_0 = 0$ . If, however,  $\bar{\mathcal{H}}^{(0)} = \hat{H}_0 \neq 0$  there is a 'non-secular' contribution to  $\bar{\mathcal{H}}^{(1)}$  which leads to improper results in the Magnus treatment. This will be illustrated below with one example :

The Bloch-Siegert Shift has been calculated using all the above techniques by different workers. The results of these calculations give the shift as follows

(a) the Magnus expansion based AHT [89]:

$$\omega = \omega_0 - \frac{\omega^2}{4\omega_0} \quad ; \quad (V.48)$$

(b) the KBM method based AHT [80] :

$$\omega = \omega_0 + \frac{\omega^2}{4\omega_0} + \dots, \quad (V.49)$$

and (c) the Floquet theorem based AHT [61] :

$$\omega = \omega_0 + \frac{b^2}{\omega_0} + \frac{b^4}{4\omega_0^3} - \frac{35b^6}{32\omega_0^5} - \dots, \quad (V.50)$$

where  $b$  in Eqn V.50 is a parameter proportional to  $\omega_1$ , the rf amplitude.

It is clear from the above, that Magnus expansion based AHT predicts erroneous value for Bloch-Siegert Shift. The KBM and Floquet theorem results match upto second order at least in the form of the expression.

Now we are in a position to compare qualitatively the three techniques for obtaining average Hamiltonian. Of all the three the Magnus expansion method seems to be most-restrictive. It imposes a special structure (i.e. of cyclicity) on the scheme of perturbation. Floquet theorem method depends only on the periodicity criterion to arrive at the average Hamiltonian. KBM is more general and, using it, we can set up an average Hamiltonian for any arbitrary time dependence. Magnus expansion method allows the observation of the system only at stroboscopic

points. On the other hand, both KBM and Floquet allow the observation of the system at all times. The convergence of Magnus expansion and Floquet theorem results has been discussed by Maricq and that of KBM can be found in the book by Krylov and Bogoliubov [88].

### V.E. Summary

In this Chapter we have reviewed the application of Floquet theorem to systems characterized by time-periodic Hamiltonians. Floquet theorem based AHT has been discussed and has been used to derive equilibrium properties in a spin  $3/2$  NQR. Finally we have made a comparative study of the various techniques for setting up the average Hamiltonian. KBM appears to be the most general method to set up the average Hamiltonian. However, we have limited ourselves in this Chapter and the following one to Floquet theorem-based methods only; the abovementioned generality of the KBM approach, although realized towards the end of our work, could not be gone into further.

In the next Chapter we shall confine ourselves to Floquet theorem based AHT to explain the results of pulsed spin-locking experiments in NQR of spin  $3/2$  solids.



## CHAPTER VI

### PULSED SPIN-LOCKING IN THE NQR OF SPIN 3/2 SOLIDS : THEORY AND EXPERIMENTS

In this Chapter we present our theoretical calculations of the response of spin 3/2 solids to spin-locking multiple-pulse sequences. A computer program has been written to evaluate and plot graphically the final expression for equilibrium magnetization during the abovementioned multiple-pulse sequence. In this program, a Monte Carlo based method called 'systematic sampling' has been used to take into account the polycrystalline (powder) nature of the samples used in our experiments. A complete listing of the Fortran program appears in Appendix A.

The experiments performed by us on powder samples of  $\text{NaClO}_3$  and  $\text{HgCl}_2$  ( $^{35}\text{Cl}$  resonance) at room temperature are then presented and interpreted in the light of our theory.

#### VI.A. The Equilibrium Magnetization in the NQR of Spin 3/2 Solids in the pulsed Spin-Locking Experiment

In pulsed spin-locking experiments the time domain signal is sampled at the echo-tops after every pulse in the sequence. Therefore, the effect of static inhomogeneous interactions,

namely, the time-independent terms in the spin Hamiltonian involving single resonant spins, such as efg inhomogeneities and heteronuclear dipolar coupling is removed completely.

The interactions that determine the behavior of the time-domain signal are therefore the ones that contribute to the width of the frequency domain signal in a homogeneous fashion, namely, the torsional oscillations of units containing the quadrupolar nuclei in the solid sample and also to a lesser extent the homonuclear dipolar couplings. The contribution of the homonuclear dipolar couplings is in general, negligibly small in spin  $3/2$  solids. Nevertheless, we will include it in our calculations. The total Hamiltonian of the combined system of spin  $3/2$  solid and spin-locking multiple-pulse sequence in QIF is, therefore written as :

$$\tilde{\mathcal{H}}' = -\omega_1(t)\bar{N} - \Delta K\bar{L} + \tilde{\mathcal{H}}'_{D(homo)}, \quad (VI.1)$$

where  $\bar{N}$ ,  $\bar{L}$  and  $\tilde{\mathcal{H}}'_{D(homo)}$  are defined in Eqns II.60a, II.32a and II.64 respectively. For this particular experiment, the rf Hamiltonian in the  $\delta$ -pulse limit (the first term in VI.1) will take the following form for the first pulse :

$$\tilde{\mathcal{H}}'_{rf(1)} = -\theta_0 \delta(t) \bar{N}_1; \quad (VI.2)$$

and for all other pulses (i.e. the pulses in the sequence), it is :

$$\tilde{\mathcal{H}}'_{rf(2)} = \theta \sum_{k=0}^{\infty} \delta\{t - \tau(2k+1)\} \bar{N}_2, \quad (\text{VI.3})$$

$$= \frac{\theta \bar{N}}{2\tau} \sum_{-\infty}^{\infty} (-1)^n \exp(in\pi\tau) \quad , \quad (\text{VI.4})$$

where  $2\tau$  is the interpulse duration or period of the pulses in the sequence. The subscripts 1 and 2 in Eqns VI.2 and VI.3 distinguish the phases of the first pulse with respect to the rest of the pulses.  $\Delta$  is a parameter that takes into account both resonance offset and the average effect of the torsional oscillations over the timescale of the experiment. It is to be noted that Eqn VI.4 is Fourier series representation of the spin-locking pulse sequence.

For the choice of the flip angle  $\theta < 1$  radian the QIF is appropriate for applying the perturbation solution for  $\tilde{\mathcal{H}}$  and  $P(t)$ . The recursion relations given in Eqns V.9 and V.10 can be used to calculate the Floquet Hamiltonians upto third order. It can also be calculated using the Baker-Campbell-Hausdorff theorem [141-151] to the evolution operator over one period :

$$U(2\tau) = \exp[-i(-\Delta \bar{L} + \tilde{\mathcal{H}}'_{D(\text{homo})})] \exp[+i\theta \bar{N}_1] \exp[-i(-\Delta \bar{L} + \tilde{\mathcal{H}}'_{D(\text{homo})})].$$

(VI.5)

A straightforward but tedious algebra\* leads us to the

\*For example, the evaluation of the integral over the discontinuities of the  $\delta$ -function has to be done painstakingly

following expressions for Floquet Hamiltonians upto third order :

$$\bar{\mathcal{H}}_1 = -\Delta K \bar{L} + \tilde{\mathcal{H}}'_{D(homo)} + \frac{\theta}{2\tau} \bar{N}_z, \quad (VI. 6)$$

$$\bar{\mathcal{H}}_2 = 0, \quad (VI. 7)$$

$$\begin{aligned} \bar{\mathcal{H}}_3 = & \frac{\theta^2}{12} \left[ \left[ \bar{N}_z, (-\Delta K \bar{L} + \tilde{\mathcal{H}}'_{D(homo)}) \right], \bar{N}_z \right], \quad (VI. 8) \\ & + \frac{\theta\tau}{12} \left[ \left[ \bar{N}_z, (-\Delta K \bar{L} + \tilde{\mathcal{H}}'_{D(homo)}) \right], (-\Delta K \bar{L} + \tilde{\mathcal{H}}'_{D(homo)}) \right]. \end{aligned}$$

(VI. 9)

Also, the periodic operators up to second order are given as :

$$P_0(t) = 1, \quad (VI. 10)$$

$$P_1(t') = -\frac{\theta}{2\pi} \bar{N}_z \sum_{n \neq 0}^{\infty} \frac{(-1)^n}{n} \exp(in\pi t'/\tau), \quad (VI. 11)$$

$$P_2(t') = \frac{\theta^2 \bar{N}_z^2}{4\pi^2} \sum_{n=-\infty}^{\infty} \sum_{p=-\infty}^{\infty} \sum_{\substack{n \neq 0 \\ n+p \neq 0}}^{\infty} \frac{(-1)^n}{p(n+p)} \exp\{i(n+p)\pi t'/\tau\}$$

$$- \left\{ \frac{\theta^2 \bar{N}_z^2}{4\pi^2} - \frac{\theta\tau}{2\pi^2} \left[ \bar{N}_z, (-\Delta K \bar{L} + \tilde{\mathcal{H}}'_{D(homo)}) \right] \right\}.$$

$$\times \sum_{n \neq 0}^{\infty} \frac{(-1)^n}{n^2} \left\{ \exp(in\pi t'/\tau) - 1 \right\} .$$

(VI.12)

In our calculations of equilibrium magnetization we also need to have the average values of periodic operators. Integrating the Eqns VI.10, VI.11 and VI.12 over the period from 0 to  $2\tau$  and dividing by  $2\tau$ , we obtain the following expressions for the average values of  $P_0(t)$ ,  $P_1(t)$  and  $P_2(t)$  :

$$\overline{P_0(t)} = 1 , \quad (VI.13)$$

$$\overline{P_1(t)} = 0 , \quad (VI.14)$$

$$\overline{P_2(t)} = -\frac{\theta}{12} \left\{ \frac{\theta}{2} \bar{N}_2^2 + \tau \left[ \bar{N}_2, -\Delta K \bar{L} + \tilde{H}'_{D(\text{homo})} \right] \right\} .$$

(V.15)

Now, the quasi-equilibrium magnetization is given by Eqn V.32, which is reproduced here:

$$\frac{M_{eq}}{M_i} = \frac{(\text{Tr } \bar{\mathcal{H}}) (\text{Tr } \{P^\dagger(t) B P(t)\}_{av} \bar{\mathcal{H}})}{(\text{Tr } \bar{\mathcal{H}}^2) (\text{tr } Q B)} . \quad (V.32)$$

Taking into consideration the perturbative expansions for  $\bar{\mathcal{H}}$  and

$P(t)$  in Eqn V.32 and arranging terms according to their order, keeping the overall order only upto three, we have :

$$\begin{aligned} & \langle P_0^\dagger(t) + P_1^\dagger(t) + P_2^\dagger(t) + \dots \rangle B \langle P_0(t) + P_1(t) + P_2(t) + \dots \rangle_{av} \\ &= B + \left[ \left\{ B\bar{P}_1 + \bar{P}_1^\dagger B \right\} + \left\{ B\bar{P}_2^\dagger \bar{P}_2 B + \left\langle P_1(t)^\dagger B P_1(t) \right\rangle_{av} \right\} \right] + \dots \end{aligned}$$

(VI.16)

Now  $\bar{P}_1 = \bar{P}_1^\dagger = 0$ ; therefore Eqn VI.16 reduces to

$$\langle P^\dagger(t) B P(t) \rangle_{av} = B + \left\{ B\bar{P}_2^\dagger \bar{P}_2 B + \langle P_1^\dagger(t) B P_1(t) \rangle_{av} \right\};$$

(VI.17)

(upto third order).

Substituting  $\bar{\mathcal{H}}^{(2)} = 0$  (Eqn VI.7) and  $\langle P^\dagger(t) B P(t) \rangle_{av}$  from Eqn VI.18 into Eqn VI.16, we obtain, upto third order :

$$\frac{M_{eq}}{M_i} = \frac{\text{Tr} \left\{ Q(\bar{\mathcal{H}}_1 + \bar{\mathcal{H}}_3) \right\} \text{Tr} \left[ B(\bar{\mathcal{H}}_1 + \bar{\mathcal{H}}_3) + \left\{ B\bar{P}_2^\dagger + \bar{P}_2 B + \langle P_1^\dagger(t) B P_1(t) \rangle_{av} \right\} \bar{\mathcal{H}}_1 \right]}{\text{Tr}(\bar{\mathcal{H}}_1 + \bar{\mathcal{H}}_3)^2 \text{Tr}(QB)}$$

(VI.18)

substituting the values of  $P_1(t)$  and  $\bar{P}_2$  from Eqns VI.11 and VI.15, it is shown straightaway that

$$B\bar{P}_2 + \bar{P}_2 B + \left\{ (P_1^\dagger(t) B P_1(t)) \right\}_{av} =$$

$$\frac{\theta^2}{24} \text{Tr} \left\{ \left[ \left[ \bar{N}_2, B \right], \bar{N}_2 \right] \bar{\mathcal{E}}_1 \right\}$$

$$+ \frac{\theta\tau}{12} \text{Tr} \left\{ \left[ \left[ \bar{N}_2, \{-\Delta K \bar{L} + \tilde{\mathcal{E}}'_{D(homo)}\} \right], B \right] \bar{\mathcal{E}}_1 \right\}. \quad (\text{VI.20})$$

Substituting Eqn VI.20 into Eqn VI.19, we obtain the final result as :

$$\frac{M_{eq}}{M_i} = \frac{\text{Tr} \left\{ (\bar{\mathcal{E}}_1 + \bar{\mathcal{E}}_2) \right\} \left[ \text{Tr} [B(\bar{\mathcal{E}}_1 + \bar{\mathcal{E}}_2)] + \frac{\theta^2}{24} \text{Tr} \left\{ \left[ \left[ \bar{N}_2, B \right], \bar{N}_2 \right] \bar{\mathcal{E}}_1 \right\} + \frac{\theta\tau}{12} \text{Tr} \left\{ \left[ \left[ \bar{N}_2, \{-\Delta K \bar{L} + \tilde{\mathcal{E}}'_{D(homo)}\} \right], B \right] \bar{\mathcal{E}}_1 \right\} \right]}{\text{Tr}(\bar{\mathcal{E}}_1 + \bar{\mathcal{E}}_2)^2 \text{Tr}(QB)} \quad (\text{VI.21})$$

The first term in the square brackets is the result that corresponds to the one obtained for the NMR of spin 1/2 nuclei by Redfield [56], who applied spin thermodynamics to the truncated Hamiltonian in the Zeeman interaction frame (the rotating frame in NMR). The second term is a correction that arises from considering the entire dynamical history of the spins and not merely the stroboscopic observation points. In other words, the oscillatory behavior of the magnetization vector about its average trajectory contributes to the equilibrium value. It is also to be noted here that the analogy of spin 3/2 NQR with spin 1/2 NMR [64,65] and spin 1 NQR [33] under multiple-pulse spin-locking

experiment is quite striking once the Hamiltonians are expressed in diagonalized representation of  $\mathcal{H}_Q$  and STO formalism.

In the next Section of this Chapter we shall describe our procedure for computing the response of a powder sample of spin  $3/2$  solid when the spin-locking multiple-pulse sequence is applied.

## VI.B. Computation of Powder Average Response

The expression  $M_{eq}/M_i$  in Eqn VI.21 is orientation dependent, due to the fact that the quadrupolar tensor (interaction matrix) is intrinsically anisotropic. In a finely crushed powder specimen quadrupolar spin sites occur with all possible orientations of their QPAS with respect to the axis of the rf detector coil. The 'powder pattern' computer simulation of the line shape is well-known in other branches of magnetic resonance such as EPR [212,213], and these techniques may be adapted for our purpose.

Now the orientation dependence of  $M_{eq}/M_i$  is in terms of  $\theta_L$  and  $\phi_L$ , which are Euler angles between QPAS major axes and rf coil axis (Figure II.I). The overall powder response of a spin  $3/2$  quadrupolar spin ensemble  $\langle M_{eq}/M_i \rangle$ , is obtained by integrating (summing and averaging) the expression  $M_{eq}/M_i$  (which is the single crystal response for any arbitrary  $\theta_L$  and  $\phi_L$ ) in the whole space  $(\theta_L, \phi_L)$ . The ranges of  $\theta_L$  and  $\phi_L$  are given as  $0 \leq \theta_L \leq \pi$  and  $0 \leq \phi_L \leq 2\pi$ .



$2\pi$  (In Figure II.I and in the following derivations, it may seem at first sight that we are rotating the detector coil axis at various  $\theta_L$ ,  $\phi_L$  for a fixed crystal orientation. This is however, equivalent to the physical reality where the 'powder' corresponds to a collection of single crystals that are at all possible orientations, which fully validates the procedure described below).

In NQR, one finds the usage of various powder averaging techniques by different authors [1,3,161,214,215]. For example Petersen [161] prescribes a procedure where averaging is done only in  $\theta_L$  space (axially symmetric cases only). In the present work, we take the more general case of non-axially symmetric NQR systems. Here the averaging is done in complete  $(\theta_L, \phi_L)$  space.

Considering the fact that the number density of orientations with respect to each  $\theta_L$  is proportional to  $\sin \theta_L$  [217] and in the  $\phi_L$  direction all orientations are equally probable, one can write the powder response as :

$$\left\langle \frac{\overline{M_{eq}}}{M_i} \right\rangle = \frac{1}{4\pi} \int_0^{2\pi} \int_0^{\pi} (M_{eq} M_i) \sin \theta_L d\theta_L d\phi_L \quad (VI.22)$$

The problem at this stage amounts to estimating this integral. Various numerical techniques including Monte Carlo [218]

procedures are in vogue for this purpose. Recently in our laboratory [219,220] a much faster Monte Carlo procedure based on systematic sampling [221,222] has been developed, which may be briefly described as follows:

In essence, our procedure considers the 'weight factor' for  $\theta_L$  and  $\phi_L$  as 'probability density functions' [221]. Accordingly, the normalized density function of  $\theta_L$  can be written as

$$P(\theta_L) = \frac{\sin \theta_L}{2} ; 0 \leq \theta_L \leq \pi , \quad (\text{IV.23})$$

and the normalization factor can be corrected later by multiplying the above response by 2. Similarly the density function of  $\phi_L$  may be understood to be of a 'uniform' type [221].

Generally in a Monte Carlo procedure one generates pseudo uniform random numbers corresponding to the integration range, and estimates the average of the integrand for the values thus generated [216]. The only difference in 'systematic sampling' is that these uniform random numbers  $R_i$  are generated systematically such that

$$R_i = \frac{(i-1/2)}{N} , \text{ where } i = 1, 2, \dots, N . \quad (\text{VI.24})$$

It is easy to see that these deterministic  $R_i$ 's also follow a uniform distribution and the estimates of averages will not change very much from those of earlier procedures.

Finally, for the range of  $\theta_L$  the  $R_i$ 's thus generated are converted to follow the density function of  $\theta_L$ ,  $P(\theta_L)$  (Eqn VI.23), in such a way that  $\theta_{Li}$ 's are obtained by solving.

$$\int_0^{\theta_{Li}} P(\theta_L) d\theta_L = \int_0^{\theta_{Li}} \frac{\sin \theta_L}{2} d\theta_L = R_i \quad (\text{VI.25})$$

Similarly, the  $\phi_i$ 's corresponding to the powder are obtained by simply scaling the uniform  $R_i$ 's for the range  $0 \leq \phi \leq \pi$ . Thus Eqn VI.22 is approximated as :

$$\langle \overline{M_{eq}/M_i} \rangle = \frac{1}{2\pi} \frac{1}{N^2} \sum_{\theta_L=\theta_{L_1}}^{\theta_{LN}} \sum_{\phi_L=\phi_{L_1}}^{\phi_{LN}} f(\theta_L, \phi_L)$$

$$\text{where } f(\theta_L, \phi_L) = M_{eq}/M_i$$

The above equations have been programmed for our calculations. The complete program listing (Fortran IV) appears in Appendix A.

In the following few pages we give the theoretical plots for  $M_{eq}/M_i$  versus various experimental parameters. The specific parameters for which the computations were performed are specified in the Figure captions. The important point to be noted is that in the Figures VI.1 (a), (b), (c), (e) and (g) we see that a finite value for the equilibrium magnetization persists even when

the contribution of the dipolar Hamiltonian to  $\mathcal{H}_{int}$  is zero. The interesting point is that spin-locking can be attained even in the presence of the torsional oscillation Hamiltonian alone. This has relevance to the experiments that we have performed in this thesis (see Section VI.C.) The internal Hamiltonian of spin 3/2 solid has a very negligible contribution from the homonuclear dipolar interaction, as pointed out in Chapter II. In the case of offset irradiation, the behavior of the equilibrium magnetization can be explained by similar curves. Another point to be noted in these Figures is the difference in the  $\theta$  dependence for the case where dipolar Hamiltonian is dominant as compared with the case when torsional Hamiltonian is dominating (refer to Figure VI.1 (a) and (d)). This difference in the  $\theta$  dependence, for example, could distinguish the mechanism that is at work in spin 3/2 solid for the establishment of spin-locked (or quasi-equilibrium) state and its subsequent decay. However, we have not pursued this point further by means of appropriate experiments. Of course, to ascertain unambiguously, the particular interaction that provides a mechanism for attainment of spin-locked state, we have to do other kinds of measurements. For example, the combined investigations of resonance line-widths and relaxation time (dipolar or quadrupolar) ought to lead to more definite conclusions. However, it is to be noted that the asymmetry parameter  $\eta$ , does not change the nature of the behavior of the  $M_{eq}/M_i$  with respect to the different parameters, as for example comparison of Figures VI.1(d) and (e) reveal.

Figure VI.1 : Quasistationary magnetization vs various experimental parameters :

(a)  $M_{eq}/M_i$  vs  $\theta$  (radians); Parameters :  $\eta = 0.0$ ,  $H_L^* = 0.0$ ,  $\Delta = 0.01$

(b)  $M_{eq}/M_i$  vs  $\Delta$  ; Parameters :  $\eta = 0.0$ ,  $H_L = 0.0$ ,  $\theta = 1.0$  radian

(c)  $M_{eq}/M_i$  vs  $\tau$  ; Parameters :  $\eta = 0.0$ ,  $H_L = 0.0$ ,  $\Delta = 0.001$

(d)  $M_{eq}/M_i$  vs  $\theta$  ; Parameters :  $\eta = 0.28$ ,  $H_L = 0.5$  Gauss,  $\Delta = 0.0$

(e)  $M_{eq}/M_i$  vs  $\theta$  ; Parameters :  $\eta = 0.28$ ,  $H_L = 0.0$ ,  $\Delta = 0.01$

(f)  $M_{eq}/M_i$  vs  $\theta$  ; Parameters :  $\eta = 0.0$ ,  $H_L = 0.50$ ,  $\Delta = 0.0$

(g)  $M_{eq}/M_i$  vs  $\theta$  ; Parameters :  $\eta = 0.0$ ,  $H_L = 0.0$ ,  $\Delta = 0.01$   $\phi_2^\dagger = 45^\circ$

---

\*

$H_L$  is local dipolar field.

$\dagger \phi_2$  is the phase of the pulses in the sequence with respect to the preparatory pulse

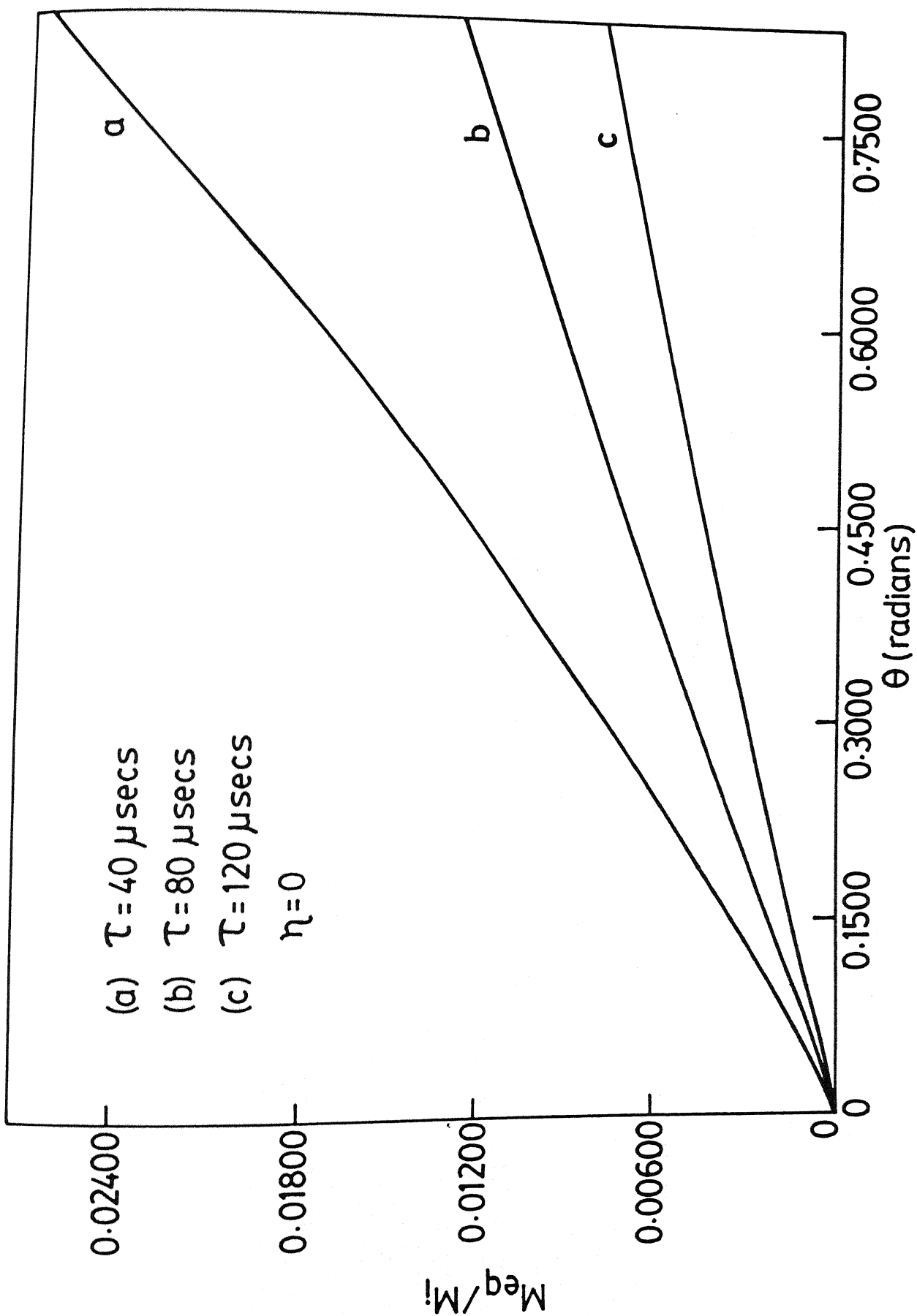


Figure VI-1(a)

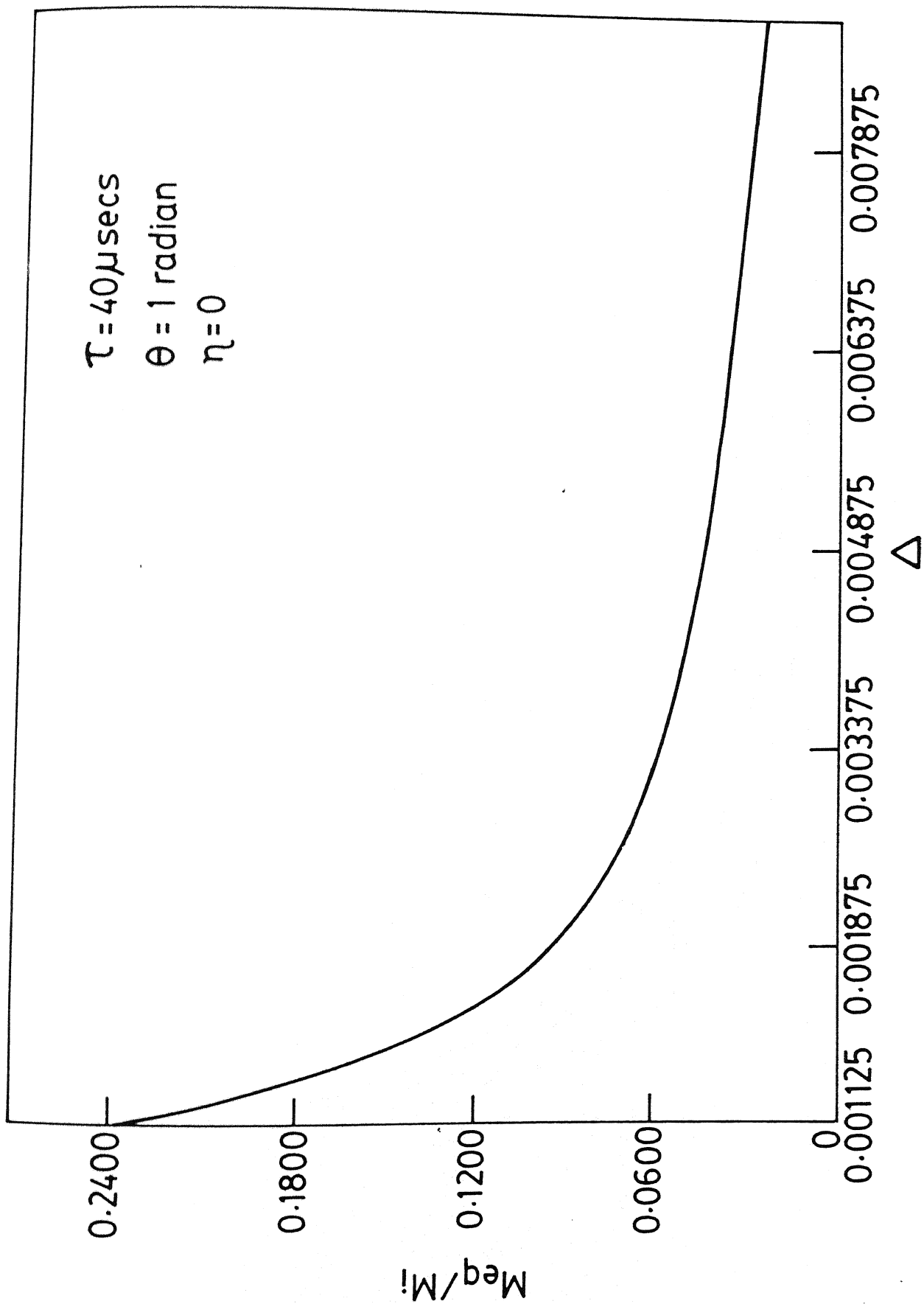


Figure VI.1(b)

- (a)  $\theta = 1.0$  radians  
(b)  $\theta = 0.8$  radians  
(c)  $\theta = 0.5$  radians

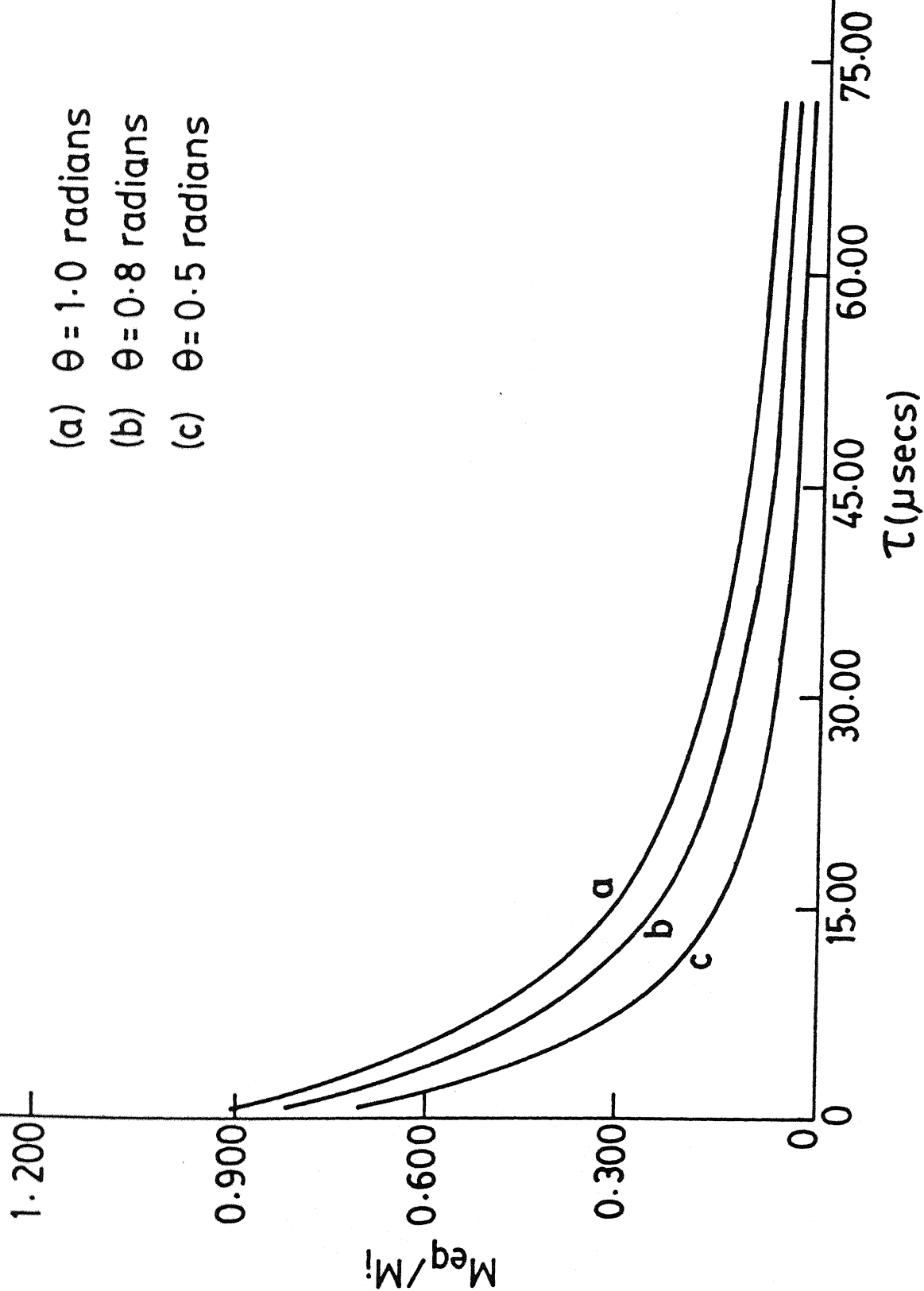


Figure VI.1(c)



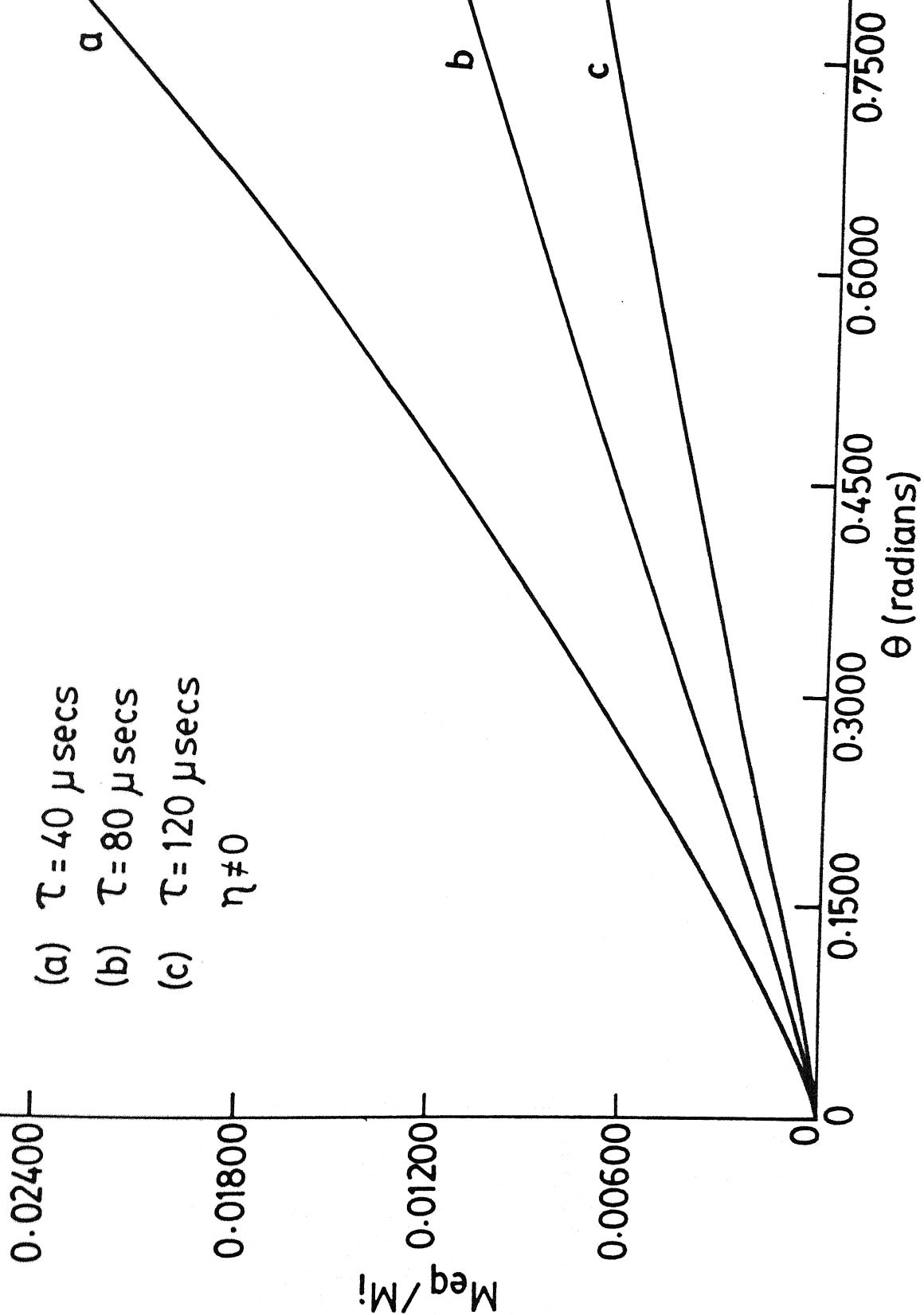


Figure VI.1(e)

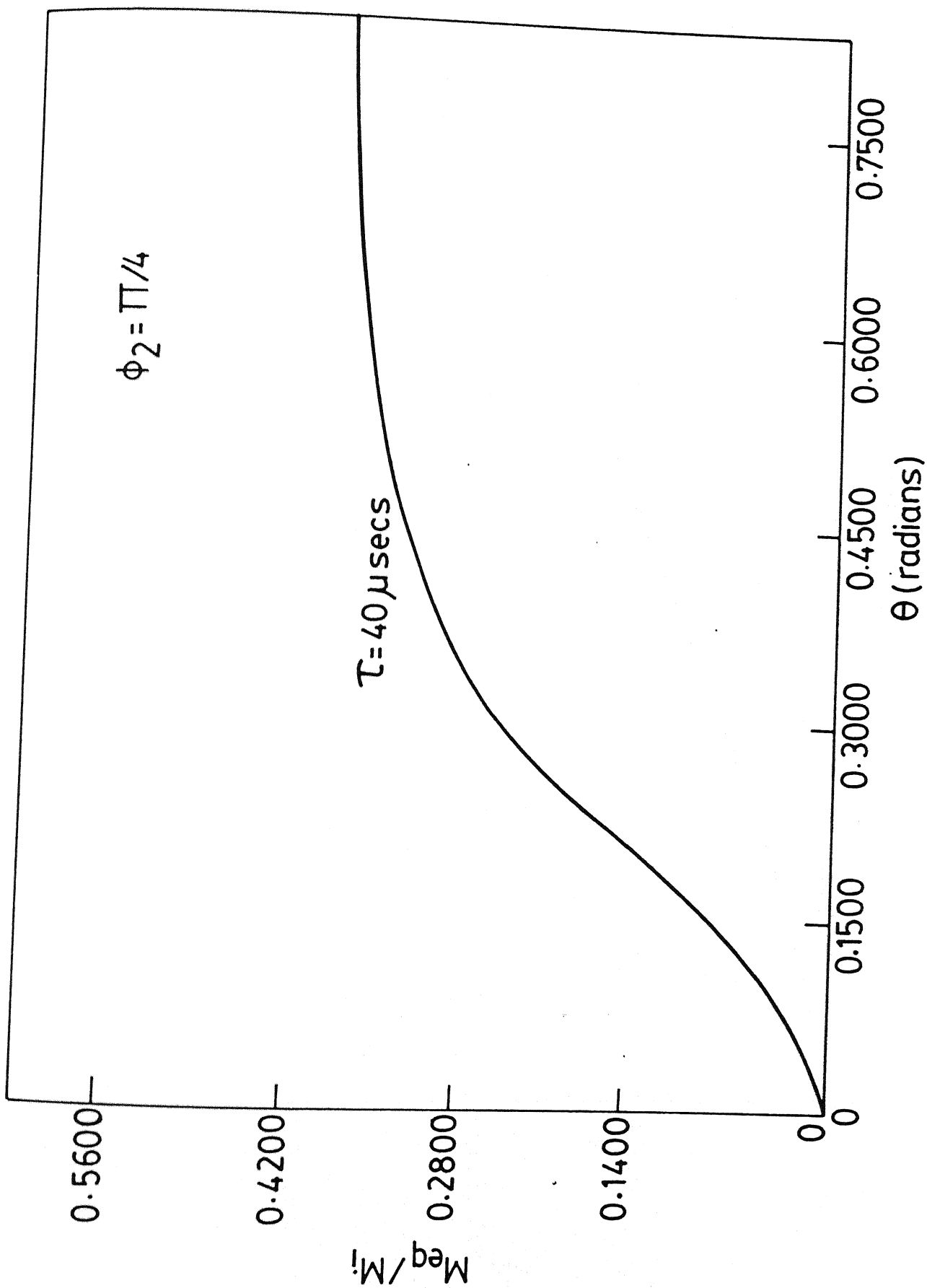


Figure VI.1(f)

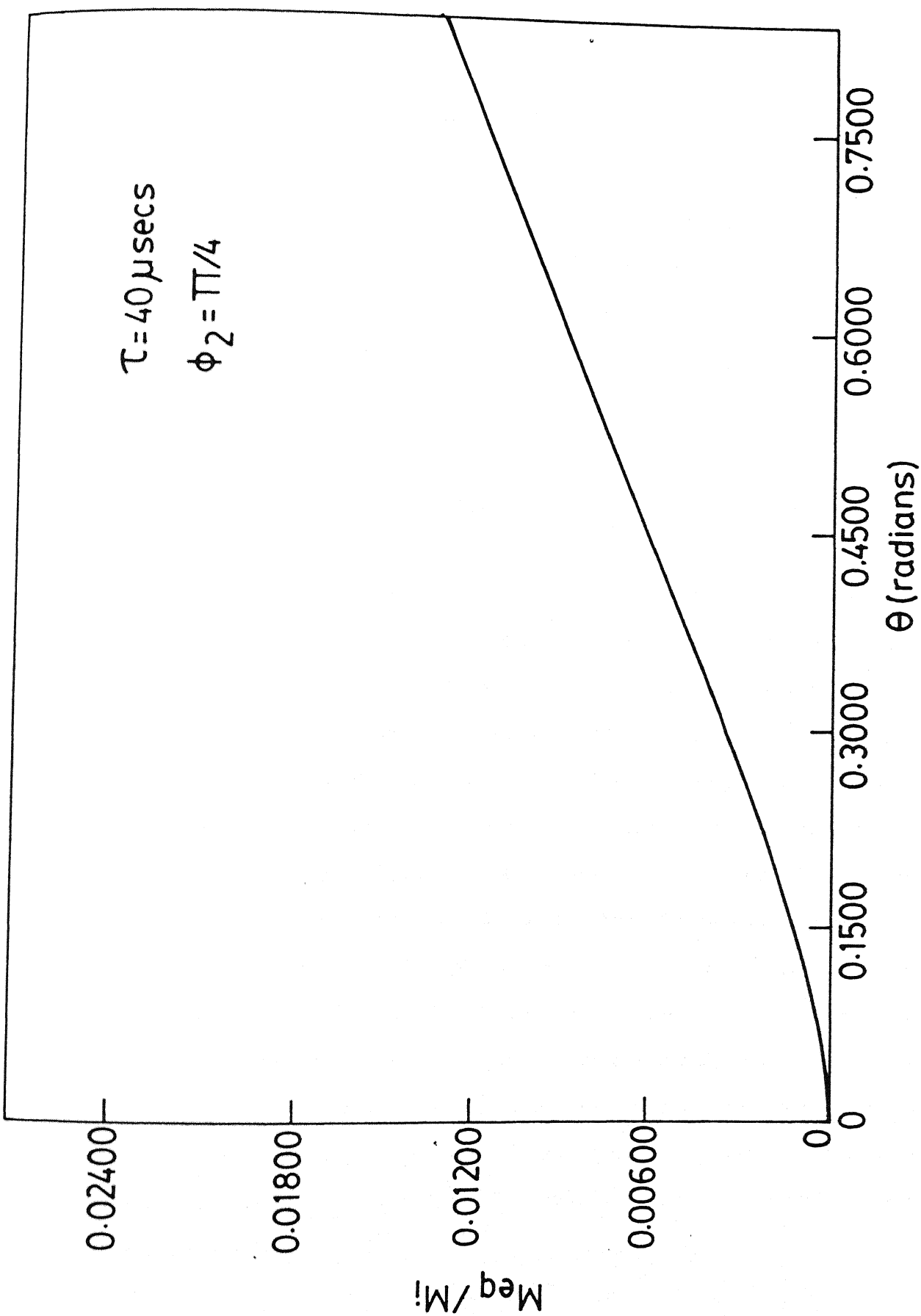


Figure VI.1(g)

### VI.C. Experimental Details and Results

As stated in Chapter IV, all the experiments were performed at the Central Leather Research Institute Madras, India. The instrument used was a Bruker CXP-90 NMR Spectrometer with its dc magnetic field switched off during the experiment. The spin-locking sequence employed was in general

$$(\theta_0)_{\phi_1} - \left\{ \tau - (\theta)_{\phi_2} - \tau \right\}_n \quad (\text{VI.26})$$

A two-pulse program, in which the second pulse would occur between 1 and 4095 counts during a loop was written and data were acquired at the end of each cycle, namely, at the 'echo tops'. The first pulse was set to be a ' $\pi/2$ ' pulse in all the experiments. The peak transmitter power employed was  $\approx$  400-500 watts corresponding to ' $\pi/2$ ' flip angle of 9  $\mu$ secs ( $^{35}\text{Cl}$  resonance in  $\text{NaClO}_3$  and  $\text{HgCl}_2$ ). A standard wide-line NMR probe (10 mm diameter) tuned to oscillate in the frequency range of 20-32 MHz was employed. The phase of the pulses in the period could be controlled in ' $\pi/2$ ' steps by using the pulse-list feature of the system's Z-17c pulser. The spectral width in this case also was  $1/4\tau$ , where  $2\tau$  is the separation between the 0 pulses in spin-locking sequence. The ambient temperature was maintained to be  $24 \pm 1^\circ\text{C}$  (for  $\text{NaClO}_3$  experiments) and  $21 \pm 1^\circ\text{C}$  (for  $\text{HgCl}_2$  experiments).

The samples chosen for the OW or MW experiments were finely crushed powder samples of  $\text{NaClO}_3$  and  $\text{HgCl}_2$ .

Sodium chlorate monocrystals have a  $\text{NaCl}$  arrangement of the ions, distorted to accomodate the  $\text{ClO}_3^-$  anions in such a way that the overall symmetry remains cubic [172]. The cubic unit cell contains four molecules. The four chlorine atoms, on one hand, and the four sodium atoms, on the other occupy equivalent lattice sites. Since oxygen is essentially nonmagnetic we neglect its presence in the discussion of the properties of the spin system of sodium chlorate. The molecular bonds, joining chlorine atoms and the associated sodium ions, are parallel to the body diagonals of the unit cell. The efg at the location of sodium and chlorine nuclei show axial symmetry ( $\eta=0$ ), resulting from (1,1,1) direction (parallel to the molecular bonds) being a three fold symmetry axis. Sodium and the two isotopes  $^{35}\text{Cl}$  and  $^{37}\text{Cl}$  of chlorine all have spin  $3/2$ . As a consequence, only one quadrupolar transition frequency is associated with each of the chlorine and sodium isotopes. As pointed out earlier we have irradiated our sample only at  $^{35}\text{Cl}$  ( $\omega_a = 29.9232$  at  $24 \pm 1^\circ\text{C}$ ).

The local field due to internal interactions in case of  $\text{NaClO}_3$  can be decomposed into the following components:

Assuming direct dipolar couplings between nuclei on an undistorted rigid lattice, the dominant contribution ( $7.050 \text{ G}^2$ ) comes from  $^{23}\text{Na}-^{23}\text{Na}$  interactions,  $^{23}\text{Na}-^{35}\text{Cl}$  interaction contribute  $3.285 \text{ G}^2$ ,  $^{23}\text{Na}-^{37}\text{Cl}$  interactions contribute  $0.742 \text{ G}^2$ . All other interactions provide almost negligible contribution, the sum being  $(H_L)^2 = 11.19 \text{ G}^2$ .

The  $\text{HgCl}_2$  single crystal, has a tetramolecular orthorhombic unit cell [172]. In this case also the local field has a negligible contribution from the homonuclear dipolar interaction. On the other hand, the angles in our theoretical computations were used for the dipolar interaction between two chlorine atoms in  $\text{HgCl}_2$ .

#### 1. Generation of $\pi/4$ phase shift

We generated ' $\pi/4$ ' phase shift by simultaneously opening two quadrature phase channel outputs of the pulser-transmitter system of the CXP-90 machine and scaling the corresponding pulse duration by a factor of  $1/\sqrt{2}$ .

#### 2. The Efficiency of Spin-locking in the Present Experiments

In general, in multiple-pulse experiments an effective field can be defined over a period (considering a periodic perturbation or pulse train). A fraction of the magnetization of the spin system gets locked and remains parallel to this effective field direction while the other fraction makes an angle with this effective field and evolves. The former component gives rise to a signal at the transmitter frequency corresponding to zero frequency in the interaction frame and is known as the pedestal. The latter gives rise to a signal with a non-zero frequency in the interaction frame- a frequency which in general reflects scaled

interactions that survive in the interaction frame under the multiple-pulse excitation.

In the case of fresh, powdered  $\text{NaClO}_3$  sample, observations on the oscilloscope traces of the FT of the quadrature detected time-domain signal, showed a signal to pedestal intensity ratio of approximately 2:1. In other words, only 33% of the magnetization remains locked in the effective field direction under our experimental conditions, while  $\sim 67\%$  of the magnetization evolves making an angle with respect to the effective field direction. It is thought that the above inefficiency in spin-locking arises essentially from poor rf inhomogeneity and/or inadequate rf field strength which might be partially compensated for either by a suitable change in the preparation pulse flip angle, rf phase alternation during the spin-locking pulse train or both [16]

### 3. The Short- and Long- time behavior of the quasiequilibrium magnetization

As far as the short-time behavior is concerned it is clear from all the spectra presented in Figure VI.5 that the spin-locked state is attained in spin  $3/2$  NQR solids also. In the following we shall examine the initial oscillatory behavior as well as the subsequent long-time decay of the magnetization.

As explained by Maricq [33,65,66] in case of spin  $1/2$  NMR and spin 1 NQR, in case of spin  $3/2$  NQR also we observe an oscillatory behavior of the magnetization initially (see Figure VI.3). During this initial portion of the signal the spins evolve effectively

Figure VI.2 : Frequency domain signal of the  $^{35}\text{Cl}$  ( $\omega_a = 29.9232$  MHz) resonance in  $\text{NaClO}_3$  powder at room temperature.

(a) Fourier transform of the one pulse FID .  
Parameters :  $\Delta = 0$ ,  $\theta = 40^\circ$ .

(b) Fourier transform of the time domain signal following a spin-locking multiple-pulse sequence (OW or MW), showing clear evidence of line narrowing (Parameters :  $\Delta=0$ ,  $\tau = 100\mu\text{sec}$ .  $\theta = 40^\circ$ )



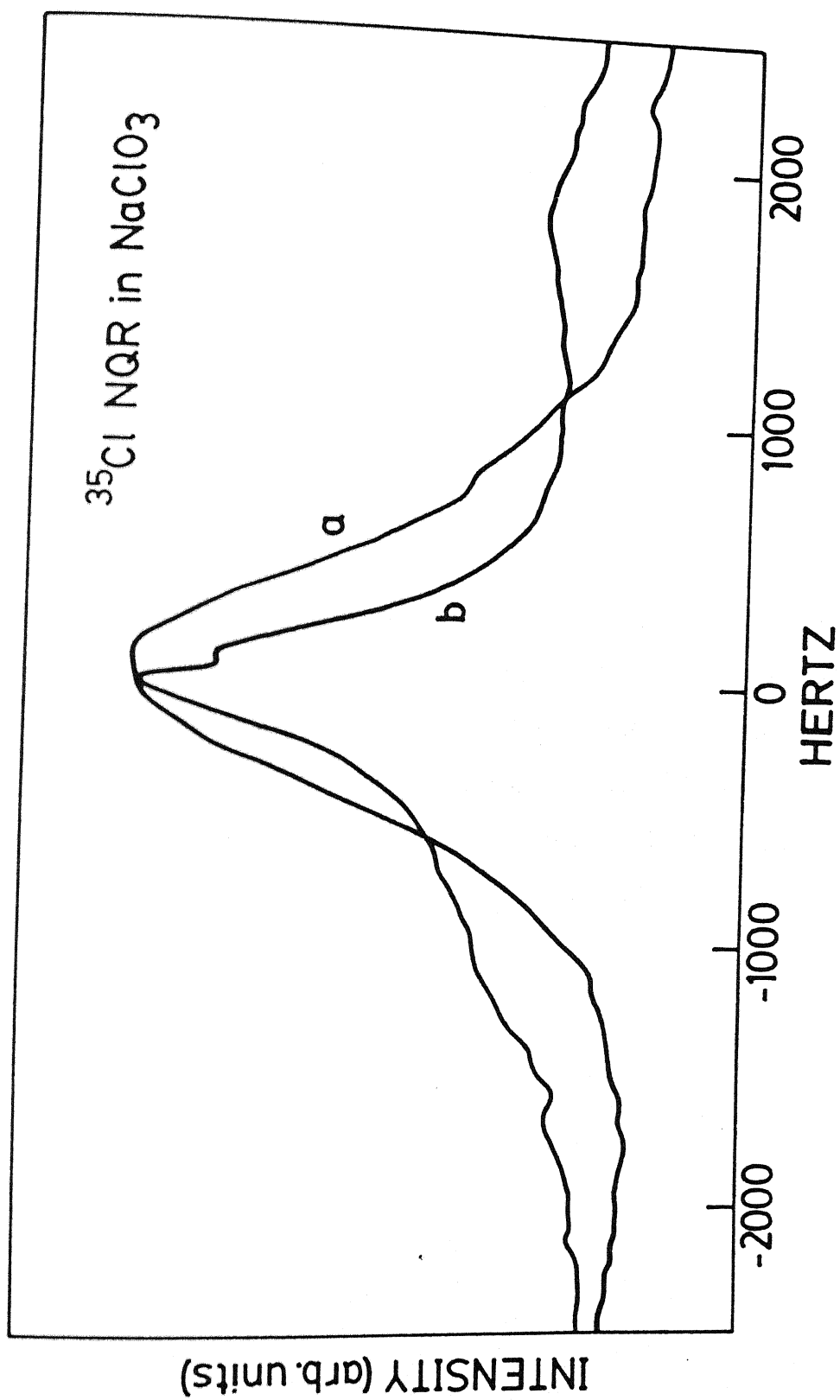


Figure VI.2

Figure VI.3 : The initial portion of the response to spin-locking multiple-pulse sequence (OW or MW) of  $^{35}\text{Cl}$  ( $\omega_a = 29.9232$  MHz) in  $\text{NaClO}_3$  powder. Parameters  $\Delta = -0.01$ ,  $\theta = \pi/4$ ,  $\tau = 40$   $\mu\text{secs}$ . The signal has been convoluted with an exponential function to reveal the initial oscillations clearly.

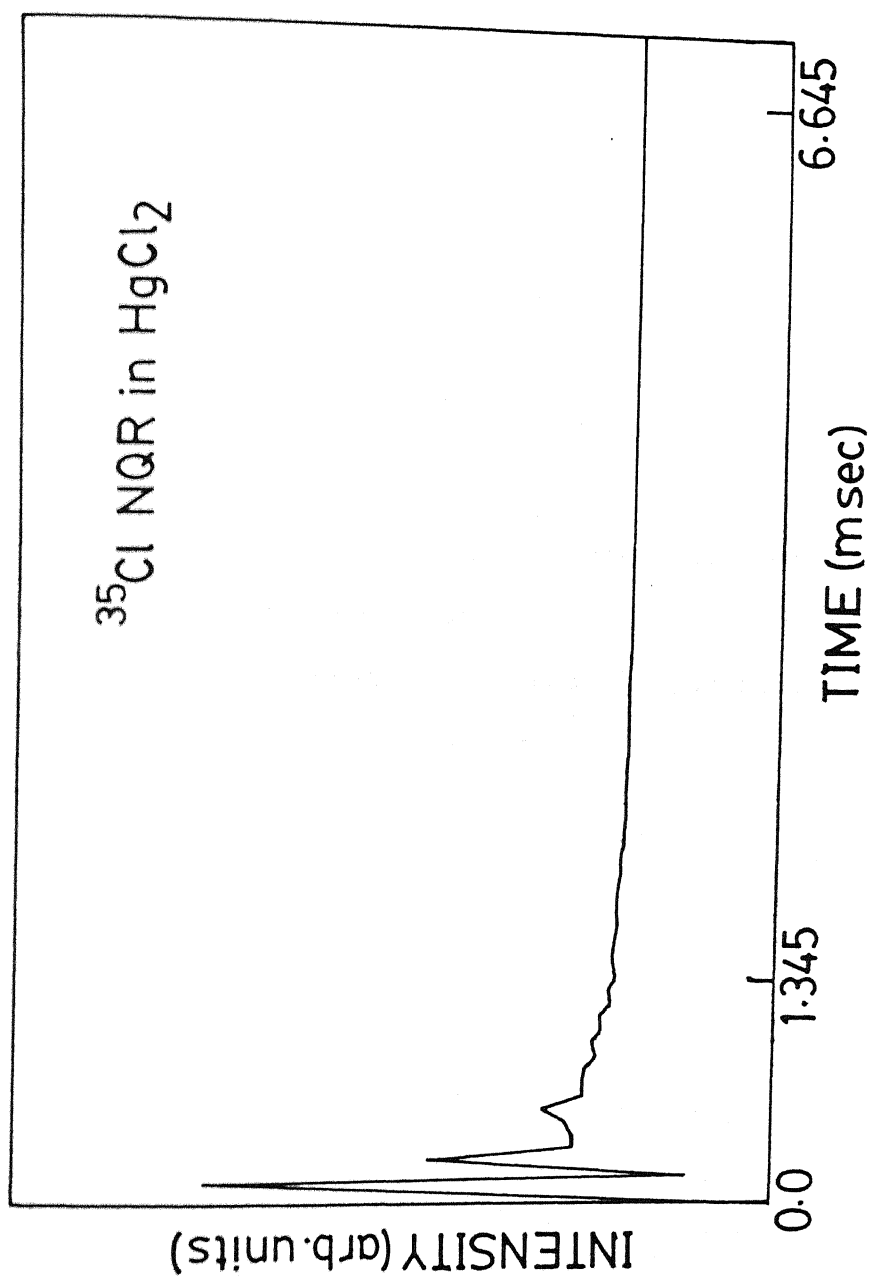


Figure VI.3

Figure VI.4 : Illustration of (a) the predicted evolution under effective Hamiltonian vs (b) the observed time-development of the magnetization for a time-periodic system [66].

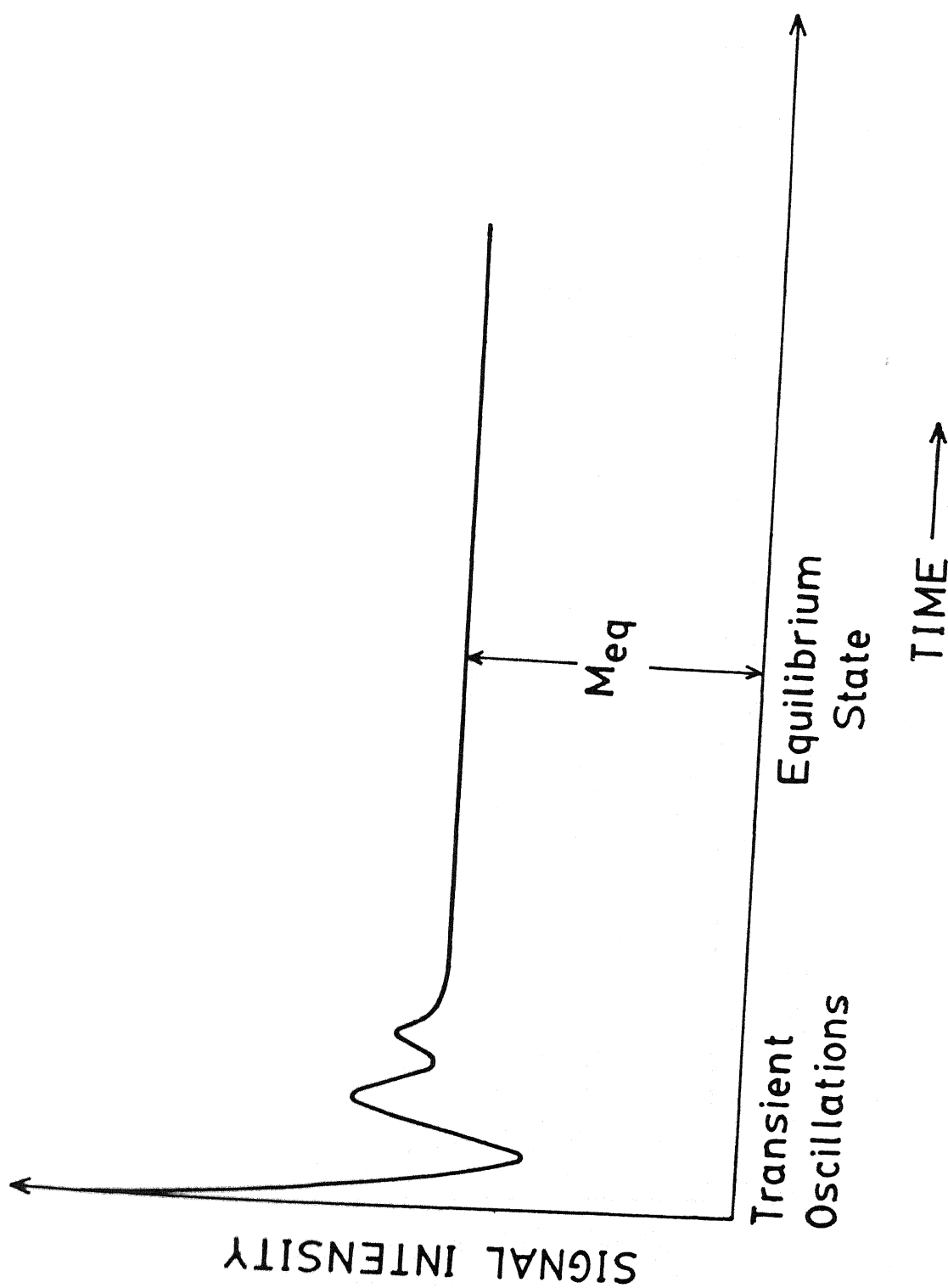


Figure VI.4(a)

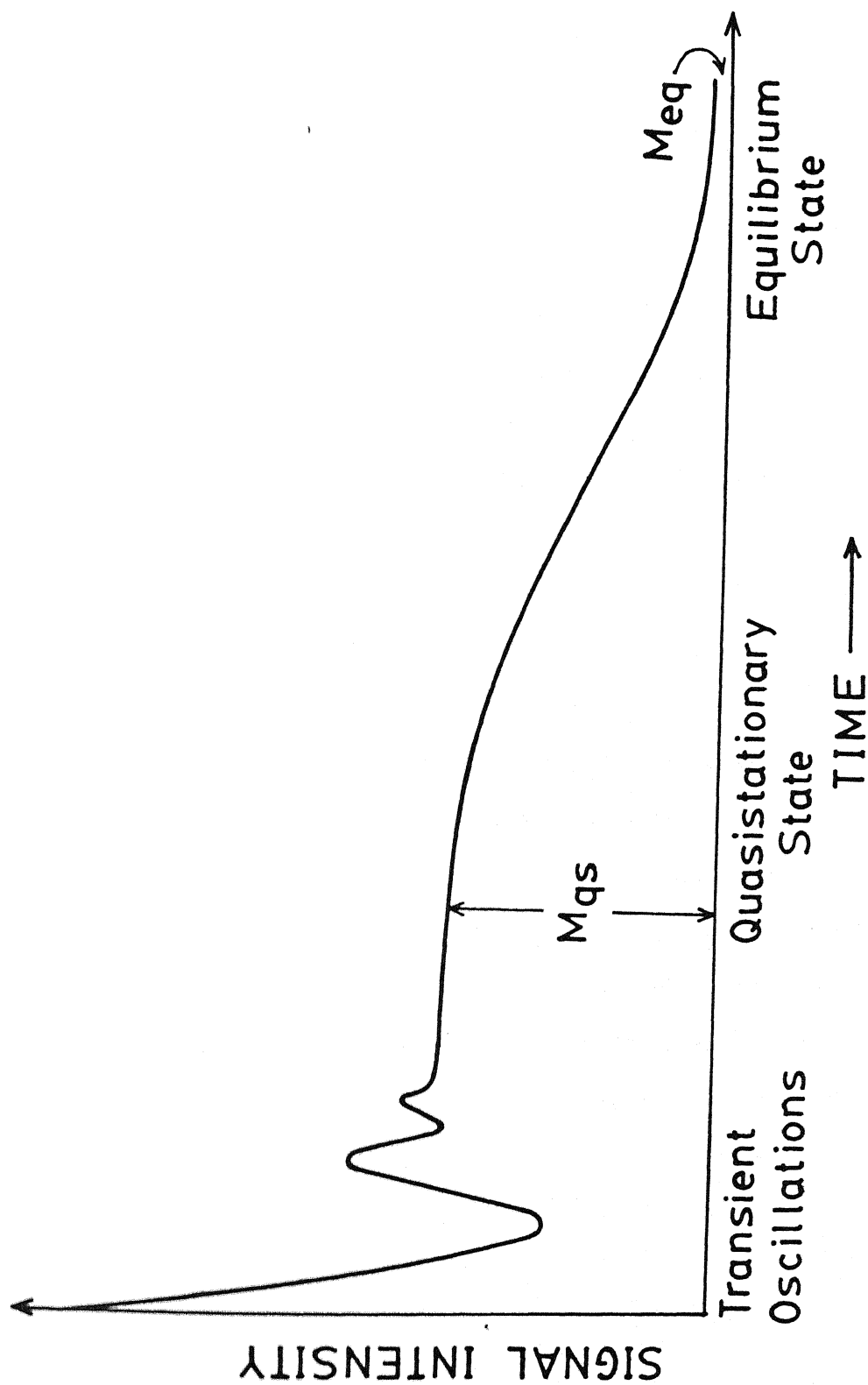


Figure VI.4(b)

Figure VI.5 : Time-domain response to OW or MW multiple-pulse sequence of the  $^{95}\text{Cl}$  signal in  $\text{NaClO}_3$  ( $\omega_a = 29.923$ ) and  $\text{HgCl}_2$  ( $\omega_z = 22.072$  MHz)

- (a)  $\text{NaClO}_3$ :  $\Delta = -5.0$  KHz ;  $\tau = 100$   $\mu\text{sec}$  ;  $\theta = 40^\circ$ .
- (b)  $\text{NaClO}_3$ :  $\Delta = +5.0$  KHz ;  $\tau = 100$   $\mu\text{sec}$  ;  $\theta = 90^\circ$ .
- (c)  $\text{HgCl}_2$ :  $\Delta = -10.0$  KHz ;  $\tau = 40$   $\mu\text{sec}$  ;  $\theta = 45^\circ$ .
- (d)  $\text{HgCl}_2$ :  $\Delta = -13.070$  KHz ;  $\tau = 40$   $\mu\text{sec}$  ;  $\theta = 55^\circ$ .
- (e)  $\text{HgCl}_2$ :  $\Delta = +4$  KHz ;  $\tau = 40$   $\mu\text{sec}$  ;  $\theta = 45^\circ$ .
- (f)  $\text{HgCl}_2$ :  $\Delta = 0.0$  KHz ;  $\tau = 40$   $\mu\text{sec}$  ;  $\theta = 90^\circ$ .
- (g)  $\text{HgCl}_2$ :  $\Delta = 0.0$  KHz ;  $\tau = 40$   $\mu\text{sec}$  ;  $\theta = 45^\circ$ .
- (h)  $\text{HgCl}_2$ :  $\Delta = -0.2$  KHz ;  $\tau = 41.955$   $\mu\text{sec}$  ;  $\theta = 29.10^\circ$ .
- (i)  $\text{HgCl}_2$ :  $\Delta = 4.0$  KHz ;  $\tau = 40$   $\mu\text{sec}$  ;  $\theta = 63.60^\circ$ ,  $\phi_2 = 45^\circ$ .
- (j)  $\text{HgCl}_2$ :  $\Delta = -14$  KHz ;  $\tau = 40$   $\mu\text{sec}$  ;  $\theta = 90^\circ$ .
- (k)  $\text{HgCl}_2$ :  $\Delta = +2.0$  KHz ;  $\tau = 41.955$   $\mu\text{sec}$  ;  $\theta = 29.10^\circ$ .
- (l)  $\text{HgCl}_2$ :  $\Delta = -10.0$  KHz ;  $\tau = 40$   $\mu\text{sec}$  ;  $\theta = 90^\circ$ .

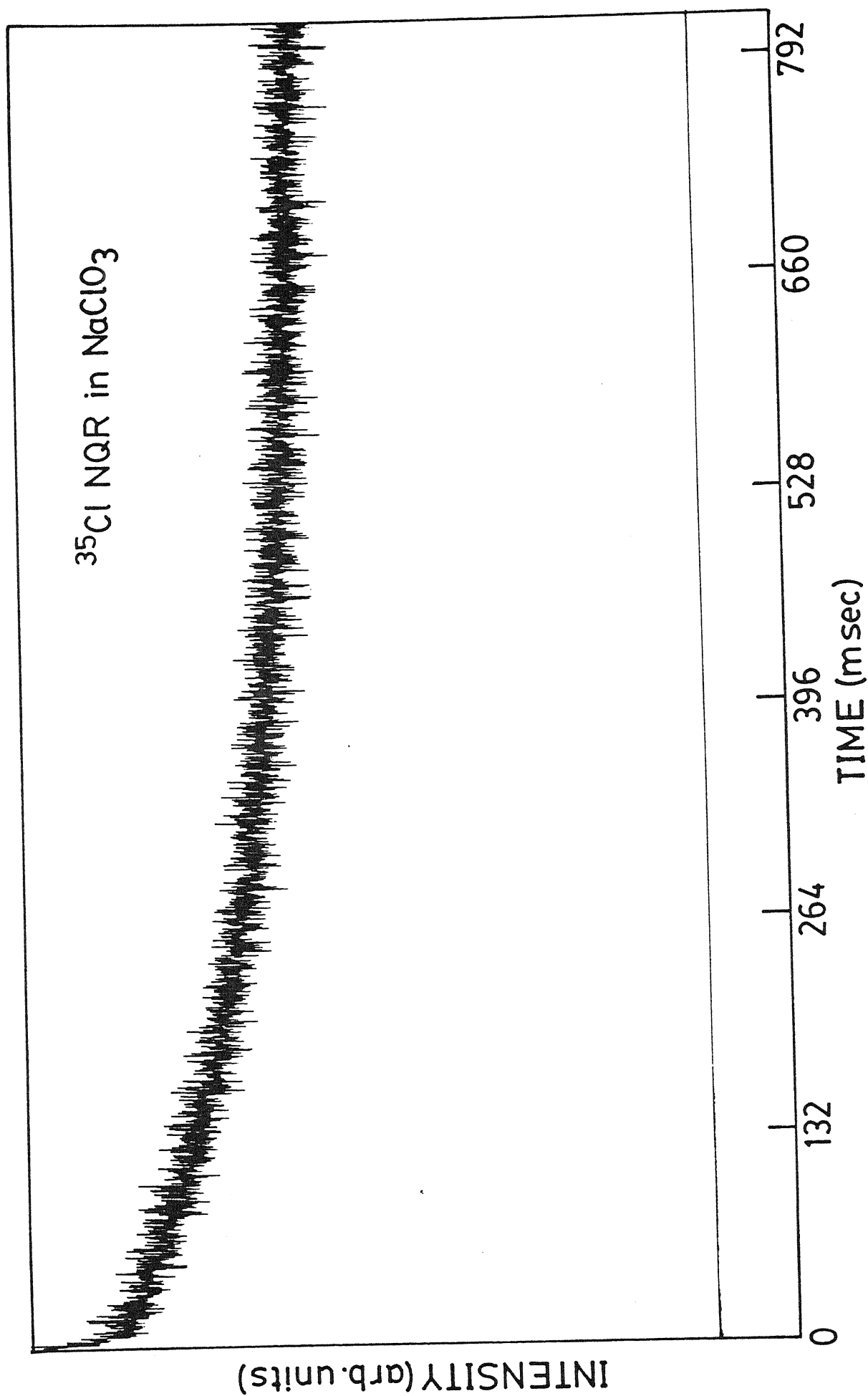


Figure VI.5(a)



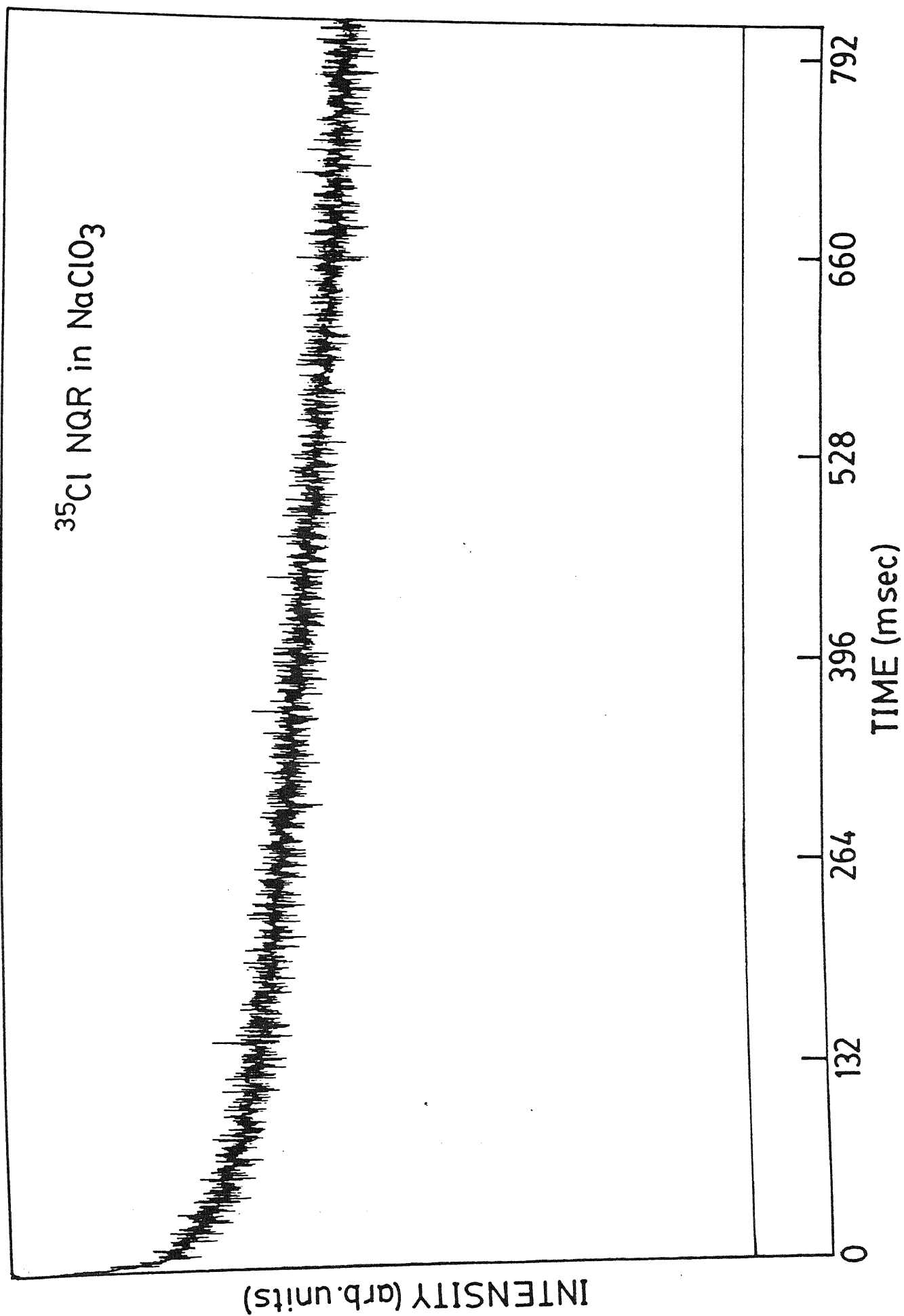


Figure VI.5(b)

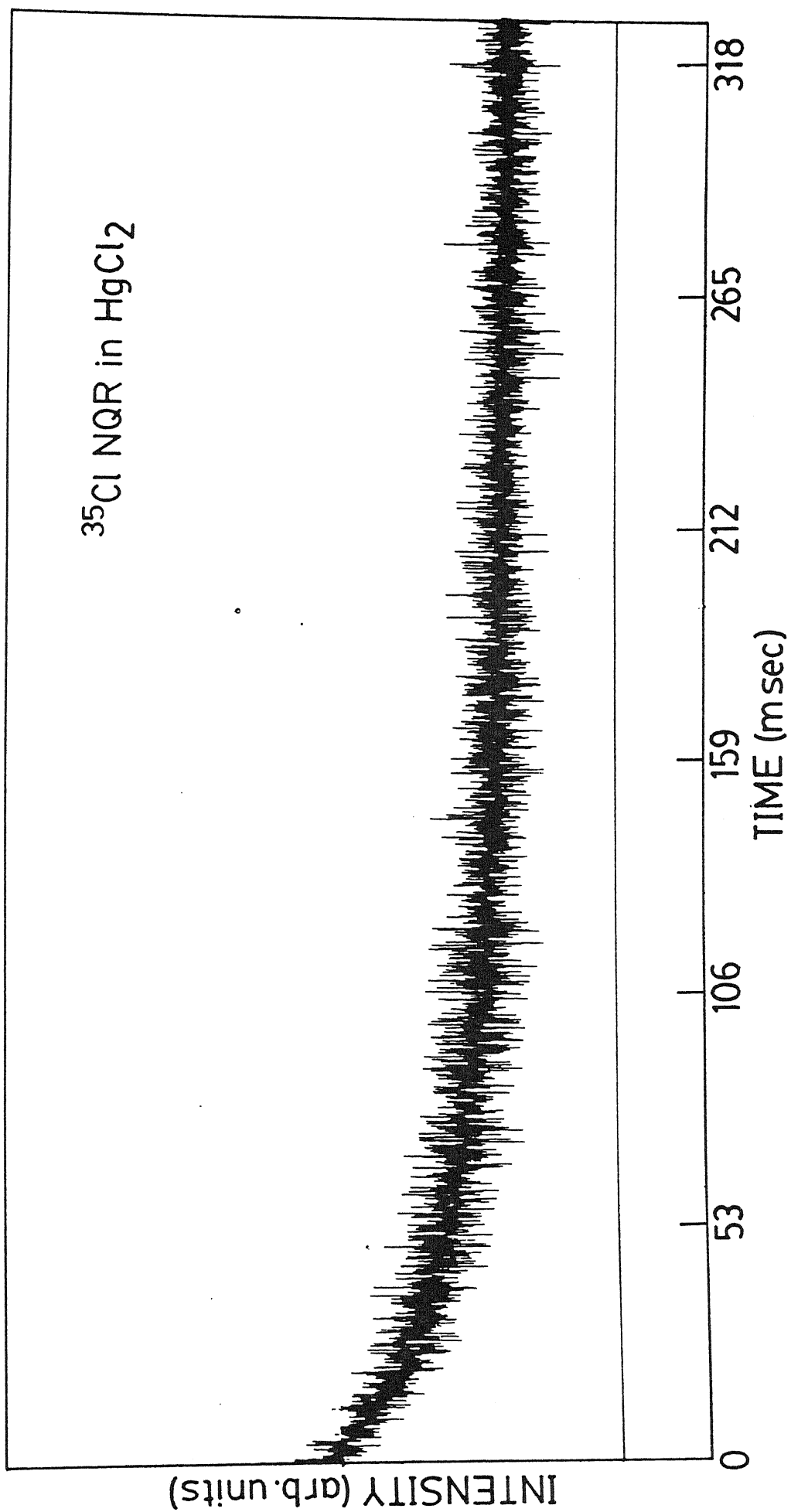


Figure VI.5(c)

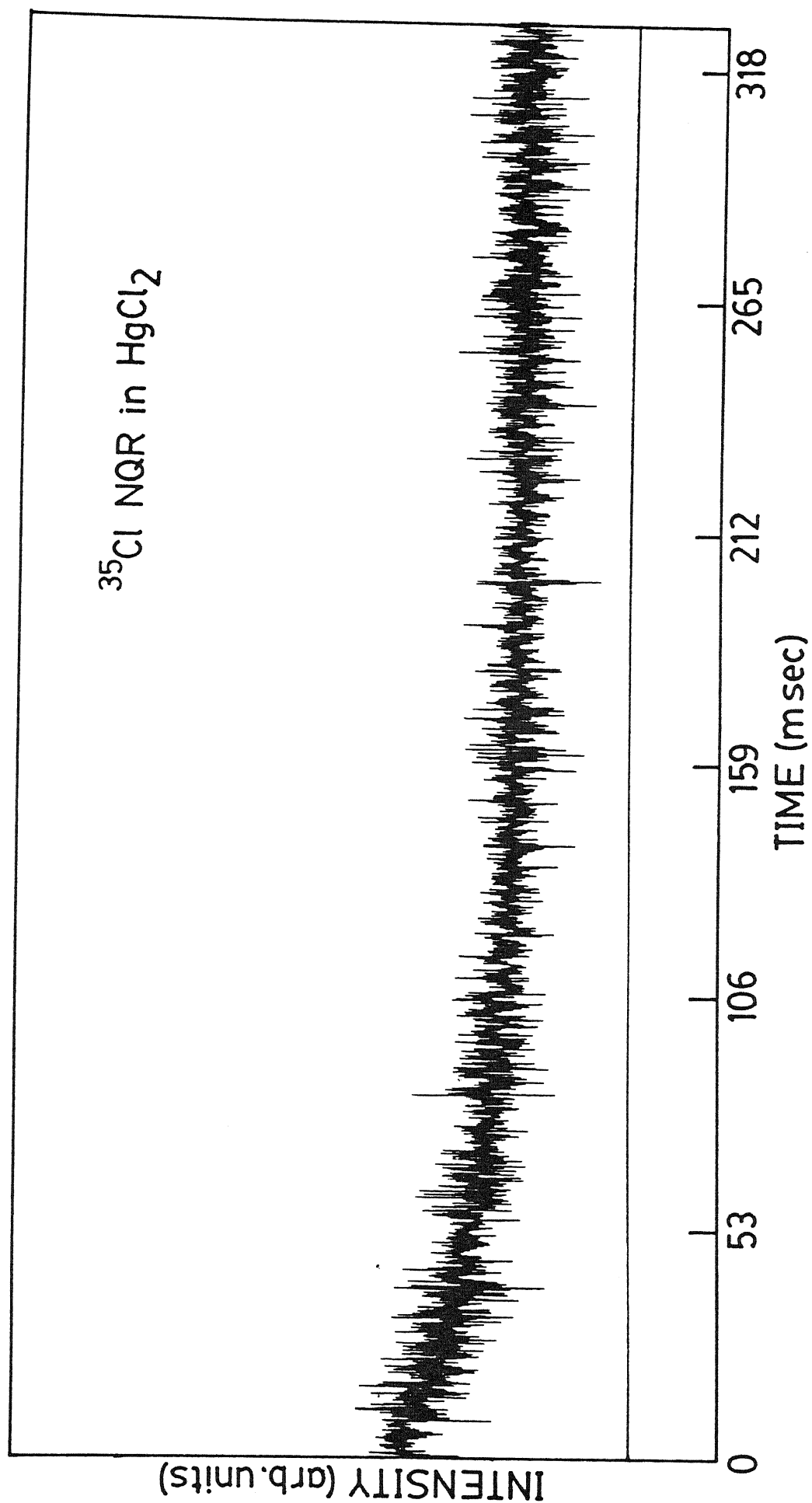


Figure VI.5(d)

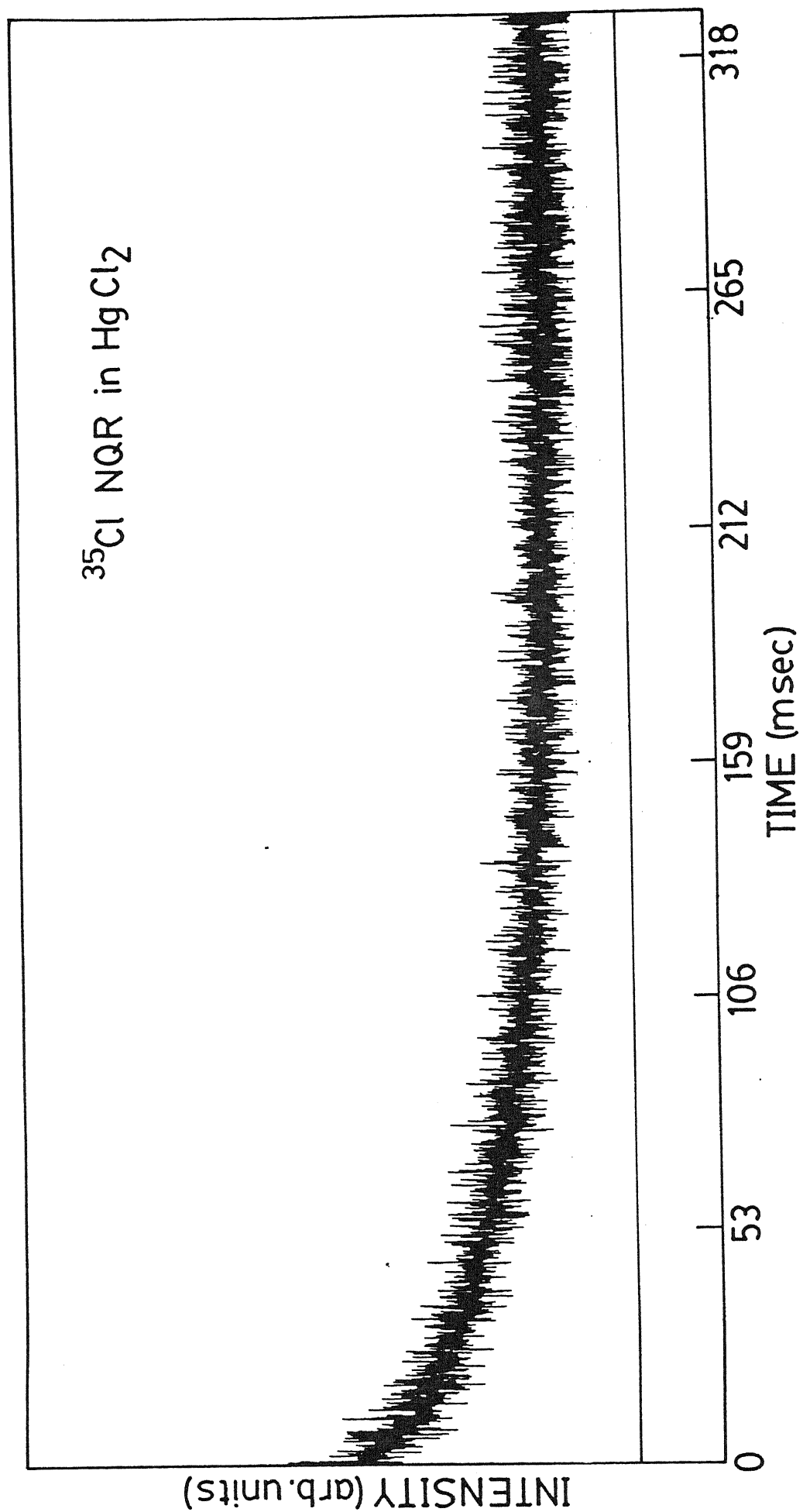


Figure VI.5(e)

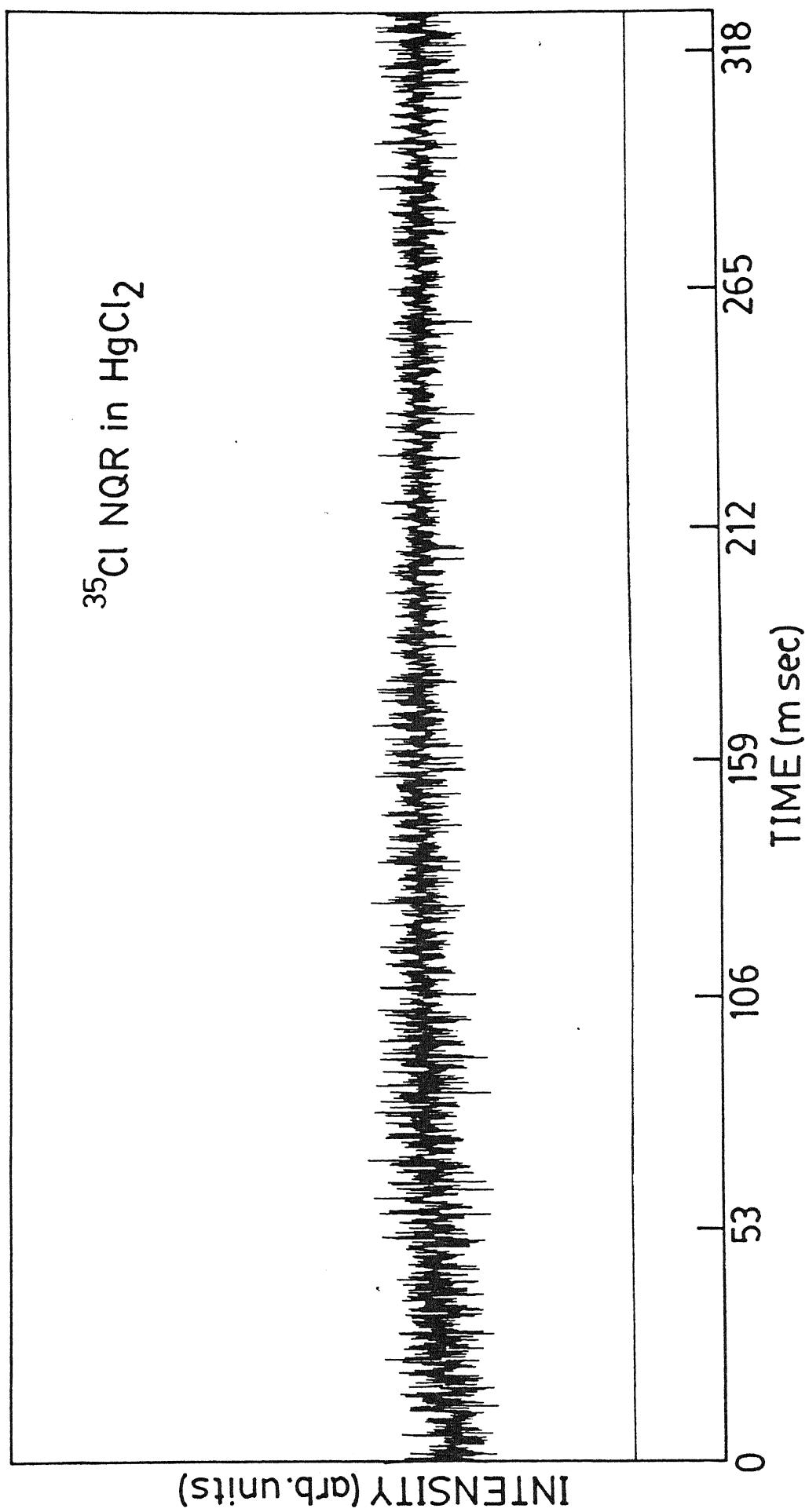


Figure VI.5(f)

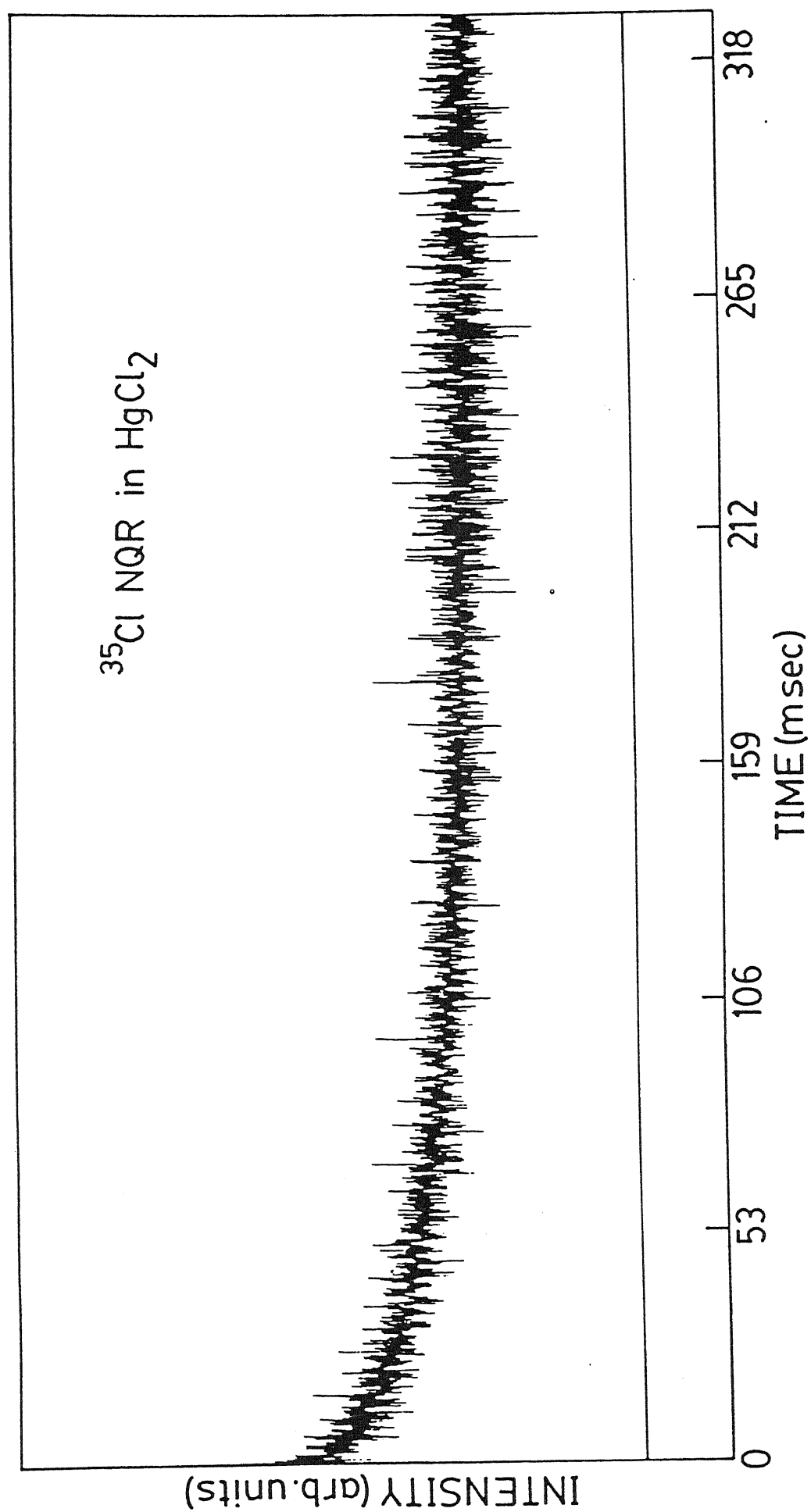


Figure VI.5(g)

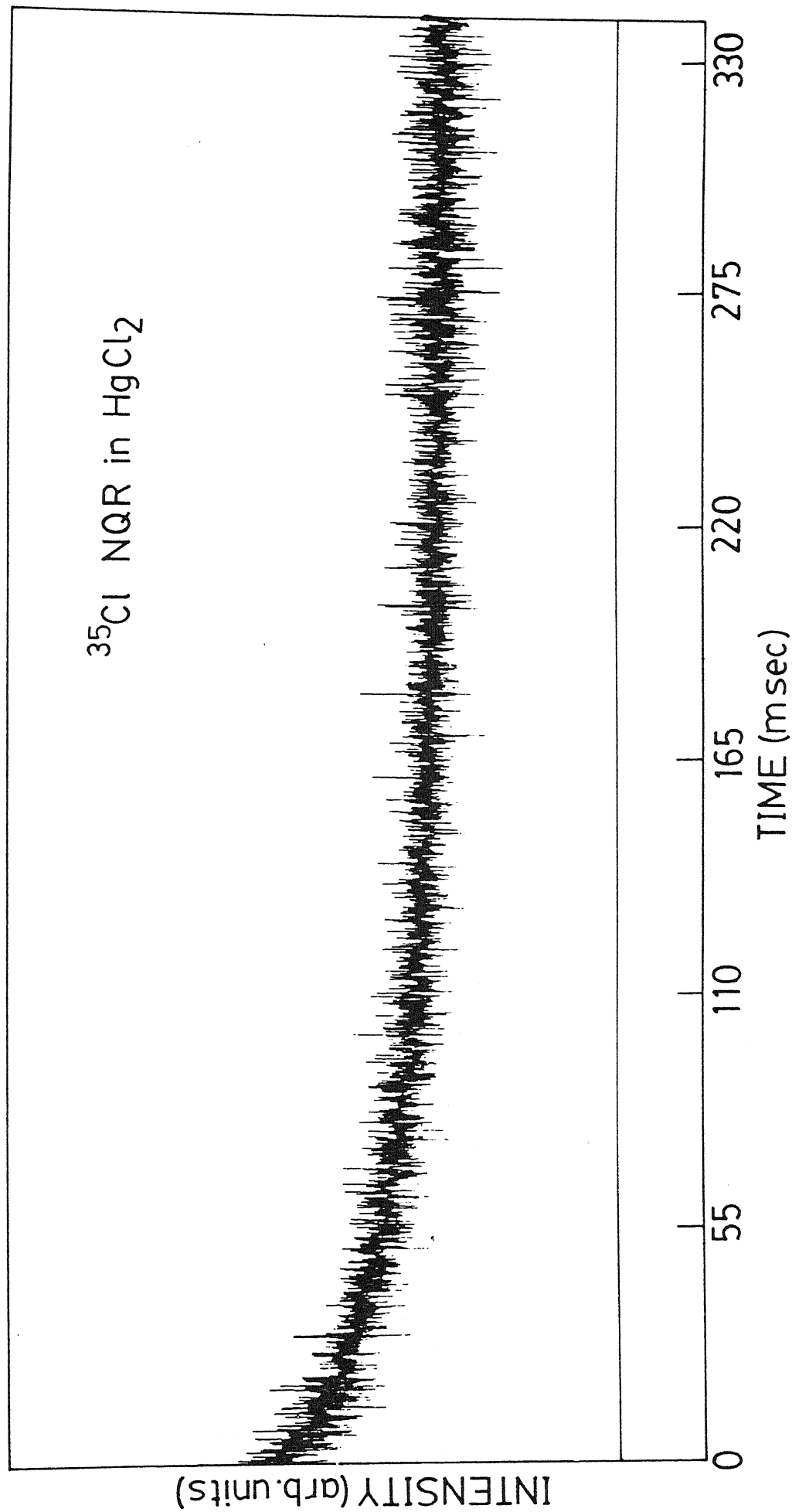


Figure VI.5(h)

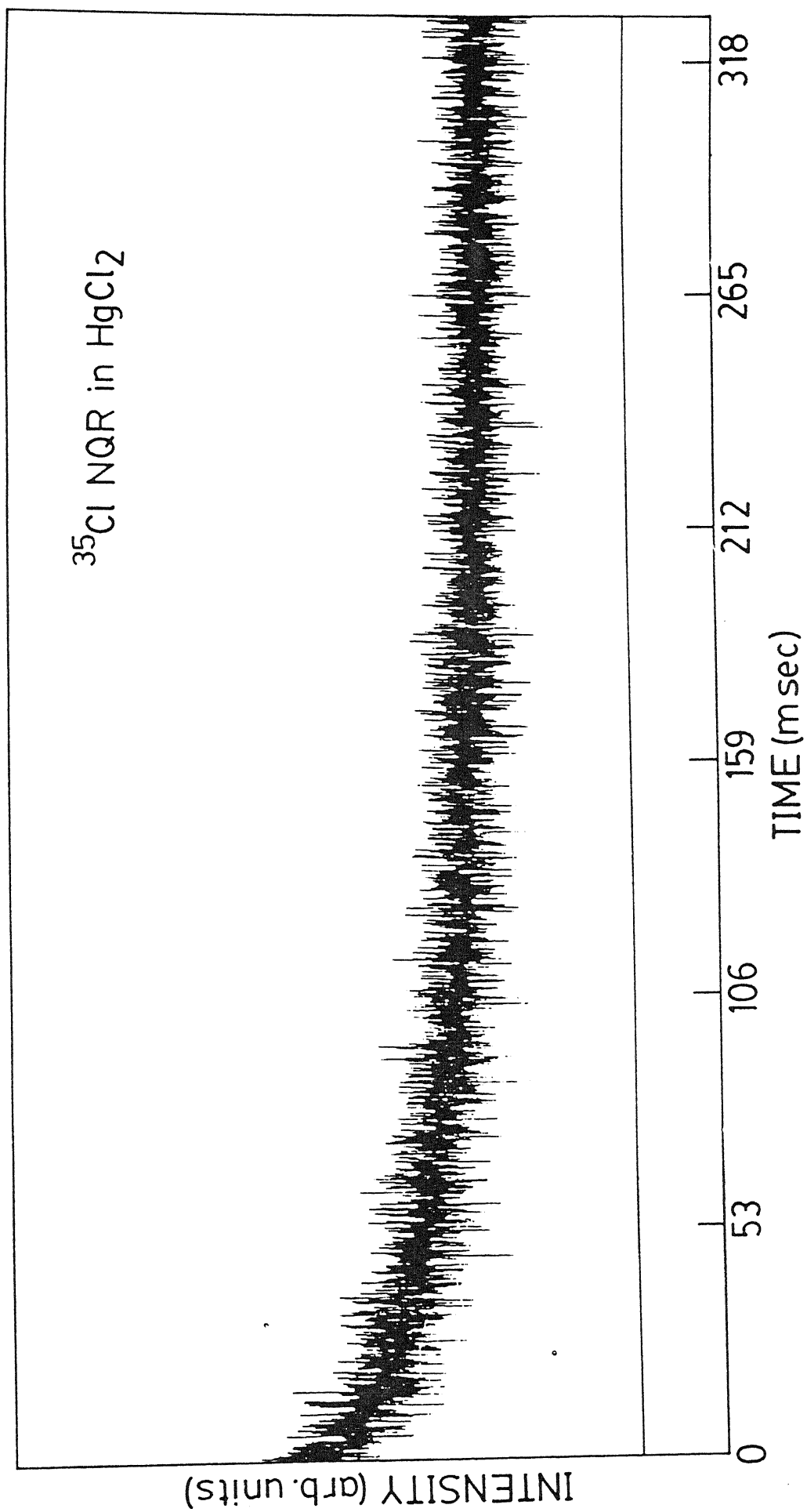


Figure VI.5(i)



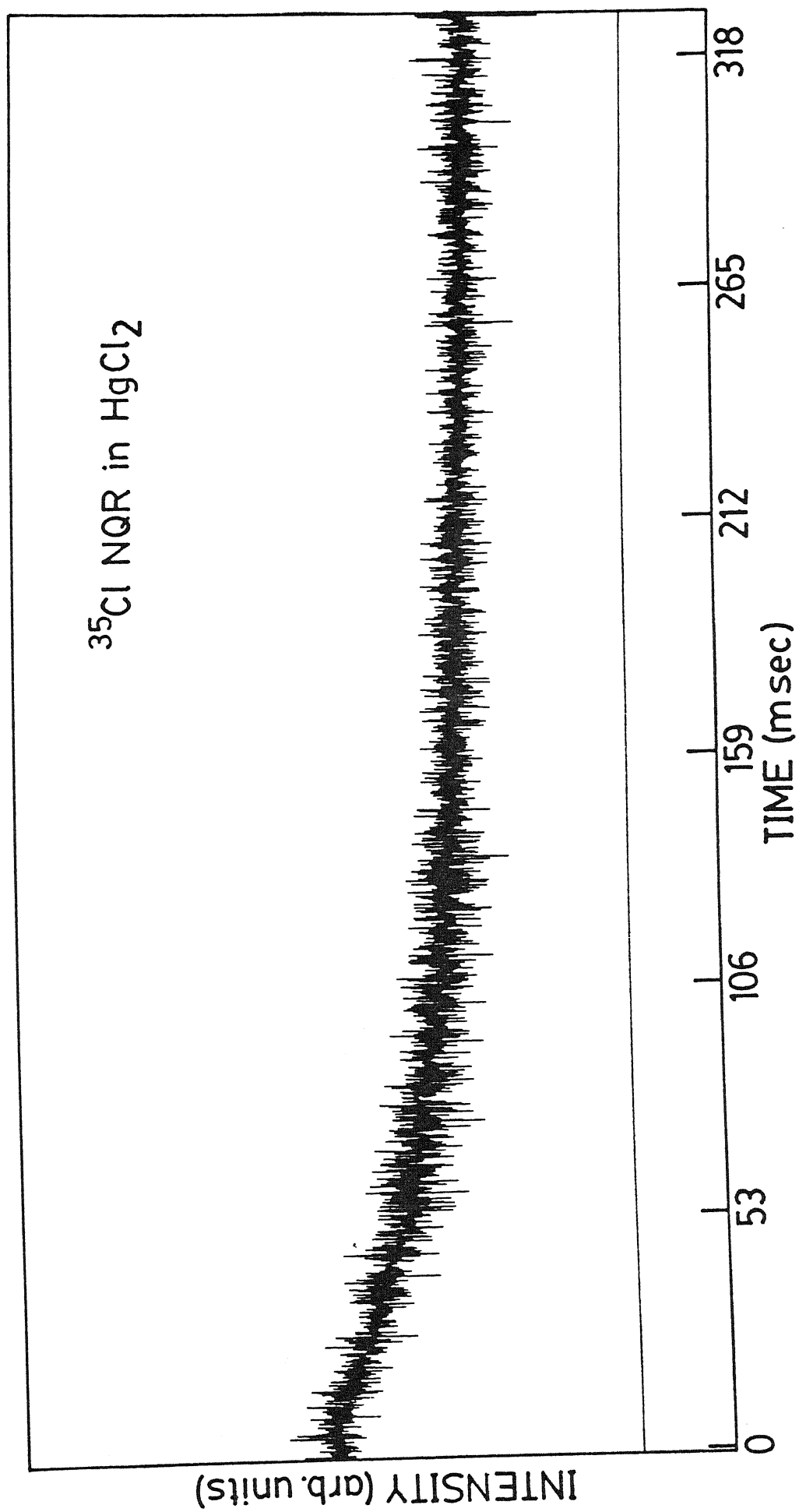


Figure VI.5(j)

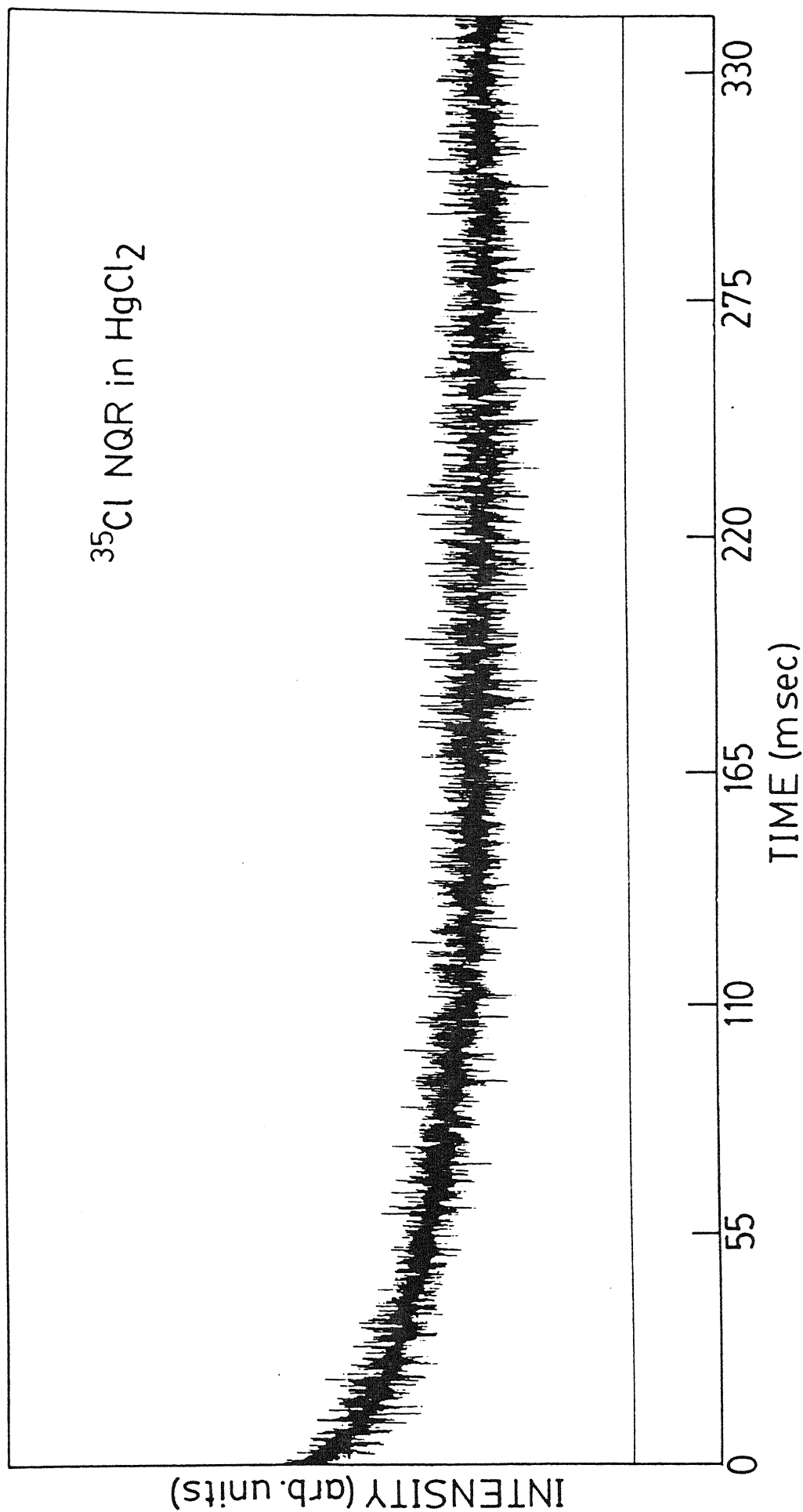


Figure VI.5(k)

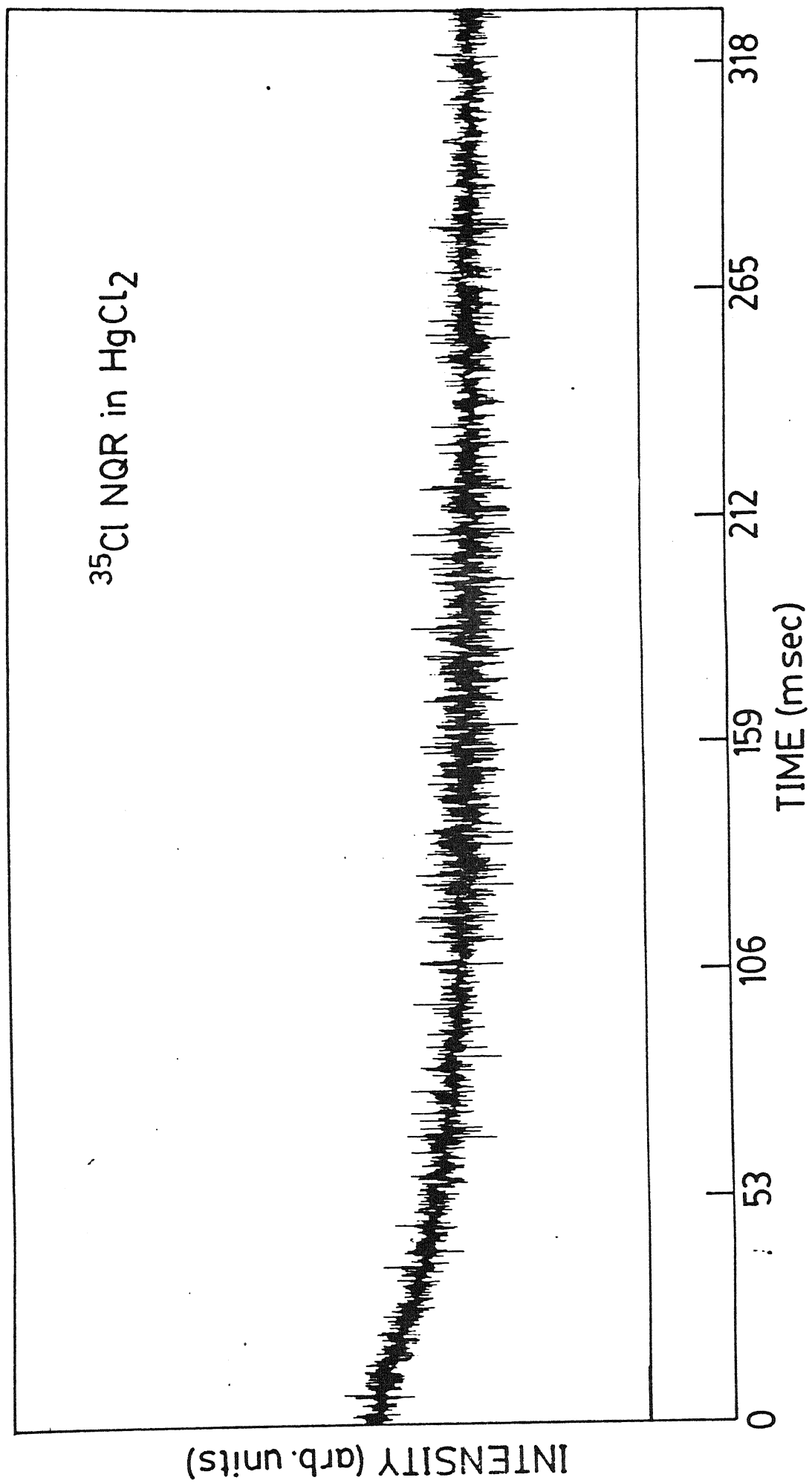


Figure VI.5(l)

under the action of  $\bar{\mathcal{H}}_1$ . This time period features a wide spectrum of oscillations of the system magnetization. This occurs because the precession rate of each spin is determined by the local magnetic field and electric field gradient surrounding it, in addition to the deviation from resonance. These oscillations arise from the component of the magnetization vector initially perpendicular to the effective rf field axis. There is, in addition a constant contribution to the magnetization that arises from the parallel component of the initial magnetization. After a time of approximately  $T_2^*$ , the transverse component decays to zero and quasistationary state is reached. The time required to arrive at this quasistationary state is determined by strength of the dominant internal interaction (torsional oscillations in case of NQR of spin  $3/2$  solids) and the flip angle  $\theta$ , employed for the pulses in the spin-locking multiple-pulse sequence. It depends only indirectly on the interval between pulses, in the sense that if  $\tau$  is too large,  $\bar{\mathcal{H}}_1$  does not represent the effective Hamiltonian even for short times.

A prior knowledge about the long-time behavior of the system of an ensemble of nuclei is important even when we restrict the problem to torsional oscillation Hamiltonian only. A very small imprecision in the initial conditions, i.e. the initial values of the parameters, can accumulate a substantial error in the subsequent evolution of the magnetization. A study of the long-time behavior from the point of view of the stability of the

equilibrium magnetization also becomes important.

When the NQR response of spin  $3/2$  solids to spin-locking multiple-pulse sequence is sampled only at observation windows once every period, the system is supposed to behave as shown in Figure VI.4(a). In actuality, however, Figure VI.4(b) represents the true behavior of the system; that is to say, the quasiequilibrium does not last long and decays over a long time scale to an equilibrium state [65,66]. In our experiments also, we have observed this behavior of the magnetization in the long-time regime. We attribute this to a case of locked quadrupolar relaxation, because of which, as seen in the Figures VI.5(a) and (b), the magnetization does not remain in the quasiequilibrium state under the spin-locked condition for long. But the important point to be noted is that the magnetization will have a definite value for periods much longer than  $5T_1$  ( $T_1$  for  $\text{NaClO}_3$ , for example, is  $\sim 45$  msec at room temperature but we see signal to be persisting for as long as 800 msec, Figure VI.5(a) and (b). Although, we have not carried out a theoretical investigation for  $\theta > 1$  radian for the flip angles of the pulses in the sequence for the OW or MW experiment, we have also presented our experimental results for this case and the conclusions are very similar to what has been said about  $\theta < 1$  radian case.

#### VI.D. Summary

In this Chapter we have derived theoretically the expression for the equilibrium magnetization in the case of spin  $3/2$  solids when irradiated with OW or MW multiple-pulse sequence. Both the theoretical curves and experimental spectra give a strong evidence of attainment of a spin-locked state in spin  $3/2$  NQR case also, as in the case of spin  $1/2$  NMR and spin 1 NQR but the difference is that in case of spin  $3/2$  NQR it is a locked quadrupolar relaxation and its mechanism is dictated by the torsional oscillations of the units containing the quadrupolar nuclei under consideration.

## CHAPTER VII

### SUMMARY OF FINDINGS AND FURTHER PROSPECTS

Although as pointed out right at the beginning of this thesis spins  $1/2$ ,  $1$  and  $3/2$  have distinct and special features of energy level splittings and transitions, it is noteworthy that the dynamics and equilibrium magnetization properties under different schemes of pulsed rf perturbation are very analogous. Indeed, the generalization seems possible that, in an ensemble of nuclei with any spin  $I$ , as long as a single frequency radiation connects only a pair of levels (degenerate or non-degenerate), the behavior will be very similar to what has been demonstrated in the past in spin  $1/2$  NMR, spin  $1$  NQR and, in the present thesis, for the case of spin  $3/2$  NQR. Theoretically we can discuss this similarity by choosing the appropriate representation and operator formalism to describe the evolution of the system.

In this thesis this fact has been demonstrated for spin  $3/2$  NQR by going to diagonalized  $\mathcal{H}_0$  representation and choosing the single transition operator (STO) formalism for the description of the Hamiltonians. An important result is the development of the special operators  $\bar{L}$ ,  $\bar{M}_i$ , and  $\bar{N}_i$  in Chapter II. We have set forth the commutation and other properties of  $\bar{L}$ ,  $\bar{M}_i$  and  $\bar{N}_i$ ;  $i = 1, 2$ , and  $3$ . It is clear that  $\bar{L}$ ,  $\bar{M}_i$  and  $\bar{N}_i$  correspond to  $I_z$ ,  $I_y$  and  $I_x$ .

respectively, used in spin  $1/2$  NMR terminology. Once we express the Hamiltonian of system in diagonalized representation and STO formalism the dynamics and equilibrium properties of spin  $3/2$  solids show striking similarity to what has been shown in the past in case of spin  $1/2$  NMR and spin 1 NQR.

The difference between the observed response now relies predominantly on only the magnitude of the various Hamiltonians in the interaction representation that governs the response of the system. In case of spin  $3/2$  NQR, for example the broadening of the line, the spin-locking and the quasi-equilibrium state have been shown to be dictated by the torsional Hamiltonian, in contrast to the preponderance of dipolar interaction in case of spin  $1/2$  NMR.

We shall now outline certain prospects for future investigations:

- (i) The theory for multiple-pulse perturbation of spin  $3/2$  NQR system has been worked out only for the limiting case of  $\delta$ -pulses. The correction due to finite pulse width needs to be worked out
- (ii) The theory for spin-locking has been worked out for the flip angle of the pulses in the sequence  $\theta < 1$  radian only. Extending the theory to investigate the results for  $\theta > 1$  radian would also be fruitful. The spin-locking experiment in case of  $\theta > 1$  radian has also been presented in this thesis, so we expect that the theory should give us a result that will be similar to what has been observed in the case  $\theta < 1$  radian.
- (iii) Going to submultiple regions of periods in the



periodic-perturbation schemes to probe the behaviour of the system deeper seems to be another interesting possibility.

(iv) Use of small magnetic fields to perturb the NQR energy levels and separate the transitions from each other, and then performance of a multiple-pulse experiments are also required. This will help us understand how the various modes of relaxation in spin  $3/2$  NQR are affected during multiple-pulse sequences.

(v) A study of the temperature-dependance of the response of multiple-pulse sequence to separate out information about various relaxation mechanisms and how they are affected during a multiple-pulse sequence perturbation will be an interesting study, and finally

(vi) Generalization to higher spin systems seems to be an interesting prospect for future.

## REFERENCES

- [1] A. K. Saha and T. P. Das, "Theory and Applications of Nuclear Induction," Saha Institute of Nuclear Physics, Calcutta, 1957.
- [2] T. P. Das and E. L. Hahn, "Nuclear Quadrupole Resonance Spectroscopy," Academic Press, New York, 1957.
- [3] A. Abragam, "The Principles of Nuclear Magnetism," Clarendon Press, Oxford, 1961.
- [4] C. P. Slichter, "Principles of Magnetic Resonance," Springer-Verlag, Berlin, 2nd Edn., 1980.
- [5] H. G. Dehmelt, Amer. J. Phys. 22, 110 (1954).
- [6] M. Bloom, E. L. Hahn and B. Herzog, Phys. Rev. 97, 1699, (1955).
- [7] M. H. Cohen and F. Reif in "Solid State Physics," Advances in Research and Applications, Vol. 5, Ed. F. Seitz and D. Turnbull, Academic Press, New York, 1957.
- [8] C. Dean, Phys. Rev. 96, 1053 (1954); Ph.D. Thesis, Harvard University, USA (1952).
- [9] P.16 of [3]
- [10] C. Hilbert, J. Clarke, T. Sleator and E.L. Hahn, Appl. Phys. Lett. 47, 637 (1985)
- [11] T. Sleator, E.L. Hahn, M.B. Heaney, C. Hilbert and J. Clarke, Phys. Rev. Lett. 57, 2756 (1986)
- [12] T. Sleator, E.L. Hahn, M.B. Heaney, C. Hilbert, and J. Clarke, Phys. Rev. B. 38, 8609 (1988)

- [13] H. A. Kramers, Proc. Acad. Sci. Amst. 33, 959 (1930).
- [14] p. 36 of [3].
- [15] P. Mansfield, Prog. NMR Spectrosc. 8, 41 (1971).
- [16] U. Haeberlen, "High Resolution NMR in Solids," Academic Press, New York, 1976.
- [17] A. Abragam and M. Goldman, "Nuclear Magnetism: Order and Disorder," Clarendon Press, Oxford, 1982.
- [18] M. Mehring, "High Resolution NMR in Solids," Springer-Verlag, Berlin, 2nd Edn., 1983.
- [19] B. C. Gerstein and C. R. Dybowski, "Transient Techniques in NMR of Solids," Academic Press Inc., Orlando, 1985.
- [20] R. A. Marino and S. M. Klainer, J. Chem. Phys. 67, 3388 (1977).
- [21] R. S. Cantor, Ph.D. Thesis, Massachusetts Institute of Technology, USA (1979).
- [22] R.S. Cantor and J. S. Waugh, J. Chem. Phys. 73, 1054 (1980).
- [23] D. Ya. Osokin, Phys. Stat. Sol.(b), 102, 681 (1980).
- [24] B. N. Provotorov and A. K. Khitrin, JETP Lett. 34, 157 (1981).
- [25] D. Ya. Osokin, J. Molec. Struct. 83, 243 (1982).
- [26] A. K. Hitrin, G. E. Karnaukh and B. N. Provotorov, J. Molec. Struct. 83, 269 (1982).
- [27] D. Ya. Osokin, Phys. Stat. Sol. (b), 109, K7 (1982).
- [28] D. Ya. Osokin, Sov. Phys. JETP, 57, 69 (1983).

- [29] G. E. Karnaukh, B. N. Provotorov and A. K. Khitrin, *Sov. Phys. JETP*, **57**, 93 (1983).
- [30] D. Ya. Osokin, *Mol. Phys.* **48**, 283 (1983).
- [31] V. L. Ermakov and D. Ya. Osokin, *Phys. Stat. Sol. (b)*, **116**, 239 (1983).
- [32] V. L. Ermakov and D. Ya. Osokin, *Mol. Phys.* **53**, 1335 (1984).
- [33] M. M. Maricq, *Phys. Rev. B*, **33** 4501 (1986).
- [34] E. L. Hahn, *Phys. Rev.* **80**, 580 (1950).
- [35] H. Y. Carr and E. M. Purcell, *Phys. Rev.* **94**, 630 (1954).
- [36] R. L. Vold, J. S. Waugh, M. P. Klein and D. E. Phelps, *J. Chem. Phys.* **48**, 3831 (1968).
- [37] R. Freeman and H. D. W. Hill in "Dynamic NMR Spectroscopy," Ed. L. M. Jackman and F. A. Cotton, Academic Press, New York, 1975.
- [38] R. L. Vold and R. R. Vold, *Prog. NMR Spectrosc.* **12**, 79 (1978).
- [39] E. O. Stejskal and J. E. Tanner, *J. Chem. Phys.* **42**, 288 (1965).
- [40] H. S. Gutowsky, R. L. Vold and E. J. Wells, *J. Chem. Phys.* **43**, 4107 (1965).
- [41] L. M. Jackman and F. A. Cotton, "Dynamic NMR Spectroscopy," Academic Press, New York, 1975.
- [42] J. I. Kaplan and G. Fraenkel, "NMR of Chemically Exchanging Systems," Academic Press, New York, 1980.

- [43] E. D. Ostroff and J. S. Waugh, *Phys. Rev. Lett.* **16**, 1097 (1966).
- [44] P. Mansfield and D. Ware, *Phys. Lett.* **22**, 133 (1966).
- [45] J. S. Waugh, *J. Mol. Spectrosc.* **35**, 298 (1970).
- [46] A. Pines, M. G. Gibby and J. S. Waugh, *J. Chem. Phys.* **59**, 569, (1973), p. 574.
- [47] J. Koo, Ph.D. Thesis, University of California, Berkeley, USA (1969).
- [48] D. T. Edmonds and P. A. Speight, *J. Magn. Reson.* **6**, 265 (1972).
- [49] R. Blinc, M. Mali, R. Osredkar, A. Prelesnik, J. Seliger, I. Zupančič and L. Ehrenberg, *J. Chem. Phys.* **57**, 5087 (1972).
- [50] J. Seliger, R. Blinc, M. Mali, R. Osredkar and A. Prelesnik, *Phys. Status Sol.(a)* **25**, K121 (1974).
- [51] T. C. Farrar and E. D. Becker, "Pulse and Fourier Transform NMR," Academic Press, New York, 1971.
- [52] D. Shaw, "Fourier Transform NMR Spectroscopy," Elsevier, Amsterdam, 2nd Edn., 1984.
- [53] M. L. Martin, J.-J. Delpuech and G. J. Martin, "Practical NMR Spectroscopy," Heyden, London, 1980.
- [54] R. R. Ernst, G. Bodenhausen and A. Wokaun, "Principles of Nuclear Magnetic Resonance in One and Two Dimensions," Clarendon Press, Oxford, 1987.

- [71] R. Reddy, Ph.D. Thesis, Indian Institute of Technology, Kanpur, India (1988).
- [72] N. E. Ainbinder, G. B. Furman, G. E. Kibrik, A. Ya. Poljakov and I. G. Shaposhnikov, Z. Naturforsch. **41a**, 366 (1986).
- [73] P. Mansfield, J. Phys. C, Solid State Phys. **4**, 1444 (1971).
- [74] P. Mansfield, M. J. Orchard, D. C. Stalker, K. H. B. Richards, Phys. Rev. B, **7**, 90 (1973).
- [75] W. -K. Rhim, D. D. Elleman, R. W. Vaughan, J. Chem. Phys. **59**, 3740 (1973).
- [76] A. N. Garroway, P. Mansfield, D. C. Stalker, Phys. Rev. B, **11**, 121 (1975).
- [77] W. -K. Rhim, D. D. Elleman, R. W. Vaughan, J. Chem. Phys. **58**, 1772 (1973).
- [78] D. Gill and S. Meiboom, Rev. Sci. Instr. **29**, 688 (1958).
- [79] M. Lee and W. I. Goldberg, Phys. Rev. A, **140**, 1261 (1965).
- [80] J. C. Pratt, P. Raghunathan and C. A. McDowell, J. Magn. Reson. **20**, 313 (1975).
- [81] J. C. Pratt, J. Molec. Struct. **111**, 113 (1983).
- [82] A. E. Mefed and B. N. Pavlov, J. Molec. Struct. **83**, 131 (1982).
- [83] O. S. Zueva, J. Molec. Struct. **83**, 379 (1982).

- [84] A. R. Kessel and O. S. Zueva, Phys. Lett. 68A, 347 (1978).
- [85] O. S. Zueva and A. R. Kessel, Sov. Phys. Solid State 21, 2032 (1979).
- [86] O. S. Zueva and A. R. Kessel, J. Molec. Struct. 83, 383 (1982).
- [87] N. E. Ainbinder and G. B. Furman, Sov. Phys. JETP 58, 575 (1983).
- [88] N. N. Bogoliubov, Y. A. Mitropolsky, "Asymptotic Methods in the Theory of Non linear Oscillations," Gordon and Breach, New York, 1961.
- [89] L. L. Buishvili and M. G. Manabde, Sov. Phys. JETP 50, 1176 (1979).
- [90] J. Jeener and P. Broekaert, Phys. Rev. 157, 232 (1967).
- [91] C. Segebarth and J. Jeener, Phys. Rev. B, 29, 1176 (1984).
- [92] M. A. Singh and R. L. Armstrong, Phys. Rev. B, 38, 50 (1988).
- [93] K. W. Vollmers, I. J. Lowe and M. Punkkinen, J. Magn. Reson. 30, 33 (1978).
- [94] M. A. Singh and R. L. Armstrong, J. Magn. Reson. 78, 538 (1988).
- [95] D. Amati, H. Bacry, J. Nuyts and J. Prentki, Nuovo Cimento, 34, 1732 (1964).

- [96] H. Lipkin, "Lie Groups for Pedestrians," North Holland Publ. Co., Amsterdam, 2nd Edn., 1986.
- [97] A. Wokaun and R. R. Ernst, J. Chem. Phys. 67, 1752 (1977).
- [98] S. Vega, J. Chem. Phys. 68, 5518 (1978).
- [99] R. V. Pound, Phys. Rev. 79, 685 (1950).
- [100] M. J. Weber, J. Phys. Chem. Solids 17, 257 (1961).
- [101] D.E. Woessner and H.S. Gutowsky, J. Chem. Phys. 39 440 (1963).
- [102] G.D. Watkins and R.V. Pound, Phys. Rev 85, 1062 (1952).
- [103] T.C. Wang, Phys. Rev 99, 566 (1955).
- [104] D.C. Douglass, Ph.D. Thesis, Cornell University, USA (1957)
- [105] R. Livingston, J. Phys. Chem. 57 , 496 (1953).
- [106] H. Bayer, Z. Physik 130, 227 (1951).
- [107] G.W. Leppelmeier and E.L. Hahn, Phys. Rev. 142, 179 (1966).
- [108] G. Ramachandran and M.V.N. Murthy, Nucl. Phys. A323, 403 (1979).
- [109] G. Ramachandran and R.K. Umerjee, Nucl. Phys. 54 665 (1964)
- [110] R. Bellman, "Introduction to Matrix Analysis," Tata McGraw-Hill Publ. Co. Ltd., New Delhi, 2nd Edn., 1974.
- [111] J.C. Pratt, Mol. Phys. 34, 539 (1977).
- [112] P. 49 of [16]
- [113] I.I. Rabi, N.F. Ramsey and J. Schwinger, Rev. Mod. Phys. 26, 167 (1954)
- [114] A. Messiah, "Quantum Mechanics," John Wiley and Sons, New York, 1976.



- [115] J. von Neumann, Göttinger Nachr. 245 and 273 (1927).
- [116] J. Von Neumann, "Mathematical Foundations of Quantum Mechanics," Princeton University Press, Princeton, N.J. 1955.
- [117] U. Fano, Rev. Mod. Phys. 29, 74 (1957).
- [118] D. ter Haar, Rep. Prog. Phys. 24, 304 (1961).
- [119] Liouville, Journ. de Math. 3, 349 (1838).
- [120] F.J. Dyson, Phys. Rev. 75, 486 (1949).
- [121] V. Ravishankar, Mol. Phys 62, 1409 (1987).
- [122] F. Bloch and A. Siegert, Phys. Rev. 57, 522 (1940).
- [123] M. J. Weber and E. L. Hahn, Phys. Rev. 120, 365 (1960).
- [124] M. J Weber, Ph.D. Thesis, University of California, USA (1960).
- [125] M. J. Weber and E.L. Hahn, Bull. Amer. Phys. Soc. 3, 324 (1958).
- [126] A.R. Edmonds, "Angular Momentum in Quantum Mechanics," Princeton University Press, Princeton, N.J., 1957.
- [127] M.E. Rose, "Elementary Theory of Angular Momentum," Wiley, New York, 1957.
- [128] D.M. Brink and G.R. Satchler, "Angular Momentum," Clarendon Press, Oxford, 1962.
- [129] L.C. Biedenharn and J.D. Louck, "Angular Momentum in Quantum Physics," Addison-Wesley Publ. Co., Reading, Massachusetts, 1981.
- [130] B. C. Sanctuary, Mol. Phys. 48, 1155 (1983).

- [131] G.J. Bowden, W.D. Hutchison and J. Khachan, J. Magn. Reson. 67, 415 (1986).
- [132] F. Bloch, Phys. Rev. 70, 460 (1946).
- [133] M. Goldman, "Spin Temperature and Nuclear Magnetic Resonance in Solid," Carendon Press, Oxford, 1970.
- [134] A. M. Portis, Phys. Rev. 91, 1071 (1953).
- [135] A. M. Stoneham, Rev. Mod. Phys. 41, 32 (1969).
- [136] J. D. Macomber, "The Dynamics of Spectroscopic Transitions, John Wiley & Sons, New York, 1976.
- [137] N. Bloembergen, E.M. Purcell and R.V. Pound, Phys. Rev. 73, 679 (1948).
- [138] N. Bloemberern, "Nuclear Magnetic Relaxation," W. A. Benjamin, New York, 1961.
- [139] T. P. Das and A. K Saha, Phys. Rev. 98, 516 (1955).
- [140] T. P. Das and D.K. Roy, Proc. Roy. Soc. A. 227, 407 (1955).
- [141] J.E. Campbell, Proc. London Math. Soc. 29, 14 (1898).
- [142] H. F. Baker, Proc. London Math. Soc. 34, 347 (1902).
- [143] H. F. Baker, Proc. London Math. Soc. 35, 333 (1903).
- [144] H.F. Baker, Proc. London Math. Soc. (Second series) 2, 293 (1904).
- [145] H.F. Baker, Proc. London Math. Soc. (Second series) 3 24 (1904).
- [146] F. Hausdorff, Ber. Verhandl, Saechs. Akad. Wiss. Leipzig. Math. Naturw. Kl. 58, 19 (1906).

- [147] W. Magnus, Algebraic Aspects of The Theory of systems of Linear Differential Equations, Research Rept. BR-3, New York University, Institute of Mathematical Sciences, June, 1953.
- [148] W. Magnus, Commun. Pure Appl. Math. 7, 649 (1954).
- [149] K. Goldberg, Duke Math. J., 23, 13 (1956).
- [150] Kuo-Tsai Chen, Ann. Math. 65, 163 (1957).
- [151] H.B. Keller and J.B. Keller, On Systems of Linear Ordinary Differential Equations, Research Rept. EM-23, New York University, Washington Square College, Mathematics Research Group, 1957.
- [152] E. Fukushima and S.B.W. Roeder, "Experimental Pulse NMR" Addison-Wesley Publ. Co., Reading, Massachusetts, 1981.
- [153] J. G. Powles and J.H. Strange, Proc. Phys. Soc. (London) 82, 6 (1963).
- [154] P. Mansfield, Phys. Rev. A 137, 961 (1965).
- [155] K. W. Vollmers, Ph.D. Thesis, University of Pittsburgh, USA (1972).
- [156] I. J. Lowe, K.W. Vollmers, and M. Punkkinen, in "Proceedings of the First Specialized Colloque Ampere," p.70, Institute of Nuclear Physics, Krakaw, Poland, 1973.
- [157] G.K. Semin, T.A. Babushkina and G.G. Yakobson, "Nuclear Quadrupole Resonance in Chemistry," John Wiley & Sons, New York, 1975.

- [158] E.A.C. Lucken, "Nuclear Quadrupole constants," Academic Press, London, 1969.
- [159] D. Van Der Putten, K.O. Prins, and N.J. Trappeniers, Rev. Sci. Instrum. 56, 803 (1985).
- [160] M. Sprik, T. Hijmans, and J.J. Trappeniers, Physica B + C 112, 285 (1982).
- [161] G.L. Petersen, Ph.D. Thesis, Brown University, USA (1975).
- [162] A. Pines, in : Proceedings of the 100th Fermi School on Physics, B. Maraviglia (Ed 3.) North Holland Publ. Co., Amsterdam, pp. 43-120 (1988).
- [163] R.M. Wilcox, J. Math. Phys. 8, 962 (1967).
- [164] P. Pechukas and J.C. Light, J. Chem. Phys. 44, 3897 (1966).
- [165] M. M. Maricq, J. Chem. Phys. 86, 5647 (1987).
- [166] W.R. Salzman, J. Chem. Phys. 85, 4605 (1986).
- [167] R. Tycko, Phys. Rev. Lett. 58, 2281 (1987).
- [168] D. Suter, G.C. Chingas, R. A. Harris and A. Pines, Mol. Phys. 61, 1327 (1987).
- [169] A. Zee, Phys. Rev. A 38, 1 (1988).
- [170] J. S. Waugh, C.H. Wang, L. M. Huber and R.L. Vold, J. Chem. Phys. 48, 662 (1968).
- [171] A. K. Dubey and P. T. Narasimhan, J. Molec. Struct. 192, 321 (1989).
- [172] R.W.G. Wyckoff, "Crystal Structures", Interscience Publ. Co., New York, 1964.

- [173] W. H. Zachariasen, Z. Krist. 71, 517 (1929).
- [174] V. I. Arnold, "Geometrical Methods in the Theory of Ordinary Differential Equations." Springer-Verlag, New York, 1983.
- [175] J. H. Poincaré, "Les Methodes Nouvelles de la Mechanique Celeste," Vols. I, II, IV, Paris, 1892, 1893, 1899.
- [176] F. Bloch, Z. Physik 52, 555 (1928).
- [177] S. H. Autler and C. H. Townes, Phys Rev. 100, 703 (1955).
- [178] J. H. Shirley, Ph. D. Thesis, California Institute of Technology, USA (1963).
- [179] V. I. Ritus, Sov. Phys. JETP 51, 1544 (1966).
- [180] Ya. B. Zel'dovich, Sov. Phys. JETP, 51, 1492 (1966).
- [181] C. Cohen-Tannoudji and S. Haroche, J. Phys. (Paris) 30, 153 (1969).
- [182] R. H. Young, W.J. Deal and N.R. Kestner, Mol. Phys. 17, 369 (1969).
- [183] Tak-San Ho, Shih-I Chu and J.V. Tietz, Chem. Phys. Lett. 86, 464 (1983).
- [184] Tak-San Ho and Shih-I Chu, J. Phys. B: At. Mol. Phys. 17, 2101 (1984).
- [185] Tak-San Ho and Shih-I Chu, Phys. Rev. A 31, 659 (1985).
- [186] Shih-I Chu, Adv. At. Mol. Phys. 21, 197 (1985).
- [187] D. R. Dion and J. O. Hirschfelder, Adv. Chem. Phys. 35, 265 (1976).

- [188] J.E. Bayfield, Phys. Rep. 51C, 317 (1979).
- [189] P. Bucci, G. Ceccarelli and C.A. Veracini, J. Chem. Phys. 50, 1510 (1969).
- [190] P. Bucci, P. Cavaliere and S. Santucci, J. Chem. Phys. 52, 4041 (1970).
- [191] P. Bucci, M. Martinelli and S. Santucci, J. Chem. Phys. 53, 4524 (1970).
- [192] S. Yatsiv, Phys. Rev. 113, 1522 (1959).
- [193] W.A. Anderson, R. Freeman and C.A. Reilly, J Chem. Phys. 39, 1518 (1963).
- [194] M. M. Maricq, Chem. Phys. 100, 203 (1985).
- [195] M. M. Maricq, Phys. Rev. Lett. 56, 1433 (1986).
- [196] M. M. Maricq, Phys. Rev. B, 37, 7215 (1988).
- [197] R. Loudon, "the Quantum Theory of Light," Clarendon Press, Oxford, 2nd Edn., 1983.
- [198] Y. Zur, M. H. Levitt and S. Vega, J.Chem. Phys. 78, 5293 (1983).
- [199] Y. Zur and S. Vega, J. Chem. Phys. 79, 548 (1983).
- [200] G. W. Series, Phys. Rep. 43C, 1 (1978).
- [201] M. H. Stone, "Linear Transformations in Hilbert Space," Am. Math. Society, p. 307, 1932.
- [202] R. C. Tolman, "The Principles of Statistical Mechanics," Oxford Univ. Press, London, 1938.

- [203] V. I. Arnold and A. Avez, "Ergodic Problems of Classical Mechanics," W.A. Benjamin, Inc., New York, 1968.
- [204] P. J. M. Bongaarts and Th. J. Siskens, *Physica (Utrecht)* 71, 529 (1978).
- [205] R. Kubo and K. Tomita, *J. Phys. Soc. Japan* 9, 88 (1954).
- [206] P. W. Atkins, A Text book of "Physical Chemistry," Oxford Univ. Press, Oxford, 3rd Edn., 1986.
- [207] D. Suwelack and J.S. Waugh, *Phys. Rev. B* 22, 5110 (1980).
- [208] Yu. N. Ivanov, B.N. Provotorov and E. B. Fel'dman, *Sov. Phy. JETP* 48, 930 (1978).
- [209] B. N. Provotorov and E. B. Fel'dman, *Sov. Phys. JETP* 52, 1116 (1980).
- [210] S. Klarsfeld and J.A. Oteo, *Phys. Rev. A* 39, 3270 (1989).
- [211] P. L. Garrido and J. Marro, *Phys. Rev. Lett.* 62, 1929 (1989).
- [212] P.C. Taylor, J. F. Baugher and H.M. Kriz, *Chem. Rev.* 75, 203 (1975).
- [213] P. Raghunathan and S.K. Sur, *J. Am. Chem. Soc.* 106, 8014 (1984)
- [214] P. J. Bryant and S. Hacobian, *Z. Naturforsch.* 41a, 141 (1986).
- [215] R. Goc and D. Fiat, *Phys. Stat. Sol. (b)* 140, 243 (1987).
- [216] J. M. Hammersley and D.C. Handscomb, "Monte Carlo Methods," Methuen, London, 1967.

- [217] J.E. Wertz and J.R. Bolton, "Electron Spin Resonance," Chapman and Hall, New York, 1986.
- [218] S. Galando and L. Gonzalez-Tovany, J. Magn. Reson. **44**, 250 (1981).
- [219] P. Raghunathan and S.C. Sivasubramanian, Proc. Indian Acad. Sci. (Chem. Sci.) **96**, 565 (1986).
- [220] S.C. Sivasubramanian, Ph.D. Thesis, Indian Institute of Technology, Kanpur, India (1989).
- [221] A. Papoulis, "Probability, Random Variables and Stochastic Processes," McGraw-Hill Inc., New York, 1965.
- [222] H.Kahn in: "Symposium on Monte Carlo Methods," H.A. Meyer (ed.), John Wiley & Sons, New York, 1956.



## APPENDIX A

```

C -----
C Program SQMGNT.(Scaled Quasiequilibrium MaGNeTization.)
C This program calculates the quasiequilibrium magnetization
C for a spin 3/2 NQR powder specimen when irradiated with an
C Ostroff-Waugh(OW) Multiple-pulse sequence.The quasiequilibrium
C magnetization is scaled down by dividing it by initial
C magnetization so that its value is always between 0.0 and 1.0.
C The internal interactions that has been taken into account in
C the theory are the homonuclear dipolar coupling between two
C nuclei and the distribution in electric field gradient (efg)
C in the vicinity of a resonant nucleus.
C The variable names are almost directly in correspondence with
C the symbols used in expressions of Chapter Six in the Thesis.
C NOTE:A digit(1-9) in column 9 means continuation line.Also ';'
C Separates a line.
C0000000011111111122222222223333333333444444444455555555556666666666777
C23456789012345678901234567890123456789012345678901234567890123456789012
PROGRAM SQMGNT
COMPLEX YP1,YP2,YN1,YN2,YP3,RMBAR,RNBAR,RBBAR
COMPLEX DC1,DC2,DC3,DC4,DC5,DC6,DC7
COMPLEX HD,DKLP,H1,H3,Q,RATIO,CON3
DIMENSION XXX(100),YYY(100),SINTL(100),COSTL(100),SINFL(100),
1 COSFL(100),TITLE(7)
COMMON/BLK1/AX,AY,AZ,B,C,D,ETA,TAU,DELWQ,THETA0,R,THETA,HL,RRKK
COMMON/BLK2/XIC,XIS,XIP1,XIN1,XIP2,XIN2
COMMON/BLK3/XP1(4,4),XP2(4,4),XN1(4,4),XN2(4,4),
1 XN3(4,4),ZN1(4,4),ZN2(4,4),ZP2(4,4),AIDEN(4,4)
COMMON/BLK4/YP1(4,4),YP2(4,4),YN1(4,4),YN2(4,4),YP3(4,4)
COMMON/BLK5/DC1(16,16),DC2(16,16),DC3(16,16),
1 DC4(16,16),DC5(16,16),DC6(16,16),DC7(16,16)
COMMON/BLK7/HD(16,16),DKLP(16,16),H1(16,16),H3(16,16),Q(16,16)
COMMON/BLK8/RK,RL,RM,RN,RP,RQ
COMMON/BLK81/R1K,R1L,R1M,R1N,R1P,R1Q
COMMON/BLK82/R2K,R2L,R2M,R2N,R2P,R2Q
COMMON/BLK9/RBBAR(16,16),RLBAR(16,16),RMBAR(16,16),RNBAR(16,16)
COMMON/BLK10/HDSMSQ,HLSQ,RSQ8
OPEN(UNIT=20,DEVICE='DSK',FILE='SQMGNT.DAT',ACCESS='SEQIN')
OPEN(UNIT=24,DEVICE='DSK',FILE='SQMGNT.OUT',ACCESS='SEQOUT')
OPEN(UNIT=6,DEVICE='DSK',FILE='SQMGNT.PLT',ACCESS='SEQOUT')
C -----
C WQ is resonance frequency of the quadrupolar nucleus (in MHz).
C (1+DELTA)*WQ is offset frequency(in MHz).
C THETA is flip angle of pulses in the sequence (in Radians).
C THETA0 is flip angle of the preparatory pulse (in Radians).
C 2*TAU is time duration between two pulses in the

```

```

C      sequence(in microsecs).
C      ETA is asymmetry parameter ( $0.0 < \text{ETA} < 1.0$ ).
C      THETAD and FID are angles that relate QPAS of a crystallite
C      to the Dipolar Principal Axis System (DPAS) (in Radians).
C      HL is local dipolar field (in Gauss).
C      FI1 is phase of the first i.e., preparatory pulse(in Radians).
C      FI2 is phase of pulses in the sequence with respect to that of
C      the preparatory pulse i.e.,first pulse (in Radians).
C      FI3 is phase of the detector with respect to first pulse.
C      IVARI indicates variation parameter:
C      IVARI=1 is for THETA variation;
C      IVARI=2 is for TAU variation;
C      IVARI=3 is for DELTA variation.
C      VINI=initial value of varying parameter.
C      VFIN=final value of varying parameter.
C      IVN=number of variation steps.
C      NT=number of THETA(LAB)S',NF=number of FI(LAB)S',used in powder
C      averaging. Typically NT=25,NF=25.
C      -----
100    READ(20,100)(TITLE(I),I=1,7)
        FORMAT(7A4)
        READ(20,*)WQ
        READ(20,*)THETA0,ETA
        READ(20,*)HL,THETAD,FID
        READ(20,*)FI1,FI2,FI3
        READ(20,*)THETA,TAU,DELTA
        READ(20,*)IVARI
        READ(20,*)VINI,VFIN,IVN
        READ(20,*)NT,NF
        CLOSE(UNIT=20)
C      -----
        WRITE(24,110)TITLE
        WRITE(6,110)TITLE
110    FORMAT(1X,'OUTPUT FROM SQMGNT'/1X,7A4)
        WRITE(24,120)WQ
        WRITE(6,120)WQ
120    FORMAT(1X,'RESONANCE FREQUENCY=',E13.6,'MHZ')
        WRITE(24,130)THETA0,ETA
        WRITE(6,130)THETA0,ETA
130    FORMAT(1X,'FLIP ANGLE OF PREPARATORY PULSE=',F9.6,'RADIANs'
1      ,2X,'ASYMMETRY PARAMETER=',F5.3)
        WRITE(24,140)HL,THETAD,FID
        WRITE(6,140)HL,THETAD,FID
140    FORMAT(1X,'LOCAL DIPOLAR FIELD=',F6.3,'GAUSS'/1X,
1      'DIPOLAR THETA=',F9.6,'RADIANs'/1X,
2      'DIPOLAR FI=',F9.6,'RADIANs')
        WRITE(24,150)FI1
        WRITE(6,150)FI1
150    FORMAT(1X,'PHASE OF THE FIRST i.e.,PREPARATORY PULSE=',F9.6
1      ,',RADIANs')

```

```

WRITE(24,160)FI2
WRITE(6,160)FI2
160  FORMAT(1X,'PHASE OF PULSES IN THE SEQUENCE W.R.T.FIRST PULSE ='
      1 ,F9.6,'RADIANS')
WRITE(24,170)FI3
WRITE(6,170)FI3
170  FORMAT(1X,'PHASE OF THE DETECTOR W.R.T. FIRST PULSE=',F9.6,
      1 'RADIANS')
GO TO(180,220,250),IVARI
180  WRITE(24,190)TAU
WRITE(6,190)TAU
190  FORMAT(1X,'TIME DURATION BETWEEN TWO PULSES IN THE SEQUENCE=',
      1 E13.6,'MICROSECS')
WRITE(24,200)DELTA
WRITE(6,200)DELTA
200  FORMAT(1X,'OFFSET PARAMETER =',E13.6)
WRITE(24,210)VINI,VFIN
WRITE(6,210)VINI,VFIN
210  FORMAT(1X,'INITIAL AND FINAL VALUES OF THETA=',F9.6,1X,',',',',1X,
      1 F9.6,'(RADIANS)')
GO TO 270
220  WRITE(24,200)DELTA
WRITE(6,200)DELTA
WRITE(24,230)THETA
WRITE(6,230)THETA
230  FORMAT(1X,'FLIP ANGLE OF THE SEQUENCE PULSES=',F9.6,'RADIANS')
WRITE(24,240)VINI,VFIN
WRITE(6,240)VINI,VFIN
240  FORMAT(1X,'INITIAL AND FINAL VALUES OF TAU=',E13.6,2X,E13.6,
      1 'MICROSEC')
GO TO 270
250  WRITE(24,230)THETA
WRITE(6,230)THETA
WRITE(24,190)TAU
WRITE(6,190)TAU
WRITE(24,260)VINI,VFIN
WRITE(6,260)VINI,VFIN
260  FORMAT(1X,'INITIAL AND FINAL VALUES OF OFFSET PARAMETER =',
      1 E13.6,2X,E13.6)
270  CONTINUE
WRITE(24,280)IVN
WRITE(6,280)IVN
280  FORMAT(1X,'NO. OF STEPS IN VARIATION=',I2)
VDEL=(VFIN-VINI)/IVN
WRITE(24,290)VDEL
WRITE(6,290)VDEL
290  FORMAT(1X,'INCREMENT IN VARIATIONS =',E13.6)
WRITE(24,300)NT,NF
WRITE(6,300)NT,NF
300  FORMAT(1X,'NO. OF THETA(LAB) VALUES=',I4/1X,'NO. OF FI(LAB)

```

1VALUES=' , I4)

C

```
-----
HL=HL*2621.4614E-06
HLSQ=HL*HL
R3=SQRT(3.0)
PI=4.0*ATAN(1.0)
WQ=WQ*2.0*PI
XI=ATAN(ETA/R3)
XIC=COS(XI)
XIS=SIN(XI)
XIP1=R3*XIC+XIS
XIN1=R3*XIC-XIS
XIP2=R3*XIS+XIC
XIN2=R3*XIS-XIC
RRKK=WQ*SQRT(1.0+ETA*ETA/3.0)
RRKK6=RRKK/6.0
DELWQ=DELTA*RRKK6
CALL INPMAT
STD=SIN(THETAD)
ST2D=SIN(2.0*THETAD)
STDD=STD*STD
CTD=COS(THETAD)
CTDD=CTD*CTD
R6=1.0/SQRT(6.0)
R5=SQRT(1.5)
SFD=SIN(FID)
CFD=COS(FID)
SF2D=SIN(2.0*FID)
CF2D=COS(2.0*FID)
E1=R5*STDD*CF2D
E2=R6*(3.0*CTDD-1.0)
AX=E1-E2
AY=-E1-E2
AZ=2.0*E2
B=R5*STDD*SF2D
C=R5*ST2D*CFD
D=R5*ST2D*SFD
CALL HDMAT
-----
```

C

C

C

C

C

C

C

C

Powder averaging preliminaries:

A Monte Carlo procedure called 'Systematic Sampling' is used.  
Reference: 1) S.C. Sivasubramanian, Ph.D. Thesis, Indian Institute  
of Technology Kanpur, India (1989).  
2) P. Raghunathan and S.C. Sivasubramanian, Proc. Indian Acad. Sci.  
(Chem. Sci.), 96 (1986) 565.

```
-----
TWOPI=PI+PI
NTNF=NT*NF
CPHAS1=COS(FI1)
SPHAS1=SIN(FI1)
```

```

CPHAS2=COS(FI2)
SPHAS2=SIN(FI2)
CPHAS3=COS(FI3)
SPHAS3=SIN(FI3)
DO 310 I=1,NT
  COSTL(I)=((1.0-2.0*I)/NT)+1.0
310  SINTL(I)=SQRT((1.0-COSTL(I)**2))
  DO 320 I=1,NF
    RND=((I-0.5)/NF)*TWOPI
    SINFL(I)=SIN(RND)
320  COSFL(I)=COS(RND)
    XXX(1)=VINI
    YYY(1)=0.0
    DO 330 I=2,IVN
      XXX(I)=XXX(I-1)+VDEL
330  YYY(I)=0.0

```

```

C -----
C Powder averaging loop starts:
C TL and FL are the angles that relate QPAS to the detection axis,
C namely, the X-axis of laboratory frame.(Crystal Orientation
C parameters).
C MEQMI is called NT*Nf times for each powder averaging.
C -----

```

```

DO 370 I=1,NT
DO 360 J=1,NF
E1=-0.5*SINTL(I)*SINFL(J)*XIP1
RK=E1*CPHAS1
R1K=E1*CPHAS2
R2K=E1*CPHAS3
RL=E1*SPHAS1
R1L=E1*SPHAS2
R2L=E1*SPHAS3
E2=0.5*COSTL(I)*(-XIN1)
RM=E2*CPHAS1
R1M=E2*CPHAS2
R2M=E2*CPHAS3
RN=-E2*SPHAS1
R1N=-E2*SPHAS2
R2N=-E2*SPHAS3
E3=SINTL(I)*COSFL(J)*XIS
RP=E3*CPHAS1
R1P=E3*CPHAS2
R2P=E3*CPHAS3
RQ=E3*SPHAS1
R1Q=E3*SPHAS2
R2Q=E3*SPHAS3
R=SQRT((RK*RK+RL*RL+RM*RM+RN*RN+RP*RP+RQ*RQ))
RSQ8=R*R*8.0
CALL HDPROJ
CALL LMNBAR

```

```

C      !!!!!!!GENERATE Q!!!!!!
      CON1=SIN(THETA0*R)/R
      CON2=COS(THETA0*R)
      CON3=CON1*(0.0,1.0)
      DO 340 ID=1,16
      DO 340 JD=1,16
340    Q(ID,JD)=RRKK*(CON2*RLBAR(ID,JD)-CON3*RMBAR(ID,JD))
C      -----
C      Parameter variation loop starts:
C      Each variation (increment by VDEL) requires one powder
C      averaging. However, we have arranged this loop in such a way that
C      powder averaging is done simultaneously for all parameter
C      (THETA,TAU or DELTA) variations.
C      -----
      DO 350 II=1,IVN
      TYPE*,II,I,J
      IF(IVARI.EQ.1)THETA=XXX(II)
      IF(IVARI.EQ.2)TAU=XXX(II)
      IF(IVARI.EQ.3)DELTA=XXX(II)
      IF(IVARI.EQ.3)DELWQ=DELTA*RRKK6
      CALL MEQMI(RATIO)
      YYY(II)=YYY(II)+REAL(RATIO)
350    CONTINUE
360    CONTINUE
370    CONTINUE
      WRITE(24,380)
380    FORMAT(1X,'VARIATION PARAMETER VS. EQ. MAGNETIZATION')
      DO 390 II=1,IVN
      YYY(II)=YYY(II)/NTNF
      WRITE(24,*)XXX(II),YYY(II)
390    CONTINUE
C      -----
      CALL PLOT(XXX,YYY,IVN)
      CLOSE(UNIT=6)
      CLOSE(UNIT=24)
      STOP
      END
C      -----
C      SUBROUTINE INPMAT
C      Generates input matrices which are Single Transition Operators.
C      -----
      COMPLEX YP1,YP2,YN1,YN2,YP3
      COMMON/BLK3/XP1(4,4),XP2(4,4),XN1(4,4),XN2(4,4),
      1 XN3(4,4),ZN1(4,4),ZN2(4,4),ZP2(4,4),AIDEN(4,4)
      COMMON/BLK4/YP1(4,4),YP2(4,4),YN1(4,4),YN2(4,4),YP3(4,4)
      DO 100 I=1,4
      DO 100 J=1,4
      XP1(I,J)=0.0;XP2(I,J)=0.0;XN1(I,J)=0.0;XN2(I,J)=0.0
      XN3(I,J)=0.0;ZP2(I,J)=0.0;ZN1(I,J)=0.0;ZN2(I,J)=0.0
      YP1(I,J)=(0.0,0.0);YP2(I,J)=(0.0,0.0);YN1(I,J)=(0.0,0.0)

```

```

100 YN2(I,J)=(0.0,0.0);YP3(I,J)=(0.0,0.0);AIDEN(I,J)=0.0
CONTINUE
XP1(1,2)=0.5;XP1(2,1)=0.5;XP1(3,4)=0.5;XP1(4,3)=0.5
XP2(1,4)=0.5;XP2(4,1)=0.5;XP2(2,3)=0.5;XP2(3,2)=0.5
XN1(1,2)=0.5;XN1(2,1)=0.5;XN1(3,4)=-0.5;XN1(4,3)=-0.5
XN2(1,4)=0.5;XN2(4,1)=0.5;XN2(2,3)=-0.5;XN2(3,2)=-0.5
XN3(1,3)=0.5;XN3(3,1)=0.5;XN3(2,4)=-0.5;XN3(4,2)=-0.5
YP1(1,2)=(0.0,-0.5);YP1(2,1)=(0.0,0.5)
YP1(3,4)=(0.0,-0.5);YP1(4,3)=(0.0,0.5)
YP2(1,4)=(0.0,-0.5);YP2(4,1)=(0.0,0.5)
YP2(2,3)=(0.0,-0.5);YP2(3,2)=(0.0,0.5)
YN1(1,2)=(0.0,-0.5);YN1(2,1)=(0.0,0.5)
YN1(3,4)=(0.0,0.5);YN1(4,3)=(0.0,-0.5)
YN2(1,4)=(0.0,-0.5);YN2(4,1)=(0.0,0.5)
YN2(2,3)=(0.0,0.5);YN2(3,2)=(0.0,-0.5)
YP3(1,3)=(0.0,-0.5);YP3(3,1)=(0.0,0.5)
YP3(2,4)=(0.0,-0.5);YP3(4,2)=(0.0,0.5)
ZN2(1,1)=0.5;ZN2(4,4)=-0.5;ZN2(2,2)=-0.5;ZN2(3,3)=0.5
ZP2(1,1)=0.5;ZP2(4,4)=-0.5;ZP2(2,2)=0.5;ZP2(3,3)=-0.5
ZN1(1,1)=0.5;ZN1(2,2)=-0.5;ZN1(3,3)=-0.5;ZN1(4,4)=0.5
AIDEN(1,1)=1.0;AIDEN(2,2)=1.0;AIDEN(3,3)=1.0;AIDEN(4,4)=1.0
RETURN
END

```

C

-----  
SUBROUTINE HDMAT

C

Generates the homonuclear Dipolar Hamiltonian.

C

```

COMPLEX YP1,YP2,YN1,YN2,YP3
COMPLEX DC1,DC2,DC3,DC4,DC5,DC6,DC7,HD,DKLP,H1,H3,Q,HDD
COMMON/BLK1/AX,AY,AZ,B,C,D,ETA,TAU,DELWQ,THETA0,R,THETA,HL,RRKK
COMMON/BLK2/XIC,XIS,XIP1,XIN1,XIP2,XIN2
COMMON/BLK3/XP1(4,4),XP2(4,4),XN1(4,4),XN2(4,4),
1 XN3(4,4),ZN1(4,4),ZN2(4,4),ZP2(4,4),AIDEN(4,4)
COMMON/BLK4/YP1(4,4),YP2(4,4),YN1(4,4),YN2(4,4),YP3(4,4)
COMMON/BLK5/DC1(16,16),DC2(16,16),DC3(16,16),
1 DC4(16,16),DC5(16,16),DC6(16,16),DC7(16,16)
COMMON/BLK6/D1(16,16),D2(16,16),D3(16,16),D4(16,16),D5(16,16),
1 D6(16,16)
COMMON/BLK7/HD(16,16),DKLP(16,16),H1(16,16),H3(16,16),Q(16,16)
COMMON/BLK10/HDSMSQ,HLSQ,RSQ8
COMMON/BLK11/HDD(16,16)
DO 100 I=1,16
DO 100 J=1,16
100 HD(I,J)=(0.0,0.0)
CALL DPSMRC(XP1,XP1,YN1,YN1,DC2,1.0)
CALL DRPRRR(XP2,XP2,D1)
CALL DPSMRR(XP2,XN2,XN2,XP2,D4,1.0)
CALL DRPRRR(XN2,XN2,D2)
E1=0.5*XIP1*XIP1
E2=XIN2*XIN2

```

```

DO 110 I=1,16
DO 110 J=1,16
HD(I,J)=HD(I,J)+(E1*DC2(I,J)+(D1(I,J)+D4(I,J)*XIN2+E2*D2(I,J))
1)*AX
110 CONTINUE
CALL DPSMRC(XN1,XN1,YP1,YP1,DC1,1.0)
CALL DRPRCC(YN2,YN2,DC2)
CALL DPSMCC(YP2,YN2,YN2,YP2,DC3,1.0)
CALL DRPRCC(YP2,YP2,DC4)
E1=0.5*XIN1*XIN1
E2=XIP2*XIP2
DO 120 I=1,16
DO 120 J=1,16
HD(I,J)=HD(I,J)+(E1*DC1(I,J)+DC2(I,J)-XIP2*DC3(I,J)+E2*DC4(I,J)
1)*AY
120 CONTINUE
CALL DRPRRR(ZN2,ZN2,D1)
CALL DPSMRR(ZN2,ZP2,ZP2,ZN2,D2,1.0)
CALL DRPRRR(ZP2,ZP2,D3)
CALL DPSMRC(XN3,XN3,YP3,YP3,DC1,1.0)
E2=2.0*XIC
E3=E2*E2
E4=2.0*XIS*XIS
DO 130 I=1,16
DO 130 J=1,16
HD(I,J)=HD(I,J)+((D1(I,J)+E2*D2(I,J)+E3*D3(I,J))+E4*DC1(I,J))*AZ
130 CONTINUE
CALL DPSMCR(YN1,XN1,XP1,YP1,DC5,-1.0)
CALL DPSMCR(YP1,XP1,XN1,YN1,DC6,-1.0)
CALL MTADCC(DC5,DC6,DC1,1.0)
CALL DPSMCR(YN2,XP2,XP2,YN2,DC2,1.0)
CALL DPSMCR(YN2,XN2,XN2,YN2,DC3,1.0)
CALL DPSMCR(YP2,XP2,XP2,YP2,DC4,1.0)
CALL DPSMCR(YP2,XN2,XN2,YP2,DC5,1.0)
E1=0.5*XIP1*XIN1
E3=XIP2*XIN2
DO 140 I=1,16
DO 140 J=1,16
HD(I,J)=HD(I,J)+(E1*DC1(I,J)-DC2(I,J)-XIN2*DC3(I,J)+XIP2*
1DC4(I,J)+E3*DC5(I,J))*B
140 CONTINUE
CALL DPSMRR(XP1,XN3,XN3,XP1,D3,1.0)
CALL DPSMCC(YN1,YP3,YP3,YN1,DC4,1.0)
CALL MTADRC(D3,DC4,DC1,1.0)
CALL DPSMRR(XP2,ZN2,ZN2,XP2,D1,1.0)
CALL DPSMRR(XP2,ZP2,ZP2,XP2,D2,1.0)
CALL DPSMRR(XN2,ZN2,ZN2,XN2,D3,1.0)
CALL DPSMRR(XN2,ZP2,ZP2,XN2,D4,1.0)
E1=-XIP1*XIS
E3=E2*XIN2

```



```

DO 150 I=1,16
DO 150 J=1,16
HD(I,J)=HD(I,J)+(E1*DC1(I,J)+(D1(I,J)+E2*D2(I,J)+XIN2*D3(I,J)+
1E3*D4(I,J))*C
150 CONTINUE
CALL DPSMCR(YP1,XN3,XN1,YP3,DC6,-1.0)
CALL DPSMCR(YP3,XN1,XN3,YP1,DC7,-1.0)
CALL MTADCC(DC6,DC7,DC1,1.0)
CALL DPSMCR(YN2,ZN2,ZN2,YN2,DC2,1.0)
CALL DPSMCR(YN2,ZP2,ZP2,YN2,DC3,1.0)
CALL DPSMCR(YP2,ZP2,ZP2,YP2,DC4,1.0)
CALL DPSMCR(YP2,ZN2,ZN2,YP2,DC5,1.0)
E1=-XIN1*XIS
E3=E2*XIP2
DO 160 I=1,16
DO 160 J=1,16
HD(I,J)=HD(I,J)+(E1*DC1(I,J)-DC2(I,J)-E2*DC3(I,J)+E3*DC4(I,J)
1 +XIP2*DC5(I,J))*D
160 CONTINUE
CALL MTMLCC(HD,HD,DC1)
HDSMSQ=0.0
DO 170 I=1,16
170 HDSMSQ=HDSMSQ+REAL(DC1(I,I))
DO 180 I=1,16
DO 180 J=1,16
180 HDD(I,J)=HD(I,J)
RETURN
END

```

```

C -----
C SUBROUTINE HDPROJ
C This subroutine projects the dipolar operator on the quadrupolar
C interaction frame (QIF).Details are given in Chapter Six.
C -----

```

```

COMPLEX HD,DKLP,H1,H3,Q,HDD
COMMON/BLK7/HD(16,16),DKLP(16,16),H1(16,16),H3(16,16),Q(16,16)
COMMON/BLK10/HDSMSQ,HLSQ,RSQ8
COMMON/BLK11/HDD(16,16)
WD=SQRT((HLSQ*RSQ8)/HDSMSQ)
DO 100 I=1,16
DO 100 J=1,16
100 HD(I,J)=HDD(I,J)*WD
RETURN
END

```

```

C -----
C SUBROUTINE LMNBAR
C Generates matrices LBAR,MBAR,NBAR and BBAR.
C BBAR is the operator that corresponds to the observable in an
C NQR experiment i.e.,the magnetization responsible for signal.
C -----
COMPLEX YP1,YP2,YN1,YN2,YP3,RMBAR,RNBAR,RBBAR

```

```

COMPLEX XC1(4,4),XC2(4,4),XC3(4,4)
COMMON/BLK1/AX,AY,AZ,B,C,D,ETA,TAU,DELWQ,THETA0,R,THETA,HL,RRKK
COMMON/BLK3/XP1(4,4),XP2(4,4),XN1(4,4),XN2(4,4),
1 XN3(4,4),ZN1(4,4),ZN2(4,4),ZP2(4,4),AIDEN(4,4)
COMMON/BLK4/YP1(4,4),YP2(4,4),YN1(4,4),YN2(4,4),YP3(4,4)
COMMON/BLK6/D1(16,16),D2(16,16),D3(16,16),D4(16,16),D5(16,16),
1D6(16,16)
COMMON/BLK8/RK,RL,RM,RN,RP,RQ
COMMON/BLK81/R1K,R1L,R1M,R1N,R1P,R1Q
COMMON/BLK82/R2K,R2L,R2M,R2N,R2P,R2Q
COMMON/BLK9/RBBAR(16,16),RLBAR(16,16),RMBAR(16,16),RNBAR(16,16)
CALL DPSMRR(ZN1,AIDEN,AIDEN,ZN1,RLBAR,1.0)
DO 100 I=1,4
DO 100 J=1,4
XC1(I,J)=(0.0,1.0)*(-RK*YN1(I,J)+RL*XP1(I,J)+RM*XN1(I,J)
1 -RN*YP1(I,J)-RP*YP3(I,J)+RQ*XN3(I,J))
XC2(I,J)=R1K*XP1(I,J)+R1L*YN1(I,J)+R1M*YP1(I,J)+
1 R1N*XN1(I,J)+R1P*XN3(I,J)+R1Q*YP3(I,J)
XC3(I,J)=R2K*XP1(I,J)+R2L*YN1(I,J)+R2M*YP1(I,J)+
1 R2N*XN1(I,J)+R2P*XN3(I,J)+R2Q*YP3(I,J)
100 CONTINUE
CALL DPSMCR(XC1,AIDEN,AIDEN,XC1,RMBAR,1.0)
CALL DPSMCR(XC2,AIDEN,AIDEN,XC2,RNBAR,1.0)
CALL DPSMCR(XC3,AIDEN,AIDEN,XC3,RBBAR,1.0)
RETURN
END

C -----
C SUBROUTINE MEQMI(RATIO)
C This calculates the ratio (eq.magnetization/ini.magnetization).
C -----
COMPLEX DC1,DC2,DC3,DC4,DC5,DC6,DC7
COMPLEX RMBAR,RNBAR,RBBAR
COMPLEX HD,DKLP,H1,H3,Q
COMPLEX TR1,TR2,TR3,TR4,TRNR,TRDR,RATIO
COMMON/BLK1/AX,AY,AZ,B,C,D,ETA,TAU,DELWQ,THETA0,R,THETA,HL,RRKK
COMMON/BLK5/DC1(16,16),DC2(16,16),DC3(16,16),
1 DC4(16,16),DC5(16,16),DC6(16,16),DC7(16,16)
COMMON/BLK7/HD(16,16),DKLP(16,16),H1(16,16),H3(16,16),Q(16,16)
COMMON/BLK9/RBBAR(16,16),RLBAR(16,16),RMBAR(16,16),RNBAR(16,16)
CALL H1H3
CALL MTADCC(H1,H3,DC1,1.0)
CALL MTMLCC(Q,DC1,DC2)
TR1=(0.0,0.0)
DO 100 I=1,16
100 TR1=TR1+DC2(I,I)
TR2=(0.0,0.0)
CALL MTMLCC(RBBAR,DC1,DC2)
DO 110 I=1,16
110 TR2=TR2+DC2(I,I)
TR3=(0.0,0.0)

```

```

TRNR=(0.0,0.0)
TRDR=(0.0,0.0)
CALL MTMLCC(DC1,DC1,DC2)
CALL MTMLCC(Q,RBBAR,DC3)
DO 120 I=1,16
120  TR3=TR3+DC2(I,I)
    TRDR=TRDR+DC3(I,I)
    TRDR=TRDR*TR3
    TR3=(0.0,0.0)
    CALL CMTRCC(RNBAR,DKLP,DC2)
    CALL CMTRCC(DC2,RBBAR,DC2)
    CALL MTMLCC(DC2,H1,DC3)
DO 130 I=1,16
130  TR3=TR3+DC3(I,I)
    TR4=(0.0,0.0)
    CALL CMTRCC(RNBAR,RBBAR,DC3)
    CALL CMTRCC(DC3,RNBAR,DC3)
    CALL MTMLCC(DC3,H1,DC1)
DO 140 I=1,16
140  TR4=TR4+DC1(I,I)
    TRNR=TR1*(TR2+(THETA*TAU*TR3/12.0)+(THETA*THETA*TR4/24.0))
    RATIO=TRNR/TRDR
    RETURN
    END

```

C

```
-----
SUBROUTINE PLOT(X,Y,N)
```

C

```
This subroutines creates a line printer plot in the file
corresponding to UNIT=6.NAG subroutine G01AGF is used!!!.
```

C

```
Execution comand should be .ex sqmgnt,/sea pub:nag.rel.
```

C

C

```
-----
DIMENSION X(N),Y(N),ISORT(100)
CALL G01AGF(X,Y,N,ISORT,110,67,1)
RETURN
END

```

C

```
-----
SUBROUTINE H1H3
```

C

```
This calculates first and third order Floquet Hamiltonian.
```

C

```
-----
COMPLEX DC1,DC2,DC3,DC4,DC5,DC6,DC7,RMBAR,RNBAR,RBBAR
COMPLEX HD,DKLP,H1,H3,Q
COMMON/BLK1/AX,AY,AZ,B,C,D,ETA,TAU,DELWQ,THETA0,R,THETA,HL,RRKK
COMMON/BLK5/DC1(16,16),DC2(16,16),DC3(16,16),
1 DC4(16,16),DC5(16,16),DC6(16,16),DC7(16,16)
COMMON/BLK7/HD(16,16),DKLP(16,16),H1(16,16),H3(16,16),Q(16,16)
COMMON/BLK9/RBBAR(16,16),RLBAR(16,16),RMBAR(16,16),RNBAR(16,16)
!!!!!!! COMPUTE H1 !!!!!!!!
CON1=THETA*0.5/TAU
CALL MTADCR(HD,RLBAR,DKLP,-DELWQ)
CALL MTADCC(DKLP,RNBAR,H1,CON1)
!!!!!!! COMPUTE H3 !!!!!!!!

```

C

C

```

CALL CMTRCC(RNBAR,DKLP,DC1)
CON1=THETA/12.0
CON2=CON1*TAU
CON1=CON1*THETA
CALL CMTRCC(DC1,RNBAR,DC2)
CALL CMTRCC(DC1,DKLP,DC3)
DO 100 I=1,16
DO 100 J=1,16
100 H3(I,J)=CON1*DC2(I,J)+CON2*DC3(I,J)
RETURN
END

```

```

C -----
C SUBROUTINE CMTRCC(A1,B1,C)
C This subroutine is written for evaluating the commutators of
C operators (complex Hermitian matrices.)
C -----
COMPLEX A1(16,16),B1(16,16),C(16,16),C1(16,16),C2(16,16)
CALL MTMLCC(A1,B1,C1)
CALL MTMLCC(B1,A1,C2)
CALL MTADCC(C1,C2,C,-1.0)
RETURN
END

C -----
C SUBROUTINE DPSMCC(A1,B1,C1,D1,D,CON)
C This and the following three subroutines are written for the
C routine evaluation of one particular kind of operation. It
C involves first taking direct product of A1 and B1, then of C1
C and D1 and finally summing the two results. The routine names can
C be decoded as follows: DP-->direct product; SM-->sum; C-->complex
C R-->real.
C -----
COMPLEX A1(4,4),B1(4,4),C1(4,4),D1(4,4),DC1(16,16),DC2(16,16),
1 D(16,16)
CALL DRPRCC(A1,B1,DC1)
CALL DRPRCC(C1,D1,DC2)
CALL MTADCC(DC1,DC2,D,CON)
RETURN
END

C -----
C SUBROUTINE DPSMRR(A1,B1,C1,D1,D,CON)
C -----
DIMENSION A1(4,4),B1(4,4),C1(4,4),D1(4,4),D2(16,16),D3(16,16),
1 D(16,16)
CALL DRPRRR(A1,B1,D2)
CALL DRPRRR(C1,D1,D3)
CALL MTADRR(D2,D3,D,CON)
RETURN
END

C -----
C SUBROUTINE DPSMCR(A1,B1,C1,D1,D,CON)

```

```

C -----
COMPLEX A1(4,4),D1(4,4),DC1(16,16),DC2(16,16),D(16,16)
DIMENSION B1(4,4),C1(4,4)
CALL DRPRCR(A1,B1,DC1)
CALL DRPRRC(C1,D1,DC2)
CALL MTADCC(DC1,DC2,D,CON)
RETURN
END

C -----
SUBROUTINE DPSMRC(A1,B1,C1,D1,D,CON)
C -----
COMPLEX C1(4,4),D1(4,4),DC2(16,16),D(16,16)
DIMENSION A1(4,4),B1(4,4),D2(16,16)
CALL DRPRRR(A1,B1,D2)
CALL DRPRCC(C1,D1,DC2)
CALL MTADRC(D2,DC2,D,CON)
RETURN
END

C -----
SUBROUTINE DRPRRR(A1,B1,C1)
C This subroutine and the following many subroutines are written
C for matrix manipulations. The routine names can be decoded as
C follows: MT->matrix; AD-> addition; ML-> multiplication;
C DRPR->direct product; R->real; C->complex.
C -----
DIMENSION A1(4,4),B1(4,4),C1(16,16)
IR=0
DO 120 I=1,4
  IC=0
  DO 110 J=1,4
    DO 100 I1=1,4
      DO 100 J1=1,4
100    C1(IR+I1,IC+J1)=A1(I,J)*B1(I1,J1)
110    IC=4*J
120    IR=4*I
  RETURN
END

C -----
SUBROUTINE DRPRRC(A1,B1,C1)
C -----
COMPLEX B1,C1
DIMENSION A1(4,4),B1(4,4),C1(16,16)
IR=0
DO 120 I=1,4
  IC=0
  DO 110 J=1,4
    DO 100 I1=1,4
      DO 100 J1=1,4
100    C1(IR+I1,IC+J1)=A1(I,J)*B1(I1,J1)
110    IC=4*J

```

```

120  IR=4*I
      RETURN
      END

```

```

C -----
C  SUBROUTINE DRPRCC(A1,B1,C1)
C -----
      COMPLEX A1(4,4),B1(4,4),C1(16,16)
      IR=0
      DO 120 I=1,4
        IC=0
        DO 110 J=1,4
          DO 100 I1=1,4
            DO 100 J1=1,4
100    C1(IR+I1,IC+J1)=A1(I,J)*B1(I1,J1)
110    IC=4*J
120    IR=4*I
      RETURN
      END

```

```

C -----
C  SUBROUTINE DRPRCR(A1,B1,C1)
C -----
      COMPLEX A1,C1
      DIMENSION A1(4,4),B1(4,4),C1(16,16)
      IR=0
      DO 120 I=1,4
        IC=0
        DO 110 J=1,4
          DO 100 I1=1,4
            DO 100 J1=1,4
100    C1(IR+I1,IC+J1)=A1(I,J)*B1(I1,J1)
110    IC=4*J
120    IR=4*I
      RETURN
      END

```

```

C -----
C  SUBROUTINE MTADCC(A1,B1,C1,CON)
C -----
      COMPLEX A1(16,16),B1(16,16),C1(16,16)
      DO 100 I=1,16
        DO 100 J=1,16
100    C1(I,J)=A1(I,J)+B1(I,J)*CON
      RETURN
      END

```

```

C -----
C  SUBROUTINE MTADRR(A1,B1,C1,CON)
C -----
      DIMENSION A1(16,16),B1(16,16),C1(16,16)
      DO 100 I=1,16
        DO 100 J=1,16
100    C1(I,J)=A1(I,J)+B1(I,J)*CON

```

RETURN  
END

C -----  
SUBROUTINE MTADRC(A1,B1,C1,CON)

C -----  
COMPLEX B1,C1  
DIMENSION A1(16,16),B1(16,16),C1(16,16)  
DO 100 I=1,16  
DO 100 J=1,16  
100 C1(I,J)=A1(I,J)+B1(I,J)\*CON  
RETURN  
END

C -----  
SUBROUTINE MTADCR(A1,B1,C1,CON)

C -----  
COMPLEX A1,C1  
DIMENSION A1(16,16),B1(16,16),C1(16,16)  
DO 100 I=1,16  
DO 100 J=1,16  
100 C1(I,J)=A1(I,J)+B1(I,J)\*CON  
RETURN  
END

C -----  
SUBROUTINE MTMLRR(A1,B1,C1)

C -----  
DIMENSION A1(16,16),B1(16,16),C1(16,16)  
DO 100 I=1,16  
DO 100 J=1,16  
C1(I,J)=0.0  
DO 100 K=1,16  
C1(I,J)=C1(I,J)+A1(I,K)\*B1(K,J)  
100 CONTINUE  
RETURN  
END

C -----  
SUBROUTINE MTMLCC(A1,B1,C1)

C -----  
COMPLEX A1(16,16),B1(16,16),C1(16,16)  
DO 100 I=1,16  
DO 100 J=1,16  
C1(I,J)=(0.0,0.0)  
DO 100 K=1,16  
C1(I,J)=C1(I,J)+A1(I,K)\*B1(K,J)  
100 CONTINUE  
RETURN  
END